Copyright
by
Vikram Chandrasekhar
2009

The Dissertation Committee for Vikram Chandrasekhar
certifies that this is the approved version of the following dissertation:

Coexistence in Femtocell-aided Cellular Architectures

Committee:

Jeffrey G. Andrews, Supervisor

Gustavo De Veciana

Robert W. Heath, Jr.

Constantine Caramanis

Yen-Hsi Richard Tsai

Coexistence in Femtocell-aided Cellular Architectures

by

Vikram Chandrasekhar, B.Tech.;M.S.

DISSERTATION

Presented to the Faculty of the Graduate School of

The University of Texas at Austin

in Partial Fulfillment

of the Requirements

for the Degree of

DOCTOR OF PHILOSOPHY

THE UNIVERSITY OF TEXAS AT AUSTIN

May 2009

Acknowledgments

This dissertation would not have materialized without the sacrifices and the discipline instilled in me by my parents. Their love, inspiration and encouragement are largely responsible for who I am today. My sister Yashodha and my brother-in-law Sriram motivated me during difficult times. My nephew Shreyas and my niece Shriya gave me new vigor before every semester. Thank you, family!

I would also like to thank my high school physics, chemistry and mathematics teachers (Professor Balasubramaniam, Professors Santhanam and Govindarajan, and Professor T.R. Subramaniam) who coached us for the arduous IIT Joint Entrance Examination. Learning calculus, taking your epic coaching tests and attending your classes were my first "trial by fire" in academia. The fundamentals that I learned from these brilliant teachers have served me well in research.

Professionally, I owe a considerable amount of my still maturing technical, writing and presentation skills to my advisor Professor Jeff Andrews. His unwavering focus and ability to multi-task efficiently (yet with the highest quality) impressed upon me very early on during graduate school. I credit my improvements on how to select the right problem to solve and how to write good papers (typical example being the 11+ iterations while writing a survey article on femtocells!) largely to Jeff's great technical feedback and writing skills. Jeff, thank you for convincing me to return to graduate school, unhesitatingly admitting me into your research group and providing me with research funding.

I am indebted to Professor Brian Evans for encouraging me to return to graduate school when I first approached him. In addition to my advisor and Prof. Evans, I thank Professors Gustavo De Veciana, Robert W. Heath Jr., Constantine Caramanis and Richard Tsai for their roles as my PhD committee members and their

useful research advice. Professor Heath, I appreciate the detailed comments that you provided on my dissertation. I specially acknowledge Professor De Veciana for his constant feedback on conducting research and his emphasis on striving for intuition. His insightful lectures (such as his coin-tossing examples to illustrate "independence" of events in EE381J) provided me with a sound background on mathematical probability.

I thank Texas Instruments for graciously supporting my research and inviting me for summer internships during 2007-08 and providing me with valuable industry experience in the wireless arena. During these internships, getting to interact and write technical papers with people of the calibre of Alan Gatherer, Zukang Shen and Tarik Muharemovic was inspiring, to say the least. As a staff engineer in the High Frequency Measurements group at National Instruments (NI), I obtained first-hand practical experience on how to prototype, design and test communication systems. I specially thank Abhay Samant and Lokesh Duriappah who mentored me and convinced me that pursuing a PhD would pay long-term dividends, even as I was grappling whether or not to return to graduate school.

I thank my best friends Bilal, Sastry, Krishna (SKK), Venkat and Vasanth in whom I could confide and get practical advice at various times. Interacting with Norberto, Andy, Jun, Marios, Ramya, Salam, Omar, Michele, Zrinka, Amin, Sriram, Behrang and all my other colleagues in the Wireless Networking and Communications Group (WNCG) was enjoyable in its camaraderie and cultural diversity.

Pursuing graduate school at the University of Texas (UT) has been a memorable journey. I thank Melanie, Janet and Paul, the ever friendly and approachable staff in the ECE graduate office and the WNCG. Together, they took care of the mystifying paper work, my tuition bills and insurance, course schedules, travel reimbursements and helping me schedule my qualifying proposal and defense. Gabriel from the ECE IT deserves my gratitude for fixing all computer issues.

I gratefully acknowledge the world-class facilities provided by UT and our industrial affiliates to conduct my research in a comfortable environment (such as the cubicles in WNCG which few universities can provide), and the excellent libraries and recreational facilities. As a potential UT Alumni, I look forward to interacting with WNCG on a long-term basis and influence further industry interaction with UT Austin.

Finally, my thank you's to Devin at JP's Java and Jessica and Monica at Ohm's Coffee. Your daily coffees will linger in my taste buds long after I will have graduated.

Coexistence in Femtocell-aided Cellular Architectures

Publication No. _____

Vikram Chandrasekhar, Ph.D.
The University of Texas at Austin, 2009

Supervisor: Jeffrey G. Andrews

The surest way to increase the capacity of a wireless system is by getting the transmitters and receivers closer to each other, which creates the dual benefits of higher quality links and more spatial reuse. In a network with nomadic users, this inevitably involves deploying more infrastructure, typically in the form of microcells, hotspots, distributed antennas, or relays. Compared to these deployments, a less expensive alternative for cellular operators is the recent concept of femtocells – also called home base-stations – which are end consumer installed data access points in the desire to get better indoor voice and data coverage. A two-tier network consisting of a conventional macrocell overlaid with shorter range wireless hotspots offers potential capacity benefits with low upfront costs to cellular operators. This dissertation addresses the key technical challenges inherent to a femtocell-aided cellular network, specifically managing radio interference and providing reliable coverage at either tier, for different physical layer technologies. Specific contributions include 1) an uplink capacity analysis and interference avoidance in two-tier networks employing Code Division Multiple Access (CDMA), 2) a decentralized power control scheme in two-tier networks with universal frequency reuse, 3) a coverage analysis of multi-antenna two-tier networks, and 4) spectrum allocation in two-tier networks employing Orthogonal Frequency Division Multiple Access (OFDMA). The goal of this research is to inspire

and motivate the use of decentralized interference management techniques requiring minimal network overhead in ongoing and future deployments of tiered cellular architectures.

Table of Contents

Acknowledgments **iv**

Abstract **vii**

List of Tables **xiii**

List of Figures **xiv**

Chapter 1. Introduction **1**

1.1 The Femtocell Concept 4

1.2 Motivation 8

1.3 Thesis Statement 11

1.3.1 Contributions and Organization 11

Chapter 2. Business and Technical Challenges facing Femtocell Deployments **14**

2.1 Business, Standardization and Deployment Aspects of Femtocells . . . 14

2.1.1 Current Standardization and Deployments 15

2.1.2 Comparison with Wi-Fi Access Points 16

2.2 Technical Challenges 17

2.2.1 Allocating Spectrum and Managing Radio Interference 17

2.2.2 Providing QoS over an Internet Backhaul 20

2.2.3 Access and Handoffs to Femtocells 20

2.2.4 Mobility of Femtocell Users and Emergency-911 services 22

2.3 Security and QoS over Internet Backhaul 23

Chapter 3. Uplink Capacity and Interference Avoidance **25**

3.1 Introduction 25

3.2 Motivation 25

3.2.1 Related Work 27

3.2.2 Contributions 28

3.3 System Model 29
3.3.1 TH-CDMA and Antenna Sectoring 31
3.3.2 Channel Model and Interference 32
3.4 Per Tier Outage Probability 35
3.5 Femtocell Exclusion Region and Tier Selection 42
3.6 Numerical Results 45
3.7 Conclusion 50

Chapter 4. Data Rate Adaptation in Closed Access 51
4.1 Introduction 51
4.1.1 Managing Cross-Interference 51
4.1.2 Prior Work 54
4.1.3 Contributions 56
4.2 System Model 57
4.3 Per-Tier SINR Contours In a Femtocell-Underlaid Macrocell 59
4.3.1 Design Interpretations 65
4.4 Utility-Based Distributed SINR Adaptation 68
4.4.1 Cellular Utility Function 71
4.4.2 Femtocell Utility Function 71
4.4.3 Existence of Nash Equilibrium 73
4.4.3.1 Femtocell Utility Selection 73
4.4.4 Reducing Femtocell SINR Targets : Cellular Link Quality Protection 75
4.5 Numerical Results 79
4.6 Conclusion 83

Chapter 5. Coverage in Multi-Antenna Two-Tier Networks 85
5.1 Introduction 85
5.2 Background on Multi-Antenna Transmission 85
5.3 Problem Definition 88
5.3.1 Related Works 91
5.3.2 Contributions 92
5.4 System Model 93
5.4.1 Terrestrial Path Loss Model 94
5.5 Per-Tier Signal-to-Interference Ratios 96

5.5.1 SIR Analysis at a Femtocell User 96
5.5.2 SIR Analysis at a Cellular User 102
5.5.3 Design Interpretations 103
5.6 Interference Management using Carrier-Sensing at Femtocells 107
5.6.1 Minimum Required Sensing Range and Per-Tier Transmit Power Ratio Bounds 108
5.6.2 Energy Detection based Carrier-Sensing of Cellular Users . . . 112
5.7 Numerical Results 113
5.8 Conclusions 117

Chapter 6. Spectrum Allocation in Two-Tier Networks 118
6.1 Introduction 118
6.1.1 The Return of FDMA 118
6.1.2 Related Work 121
6.1.3 Contributions 122
6.2 System Model 123
6.2.1 Per-Tier Spectrum Access 123
6.2.2 Channel Model and Variable Rate Transmission 125
6.3 Spectrum Allocation and Per-Tier Expected Throughputs 126
6.3.1 Macrocell Throughput: RR Scheduling 128
6.3.2 Macrocell Throughput: PF Scheduling 132
6.3.3 Femtocell Throughput 133
6.4 Numerical Results 140
6.5 Conclusions 143

Chapter 7. Conclusions and Future Work 146
7.1 Conclusions 146
7.2 Future Work 148

Appendices 150

Appendix A. Appendix to Chapter 3 151
A.1 Lemma 1 151
A.2 Theorem 1 152
A.3 Theorem 2 153
A.4 Theorem 3 154

A.5 Theorem 4 156
A.6 Lemma 2 157
A.7 Lemma 3 158

Appendix B. Appendix to Chapter 4 **160**
B.1 Theorem 9 160
B.2 Lemma 6 161

Appendix C. Appendix to Chapter 5 **163**
C.1 Theorem 10 163
C.2 Proposition 2 164
C.3 Corollary 4 165
C.4 Theorem 11 166
C.5 Distribution of the product of independent Beta distributed and Gamma distributed random variates 169
C.6 A new expression for the regularized incomplete Beta function 170

Appendix D. Appendix to Chapter 6 **172**
D.1 Lemma 8 172

Bibliography **174**

Vita **194**

List of Tables

3.1 System Parameters 46

4.1 Example: Link quality protection for a cellular user (row 2) with $N =$ 16 femtocells 78

4.2 System Parameters 79

5.1 System Parameters 114

6.1 System Parameters 141

List of Figures

1.1 The underlying architecture in a microcell-aided cellular network. . . 5

1.2 The underlying architecture in a cellular system employing distributed antennas. 5

1.3 The underlying architecture in a multi-hop relayed cellular system . . 6

1.4 The underlying architecture in a femtocell-aided cellular network. . . 7

1.5 Dead zones caused by cross-tier interference with universal frequency reuse. 10

2.1 Example demonstrating cross-tier interference at cellular user. 18

3.1 A two-tier femtocell network. 30

3.2 Interference experienced at sectorized femtocell antenna aligned at θ. 31

3.3 Intra-tier and cross-tier interference with universal frequency reuse. . 33

3.4 CDMA transmission with per-tier SIR target Γ. 36

3.5 Femtocell outage probabilities with joint and independent hopping protocols. Solid lines represent joint hopping when all users within a femtocell are assigned a common set of CDMA hopping slots. Dotted lines assume each femtocell user is individually randomly assigned a set of CDMA hopping slots. 37

3.6 Interior femtocell outage probability. 41

3.7 Theoretical (dotted) and empirical (solid) $\mathbb{P}^f_{\text{out}}$ for an interior and corner femtocell. 41

3.8 Macrocell outage probability for different femtocell densities with a femtocell exclusion region ($N_c = 24$ users, $P^f_r = P^c_r$). Dotted lines represent the theoretical lower bounds on outage probability and solid lines represent the empirically estimated probabilities. 43

3.9 Macrocell OCs with $N_{\text{hop}} = 1, N_{\text{sec}} = 3$. Solid lines show the empirical OCs, while dotted lines show the theoretically obtained OC curves. . 47

3.10 Cell Interior Femtocell OCs with $N_{\text{hop}} = 1, N_{\text{sec}} = 3$. Solid lines show the empirical OCs, while dotted lines show the theoretically obtained OC curves. 47

3.11 Network OCs for different macrocell-femtocell received power ratios ($N_{\text{hop}} = 4, N_{\text{sec}} = 3$) for a cell edge femtocell (distance to macrocell $= R_c$). 47

3.12 Network OCs with different hopping slots ($\frac{P_r^f}{P_r^c} = 10, N_{\text{sec}} = 3$) for a cell edge femtocell (distance to macrocell = R_c). 48

3.13 Network OCs with different hopping slots ($\frac{P_r^f}{P_r^c} = 10, N_{\text{sec}} = 3$) for a cell interior femtocell (distance to macrocell = $0.5R_c$). 48

3.14 Network OCs with tier selection and femtocell exclusion ($\frac{P_r^f}{P_r^c} = 10, N_{\text{sec}} = 3, R_{f,\text{exc}} = 20$) for a cell interior femtocell (distance to macrocell = $0.5R_c$). 48

4.1 A two-tier cellular system with varying SINR targets 52

4.2 Simple example with $N = 2$ femtocells for determining how link budgets vary with the normalized interference distance $D_f D_c / R_f D$. . . . 64

4.3 Single transmitting cellular user coexisting with an underlaid grid of cochannel femtocells. 66

4.4 Per-Tier SINR contours for different cellular user and femtocell locations 67

4.5 Decibel link budget $10 \log_{10}(1/\mathbf{q}_c^T \mathbf{q}_f)$ considering a square femtocell grid and randomly placed femtocells 69

4.6 Mean femtocell SINR targets (grid center at cell-edge) for different reward and cost coefficients. 81

4.7 Mean femtocell SINR targets with distributed power control and cellular link quality protection. 81

4.8 Femtocell SINR reduction when cellular SINR target is uniformly distributed in $[3, 10]$ dB, and initial femtocell SINR targets are uniformly distributed in $[5, 25]$ dB 82

5.1 Single user multiple antenna transmission 88

5.2 Multi-user multiple antenna transmission 89

5.3 No-coverage femtocell radius D_f 90

5.4 Cellular coverage radius D_c. 91

5.5 No-coverage femtocell radius for different values of $\frac{P_f}{P_c}$. 104

5.6 Maximum number of simultaneous femtocell transmissions $N_f U_f$ computed with SU and MU precoding at each femtocell. 104

5.7 Maximum number of simultaneous femtocell transmissions $N_f U_f$ for different values of α_{fo}. 105

5.8 Maximum number of simultaneous femtocell transmissions given a maximum outage probability constraint ϵ per cellular user. 106

5.9 Required sensing range (in meters) per femtocell (assuming SU transmission in each tier) as a function of the path loss exponents α_c, α_f and the normalized distance D of the cellular user. 110

5.10 Lower and upper bounds on P_c/P_f with SU transmission as a function of the distance D. Shaded region shows feasible P_c/P_f's at location D, which satisfies the per-tier outage probability requirement for different average numbers of femtocells per cell-site. 111
5.11 Maximum sensing range (in meters) at each femtocell as a function of the sensing time-bandwidth product and uplink pilot transmission powers. 114
5.12 Cumulative distribution function of the cellular data rate (in b/s/Hz) with SU transmission in each tier. 116
5.13 Conditional cumulative distribution function of the femtocell data rate (in b/s/Hz) (assuming a carrier-sensed cellular user at distance $D_{\text{sense}}/2$). Single-user transmission is employed in each tier. 116

6.1 Spectrum partitioning in a two-tier network. 119
6.2 S_c (in bps/Hz) versus outdoor path loss exponent α_c. 134
6.3 S_c (in bps/Hz) with RR and PF Scheduling, $\alpha_c = 4$. 134
6.4 Theoretical and empirical throughput per femtocell $\rho_f S_f$ (b/s/Hz). . 137
6.5 Femtocell ASE Vs F-ALOHA access probability. 138
6.6 Femtocell ASEs and subchannel throughputs. 139
6.7 Optimal spectrum allocation ρ for varying QoS parameter η. 142
6.8 Area Spectral Efficiencies in a two-tier network for varying QoS parameter η. 143
6.9 Average network-wide throughput $\rho_f S_f(1-\rho)$ (in b/s/Hz) provided by femtocells in their allocated spectrum $(1-\rho)$. 144
6.10 Required spectrum WF meeting a target average data rate of $D_c = 0.1$ Mbps for each macrocell user, given Round-Robin and Proportional-Fair scheduling at the macrocell. 145

Chapter 1

Introduction

The advances in digital signal processing, integrated circuit (IC) technology and microprocessors towards the latter half of the 20th century has, among other things, ushered in a new era of telephony, providing people the ability to communicate over the wireless medium. It is one of the crowning achievements of the human age that a vehicular user traveling at 80 plus miles per hour can yet communicate reliably over wireless. Due to technological advances in semiconductor fabrication and manufacturing, the number of transistors that can be placed on an IC has increased exponentially, doubling nearly every two years – known as the *Moore's law*. Indeed, cellular telephony has experienced exponential growth over the last decade, and it is estimated that there are about two billion users worldwide [56]. A further consequence has been that heterogeneous tasks hitherto carried out by different devices – cell phones for voice telephony, desktop computers for video downloads, cameras for taking pictures, MP3 players for music – have been aggregated onto single computing platforms endowed with wireless capability, thereby accelerating social change.

This technological "convergence" has created an unrelenting demand for higher data rates in wireless networks, and has triggered the design and development of new data-minded cellular standards such as the Worldwide Interoperability for Microwave Access (WiMAX) (IEEE 802.16e), the 3rd Generation Partnership Project's (3GPP) High Speed Packet Access (HSPA) and Long Term Evolution (LTE) standards, and 3GPP2's Evolution Data Optimized (EVDO) standard. In parallel, Wireless-Fidelity (Wi-Fi) mesh networks also are being developed to provide nomadic high-rate data services in a more distributed fashion [147]. Although the Wi-Fi networks will not

be able to support the same level of mobility and coverage as the cellular standards, to be competitive for home and office use, cellular data systems will need to provide service roughly comparable to that offered by Wi-Fi networks.

This conglomeration of differing wireless technologies such as cellular telephony, Wi-Fi, Bluetooth, ZigBee etc. has created an unprecedented growth in the ability to reliably communicate at ever increasing data rates over the wireless medium. Indeed, this growth in wireless capacity is exemplified by this observation from Martin Cooper of Arraycomm: "The wireless capacity has doubled every 30 months over the last 104 years". This translates into an approximately million-fold capacity increase since 1957. Breaking down these gains shows a 25x improvement from wider spectrum, a 5x improvement by dividing the spectrum into smaller slices, a 5x improvement by designing better modulation schemes, and a whopping 1600x gain through reduced cell sizes and transmit distance. The enormous gains reaped from smaller cell sizes arise from efficient spatial reuse of spectrum, or alternatively, a higher area spectral efficiency [7] measured in bits per second per hertz per unit area.

In conventional macrocellular systems (providing a wide area coverage typically of the order of a kilometer or more), providing reliable wireless performance – for example, a guaranteed minimum data rate with a maximum tolerable outage probability – is difficult because of path losses, the random wireless channel fluctuations (known as *fading*), and most seriously, cochannel interference from neighboring base-station (BS) transmissions. Existing and upcoming wireless standards – such as the IS136, the European GSM, the WiMAX (IEEE 802.16e) and the 3GPP LTE standards – negotiate the interference problem by requiring that adjacent BSs transmit on different frequency resources. Frequency reuse, however, requires centralized control, and more importantly incurs a poor spatial reuse of expensive spectrum. Therefore, cellular systems often encounter conflicting requirements between either providing reliable communication or obtaining higher spatial reuse of spectrum.

The surest way to resolve this tradeoff is by getting the transmitter and receiver

closer to each other, which creates the dual benefits of higher-quality links and more spatial reuse. In a network with nomadic users, this inevitably involves deploying more infrastructure, typically in the form of microcells, distributed antennas, or relays as described below.

Microcells. Microcells are operator installed cell towers (Fig. 1.1) that improve coverage in urban areas experiencing poor reception. A microcell [77] has a large radio range (100-500 m), and generally implies centralized deployment, i.e. by the service-provider. This allows the operator to either load balance users [113, 152] or preferentially assign high data rate cellular users to the microcell [99, 130] because of its inherently larger capacity. The disadvantage associated with microcells are the high costs associated with installation and maintenance of new cell towers. Moreover, microcells do not guarantee reliable indoor coverage.

Distributed Antennas (DAs). Distributed antennas cellular systems comprise of a conventional macrocell BS augmented with operator installed spatially separated antenna elements (AEs) [123], thereby forming a spatially separated macroscopic multi-antenna system. Each antenna module is connected to the central macrocell BS via dedicated wires, fiber optic or an exclusive RF backhaul link (Fig. 1.2). Coverage holes are eliminated since users previously experiencing poor reception to the macrocell BS are likely proximate to an antenna element. Because the AEs are centrally controlled, the operator can vary the transmission strategy – as an instance, choosing which AEs to transmit and how much transmit power to assign to each AE – for optimizing system performance. Previous research has shown that DAs cause lower other-cell interference and provide substantial capacity gains [35, 79], especially for users on their cell-edge. The shortcomings of DAs are that they do not necessarily guarantee reliable indoor coverage, the high costs associated with backhaul provisioning, and radio interference in the same bandwidth from nearby AEs which will likely diminish capacity.

Relays. Relays are operator deployed infrastructure points which route the

data between the source and destination, thereby enhancing the overall end-to-end performance. Relays are currently the focus of intense research in the area of *cooperative communications* [114, 117] as well as in upcoming deployments of *multihop cellular networks* (MCN) – for example, the IEEE 802.16j, the multihop relay specification for the IEEE 802.16e (WiMAX) wireless standard. Relays can fill coverage holes in existing cellular systems (at the cell-edge, at tunnels/subways), or end-user deployed in poor coverage areas, or even provide temporary coverage (for example, during public events). Additionally, relays enhance signal strength at users experiencing already experiencing good coverage at their BS. In practice, however, deploying relays requires prior planning by the service provider – for example, where to place the relays for maximum coverage benefit [105] – and identifying locations experiencing poor cellular coverage. From a communications perspective, relays will require to be tightly synchronized with the macrocell BS for ensuring coherent reception and consequent improved signal strength at the user terminal [117]. Finally, non-transparent relaying – for relays serving mobiles unable to communicate with the macrocell BS – will require relays to transmit control information, implying potentially increased costs and sophisticated design.

The common problems associated with each of the above infrastructures are that a) the network infrastructure for doing so is potentially expensive and b) high quality indoor reception is not guaranteed especially in microcells and DA systems. In the following section, we shall describe an alternative approach for coverage and capacity enhancement by end-user deployment through the recent concept of *femtocells*.

1.1 The Femtocell Concept

Femtocells, also called home base-stations, are short range, low cost and low power access points (APs), installed by the *end-consumer* for better indoor voice and data reception. The user-installed femtocell device communicates with the cellular

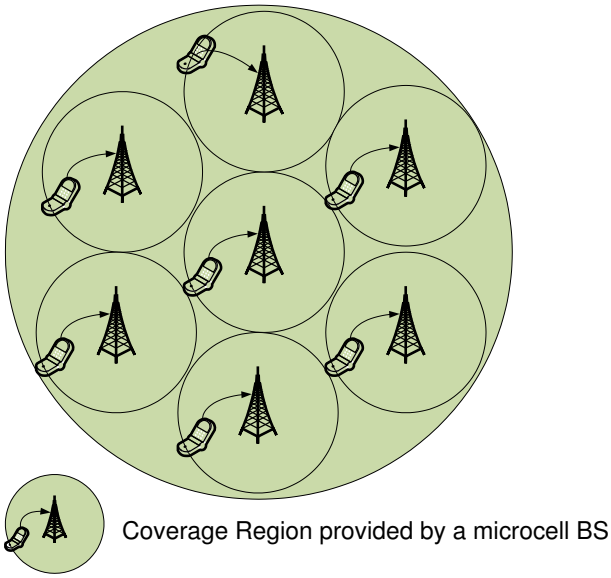

Figure 1.1: The underlying architecture in a microcell-aided cellular network.

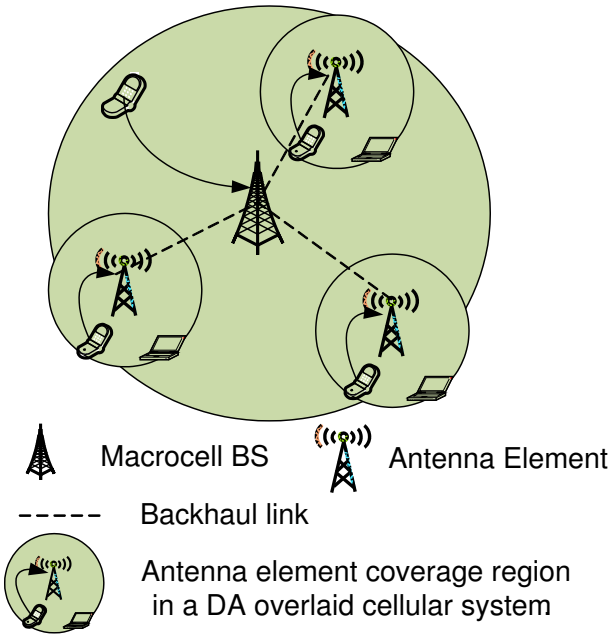

Figure 1.2: The underlying architecture in a cellular system employing distributed antennas.

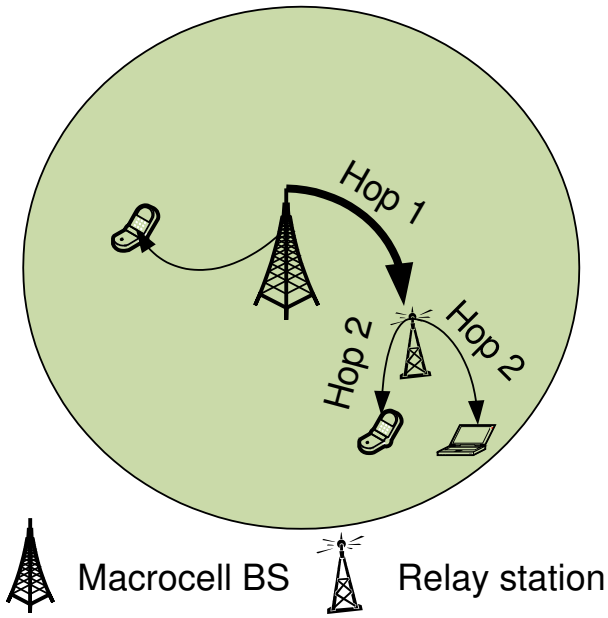

Figure 1.3: The underlying architecture in a multi-hop relayed cellular system

network over a broadband connection such as Digital Subscriber Line (DSL), cable modem, or a separate wireless backhaul channel (see Fig. 1.4). Like microcells, DAs and relays, due to their short transmit-receive distance, femtocells can greatly lower transmit power, prolong handset battery life, and achieve a higher signal-to-interference-plus-noise ratio (SINR). These translate into improved reception – the so-called five-bar coverage – and higher capacity. Because of the reduced interference, more users can be packed into a given area in the same region of spectrum, thus increasing the area spectral efficiency [7], or equivalently, the total number of active users per Hz per unit area.

Compared to other techniques for increasing system capacity, such as distributed antenna systems, microcells and relays, the key advantages of femtocells are that there is very little upfront cost to the service provider, further, they require relatively minimal coordination (implying minimal network overhead) with the macrocell

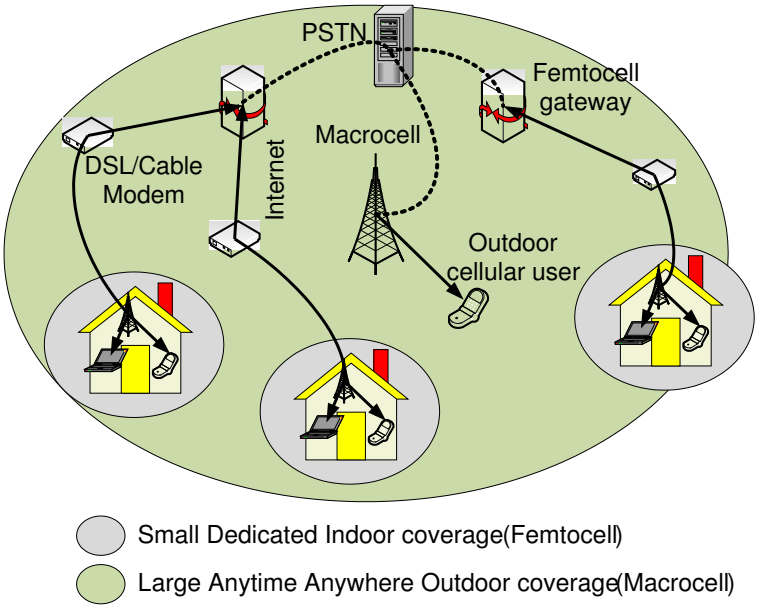

Figure 1.4: The underlying architecture in a femtocell-aided cellular network.

BS [29]. Moreover, because femtocells are installed by end-consumers in their self-interest, they can be placed at random locations in each cell-site; in contrast, other infrastructure such as fixed relays will need to be placed by the service provider for realizing their benefits, implying increased network planning.

Studies on wireless usage show that more than 50% of all voice calls and more than 70% of data traffic originates indoors [118]. Voice networks are engineered to tolerate low signal quality, since the required data rate for voice signals is very low, on the order of 10 Kbps or less. Data networks, on the other hand, require much higher signal quality in order to provide the multi-Mbps data rates users have come to expect. For indoor devices, particularly at the higher carrier frequencies likely to be deployed in many wireless broadband systems, attenuation losses will make high signal quality and hence high data rates very difficult to achieve. Poor in-building coverage causes customer dissatisfaction, encouraging them to either switch operators or maintain a separate wired line whenever indoors.

This raises the obvious question: why not encourage the end-user to install a short-range low-power link in these locations? This is the essence of the win-win of the femtocell approach. The subscriber is happy with the higher data rates and reliability; the operator reduces the amount on traffic on their expensive macrocell network, and can redirect its resources to provide better coverage to truly mobile users. The enhanced home coverage provided by femtocells will reduce motivation for home users to switch carriers.

However, the coverage and capacity benefits of femtocells are not realizable, without first addressing radio interference across tiers, i.e. between the primary tier 1 cellular network and the secondary tier 2 femtocell network. Interference in such a tiered cellular architecture arises because users in both tiers inhabit the same region of spectrum, termed as *universal frequency reuse*.

Universal frequency reuse is desirable for reasons of economy and flexible deployment. With universal frequency reuse however, cochannel radio interference between cellular users and femtocell users will likely limit the performance of such tiered cellular systems. Interference management in two-tier networks faces practical challenges from the lack of coordination between the macrocell base-station (BS) and femtocell APs due to reasons of scalability, security and limited availability of backhaul bandwidth [160]. Consequently, even though it may be easier to operate the macrocell and femtocells in a common spectrum from an infrastructure or spectrum availability perspective, at the same time, *pragmatic solutions are necessary to reduce cross-tier interference*. The motivation of this thesis is to provide decentralized radio interference management strategies in femtocell-aided cellular architectures.

1.2 Motivation

The motivation behind this research is to address radio interference management in practical femtocell deployments and ensure that both cellular users and

hotspot users can achieve their desired target data rates (or coexist) when they either operate in the same spectrum, or operate in orthogonal spectrum. Shared spectrum operation may be desirable to operators because of the scarce availability of spectrum and flexibility during deployment [72]. With shared spectrum between tiers however, radio interference between cellular users to femtocell hotspots, and between hotspot users to the macrocell BS, is likely to be the capacity-limiting factor.

Contemporary wireless systems employ power control to assist users experiencing poor channels and to limit interference caused to neighboring cells. In a two-tier network however, cross-tier interference may significantly hinder the performance of conventional power control schemes. For example, during cellular uplink (mobile to BS) transmission, a cellular user at the edge of its macrocell transmits with higher power to meet its receive power target, and causes excessive cross-tier interference at nearby femtocells. During downlink (BS to mobile) transmissions, a cellular user may experience excessive interference from nearby cochannel femtocell transmissions, especially when the received signal strength from the macrocell BS transmission is low (typically at the edge of the macrocell). Cellular users and femtocell users consequently experience unacceptable cross-tier interference in these resulting coverage "dead zones" (see Fig. 1.5), thereby satisfy their minimum desired Quality-of-Service (QoS) requirements.

Addressing cross-tier interference at a cellular user is especially important because the service (data rates) provided to cellular users should remain unaffected by a femtocell underlay which operates in the same spectrum. In other words, *the addition of femtocells should not deteriorate the performance of the conventional macrocellular network*. Three main reasons are a) the macrocell BS's primary role of an anytime anywhere infrastructure, especially for mobile and "isolated" users without hotspot access, b) the greater number of users served by each macrocell BS, and c) the end user deployment of femtocells in their self-interest. The macrocell is consequently modeled as *primary infrastructure*, meaning that the service provider's foremost obli-

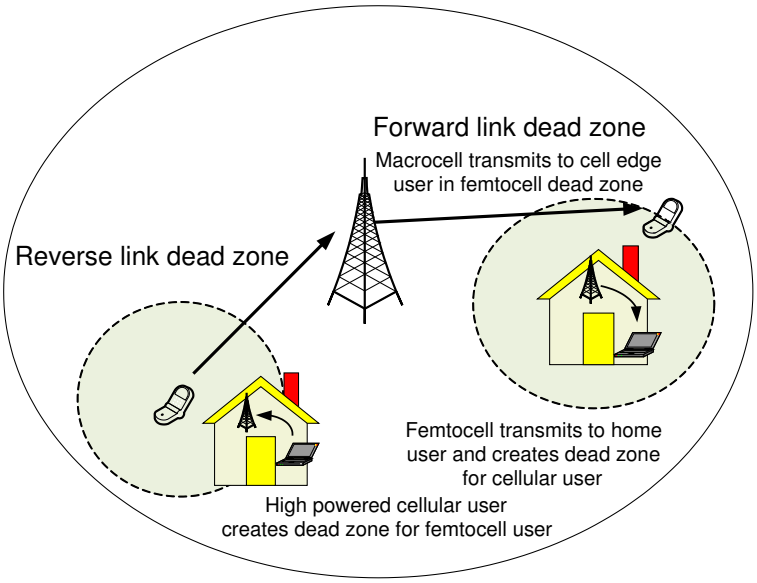

Figure 1.5: Dead zones caused by cross-tier interference with universal frequency reuse.

gation is to ensure that an outdoor cellular user achieves its desired quality of service, despite cross-tier femtocell interference.

Due to reasons of scalability and limited availability of backhaul bandwidth, the macrocell and femtocell BSs may not be able to coordinate their transmissions (for example, using a centralized scheduler or centralized power assignments to users) for minimizing cross-tier interference. The implication is that the macrocell BS and femtocell APs should not only provide reliable coverage to their own users, but ensure that they do not cause unacceptable interference to users in the other tier in a *distributed fashion*. By distributed, we mean that there is little or zero control information exchanged – for instance, the indices of the currently active cellular or femtocell user – either between the macrocell BS and femtocell APs, or between femtocell APs. This motivates employing *decentralized interference management* schemes – which is the main focus of this thesis – for ensuring acceptable performance at either tier. In the following section, we focus on the main contributions of this research for

ensuring coexistence in femtocell-aided cellular architectures.

1.3 Thesis Statement

Our main thesis is that without managing interference, deploying tiered networks will likely be self-defeating due to near-far effects with universal frequency reuse. This dissertation addresses decentralized radio interference management in femtocell-aided cellular architectures, encompassing a variety of physical layer technologies, through a combination of interference avoidance, power control and spectrum allocation techniques for alleviating cross-tier interference and improving wireless capacity.

1.3.1 Contributions and Organization

The following are the contributions of this dissertation.

Uplink Capacity and Interference Avoidance. Due to the scarcity of spectrum, it is desirable to operate both macrocell and femtocell users to operate in the same bandwidth, if at all possible. The location dependent cross-tier co-channel interference (CCI) experienced at femtocells from the "near-far" problem causes significant deterioration in the user capacity of a two-tier network. This research addresses the total two-tier system capacity – defined as the total number of cellular users and femtocell APs – when Code Division Multiple Access (CDMA) transmission is employed in either tier. This work also demonstrates an interference avoidance strategy for combating the near-far problem, which results in superior user capacity, compared with a two-tier network which splits the spectrum between each tier.

Data Rate Adaptation in Closed Access. To quantify near-far effects in a femtocell-aided cellular network with universal frequency reuse, this research derives a fundamental relation providing the largest feasible macrocell SINR, given any set of feasible femtocell SINRs. A distributed utility-based SINR adaptation at femtocells is proposed in order to alleviate cross-tier interference at the macrocell from overlaid

femtocell infrastructure. The Foschini-Miljanic (FM) algorithm is a special case of the adaptation. Each femtocell maximizes their individual utility consisting of a SINR based reward less an incurred cost (interference to the macrocell). Numerical results show greater than 30% improvement in mean femtocell SINRs relative to FM. In the event that cross-tier interference prevents a cellular user from obtaining its SINR target, an algorithm is proposed that adaptively curtails transmission powers of the strongest femtocell interferers.

Coverage in Multi-Antenna Networks. In two-tier networks with universal frequency reuse, the near-far effect from cross-tier interference creates dead spots where reliable coverage cannot be guaranteed to users in either tier. Equipping the macrocell and femtocells with multiple antennas enhances robustness against the near-far problem and improves spatial reuse. Using tools from stochastic geometry, this research has derived the maximum number of simultaneously transmitting multiple antenna femtocells meeting a per-tier outage probability constraint. Per-tier coverage zones are presented wherein cross-tier interference bottlenecks cellular and hotspot coverage. Two operational regimes have been shown namely 1) a cellular-limited regime in which femtocell users experience unacceptable cross-tier interference and 2) a hotspot-limited regime wherein both femtocell users and cellular users are limited by hotspot interference. The analysis accounts for the per-tier transmit powers, the number of transmit antennas (single antenna transmission being a special case) and terrestrial propagation such as the Rayleigh fading and the path loss exponents. Single user (SU) multiple antenna transmission at each tier is shown to provide significantly superior coverage and spatial reuse relative to multiuser (MU) transmission. Finally, a decentralized carrier-sensing approach has been proposed to regulate femtocell transmission powers based on their location.

Spectrum Allocation. In two-tier networks providing frequency division based access (FDMA), the absence of coordination between cellular and femtocell transmissions will cause spectrum partitioning between tier to be more viable, compared to

centralized frequency assignment strategies. This research has proposed and analyzed the performance of an optimum decentralized spectrum allocation policy that maximizes the Area Spectral Efficiency (ASE) of a two-tier network employing FDMA, and is subjected to a sensible QoS requirement, which guarantees that both macrocell and femtocell users attain at least a prescribed data rate.

This dissertation is organized as follows. In **Chapter 2**, we examine the key technical and business challenges facing femtocell deployments. Thereafter, the technical contributions of this dissertation are covered in **Chapters 3** through **6**.

In **Chapter 3**, we describe an uplink capacity analysis and an interference avoidance strategy in a two-tier network employing CDMA transmission with universal frequency reuse. Next, **Chapter 4** presents a utility-based femtocell Signal-to-Interference-Plus Noise Ratio (SINR) adaptation scheme which minimizes cross-tier interference to cellular users. Moving from single antenna transmission to multi-antenna transmission, **Chapter 5** studies how equipping the macrocell BS and femtocell APs with multiple transmit antennas influences coverage provided to cellular and femtocell users, and presents a carrier-sensing based femtocell interference management strategy to combat cross-tier interference. The final contribution in **Chapter 6** presents a spectrum allocation strategy and derives area spectral efficiencies in frequency division access based two-tier networks. The dissertation concludes with **Chapter 7**, which summarizes the key contributions of this thesis and highlights open avenues for future research in femtocell networks.

Chapter 2

Business and Technical Challenges facing Femtocell Deployments

This chapter examines the key business and technical challenges encountering practical femtocell deployments. We first discuss the daunting requirements for keeping femtocell manufacturing costs and their prices low for effectively competing against the ubiquitous Wi-Fi technology. Next, we discuss the state of ongoing femtocell deployments and standardization efforts spearheaded by the *Femto-Forum*. Key technical challenges in a practical femtocell deployment are presented, including managing cross-tier radio interference, resource allocation between tiers, providing QoS over an internet backhaul, allowing access to femtocells, handoffs and mobility issues, and finally, how to provide reliable QoS and security over the cable modem/DSL based internet backhaul.

2.1 Business, Standardization and Deployment Aspects of Femtocells

Even though femtocells offer savings in site lease, backhaul and electricity costs for the operator, they incur strategic investments. Operators will need to aggressively price femtocells despite tight budgets and high manufacturing costs, to compete with ubiquitous Wi-Fi. This may necessitate innovative business solutions such as the cellular operator subsidizing the femtocell for purchase by the customer, or alternatively charging reduced prices per call to incentivize consumers using their home BS. For example, the North American operator Sprint charges a subsidized price of $99.99 per

Airave femtocell (introduced in September 2007), for subscribing to a $20 per month family plan. At the same time, the features that femtocells have to provide are in many ways more sophisticated than what is in a consumer grade Wi-Fi access point. The nascent femtocell vendors are facing cost targets set by the mature high-volume Wi-Fi market and by the demands of the operators for minimal subsidy to reduce Return-on-Investment (ROI) time. Consequently, cost issues are in most cases, the central factor driving the selection of solutions to each technical challenge.

Claussen *et al.* [36] have performed a financial analysis of the operating and capital expenditures incurred in a femtocell deployment. Assuming open access (or public access to all users within radio range of a femtocell), the key conclusions of their study are that 1) the macrocell expenses initially decrease very quickly because of the high degree of coverage even with a few installed femtocells and 2) the overall network costs (considering operating expenses of both the macrocell and femtocells) are minimal with nearly 30% of consumers having an installed femtocell. A predictive cost breakup in a femtocell network deployment conducted by Airvana and Gartner [118] has shown that after 1.5 years, operator investment will be recovered, allowing future profits.

2.1.1 Current Standardization and Deployments

Given the aggressive cost challenges, standardization of requirements across customers is important to accomplish a low cost femtocell solution. Towards this end, a collaborative organization called the Femto-Forum comprised of operators and femtocell vendors was formed in 2007 with the objective of developing open standards for product interoperability. During April 2009, the 3rd generation partnership project (3GPP), in collaboration with the Femto-Forum and the Broadband Forum released the world's first femtocell standard. This standard covers different aspects of femtocell deployments including the network architecture, radio interference, femtocell management, provisioning and security.

As of the writing of this dissertation (February-April 2009), the cellular operator Sprint provides CDMA 1x EVDO services through its "Airave" femtocell (manufactured by Samsung) in the United States of America (USA). Verizon has launched its femtocell operation in USA–called the "Verizon Home Network Expander" for providing Code Division Multiple Access (CDMA) service. Concurrently, a number of operators-AT &T (USA), O2 Telefonica and Motorola (Europe) and Softbank (Japan)-are conducting femtocell trials prior to market. ABI Research [118] predicts 102 million users worldwide on more than 32 million femtocells by 2012.

2.1.2 Comparison with Wi-Fi Access Points

For users possessing dual-mode handsets endowed with both cellular and Wi-Fi capability (for example, the iPhone), it is likely that such users would rather communicate with an indoor Wi-Fi AP – using for example, a Skype-enabled software application on their handset device – for making telephone calls over the internet. Indeed, it is hard to make a convincing case to motivate such users to install femtocells. On the contrary, significant numbers of cellular devices are not equipped with dual-mode capabilities; the value proposition for femtocells lies in encouraging such users to install femtocell APs for enhancing their indoor cellular coverage.

One would note the demerits of Wi-Fi access including a) the QoS (example, guarantees on the maximum end-to-end latencies at a packet level) provided by IEEE 802.11x Wi-Fi standards are in general inferior to those provided by the cellular standards, b) interference between Wi-Fi devices since they operate in unlicensed spectrum and c) seamless switching on dual-mode devices between the 3G/2G cellular networks and Wi-Fi networks may be difficult.

Having considered the business aspects, the following sections now examine equally compelling technical challenges that will require to be addressed by femtocells.

2.2 Technical Challenges

This section overviews the key technical challenges facing practical deployments of femtocell networks namely a) managing radio interference between cellular users and femtocell users, b) resource allocation between tiers, c) providing QoS over an internet backhaul, d) allowing access to femtocells and e) handoffs, mobility and providing Emergency-911 services .

2.2.1 Allocating Spectrum and Managing Radio Interference

Confronting cellular operators will be the dual problems of mitigating radio interference and efficiently allocating spectrum in femtocell-aided cellular networks. Interference mitigation will require innovative solutions since the low-cost target potentially necessitates scaled-down signal processing capabilities inside femtocells. The interference will arise from a) Macrocell to femtocell interference, b) Femtocell to femtocell interference and c) Femtocell to macrocell interference. The near-far effect – due to uneven spatial distribution of receive power – is the main contributor for a) and c), while femtocell to femtocell interference is relatively smaller due to low transmit power and penetration losses.

Example. Assume a cellular user located at a distance of $D = 1000$ meters from their macrocell BS, whose transmission power equals $P_{\text{tx,dBm}} = 43$ dBm (approximately 20 Watts) [1]. Considering a path loss based signal strength decay using the IMT-2000 propagation model [1], the average received signal strength – disregarding fast fading and random channel fluctuations – at the cellular user terminal equals

$$S_{\text{rx,dBm}} = P_{\text{tx,dBm}} - 10\alpha_c \log_{10} D - 30 \log_{10} f_c + 71.$$

[1] The dBm notation refers to the decibel signal power level relative to 1 milliwatt (mW). A signal power level P (in milliwatts) is equivalent to $10 \log_{10} P$ dBm. A power level of 1 mW therefore equals 0 dBm. The dBm notation is convenient for expressing both small and large signal power values in a short form.

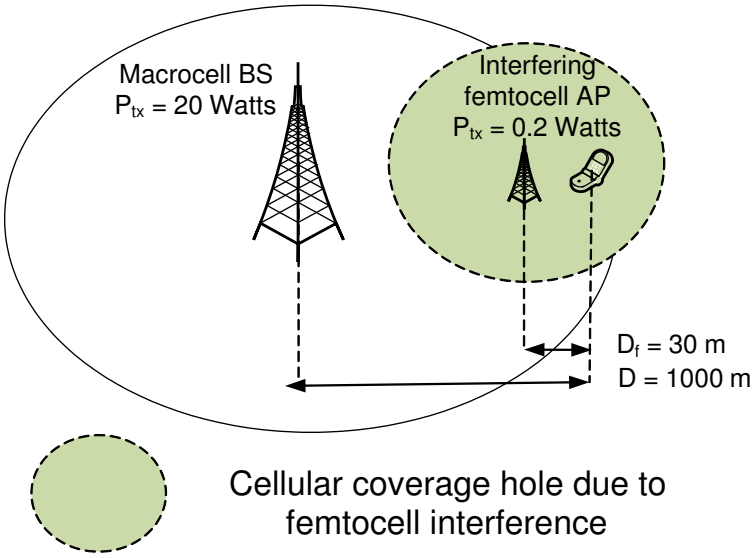

Figure 2.1: Example demonstrating cross-tier interference at cellular user.

Here f_c denotes the carrier frequency (in MHz) and α_c denotes the path-loss exponent [56]. Choosing $f_c = 2000$ MHz and a typical cellular path-loss exponent $\alpha_c = 3.8$, the receive power $S_{\text{rx,dBm}}$ is nearly -99 dBm.

Now, assume an interfering femtocell at a distance of $D_f = 30$ meters from the cellular user (see Fig. 2.1). This choice of D_f represents a scenario of a cellular user passing near the immediate vicinity of an actively transmitting femtocell AP. The average interference power at the cellular user due to the femtocell is well modeled as

$$I_{\text{rx,dBm}} = P_{\text{tx,dBm}} - 10\alpha_{fo} \log_{10} D_f - W_{\text{dB}} - 37.$$

With a femtocell transmit power equaling 23 dBm – 100x smaller than the macrocell transmit power – and the path loss exponent $\alpha_{fo} = 3.8$, the received interference power $I_{\text{rx,dBm}}$ at the cellular user is nearly -75 dBm. In other words, the decibel signal-to-interference ratio at the cellular user equals -24 dB, implying that successful reception at the cellular user is *infeasible*. This indicates that cross-tier interference, arising from the uneven distribution of receive powers, is potentially likely to be the

key technical challenge facing practical femtocell deployment.

The 3GPP LTE and WiMAX (IEEE 802.16e) standards ensure intra-cell orthogonality among cellular users and mitigate inter-cell interference through fractional frequency reuse [10]. Since femtocells will be placed by end consumers, the ad-hoc locations of femtocells will render centralized frequency planning difficult. Owing to the absence of coordination between the macrocell and femtocells and between femtocells, decentralized spectrum allocation between macrocell and femtocell users is an open research problem, which can provide answers to the following questions.

1. Should macrocell and femtocell users be orthogonal through bandwidth splitting? Is there an "optimal" splitting policy? How does this vary with the femtocell density?

2. Alternatively, with shared bandwidth (i.e. universal frequency reuse), what fraction of the spectrum should the macrocell and femtocells assign their users?

3. Which of these two schemes is "better" in various configurations?

Because of the scarce availability of spectrum and for reasons of economy, flexibility and ease of deployment [72, 89], cellular operators will likely prefer assigning the same region of spectrum to both cellular and hotspot users. With shared spectrum, practical challenges stem from the absence of coordination between the macrocell and femtocell due to reasons of scalability, security and limited backhaul capacity [29]. Due to the near-far effect in a closed-access femtocell deployment, cross-tier interference will likely be the capacity-limiting factor with universal frequency reuse. When femtocells are added, power control employed by cellular users creates dead-zones leading to non-uniform coverage. On the reverse link (user transmitting to their BS), a cell edge macrocell user transmitting at maximum power causes unacceptable interference to nearby femtocells. Consequently, cell edge femtocells experience significantly higher interference compared to interior femtocells. On the forward link (BS

transmitting to served user), at the cell edge – where femtocells are most needed – cellular users are disrupted by nearby femtocell transmissions, since they suffer higher path loss compared to cell interior users.

2.2.2 Providing QoS over an Internet Backhaul

The IP backhaul needs QoS for delay-sensitive traffic and providing service parity with macrocells. Additionally, it should provide sufficient capacity to avoid creating a traffic bottleneck. While existing macrocell networks provide latency guarantees within 15 ms, current backhaul networks are not equipped to provide delay resiliency. Lack of net neutrality poses a serious concern, except in cases where the wireline backhaul provider is the same company or in a tight strategic relationship with the cellular operator.

Another issue arises when femtocell usage occurs when the backhaul is already being used to deliver Wi-Fi traffic. Trials by Telefonica reveal that when users employed Wi-Fi, femtocells experienced difficulty transferring data and even low-bandwidth services like voice [118]. This is especially important considering that improved voice coverage is expected to be a main driver for femtocells. In this respect, other infrastructures such as DAs and relays – typically being operator deployed – can ensure satisfactory backhaul performance because the operator may optimize the backhaul for providing reliable QoS to serviced users.

2.2.3 Access and Handoffs to Femtocells

A closed access femtocell – also called managed access – has a fixed set of subscribed home users-for privacy and security-that are licensed to use the femtocell. Tackling radio interference is complicated due to the limited coordination between the macrocell BS and femtocell APs for reasons of scalability, security and limited backhaul [29]. Managing cross-tier radio interference from cellular users to femtocell users and vice-versa (see preceding subsection) in closed-access femtocell deployments

is potentially the biggest challenge confronting cellular operators.

Open access femtocells, on the other hand, provide service to macrocell users, if they pass nearby. Radio interference is managed by allowing strong macrocell interferers to communicate with nearby femtocells. Although open access reduces the macrocell load, the higher numbers of users communicating with each femtocell will strain the backhaul to provide sufficient capacity and raise privacy concerns for home users. Open access will need to avoid "starving" the paying home user-so they shouldn't ever see "all circuits busy." Since femtocells are typically marketed as offering flat-rate calling, open access will need to differentiate between the zero-tariff home users from the pay-per-minute visitor. For both reasons, operators are looking at hybrid models where some of the femtocell's resources are reserved for registered family members, while others are open for roamers. Alternatively, the cellular operator could potentially reward the paying home consumer – either in money or calling minutes – for enabling open access especially in cellular coverage dead-zones.

In current commercial femtocell offerings, cellular operators are typically offering both open access and closed access operation which are configurable by users. For example, Verizon's home expander (femtocell) allows open access by default, but provides the user the capability to choose closed access operation with priority access for up to 50 callers. Sprint's Airave femtocell offers a similar access operation. Because of federal regulations however, all users can potentially access the home expander for Emergency (E911) calls.

In general, handoff from a femtocell to the macrocell network is significantly easier – as there is only one macrocell BS – as compared to handoffs from the macrocell to the femtocell. Current 2nd generation (2G) and 3rd generation (3G) cellular systems broadcast a neighbor list which a mobile attached to the current cell uses to learn where to search for potential handover cells. Such a handoff protocol does not scale to the large numbers of femtocells that "neighbor" (actually underlay) the

macrocell, and the underlying network equipment isn't designed to rapidly change the lists as femtocells come and go. This motivates upcoming 4th generation (4G) standards to implement handover procedures to account for the presence of femtocells.

In open access, channel fluctuations may cause a passing macrocell user to perform multiple handovers. In co-channel deployments, Claussen *et al.* [37] have proposed auto configuration that periodically reduces the pilot power inside a femtocell when no active calls are in progress thereby minimizing handoffs from passing macrocell users. An open research area is to develop low complexity algorithms for predicting the dwell time before handing off a macrocell user onto a nearby femtocell. Yeung and Nanda [156] have proposed controlling handoff events by choosing velocity thresholds based on the user mobility and sojourn times when a macrocell user travels in the vicinity of a femtocell.

2.2.4 Mobility of Femtocell Users and Emergency-911 services

The portability of the femtocell presents a conundrum: Unlike Wi-Fi networks that operate in unlicensed spectrum in which radio interference is not actively managed, femtocell networks will operate in licensed spectrum. Femtocell mobility can cause problems when a subscriber with operator A carries their femtocell to another location where the only service provider is a rival operator B. In such a scenario, should the femtocell be allowed to transmit on operator B's spectrum? Viable options are providing Global Positioning System (GPS) inside femtocells for location tracking and locking the femtocell within a geographical area. Alternatively, inter-operator agreements facilitate charging the home subscriber on roaming.

Government mandated Emergency-911 services require operators to provision femtocells for transmitting location information during emergency calls. Femtocell location may be obtained by either using GPS inside femtocells (added cost with possibly poor indoor coverage), or querying the service provider for location over the backhaul, or gathering information from the macrocell providing the femtocell

falls within the macrocell radio range, or even inferring the location from the mobile position (estimated by the macro network) at handoff to the femtocell.

Ethical/legal dilemmas can arise on whether a femtocell should service macrocell users with poor outdoor coverage for making emergency calls, if they are located within its radio range. In open access networks, this problem can be solved by handoff. Closed access femtocells should be provisioned to allow communication with unsubscribed users in the event of emergencies.

2.3 Security and QoS over Internet Backhaul

In a femtocell environment the operator will need to provide a secure and scalable interface over the Internet at a reasonable cost. Traditional radio network controllers (RNCs) are equipped to handle tens to hundreds of macrocells. *How will they provide equal parity service to femtocells over the Internet?*

Three network interfaces have been proposed, of which the IP multimedia subsystem (IMS)/Session Initiation Protocol (SIP) and unlicensed mobile access (UMA)-based interfaces appear to be the architectures of choice.

Iu-b over IP. Existing RNCs connect to femtocells through standard Iu-CS (circuit-switched) and Iu-PS (packet-switched) interfaces present in macrocell networks. The advantage is that the capital expenditure is comparatively low insofar as the operator can leverage existing RNCs. The shortcomings are the lack of scalability and that the interface is not yet standardized.

IMS/SIP. The IMS/SIP interface provides a core network residing between the femtocell and the operator. The IMS interface converts subscriber traffic into IP packets and employs voice over IP (VoIP) using SIP, and coexists with the macrocell network. The main advantages are scalability and rapid standardization. Disadvantages include the capital expenditure for upgrade, and the operating expenditure in maintaining two separate core networks for the macrocell and femtocell respectively.

RAN-gateway-based UMA. A radio access network (RAN) gateway exists between the IP and operator networks, aggregating traffic from femtocells. This gateway is connected to the operator network using a standard Iu-PS/CS interface. Between the femtocell and the RAN gateway, the UMA protocol makes use of secure IP tunneling for transporting the femtocell signals over the Internet. Current UMA-enabled services such as T-Mobiles Hotspot@Home require dual-mode handsets for switching between in-home Wi-Fi and outdoor cellular access. Integrating the UMA client inside femtocells rather than the mobile would enable future deployments support use of legacy handsets.

This chapter has shown that there are numerous challenges that will require to be addressed by the service provider, in order for femtocells to provide tangible benefits. From a technical standpoint, the main focus of this thesis is on proposing interference management schemes for alleviating cross-tier interference in two-tier networks. In the following chapters, we present each thesis contribution in detail. In Chapter 3, we consider a two-tier network employing CDMA transmission at both tiers. An uplink capacity analysis is derived and an interference avoidance strategy is presented in such a network. We show that substantial capacity gains are obtainable through interference avoidance, thereby enabling the robust design of two-tier networks with universal frequency reuse.

Chapter 3

Uplink Capacity and Interference Avoidance

3.1 Introduction

In a two-tier network employing CDMA transmission with universal frequency reuse, cross-tier interference causes unacceptable outage probability. This chapter presents an uplink capacity analysis and an interference avoidance strategy in a two-tier CDMA network. We present a network-wide area spectral efficiency metric called the *Operating Contour* (OC) defined as the Pareto-optimal pairs of the average number of active cellular users and femtocell access points in each cell-site which ensures that all users attain a certain minimum Signal-to-Interference Ratio (SIR) subject to a maximum outage probability (call drop probability) constraint. The capacity analysis accurately models the uplink outage probability, accounting for power control, path loss and lognormal shadowing. The research also demonstrates substantial benefits obtained using an interference avoidance strategy thereby enabling the robust design of two-tier networks with universal frequency reuse.

3.2 Motivation

Conventional CDMA networks (without femtocells) employ fast power control to compensate for path loss, shadowing and fading, and to provide uniform coverage. When femtocells are added, the very same power control can create dead-zones leading to non-uniform coverage for both macrocell and femtocell users. On the reverse link, a cell edge cellular user transmitting at maximum power causes unacceptable interference to nearby femtocells. Consequently, cell edge femtocells experience significantly

higher interference compared to interior femtocells [28]. Consequently, an operator faces two choices: either allocate different frequency bands to macrocell and femtocell users to reduce cross-tier interference, or alternatively, serving both macrocell and femtocell users in the same region of bandwidth, to maximize area spectral efficiency. Considering the scarce availability of radio resources and ease of deployment, using the same region of bandwidth is preferable, if at all possible. The system capacity in such a macrocell-femtocell deployment with shared spectrum is determined by the maximum number of simultaneous macrocell and femtocell transmissions, subject to an outage probability constraint per BS. The focus of the research is to answer the following questions:

- What is the two-tier uplink capacity in a typical macrocell with randomly scattered hotspots, assuming a randomly distributed population of actively transmitting users per femtocell?
- Is it possible to accurately characterize the statistics of the cross-tier interference? What is the effect of the femtocell hotspot density, macrocell-femtocell power ratio and femtocell size?
- How much benefit is accrued by interference avoidance using antenna sectoring and time hopping in CDMA transmission?

By addressing these questions, this work augments existing research on capacity analysis and interference mitigation in two-tier networks. We show that creating a suitable infrastructure for curbing cross-tier interference can actually increase the uplink capacity for a shared spectrum network.

3.2.1 Related Work

From a physical layer viewpoint, prior research has mainly focused on analyzing the uplink capacity, assuming either a single microcell[1] or multiple regularly spaced microcells in a macrocell site[4, 51, 93]. This model has assumed significance for its analytical tractability, nonetheless, it has limited applicability owing to the inherent variability in microcell locations in realistic scenarios.

The ideas presented in this work are most closely related to the work by Kishore *et al.* The downlink cellular capacity of a two-tier network was derived in [92]. Considering a single macrocell with an embedded microcell, their results showed that the per-tier user capacity is uplink-limited when fast power control is employed. In [95], the user capacities in a two-tier network were derived for different tier-selection schemes. Further work by the same author [94, 96] extended the framework to multiple microcells embedded inside multiple macrocells. The cross-tier interference was approximated by its average and cross-tier microcell to microcell interference is ignored. Their resulting analysis was accurate only up to 8 microcells per macrocell. Our results, on the other hand, are accurate over a wide range of femtocell densities, without approximating the interference statistics.

Related work includes [90], which discusses the benefits of having a tilted antenna radiation pattern and macrocell-microcell power ratio control. In [89, 149], a regular network comprising a large hexagonal macrocell and smaller hexagonal microcells is considered. Citing near far effects, the authors conclude that it is more practical to operate both tiers in separate spectrum. The reason being that the loss in trunking efficiency by splitting the spectrum is lower than the increase in outage probability in a shared spectrum two-tier network. This work, in contrast, shows a higher user capacity for a shared spectrum network by enforcing *higher spatial reuse*

[1] A microcell has a much larger radio range (100-500 m) than a femtocell.

through small femtocells and *interference avoidance* by way of antenna sectoring and Time Hopped CDMA (TH-CDMA) in each tier.

Finally, from a network perspective, Joseph *et al.* [87] study impact of user behavior, load balancing and different pricing schemes for interoperability between Wi-Fi hotspots and cellular networks. In [51], the design of a multitiered wireless network with Poisson call arrivals is formulated as an constrained optimization problem, and the results highlight the economic benefits of a two-tier network infrastructure: increased stability in system cost and a more gradual performance degradation as users are added.

3.2.2 Contributions

This work employs a stochastic geometry framework for modeling the *random* spatial distribution of users/femtocells, in contrast to prior work [77, 89, 94–96, 149]. Hotspot locations are likely to vary from one cellsite to another, and be opportunistic rather than planned: Therefore a capacity analysis that embraces instead of neglecting randomness will naturally provide more accurate results and more plausible insights. To model the user/hotspot locations therefore, cellular users and femtocell BS are assumed to be randomly distributed as a Homogeneous Spatial Poisson Point Process (SPPP) (see [65, 91, 142] for background and survey, prior works include [14, 26, 48, 160]). The three key contributions of this work are given below.

- First, a novel outage probability analysis is presented, accounting for cellular geometry, cross-tier interference and shadowing effects. We derive tight lower bounds on statistics of macrocell interference at any femtocell hotspot BS along the hexagonal axis. Next, assuming small femtocell sizes, a Poisson-Gaussian model for macrocell interference and alpha-stable distribution for cross-tier femtocell interference is shown to accurately capture the statistics at the macrocell BS. In the analysis, outage events are explicitly modeled rather than considering average interference as in [77, 149]. For doing so, the properties of Poisson shot-noise processes [78, 107] and Poisson void

probabilities [91] are used for deriving the uplink outage probabilities.

• Second, robust interference avoidance is shown to enable two-tier networks with universal frequency reuse to achieve higher user capacity. With interference avoidance, an equitable distribution of users between tier 1 and tier 2 networks is shown to be achieved with an order-wise difference in the ratio of their received powers. Even considering the worst case cross-tier interference at a corner femtocell, results for moderately loaded cellular networks reveal that interference avoidance provides a 7x increase in the mean number of femtocells over split spectrum two-tier networks.

• Third, additional interference avoidance using a combination of femtocell exclusion and tier selection based femtocell handoff offers modest improvements in the network OCs. This suggests that at least for small femtocell sizes, time hopping and antenna sectoring offer the largest gains in user capacity for shared spectrum two-tier networks.

3.3 System Model

Denote $\mathcal{H} \subset \mathbb{R}^2$ as the interior of a reference hexagonal macrocell C of radius R_c. The tier 1 network consists of low density cellular users that are communicating with the central BS in each cellsite. Cellular users are distributed on $\mathbb{R}^2$ according to a homogeneous SPPP Ω_c of intensity λ_c. The underlying femtocells forms a homogeneous SPPP[2] Ω_f with intensity λ_f. Each femtocell hotspot includes a Poisson distributed population of actively transmitting users[3] with mean U_f in a circular coverage area of radius $R_f, R_f \ll R_c$. To maximize user capacity per cellsite, it is desirable to have $\lambda_f \gg \lambda_c$; as will be shown, cross-tier interference at a macrocell BS

[2]The system model allows a cellular user to be present inside a femtocell as the governing process Ω_c is homogeneous.

[3]A hard handoff is assumed to allocate only licensed subscribed hotspot users to a femtocell, provided they fall within its radio range.

limits λ_f for a given λ_c. Defining $|\mathcal{H}| \triangleq 2.6R_c^2$ as the area of the hexagonal region $\mathcal{H}$, the mean number of cellular users and femtocell BS's per cellsite are given as $N_c = \lambda_c \cdot |\mathcal{H}|$ and $N_f = \lambda_f \cdot |\mathcal{H}|$ respectively. Table 3.1 shows a summary of important parameters and typical values for them, which are used later in numerical simulations.

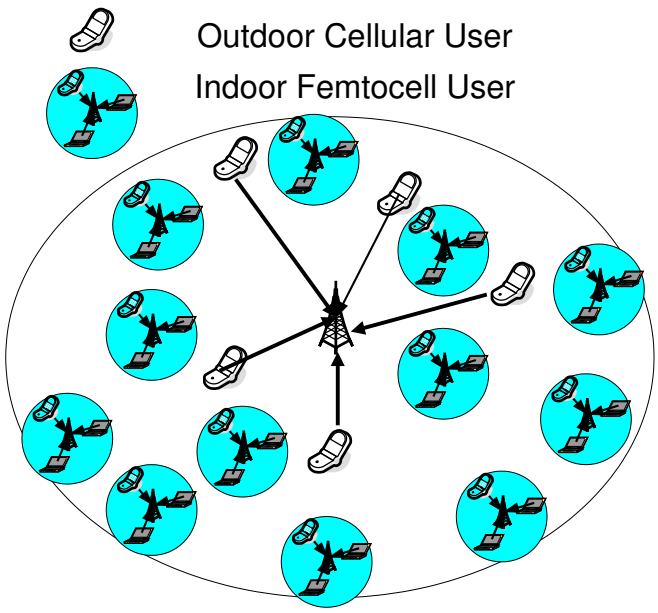

Figure 3.1: A two-tier femtocell network.

Users in each tier employ Direct Sequence-CDMA transmission with processing gain G. Uplink power control adjusts for propagation losses and log-normal shadowing, which is standard in contemporary CDMA networks. The macrocell and femtocell receive powers are denoted as P_r^c and P_r^f respectively. Any power control errors [80] and short-term fading effects are ignored for analytical convenience. We affirm this assumption as reasonable, especially in a wide-band system with significant frequency diversity and robust reception (through RAKE receiver, coding and interleaving).

3.3.1 TH-CDMA and Antenna Sectoring

Suppose that the CDMA period $T = G \cdot T_c$ is divided into N_{hop} hopping slots, each of duration T/N_{hop}. Every cellular user and all users within an active femtocell independently, randomly select a hopping slot for transmission, and remain silent over the remaining $N_{\text{hop}} - 1$ slots. Because the process of selecting the hopping slots are independent across users, the resulting intra- and cross-tier interference at the macrocell BS and femtocell APs are "thinned" by a factor of N_{hop} [91]. Using TH-CDMA, users in each tier effectively sacrifice a factor N_{hop} of their processing gain, but benefit by thinning the interfering field by the same factor. We further assume

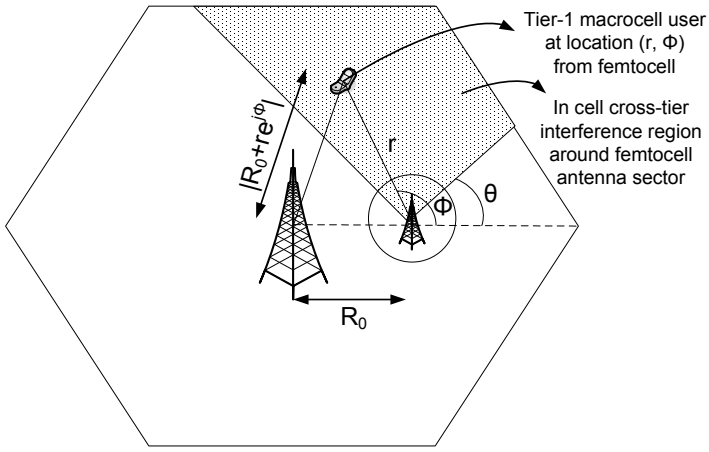

Figure 3.2: Interference experienced at sectorized femtocell antenna aligned at θ.

sectorized antenna reception in both the macrocell and femtocell BS, with antenna alignment angle θ and sector width equaling $2\pi/N_{\text{sec}}$ (Fig. 3.2). While antenna sectoring is a common feature at the macrocell BS in practical cellular systems, this work proposes to use sectorized antennas at femtocell BS's as well. The reason is that the cross-tier interference caused by nearby cellular users can lead to unacceptable outage performance over the femtocell uplink; this motivates the need for directed femtocell antennas.

The following definitions will be useful in the remainder of the paper.

Definition 1. *Denote $\mathcal{H}_{sec} \subseteq \mathcal{H}$ (region within the reference cellsite) over which the femtocell BS antenna sector experiences interference. For example, $\mathcal{H}_{sec} = \mathcal{H}$ for an omnidirectional femtocell located at the corner of the reference macrocell.*

Definition 2. *Denote $\hat{\Omega}_c$ and $\hat{\Omega}_f$ as the heterogeneous SPPPs composed of active macrocell and femtocell interferers as seen at an antenna sector in each tier. Denote the equivalent mapped homogeneous SPPPs over $\mathbb{R}^2$ by Φ_c and Φ_f whose intensities are given by η_c and η_f respectively.*

The spatial thinning effect of TH-CDMA transmission and antenna sectoring is analytically derived in the following lemma.

Lemma 1 (Spatial thinning by interference avoidance)**.** *With TH-CDMA transmission over N_{hop} slots and antenna sectoring with N_{sec} directed BS antennas in each tier, the interfering field at a given antenna sector can be mapped to the SPPPs Φ_c and Φ_f on $\mathbb{R}^2$ with intensities $\eta_c = \lambda_c/(N_{hop}N_{sec})$ and $\eta_f = \lambda_f(1 - e^{-U_f})/(N_{hop}N_{sec})$ respectively.*

Proof. See Appendix A.1. □

Definition 3. *Denote the restriction of $\hat{\Omega}_c$ and $\hat{\Omega}_f$ to $\mathcal{H}$ by the SPPPs Π_c and Π_f respectively.*

3.3.2 Channel Model and Interference

The channel is represented as a combination of path loss and log-normal shadowing. The path loss exponents are denoted by α (outdoor transmission) and β (indoor femtocell transmission) with random lognormal shadowing standard deviation σ_{dB}. Through uplink power control, a cellular user transmitting at a random position X w.r.t the reference macrocell BS C chooses a transmit power level

$P_t^c = P_r^c/g_c(|X|)$. Here $g_c(|X|)$ is the attenuation function for outdoor propagation, defined as $g_c(|X|) = K_c(d_{0c}/|X|)^\alpha \Theta_C$ where $10\log_{10}\Theta_C \sim \mathcal{N}(0, \sigma_{dB}^2)$ is the log-normal shadowing from user to C, $K_c \triangleq [c/(4\pi f_c d_{0c})]^2$ is a unitless constant that depends on the wavelength of the RF carrier c/f_c and outdoor reference distance d_{0c}. Similarly,

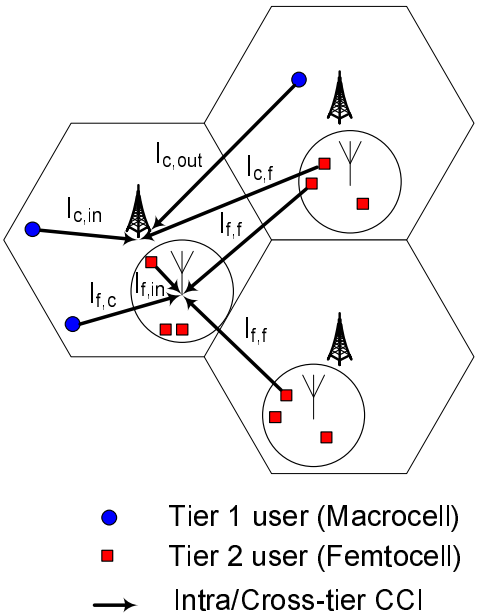

Figure 3.3: Intra-tier and cross-tier interference with universal frequency reuse.

a femtocell user at a random position Y within a femtocell BS F chooses a transmit power $P_t^f = P_r^f/g_f(|Y|)$, where $g_f(|Y|) = K_f(d_{0f}/|Y|)^\beta \Theta_F$ represents the indoor attenuation, $10\log_{10}\Theta_F \sim \mathcal{N}(0, \sigma_{dB}^2)$ and $K_f \triangleq [c/(4\pi f_c d_{0f})]^2$. Here d_{0f} is the reference distance for calculating the indoor propagation loss. Note that in reality, K_c and K_f are empirically determined. The interference in each tier (Fig. 3.3) can be grouped as:

Macrocell interference at a macrocell. Through power control, all cellular users within $\mathcal{H}_{\text{sec}}$ are received with constant power P_r^c, so the in-cell interference equals $(N-1)P_r^c$, where $N \sim \text{Poisson}(N_c/N_{\text{hop}})$. As such, inferring the exact statis-

tics of out-of-cell cellular interference $I_{c,\text{out}}$ is analytically intractable; it is assumed that $I_{c,\text{out}}$ is distributed according to a scaled Gaussian pdf [26]. Defining μ and σ^2 to be the empirically determined parameters of the Gaussian, the pdf of $I_{c,\text{out}}$ is given as $f_{I_{c,\text{out}}}(y) = \frac{2e^{-\frac{1}{2}(y-\mu)^2/\sigma^2}}{\sqrt{2\pi\sigma^2}[2-\text{erfc}(\frac{\mu}{\sqrt{2}\sigma})]}$, where $\text{erfc}(t) \triangleq \sqrt{\frac{2}{\pi}} \int_{t\sqrt{2}}^{\infty} e^{-x^2/2} dx$.

Femtocell interference at a macrocell. Say femtocell F_i with $U_i \sim \text{Poisson}(U_f)$ users is located at random position X_i w.r.t the reference macrocell BS C. A femtocell user j at distance Y_j from their femtocell BS F_i transmits with power $P_t^f(j) = P_r^f / g_f(Y_j)$. The interference caused at C from user j is given as

$$I_{c,f}(F_i, j) = P_r^f g_c(|X_i + Y_j|)/g_f(|Y_j|) \approx P_r^f g_c(|X_i|)/g_f(R_f) = Q_f \Theta_{j,C}/\Theta_{j,F_i}|X_i|^{-\alpha} \tag{3.1}$$

where $Q_f \triangleq P_r^f R_f^{\beta}(\frac{K_c}{K_f})(\frac{d_{0c}^{\alpha}}{d_{0f}^{\beta}})$. In doing so, we make two important assumptions namely

AS 1. *For small sized femtocells ($R_f \ll R_c$), a femtocell or macrocell BS sees interference from other femtocells as a point source, implying $g_c(|X_i + Y_j|) \approx g_c(|X_i|)$.*

AS 2. *When analyzing the interference caused by a random femtocell F_i at any other location, the U_i femtocell users can be modeled as transmitting with maximum power, so that $g_f(|Y_j|) \approx g_f(R_f)$. This is for analytical tractability and modeling worst-case interference.*

Using (3.1), the cumulative cross-tier interference at the reference macrocell C is represented by the Poisson Shot-Noise Process (SNP) [107],

$$I_{c,f} = \sum_{F_i \in \hat{\Omega}_f} Q_f \Psi_i |X_i|^{-\alpha} \tag{3.2}$$

where $\Psi_i \triangleq \sum_{l=1}^{U_i} \Theta_{l,C}/\Theta_{l,F_i}$ defines the cumulative shadowing gain between actively transmitting users in femtocell F_i and the macrocell BS C.

Neighboring femtocell interference at a femtocell. By an identical argument as above, the interference caused at the antenna sector of femtocell F_j from other femtocells $F_i, i \neq j$ is a Poisson SNP given by $I_{f,f} = \sum_{F_i \in \hat{\Omega}_f} Q_f \Psi_i |X_i|^{-\alpha}$, where $|X_i|$ refers to the distance between (F_i, F_j) and $\Psi_i \triangleq \sum_{l=1}^{U} \Theta_{l,F_j}/\Theta_{l,F_i}$.

Interference from active users within a femtocell. Conditioned on the femtocell containing U actively transmitting users ($U \geq 1$), the intra-tier interference experienced by the user of interest arising from simultaneous transmissions within the femtocell is given as $I_{f,\text{in}} = (U-1)P_r^f, \mathbb{E}[U] = \frac{U_f}{1-e^{-U_f}}$.

Macrocell interference at a femtocell. This work analyzes outage probability at a femtocell BS F_j located on the hexagonal axis, considering the effect of in-cell cellular interference. The cellular interference $I_{f,c}$ is lower bounded by the interference caused by the set of cellular interferers inside the reference macrocell Π_c. This lower bound is represented as $I_{f,c} \geq I_{f,c}^{lb} = \sum_{i \in \Pi_c} P_r^c \Psi_i (\frac{|X_i|}{|Y_i|})^\alpha$, where $\Psi_i \triangleq \Theta_{i,F_j}/\Theta_{i,C}, 10\log_{10}\Psi_i \sim \mathcal{N}(0, 2\sigma_{dB}^2)$ is the LN shadowing term and $|X_i|, |Y_i|$ represent the distances of cellular user i to the macrocell BS and femtocell BS respectively. Because a corner femtocell experiences a significantly higher cellular interference relative to an interior femtocell, the statistics of $I_{f,c}$ are non-stationary.

3.4 Per Tier Outage Probability

To derive the OCs, an uplink outage probability constraint is formulated in each tier. Define N_f and N_c as the average number of femtocell BS's and cellular users per cellsite respectively.

A user experiences outage if their instantaneous received Signal-to-Interference Ratio (SIR) over a transmission (Fig. 3.4) is below a threshold Γ. The outage probabilities $\mathbb{P}_{\text{out}}^c(N_f, N_c)$ [resp. $\mathbb{P}_{\text{out}}^f(N_f, N_c)$] are defined as the probabilities that the despread narrowband SIR for a cellular user [femtocell user] at the tier 1 [tier 2] antenna sector is below Γ. Assuming the PN code cross-correlation equals N_{hop}/G[4],

[4]With $N_{\text{hop}} = G = 1$, the model reduces to a non CDMA narrowband transmission; with $N_{\text{hop}} = G \gg 1$, the model reduces to slotted ALOHA transmission

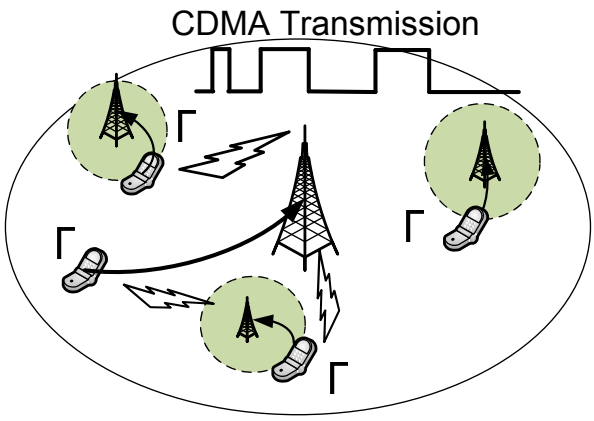

Figure 3.4: CDMA transmission with per-tier SIR target Γ.

define

$$\mathbb{P}^c_{\text{out}}(N_f, N_c) = \mathbb{P}\left[\frac{G/N_{\text{hop}}P^c_r}{I_{c,\text{in}} + I_{c,\text{out}} + I_{c,f}} \leq \Gamma \middle| |\hat{\Omega}_c| \geq 1\right]$$
$$\mathbb{P}^f_{\text{out}}(N_f, N_c) = \mathbb{P}\left[\frac{G/N_{\text{hop}}P^f_r}{(U-1)\cdot P^f_r + I_{f,f} + I_{f,c}} \leq \Gamma \middle| U \geq 1\right] \tag{3.3}$$

where $|\hat{\Omega}_c|$ denotes the number of points in $\hat{\Omega}_c$ and the unconditioned $U \sim \text{Poisson}(U_f/N_{\text{sec}})$. Any feasible $(\tilde{N}_f, \tilde{N}_c)$ satisfies the outage probability requirements $\mathbb{P}^f_{\text{out}}(N_f, N_c) \leq \epsilon, \mathbb{P}^c_{\text{out}}(N_f, N_c) \leq \epsilon$ in each tier.

Definition 4. *Define the tuple* $\mathbf{N} \triangleq (N_f, N_c)$ *as being a feasible tuple if* $\mathbb{P}^c_{out}(N_f, N_c) \leq \epsilon$ *and* $\mathbb{P}^f_{out}(N_f, N_c) \leq \epsilon$.

Definition 5. *Given two feasible tuples* $\mathbf{N}$ *and* $\mathbf{N}'$*, define* $\mathbf{N} \succ \mathbf{N}'$ *when ever either a)* $N_f > N'_f$ *and* $N_c \geq N'_c$*, or alternatively b)* $N_f \geq N'_f$ *and* $N_c > N'_c$ *is satisfied.*

The OCs for the macrocell [resp. femtocell] are obtained by computing the Pareto optimal set of tuples $\mathbf{N}$ pairs which satisfy a target outage constraint ϵ. More

formally,

$$\mathrm{OC} \triangleq \{\mathbf{N} : \nexists \tilde{\mathbf{N}} \succ \mathbf{N} \text{ such that } \tilde{\mathbf{N}} \text{ is feasible}\}. \tag{3.4}$$

Theorem 1. *With a path loss exponent $\alpha = 4$, the interference terms $I_{c,f}$ and $I_{f,f}$ are identically distributed as a Poisson SNP $Y = \sum_{i \in \Phi_f} Q_f \Psi_i |X_i|^{-\alpha}$ with identical and independently distributed marks Ψ_i and probability density function (pdf) and cumulative distribution function (cdf) given as*

$$f_Y(y) = \sqrt{\frac{\kappa_f}{\pi}} y^{-3/2} e^{-\kappa_f / y}, F_Y(y) = \mathrm{erfc}\left(\sqrt{\frac{\kappa_f}{y}}\right) \tag{3.5}$$

where $\kappa_f \triangleq \eta_f^2 \pi^3 Q_f (\mathbb{E}[\Psi^{1/2}])^2 / 4$.

Proof. See Appendix A.2. □

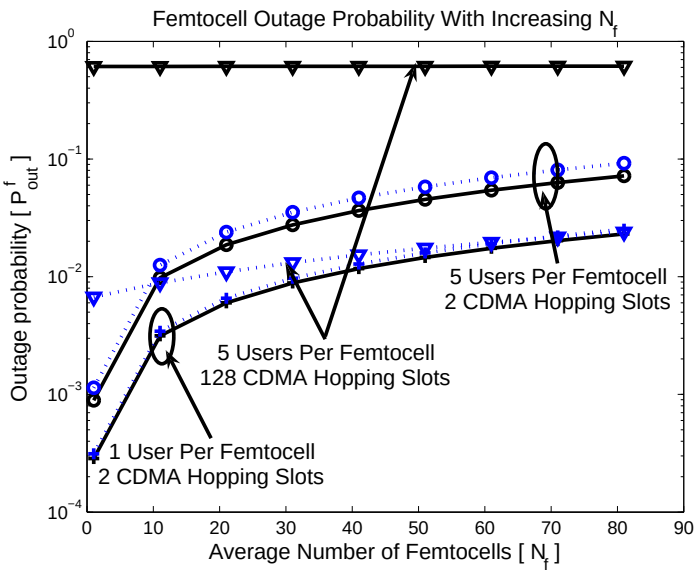

Figure 3.5: Femtocell outage probabilities with joint and independent hopping protocols. Solid lines represent joint hopping when all users within a femtocell are assigned a common set of CDMA hopping slots. Dotted lines assume each femtocell user is individually randomly assigned a set of CDMA hopping slots.

Remark 1 (Femtocell size)**.** *Increasing femtocell size (R_f)* strictly increases *the outage probabilities arising from the femtocell interference $I_{f,f}$ and $I_{c,f}$ in a two-tier network. To elucidate this, observe that an increase in R_f causes κ_f to increase by a factor R_f^β. By monotonicity of* $\mathrm{erfc}(\cdot)$*, the cdf's $F_{I_{f,f}}(\cdot), F_{I_{c,f}}(\cdot)$ decrease as κ_f increases, causing a higher outage probability per tier. Intuitively, a femtocell user located on the edge of a femtocell will cause excessive interference at a nearby femtocell BS; this edge effect appears as a power control factor R_f^β in* (3.5)*.*

All Tier 2 users within a femtocell are assumed to jointly choose a hopping slot. Suppose we compare this against an independent hopping protocol, where users within a femtocell are independently assigned a hopping slot. With independent hopping, the intensity of Φ_f equals $\tilde{\eta}_f = \frac{\lambda_f}{N_{\text{sec}}} \cdot (1 - e^{-U_f/N_{\text{hop}}})$ (note the difference from η_f in Lemma 1) and the average number of interfering users in an actively transmitting femtocell equals $\frac{U_f/N_{\text{hop}}}{1-e^{-U_f/N_{\text{hop}}}}$. With an outage threshold of $P_r^f G/(\Gamma N_{\text{hop}})$ (3.3) at a femtocell BS, two observations are in order:

TH-CDMA transmission. When $\frac{G}{N_{\text{hop}}} \gg 1$, joint hopping is preferable from an outage probability perspective. Intuitively, joint hopping reduces λ_f by a factor N_{hop}, causing a quadratic decrease in κ_f in (3.5); independent hopping decreases the number of interfering users per active femtocell, causing a sub-quadratic decrease in $\mathbb{E}[\Psi^{1/2}]^2$. The consequence is that joint hopping results in a greater decrease in $\mathbb{P}_{\text{out}}^f$. Using $N_{\text{hop}} = 2$, Fig. 3.5 confirms this intuition; notably, the gap in outage performance is dictated by the hotspot user density: In heavily loaded femtocells ($U_f \gg 1$), a joint hopping scheme is clearly superior. For lightly loaded femtocells, $\eta_f \simeq \tilde{\eta}_f \approx \frac{\lambda_f U_f}{N_{\text{sec}} \cdot N_{\text{hop}}}$, implying that independent and joint hopping schemes perform nearly identical.

Random access transmission. When $N_{\text{hop}} = G \gg 1$, the femtocell outage threshold is P_r^f/Γ; by consequence, it is preferable to use independent hopping across the tier 2 network (see Fig. 3.5). With joint hopping, even a *single interferer* within

a femtocell can cause outage for the user of interest as there is no CDMA interference averaging ; an independent hopping scheme offers increased interference avoidance since the likelihood of two femtocell users sharing a hopping slot is negligible. Consequently, in non-CDMA two-tier cellular networks employing interference avoidance, an independent assignment of hopping slots is preferable from an outage viewpoint.

Theorem 2 (Macrocell outage probability)**.** *Let the outdoor path loss exponent $\alpha = 4$. With Poisson in-cell macrocell interference $I_{c,in}$, Gaussian out-of-cell interference $I_{c,out}$ and Lévy-stable femtocell interference $I_{c,f}$ given by* (3.5)*, the outage probability at the macrocell BS antenna sector is given as*

$$\epsilon \geq \mathbb{P}^c_{out} = 1 - \frac{1}{1 - e^{-\eta_c|\mathcal{H}|}} \sum_{m=1}^{\lfloor \rho_c / P_r^c \rfloor} \frac{e^{-\eta_c|\mathcal{H}|}(\eta_c|\mathcal{H}|)^m}{m!} G_c(\tilde{\rho}_c) \tag{3.6}$$

where $\eta_c = \frac{\lambda_c}{N_{hop}N_{sec}}, \rho_c = \frac{P_r^c G}{\Gamma N_{hop}}, \tilde{\rho}_c = \rho_c - (m-1)P_r^c$ *and* $G_c(t) \triangleq \int_0^t f_{I_{c,out}}(t - y) F_{I_{c,f}}(y) dy$.

Proof. See Appendix A.3. □

Theorems 1 and 2 provide the tools to quantify the largest N_f that can be accommodated at a given N_c subject to an outage constraint ϵ. The next step is to compute the outage probability at a femtocell as defined in (3.3). To do so, assume that the femtocell is located on the axis at a distance R_0 from the macrocell center and the femtocell antenna sector is aligned at angle θ w.r.t the hexagonal axis. The following theorem derives a lower bound on the tail probability distribution of the cross-tier interference $I_{f,c}$ at any femtocell located along the hexagonal axis.

Theorem 3 (Lower bound on cellular interference)**.** *At any femtocell antenna sector located at distance $0 < R_0 \leq R_c$ from the macrocell BS along the hexagonal axis:*

1. *The complementary cumulative distribution function (ccdf) of the cross-tier interference $I_{f,c}$ at a femtocell antenna sector is lower bounded as $\bar{F}_{I_{f,c}}(y) \geq 1 - F^{lb}_{I_{f,c}}(y)$,*

where

$$F^{lb}_{I_{f,c}}(y) = \exp\left\{-\frac{\lambda_c}{N_{hop}}\iint\limits_{\mathcal{H}_{sec}} S(r,\phi;y) r\,dr\,d\phi\right\}, S(r,\phi;y) \triangleq \bar{F}_\Psi\left[\frac{yr}{P^c_r(|re^{\mathbf{i}\phi}+R_0|)^\alpha}\right] \tag{3.7}$$

Here $\bar{F}_\Psi$ *is the ccdf of* $\Psi : 10\log_{10}\Psi \sim \mathcal{N}(0, 2\sigma^2_{dB})$, $\mathbf{i} \triangleq \sqrt{-1}$, θ *is the femtocell BS antenna alignment angle and* $\mathcal{H}_{sec} \subseteq \mathcal{H}$ *denotes the region inside the reference macrocell enclosed between* $\theta \leq \phi \leq \theta + 2\pi/N_{sec}$.

2. *For a corner femtocell* $R_0 = R_c$ *with an omnidirectional femtocell antenna* $N_{sec} = 1$, *the ccdf of* $I_{f,c}$ *is lower bounded as* $\bar{F}_{I_{f,c}}(y) \geq 1 - F^{lb}_{I_{f,c}}(y)$, *where*

$$F^{lb}_{I_{f,c}}(y) = \exp\left\{-3\frac{\lambda_c}{N_{hop}}\iint\limits_{\mathcal{H}} S(r,\phi;y) r\,dr\,d\phi\right\}. \tag{3.8}$$

Proof. See Appendix A.4. □

Corollary 1. *With the above definitions, assuming a pure path loss model (no shadowing),* (A.5) *and* (3.8) *hold with* $S(r,\phi;y) \triangleq \mathbf{1}\left[P^c_r \cdot (|re^{\mathbf{i}\phi}+R_0|/r)^\alpha \geq y\right]$.

Theorem 3 characterizes the relationship between the intensity of cellular users and the femtocell outage probability. Increasing N_{hop} "thins" the intensity of Π_c, thereby mitigating cross-tier interference at the femtocell BS.

The thesis of this work revolves around a two-tier CDMA network with interference avoidance. Below, we elucidate why successful application of sectorization is required in a CDMA two-tier network.

Infeasibility of omnidirectional femtocells. Irrespective of the orientation of the sector inside a femtocell, the femtocell outage probability is no worse than a sectorized femtocell located on the cell edge. Results (see Fig. 3.7) show that an omnidirectional femtocell located in the cell interior has a higher outage probability than a sectorized femtocell on the cell edge. The implication is that *CDMA two-tier*

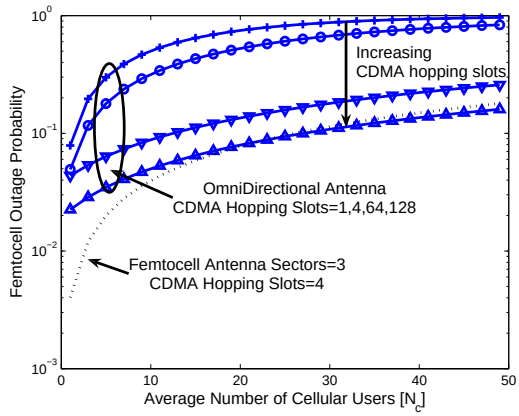

Figure 3.6: Interior femtocell outage probability.

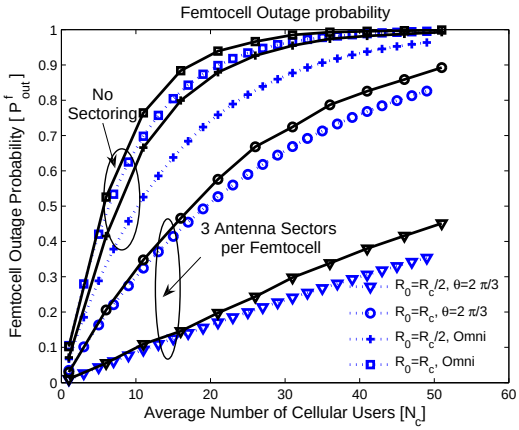

Figure 3.7: Theoretical (dotted) and empirical (solid) $\mathbb{P}^{f}_{\text{out}}$ for an interior and corner femtocell.

networks with universal frequency reuse perform poorly with omnidirectional femtocell antennas. Additionally, irrespective of how a consumer places the antenna sector, using sectorized femtocells benefits the end consumer.

Benefits of Time-hopping. Figure 3.6 compares the performance of increasing the number of CDMA hopping slots while employing an omnidirectional femtocell antenna, versus using a fixed CDMA hopping factor and using three antenna sectors. Results indicate that a femtocell which uses a combination of interference averaging and interference avoidance (3 antenna sectors and 4 CDMA hopping slots) shows a near identical outage probability, in comparison to random TDMA transmission (using 128 CDMA hopping slots). This shows that an alternative non-CDMA scheme (random TDMA) offers the same benefits as a CDMA two-tier network with sectorized femtocell BSs.

As seen in Fig. 3.7, the closeness between the empirical and theoretical outage probabilities in (A.5) and (3.8) shows that the cross-tier interference $I_{f,c}$ is primarily impacted by the set of *dominant cellular interferers* (A.7). Moreover, the magnitude of outage is more severe in femtocells that are located on the edge of the macrocell,

relative to interior femtocells. The implication is that one can perform accurate outage analysis at a femtocell by considering only cellular users whose transmissions are strong enough to individually cause outage. This agrees with the observations in [143, 144].

Using Theorems 1 and 3, the femtocell outage probability (3.3) is stated in the next theorem.

Theorem 4 (Femtocell outage probability)**.** *For small λ_c, the femtocell outage probability $\mathbb{P}^f_{out}$ is lower bounded as*

$$\epsilon \geq \mathbb{P}^{f,lb}_{out} \approx 1 - \frac{e^{-U_{f,sec}}}{1 - e^{-U_{f,sec}}} \sum_{m=1}^{\lfloor \rho_f / P^f_r \rfloor} \frac{U^m_{f,sec}}{m!} \cdot G_f(\tilde{\rho}_f) \tag{3.9}$$

where $U_{f,sec} \triangleq \frac{U_f}{N_{sec}}, \rho_f \triangleq \frac{GP^f_r}{N_{hop} \cdot \Gamma}$, $\tilde{\rho}_f = \rho_f - (m-1) \cdot P^f_r$ and $G_f(t) \triangleq F_{I_{f,f}}(t) + \int_0^t f_{I_{f,f}}(t-y) \ln\left(F^{lb}_{I_{f,c}}(y)\right)\, dy$.

Proof. See Appendix A.5. □

For a given N_f, Theorem 4 computes the largest N_c which ensures the SIR threshold Γ is satisfies for a fraction $(1-\epsilon)$ of the time. Furthermore, the lower bound $F^{lb}_{I_{f,c}}(\cdot)$ was shown to be tight, hence the computed N_c is not overly optimistic. Using Theorems 2 and 4, the OCs for the two-tier network with interference avoidance can now be readily obtained. The following section studies using a femtocell exclusion region around the macrocell BS and a tier selection based femtocell handoff policy, in addition to the interference avoidance strategies discussed hitherto.

3.5 Femtocell Exclusion Region and Tier Selection

Suppose the reference macrocell BS has a femtocell exclusion region $\mathcal{R}^{exc}_f \subset \mathcal{H}$ surrounding it. This idea is motivated by the need to silence neighboring femtocell transmissions which are strong enough to individually cause outage at a macrocell BS;

similar schemes have been proposed in [68] and adopted in the CSMA scheduler in the 802.11 standard. The tier 2 femtocell network then forms a heterogeneous SPPP on $\mathcal{H}$ with the average number of femtocells in each cell-site equaling $\lambda_f \cdot (|\mathcal{H}| - |\mathcal{R}_f^{exc}|)$. The following theorem derives a lower bound on the ccdf of the cross-tier femtocell interference $I_{c,f}$ considering the effect of a femtocell exclusion region.

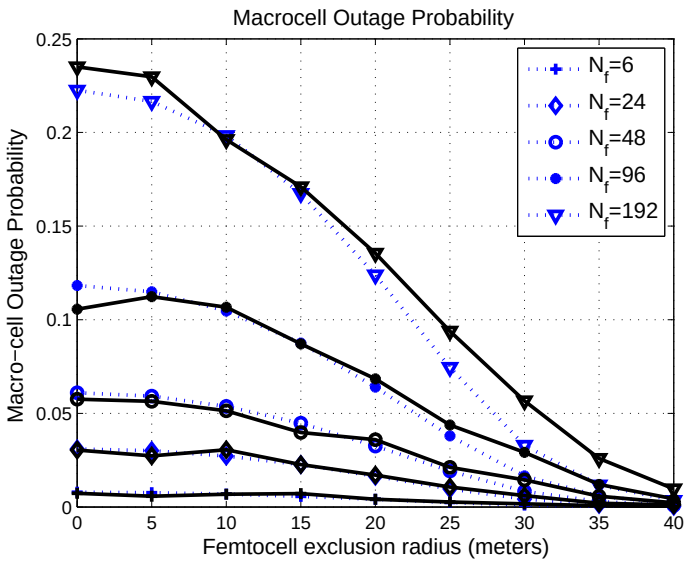

Figure 3.8: Macrocell outage probability for different femtocell densities with a femtocell exclusion region ($N_c = 24$ users, $P_r^f = P_r^c$). Dotted lines represent the theoretical lower bounds on outage probability and solid lines represent the empirically estimated probabilities.

Lemma 2 (Femtocell exclusion region)**.** *With a femtocell exclusion region of radius $R_{f,exc}$ around the reference macrocell BS, the ccdf of cross-tier femtocell interference $I_{c,f}$ is lower bounded as*

$$\bar{F}_{I_{c,f}}(y) \geq 1 - e^{-\pi\eta_f H(y)} \tag{3.10}$$

where $H(y)$ is defined as,

$$H(y) \triangleq \left(\frac{Q_f}{y}\right)^{\delta} (\mathbb{E}[\Psi^{\delta}] - F_{\Psi}(u)\mathbb{E}[\Psi^{\delta}|\Psi \leq u]) - (R_{f,exc})^2 \bar{F}_{\Psi}(u)$$
$$\Psi = \sum_{i=1}^{U} \Psi_i, \text{ where } 10\log_{10}\Psi_i \sim \mathcal{N}(0, 2\sigma_{dB}^2)$$
$$\delta = 2/\alpha, u = \frac{yR_{f,exc}^{2/\delta}}{Q_f}, U \sim X|X \geq 1, X \sim \text{Poisson}(U_f) \tag{3.11}$$

Proof. See Appendix A.6. □

Fig. 3.8 depicts the macrocell outage performance as a function of the femtocell exclusion radius. A small exclusion radius $R_{f,\text{exc}}$ results in a significant decrease in $\mathbb{P}_{\text{out}}^{c}$. The implication is that a femtocell exclusion region can substantially increase the number of simultaneous active femtocell transmissions, while satisfying the macrocell outage constraint $\mathbb{P}_{\text{out}}^{c} \leq \epsilon$. The close agreement between analysis and simulation shows that only the nearby dominant femtocell interferers influence outage events at the macrocell BS.

Corollary 2. *With no femtocell exclusion ($R_{f,exc} = 0$), the complementary cumulative distribution function of the cross-tier femtocell interference $I_{c,f}$ at a macrocell is lower bounded as $\bar{F}_{I_{c,f}}(y) \geq 1 - e^{-\pi\eta_f Q_f^{\delta}\mathbf{E}[\Psi^{\delta}]y^{-\delta}}$.*

Corollary 2 is the two-tier cellular network equivalent of Theorem 3 in Weber *et al.* [143], which derives a lower bound on the outage probability for ad hoc networks with randomized transmission and power control. Finally, this work considers the influence of a femtocell tier selection based handoff policy wherein any tier 1 cellular user within the radius R_f of a femtocell BS undergoes handoff to the femtocell. In essence, the interference caused by the nearest cellular users is mitigated since these users are power controlled to a femtocell BS.

Lemma 3. *With a tier selection policy in which any user within a radius R_f of a femtocell undergoes handoff to the femtocell BS, the intensity of tier 1 users within $\mathcal{H}$ after handoff is given as $\lambda_c^{TS}(r) = \lambda_c e^{-\lambda_f \pi {R_f}^2}$ whenever $r > R_{f,exc}$, where $R_{f,exc}$ is the femtocell exclusion radius.*

Proof. See Appendix A.7. □

Remark 2. *For small λ_f and $r > R_{f,exc}$, a first-order Taylor approximation shows that $\lambda_c^{TS} \approx \lambda_c \cdot (1 - \lambda_f \pi R_f^2)$. The interpretation is that tier-selection offers marginal benefits for small femtocell sizes ($R_f \ll R_c$). Intuitively, a small sized femtocell does not cover "enough space" for significant numbers of cellular users in Ω_c to accomplish femtocell handoff. However, Theorem 1 shows that a small femtocell size does lead to a lower uplink outage probability.*

Remark 3. *The network OCs considering the effects of a femtocell exclusion region and tier selection can be obtained by applying Lemmas 2 and 3 in Theorems 2 and 4 respectively. In doing so, we approximate $I_{f,f}$ as a Poisson SNP whose cdf is described by* (1).

3.6 Numerical Results

System parameters are given in Table 3.1. The setup consists of the region $\mathcal{H}$ surrounded by 18 macrocell sites to consider two rings of interferers and $2\pi/3$ sectorized antennas at each BS. In (3.10), the statistics of the shadowing gain Ψ were empirically estimated using the MATLAB functions `ksdensity` and `ecdf` respectively. The OCs were analytically obtained using Theorems 1-4 for an outage constraint $\epsilon = 0.1$ in (3.4). The following plots compare the OCs for a shared spectrum network with interference avoidance against a split spectrum network with omnidirectional femtocells.

Figs. 3.9-3.10 plot the OC curves for a macrocell and an interior femtocell with $P_r^f/P_r^c = 1, 10, 100$ and $N_{\text{hop}} = 1$. The femtocell uses a sectorized receive

Table 3.1: System Parameters

Symbol	Description	Value
$\mathcal{H}$	Region inside reference cellsite	N/A
Ω_c, Ω_f	SPPPs defining Tier 1, Tier 2 users	N/A
R_c, R_f	Macro/Femtocell Radius	$500, 20$ meters
U_f	Poisson mean users per femtocell	5
N_{sec}	Macrocell/Femtocell antenna sectors	3
N_{hop}	CDMA Hopping slots	$1, 2, 4$
G	Processing Gain	128
Γ	Target SIR per tier	2 [C/I=3 dB]
ϵ	Target Outage Probability	0.1
P_r^c	Macrocell receive power	1
P_r^f	Femtocell receive power	$1, 10, 100$
σ_{dB}	Lognormal shadowing parameter	4 dB
α, β	Path loss exponents	$4, 2$
d_{0c}, d_{0f}	Reference distances	$100, 5$ meters
f_c	Carrier Frequency	2 GHz

antenna with $N_{\text{sec}} = 3, \theta = 2\pi/3$. The close agreement between the theoretical and empirical OC curves indicates the accuracy of the analysis. Observe that the outage constraints oppose one another: Relative to the macrocell, increasing P_r^f/P_r^c decreases the largest sustainable N_f for a given N_c. From the femtocell standpoint, increasing P_r^f/P_r^c increases the largest sustainable N_c sustainable for a given N_f.

Figs. 3.11 through 3.13 plot the performance of the shared spectrum network employing interference avoidance for a corner and an interior femtocell, as a function of N_{hop} and P_r^f/P_r^c. Fig. 3.11 shows that with $P_r^f/P_r^c = 1$ and a lightly loaded tier 1 network, the corner femtocell can achieve greater than 7x improvement in N_f relative to the split spectrum network. Intuitively, with $P_r^f/P_r^c = 1$, a macrocell BS tolerates a large cross-tier interference; the downside being that the femtocell BS experiences higher cross-tier interference arising from cellular users transmitting at maximum power near the cell edge. This explains why N_f decreases rapidly with increasing N_c in the OC curves for a corner femtocell. This also suggests that achieving load balancing by increasing N_c at the expense of N_f requires an order wise difference

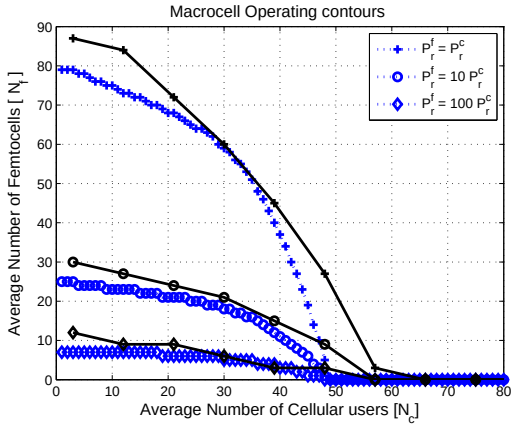

Figure 3.9: Macrocell OCs with $N_{\text{hop}} = 1, N_{\text{sec}} = 3$. Solid lines show the empirical OCs, while dotted lines show the theoretically obtained OC curves.

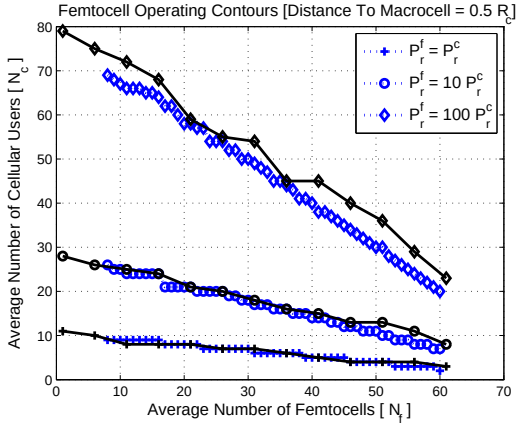

Figure 3.10: Cell Interior Femtocell OCs with $N_{\text{hop}} = 1, N_{\text{sec}} = 3$. Solid lines show the empirical OCs, while dotted lines show the theoretically obtained OC curves.

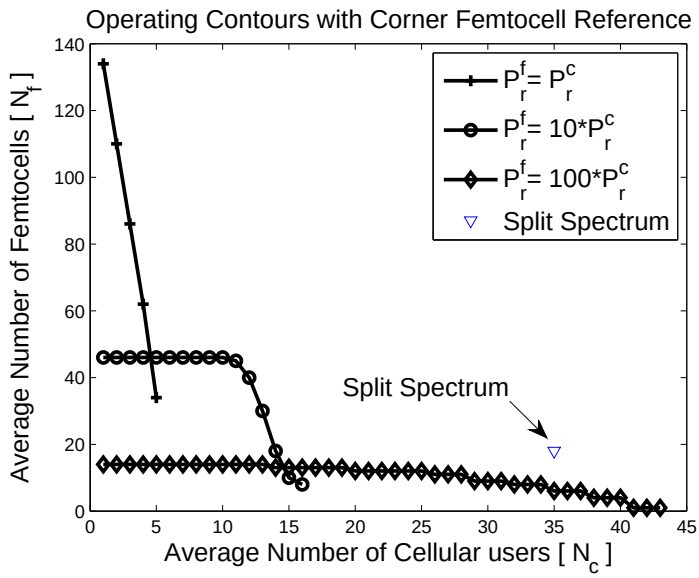

Figure 3.11: Network OCs for different macrocell-femtocell received power ratios ($N_{\text{hop}} = 4, N_{\text{sec}} = 3$) for a cell edge femtocell (distance to macrocell = R_c).

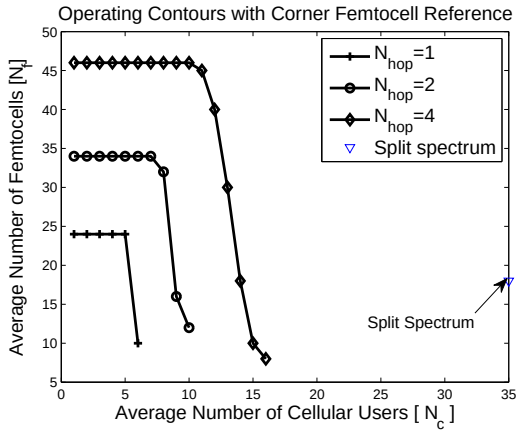

Figure 3.12: Network OCs with different hopping slots ($\frac{P_r^f}{P_r^c} = 10, N_{\text{sec}} = 3$) for a cell edge femtocell (distance to macrocell $= R_c$).

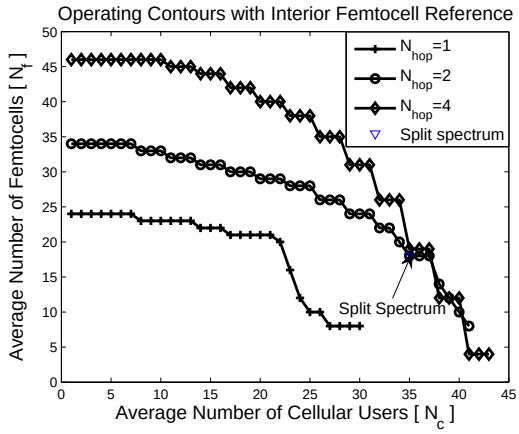

Figure 3.13: Network OCs with different hopping slots ($\frac{P_r^f}{P_r^c} = 10, N_{\text{sec}} = 3$) for a cell interior femtocell (distance to macrocell $= 0.5R_c$).

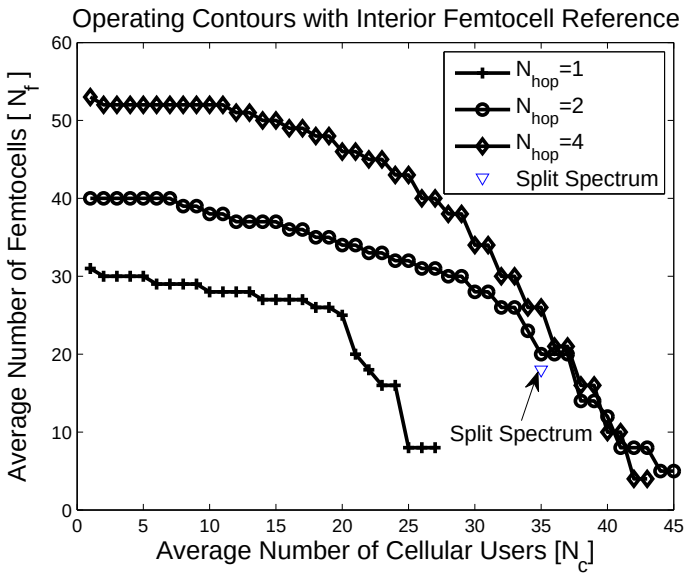

Figure 3.14: Network OCs with tier selection and femtocell exclusion ($\frac{P_r^f}{P_r^c} = 10, N_{\text{sec}} = 3, R_{f,\text{exc}} = 20$) for a cell interior femtocell (distance to macrocell $= 0.5R_c$).

in the femtocell-macrocell receive power ratio. We suggest that a practical wireless system use a larger femtocell-macrocell receive power ratio (P_r^f/P_r^c) at the corner

femtocell, relative to an interior femtocell. Such a position based variable power ratio would ensure that both the interior and corner femtocells can tolerate interference from an almost identical number of tier 1 users.

With $P_r^f/P_r^c = 10$, Fig. 3.13 shows that up to $N_c = 43$ cellular users (a nearly 1.2x improvement in the number of cellular users compared to a split spectrum network) can be accommodated by an interior femtocell. With $P_r^f/P_r^c = 10$ and $N_{\text{hop}} = 4$ slots, Figs. 3.12-3.13 show a nearly 2.5x improvement in N_f compared to the split spectrum network.

Fig. 3.14 shows the OCs with a femtocell exclusion region and a tier selection policy for femtocell handoff. We observe an increase in N_f by up to 10 additional femtocells (or $10 * U_f = 50$ users) for $N_c < 30$ users. Both femtocell exclusion and tier selection do not result in a higher N_c. The reason is that a femtocell exclusion region does not alleviate tier 1 interference at a femtocell. Furthermore, an explanation for the conservative gains in N_f is that there is a maximum tolerable interference to sustain the outage requirements at a given femtocell, that prevents a substantial increase in the number of actively transmitting femtocells. Next, owing to small femtocell sizes, a tier selection policy succeeds in curbing cellular interference mainly for a large N_f, which is sustainable when N_c is small (to satisfy $\mathbb{P}_{out}^c \leq \epsilon$). This explains the dominant gains in N_f at a low-to-moderate N_c.

A relevant question is to ask: *"How does the system capacity with randomly placed users and hotspots compare against a two-tier network with a given configuration?"* Kishore *et al.* [96, Page 1339] have performed a capacity analysis with a given configuration of cellular users and hotspots. Their results show diminishing system capacity gains without interference avoidance, because the configuration contains high levels of cross-tier interference.

Kishore [95] considers an operator administered macrocell-microcell underlay and proposes to improve two-tier cellular capacity assuming that the macrocell can

offload its traffic by handing off users to the microcell. Our model assumes that femtocells (placed by end consumer) operate with closed access. Consequently, due to reasons of security, handing off unsubscribed users from macrocell to a femtocell hotspot may not be practical. This necessitates an interference avoidance strategy.

3.7 Conclusion

This chapter has presented an uplink capacity analysis and interference avoidance strategy for a shared spectrum two-tier DS-CDMA network. We derive exact outage probability at a macrocell BS and tight lower bounds on the outage probability at a femtocell. Interference avoidance through a TH-CDMA physical layer coupled with sectorized receive antennas is shown to consistently outperform a split spectrum two-tier network with omnidirectional femtocell antennas. Considering the worst-case interference at a corner femtocell, the network OCs show a 7x improvement in femtocell density. Load balancing users in each tier is achievable through a orderwise difference in receive powers in each tier. Additional interference avoidance using a femtocell exclusion region and a tier selection based femtocell handoff offers conservative improvements in the OCs. The message is clear: Interference avoidance strategies can make shared spectrum two-tier networks a viable proposition in practical wireless systems.

The uplink capacity analysis presented in this chapter assumes that a) channel-inversion based power control is adopted at either tier, and b) users seek a common minimum SINR at their respective BSs. The next chapter relaxes these assumptions and derives a fundamental relationship between the set of feasible SINR targets at femtocells and the set of feasible cellular SINR targets. A utility-based femtocell power control scheme is presented, along with an algorithm which ensures that cellular users can satisfy their minimum target data rates in the presence of interfering hotspots.

Chapter 4

Data Rate Adaptation in Closed Access

4.1 Introduction

In a two-tier network with closed access and universal frequency reuse, because of the lack of coordination between cellular users and hotspot users, the SINRs of cellular users and hotspot users are coupled. This chapter provides three contributions. First, given a cellular user and N cochannel femtocells, the highest feasible cellular SINR target is derived, given a set of N femtocell SINR targets over all power control strategies. A Link Budget bound is presented which enables a simple and accurate performance analysis in a two-tier network. Next, a utility-based femtocell SINR adaptation is proposed which comprises of a SINR-based reward less an incurred cost (namely cross-tier interference to the macrocell). We show improved performance of this utility adaptation in contrast to conventional closed-loop power control schemes. Lastly, to guarantee that a cellular user satisfies its SINR target, a distributed link quality protection algorithm is proposed to adaptively reduce transmission powers of the strongest femtocell interferers.

4.1.1 Managing Cross-Interference

Contemporary wireless systems employ power control to assist users experiencing poor channels and to limit interference caused to neighboring cells. However, in a two-tier network, cross-tier interference may significantly hinder the performance of conventional power control schemes. For example, signal strength based power control (channel inversion) employed by cellular users results in unacceptable deterioration of femtocell SINRs [28]. The reason is because a user on its cell-edge transmits

with higher power to meet its receive power target, and causes excessive cross-tier interference at nearby femtocells.

Due to cross-tier interference in a two-tier network with shared spectrum, the target per-tier SINRs among macrocell and femtocell users are coupled. The notion of a SINR "target" models a certain application dependent minimum QoS requirement per user. It is reasonable to expect that femtocell users and cellular users seek different SINRs (data rates) – typically higher data rates using femtocells – because home users deploy femtocells in their self interest, and because of the proximity to their BS (Fig. 4.1). However, the QoS improvement arising from femtocells should come at an expense of reduced cellular coverage.

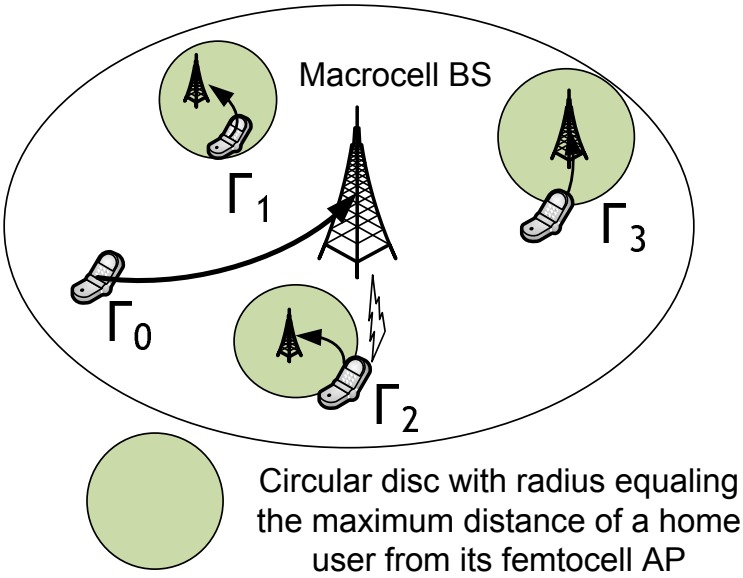

Figure 4.1: A two-tier cellular system with varying SINR targets

Interference management in two-tier networks faces practical challenges from the lack of coordination between the macrocell base-station (BS) and femtocell APs due to reasons of scalability, security and limited availability of backhaul bandwidth

[160]. From an infrastructure or spectrum availability perspective, it may be easier to operate the macrocell and femtocells in a common spectrum; at the same time, pragmatic solutions are necessary to reduce cross-tier interference. An open access (OA) scheme [36], which performs radio management by vertical handoffs – forcing cellular users to communicate with nearby femtocells to load balance traffic in each tier – is one such solution. A drawback of OA is the network overhead [29, 113] and the need for sufficient backhaul capacity to avoid starving the paying home user. Additionally, OA potentially compromises security and QoS for home users.

This work assumes *Closed Access* (CA), which means only licensed home users within radio range can communicate with their own femtocell. With CA, cross-tier interference from interior femtocells may significantly deteriorate the SINR at the macrocell BS. The motivation behind this work is ensuring that the service (data rates) provided to cellular users remain unaffected by a femtocell underlay which operates in the same spectrum. Three main reasons are 1. the macrocell's primary role of an anytime anywhere infrastructure, especially for mobile and "isolated" users without hotspot access, 2. the greater number of users served by each macrocell BS, and 3. the end user deployment of femtocells in their self-interest. The macrocell is consequently modeled as *primary infrastructure*, meaning that the operator's foremost obligation is to ensure that an outdoor cellular user achieves its minimum SINR target at its BS, despite cross-tier femtocell interference. Indoor users act in their self interest to maximize their SINRs, but incur a SINR penalty because they cause cross-tier interference.

Considering a macrocell BS with N cochannel femtocells and one transmitting user per slot per cell over the uplink, the following questions are addressed in this work:

- Given a set of feasible target SINRs inside femtocell hotspots, what is the largest cellular SINR target for which a non-negative power allocation exists for all users in the system?

- How does the cellular SINR depend on the locations of macrocell and femtocell users and cellular parameters such as the channel gains between cellular users and femtocells?
- Given an utility-based femtocell SINR adaptation with a certain minimum QoS requirement at each femtocell, what are the ensuing SINR equilibria and can they be achieved in a distributed fashion?
- When a cellular user cannot satisfy its SINR target due to cross-tier interference, by how much should femtocells reduce their SINR target to ensure that the cellular user's SINR requirement is met?

The first question poses a problem of determining the radio link quality (feasible SINR target) for a cellular user, given a set of N transmitting femtocells with different SINR targets. Questions 2 & 3 seek to determine the data rates at femtocells when home users adapt their SINR targets based on a utility function accounting for cross-tier interference; providing link quality protection to an active cellular user may necessitate femtocells to deliberately lower their SINR targets.

Although this work exclusively focusses on the uplink in a tiered cellular system, we would like to clarify that portions of our analysis (Section III) are also applicable in the downlink with potentially different conclusions. Due to space limitations, the downlink extension is omitted for future work.

4.1.2 Prior Work

Prior research in cellular power control and rate assignments in tiered networks mainly considered an operator planned underlay of a macrocell with single/multiple microcells [51, 93]. In the context of this work, a microcell has a much larger radio range (100-500 m) than a femtocell, and generally implies centralized deployment, i.e. by the service-provider. A microcell underlay allows the operator to handoff and load

balance users between each tier [29]. For example, the operator can preferentially assign high data rate users to a microcell [93, 99, 130] because of its inherently larger capacity. In contrast, femtocells are consumer installed and the traffic requirements at femtocells are user determined without any operator influence. Consequently, distributed interference management strategies may be preferred.

Our work ties in with well known power control schemes in conventional cellular networks and prior work on utility optimization based on game theory. Results in Foschini *et al.* [46], Zander [159], Grandhi *et al.* [59] and Bambos *et al.* [17] provide conditions for SINR feasibility and/or SIR balancing in cellular systems. Specifically, in a network with N users with target SINRs $\Gamma_i, 1 \leq i \leq N$, a feasible power allocation for all users exists iff the spectral radius of the normalized channel gain matrix is less than unity. Associated results on centralized/distributed/constrained power control, link admission control and user-BS assignment are presented in [59, 67, 135, 139, 154, 155, 158] and numerous other works.

The utility-based non-cooperative femtocell SINR adaptation presented here is related to existing game theory literature on non-cooperative cellular power control [8, 57, 81, 100, 126, 151] (see [9] for a survey). The adaptation forces stronger femtocell interferers to obtain their SINR equilibria closer to their minimum SINR targets, while femtocells causing smaller cross-tier interference obtain higher SINR margins. This is similar to Xiao and Shroff[151]'s utility-based power control (UBPC) scheme, wherein users vary their target SIRs based on the prevailing traffic conditions. Unlike the sigmoidal utility in [151], our utility function has a more meaningful interpretation because it models 1. the femtocell user's inclination to seek higher data-rates and 2. the primary role of the macrocell while penalizing the femtocell user for causing cross-tier interference. Our SINR equilibria is simple to characterize unlike the feasibility conditions presented in prior works e.g [8].

To minimize cross-tier interference, prior femtocell research has proposed open access [36], varying femtocell coverage area [72], hybrid frequency assignments [62],

adjusting the maximum transmit power of femtocell users [86] and adaptive access operation of femtocells [33]. In contrast, this work addresses SINR adaptation and ensuring acceptable cellular performance in closed access femtocells. Related works in cognitive radio (CR) literature such as [74, 119] propose that secondary users limit their transmission powers for reducing interference to primary users (PUs). In [74], CR users regulate their transmit powers to limit PU interference, but their work does not address individual rate requirements at each CR. Qian *et al.* [119] propose a joint power and admission control scheme, but provide little insight on how a CR user's data-rate is influenced by a PU's rate. In contrast, our results are applicable in CR networks for determining the *exact relationship* between the feasible SINRs of primary and CR users; further our SINR adaptation can enable CR users to vary their data-rates in a decentralized manner based on instantaneous interference at PU receivers.

4.1.3 Contributions

Pareto SINR Contours. Near-far effects in a cochannel two-tier network are captured through a theoretical analysis providing the highest cellular SINR target– for which a non-negative power allocation exists between all transmit-receive pairs– given any set of femtocell SINRs and vice versa. With a common SINR target at femtocells and neglecting interference between femtocells, the per-tier Pareto SINR pairs have an intuitive interpretation: the sum of the decibel (dB) cellular SINR and the dB femtocell SINR equals a constant. Design interpretations are provided for different path loss exponents, different numbers of femtocells and varying locations of the cellular user and hotspots.

Utility-based Femtocell SINR Adaptation. Femtocells individually maximize an objective function consisting of a SINR dependent reward, and a penalty proportional to the interference at the macrocell. We obtain a *channel-dependant SINR equilibrium* at each femtocell. The equilibrium discourages strongly interfering

femtocells to use large transmit powers. This SINR equilibrium is attained using distributed power updates[155]. For femtocell users whose objective is to simply equal their minimum SINR targets, our adaptation simplifies to the Foschini-Miljanic (FM) update. Numerical results show that the utility adaptation provides up to 30% higher femtocell SINRs relative to FM.

Cellular Link Quality Protection. To alleviate cross-tier interference when the cellular user does not achieve its SINR target, we propose a distributed algorithm to progressively reduce SINR targets of strongest femtocell interferers until the cellular SINR target is met. Numerical simulations with 100 femtocells/cell-site show acceptable cellular coverage with a worst-case femtocell SINR reduction of only 16% (with typical cellular parameters).

4.2 System Model

The system consists of a single central macrocell B_0 serving a region $\mathcal{C}$. The macrocell is underlaid with N cochannel femtocells APs $B_i, i \geq 1$. Femtocell users are located on the circumference of a disc of radius R_f centered at their femtocell AP. Orthogonal uplink signaling is assumed in each slot (1 scheduled active user per cell during each signaling slot), where a slot may refer to a time or frequency resource (the ensuing analysis leading up to Theorem 5 apply equally well over the downlink).

AS 3. *For analytical tractability, cochannel interference from neighboring cellular transmissions is ignored.*

During a given slot, let $i \in \{0, 1, \cdots, N\}$ denote the scheduled user connected to its BS B_i. Designate user i's transmit power to be p_i Watts. Let σ^2 be the variance of Additive White Gaussian Noise (AWGN) at B_i. The received SINR γ_i of user i at B_i is given as

$$\Gamma_i \leq \gamma_i = \frac{p_i g_{i,i}}{\sum_{j \neq i} p_j g_{i,j} + \sigma^2}. \tag{4.1}$$

Here Γ_i represents the minimum target SINR for user i at B_i. The term $g_{i,j}$ denotes the channel gain between user j and BS B_i. Note that $g_{i,i}$ can also account for post-processing SINR gains arising from, but not restricted to, diversity reception or interference suppression (e.g. CDMA). In matrix-vector notation, (4.1) can be written as

$$\mathbf{p} \geq \mathbf{\Gamma G p} + \boldsymbol{\eta} \text{ and } \mathbf{p} \geq 0. \tag{4.2}$$

Here $\mathbf{\Gamma} \triangleq \text{diag}(\Gamma_0, \ldots \Gamma_N)$ while the vector $\mathbf{p} = (p_0, p_1, \cdots p_N)$ denotes the transmission powers of individual users, and the normalized noise vector equals $\boldsymbol{\eta} = (\eta_0, \ldots \eta_N), \eta_i = \sigma^2 \Gamma_i / g_{i,i}$. The $(N+1) \times (N+1)$ matrix $\mathbf{G} \geq 0$ is assumed to be irreducible – meaning its directed graph is strongly connected [73, Page 362]– with elements given as

$$G_{ij} = \frac{g_{i,j}}{g_{i,i}}, i \neq j \text{ and 0 else.} \tag{4.3}$$

Since $\mathbf{\Gamma G}$ is nonnegative, the spectral radius $\rho(\mathbf{\Gamma G})$ (defined as the maximum modulus eigenvalue $\max\{|\lambda| : \mathbf{\Gamma G} - \lambda \mathbf{I}_{N+1} \text{ is singular}\}$) is an eigenvalue of $\mathbf{\Gamma G}$ [73, Theorem 8.3.1]. Applying Perron-Frobenius theory [73] to $\mathbf{\Gamma G}$, (4.2) has a nonnegative solution $\mathbf{p}^*$ (or $\mathbf{\Gamma}$ constitutes a *feasible* set of target SINR assignments) *iff* the spectral radius $\rho(\mathbf{\Gamma G})$ is less than unity[17, 59]. Consequently,

$$\forall \boldsymbol{\eta} \geq \mathbf{0}, (\mathbf{I} - \mathbf{\Gamma G})^{-1} > 0 \Leftrightarrow (\mathbf{I} - \mathbf{\Gamma G})^{-1} \boldsymbol{\eta} \geq \mathbf{0} \Leftrightarrow \rho(\mathbf{\Gamma G}) < 1. \tag{4.4}$$

The solution $\mathbf{p}^* = (\mathbf{I} - \mathbf{\Gamma G})^{-1} \boldsymbol{\eta}$ guarantees that the target SINR requirements are satisfied at all BSs. Further, $\mathbf{p}^*$ is Pareto efficient in the sense that any other solution $\mathbf{p}$ satisfying (4.2) needs at least as much power componentwise[17]. When $\mathbf{\Gamma} = \gamma \mathbf{I}_{N+1}$, then the max-min SIR solution γ^* to (4.4) is given as

$$\mathbf{\Gamma} = \Gamma \mathbf{I}_{N+1} \Rightarrow \Gamma^* = \frac{1}{\rho(\mathbf{G})}. \tag{4.5}$$

In an interference-limited system (neglecting $\boldsymbol{\eta}$), the optimizing vector $\mathbf{p}^*$ equals the Perron-Frobenius eigenvector of $\mathbf{\Gamma G}$ [159].

4.3 Per-Tier SINR Contours In a Femtocell-Underlaid Macrocell

In a two-tier network, let $\Gamma_c = \Gamma_0$ and $\Gamma_i (i \geq 1)$ denote the per-tier SINR targets at the macrocell and femtocell BSs respectively. Define $\mathbf{\Gamma}_f \triangleq \text{diag}(\Gamma_1, \Gamma_2, \ldots, \Gamma_N)$ and $\mathbf{\Gamma} = \text{diag}(\Gamma_c, \mathbf{\Gamma}_f)$. Any feasible SINR tuple ensures that the spectral radius $\rho(\mathbf{\Gamma G}) < 1$ with a feasible power assignment given by (4.4). This section derives the relationship between Γ_c and Γ_i as a function of κ and entries of the $\mathbf{G}$ matrix.

Using the above notation, $\mathbf{\Gamma G}$ simplifies as

$$\mathbf{\Gamma G} = \begin{pmatrix} 0 & \Gamma_c \mathbf{q}_c^T \\ \mathbf{\Gamma}_f \mathbf{q}_f & \mathbf{\Gamma}_f \mathbf{F} \end{pmatrix}. \tag{4.6}$$

Here the principal submatrix $\mathbf{F}$ consists of the normalized channel gains between each femtocell and its surrounding $N-1$ cochannel femtocells. The vector $\mathbf{q}_C^T = [G_{01}, G_{02}, \ldots, G_{0N}]$ consists of the normalized cross-tier channel gains between the transmitting femtocell users to the macrocell BS. Similarly, $\mathbf{q}_F = [G_{10}, G_{20}, \ldots G_{N0}]^T$ consists of the normalized cross-tier channel gains between the cellular user to surrounding femtocell BSs.

Below, we list two simple but useful properties of $\mathbf{\Gamma G}$:

Property 1. $\rho(\mathbf{\Gamma G})$ is a non-decreasing function of $\mathbf{\Gamma}$. That is, $\mathbf{\Gamma}' \geq \mathbf{\Gamma} \Rightarrow \rho(\mathbf{\Gamma}'\mathbf{G}) \geq \rho(\mathbf{\Gamma G})$.

Property 2. $\rho(\mathbf{\Gamma G}) \geq \rho(\mathbf{\Gamma}_f \mathbf{F})$.

Property 1 is a consequence of [73, Corollary 8.1.19] and implies that increasing the per-tier SINRs in $\mathbf{\Gamma}$ drives $\rho(\mathbf{\Gamma G})$ closer to unity. This decreases the margin for existence of a nonnegative inverse of $\mathbf{I} - \mathbf{\Gamma G}$ in (4.4). Therefore, assuming a fixed set of femtocell SINRs given by $\mathbf{\Gamma}_f$, the maximum cellular SINR target Γ_0 monotonically increases with $\rho(\mathbf{\Gamma G})$. Property 2 arises as a consequence of $\mathbf{\Gamma}_f \mathbf{F}$ being a principal submatrix of $\mathbf{G}$, and applying [73, Corollary 8.1.20]. Intuitively, any feasible femtocell

SINR in a tiered network is also feasible when the network comprises only femtocells since $\rho(\mathbf{\Gamma G}) < 1 \Rightarrow \rho(\mathbf{\Gamma}_f\mathbf{F}) < 1$. From (4.4), the condition $\rho(\mathbf{\Gamma}_f\mathbf{F}) < 1 \Leftrightarrow (\mathbf{I}-\mathbf{\Gamma}_f\mathbf{F})^{-1}$ is non negative with expansion given as $\sum_{k=0}^{\infty}(\mathbf{\Gamma}_f\mathbf{F})^k$.

We restate a useful lemma by Meyer [109] for obtaining $\rho(\mathbf{\Gamma G})$ in terms of $\mathbf{F}, \mathbf{q}_f, \mathbf{q}_c, \Gamma_c$ and $\mathbf{\Gamma}_f$.

Lemma 4. *[109, Meyer]* Let $\mathbf{A}$ be a $m \times n$ nonnegative irreducible matrix with spectral radius ρ and let $\mathbf{A}$ have a k-level partition

$$\mathbf{A} = \begin{pmatrix} \mathbf{A}_{11} & \mathbf{A}_{12} & \dots & \mathbf{A}_{1k} \\ \mathbf{A}_{21} & \mathbf{A}_{22} & \dots & \mathbf{A}_{2k} \\ \vdots & \vdots & \ddots & \vdots \\ \mathbf{A}_{k1} & \mathbf{A}_{k2} & \dots & \mathbf{A}_{kk} \end{pmatrix} \tag{4.7}$$

in which all diagonal blocks are square. For a given index i, let $\mathbf{A}_i$ represent the principal block submatrix of $\mathbf{A}$ by deleting the ith row and ith column of blocks from $\mathbf{A}$. Let $\mathbf{A}_{i*}$ designate the ith row of blocks with $\mathbf{A}_{ii}$ removed. Similarly, let $\mathbf{A}_{*i}$ designate the ith column of blocks with $\mathbf{A}_{ii}$ removed. Then each Perron complement $\mathbf{P}_{ii} = \mathbf{A}_{ii} + \mathbf{A}_{i*}(\rho\mathbf{I} - \mathbf{A}_i)^{-1}\mathbf{A}_{*i}$ is also a nonnegative matrix whose spectral radius is again given by ρ.

Using Lemma 4, we state the first result in this work.

Theorem 5. Assume a set of feasible femtocell SINRs targets $\Gamma_i (i \geq 1)$ such that $\rho(\mathbf{\Gamma}_f\mathbf{F}) < 1$, and a target spectral radius $\rho(\mathbf{\Gamma G}) = \kappa, \rho(\mathbf{\Gamma}_f\mathbf{F}) < \kappa < 1$. The highest cellular SINR target maintaining a spectral radius of κ is then given as

$$\Gamma_c = \frac{\kappa^2}{\mathbf{q}_c^T[\mathbf{I} - (\mathbf{\Gamma}_f/\kappa)\mathbf{F}]^{-1}\mathbf{\Gamma}_f\mathbf{q}_f}. \tag{4.8}$$

Proof. From Lemma 4, the Perron complement of the entry "0" of $\mathbf{\Gamma G}$ in (4.6) is a nonnegative scalar equaling κ. This implies,

$$\kappa = 0 + \Gamma_c\mathbf{q}_c^T[\kappa\mathbf{I} - \mathbf{\Gamma}_f\mathbf{F}]^{-1}\mathbf{\Gamma}_f\mathbf{q}_f. \tag{4.9}$$

Rearranging terms, we obtain (4.8). Note that since $\kappa > \rho(\mathbf{\Gamma}_f\mathbf{F})$, the inverse $[\mathbf{I} - (\mathbf{\Gamma}_f/\kappa)\mathbf{F}]^{-1} = \sum_{k=0}^{\infty}(\Gamma_f/\kappa)^k\mathbf{F}^k$ exists and is nonnegative. □

Remark 4. *Alternatively, one may use the block determinant formula*

$$\det(\mathbf{D}) \neq 0 \Rightarrow \det\begin{pmatrix}\mathbf{A} & \mathbf{B}\\ \mathbf{C} & \mathbf{D}\end{pmatrix} = \det(\mathbf{D})\det(\mathbf{A} - \mathbf{B}\mathbf{D}^{-1}\mathbf{C}). \tag{4.10}$$

Let λ be an eigenvalue of $\mathbf{\Gamma G}$. Whenever $\lambda\mathbf{I} - \mathbf{\Gamma}_f\mathbf{F}$ is invertible, applying the block determinant formula implies

$$\det(\lambda\mathbf{I} - \mathbf{\Gamma G}) = 0 \tag{4.11}$$

$$\Rightarrow \det(\lambda\mathbf{I} - \mathbf{\Gamma}_f\mathbf{F}) \cdot \det(\lambda - \Gamma_c\mathbf{q}_c^T(\lambda\mathbf{I} - \mathbf{\Gamma}_f\mathbf{F})^{-1}\mathbf{\Gamma}_f\mathbf{q}_f) = 0 \tag{4.12}$$

$$\Rightarrow \det(\lambda - \Gamma_c\mathbf{q}_c^T(\lambda\mathbf{I} - \mathbf{\Gamma}_f\mathbf{F})^{-1}\mathbf{\Gamma}_f\mathbf{q}_f) = 0 \tag{4.13}$$

We claim that $\det(\kappa\mathbf{I} - \mathbf{\Gamma}_f\mathbf{F}) \neq 0$ because 1. the spectral radius $\rho(\mathbf{\Gamma G}) = \kappa$ is also an eigenvalue of $\mathbf{\Gamma G}$ and 2. Property 2 ensures that $(\kappa\mathbf{I} - \mathbf{\Gamma}_f\mathbf{F})$ is non-singular. Replacing λ in (4.13) with κ, one obtains $\kappa = \Gamma_c\mathbf{q}_c^T(\kappa\mathbf{I} - \mathbf{\Gamma}_f\mathbf{F})^{-1}\mathbf{\Gamma}_f\mathbf{q}_f$. Consequently, (4.8) follows.

Given a set of N feasible femtocell SINR targets, Theorem 5 provides a fundamental relationship describing the maximum SINR target at the macrocell over all power control strategies. Given a κ (e.g. $\kappa = 1 - \epsilon$, where $0 < \epsilon < 1 - \rho(\mathbf{\Gamma}_f\mathbf{F})$), one obtains the highest Γ_c for a given $\mathbf{\Gamma}_f$.

Example 6 (One Femtocell). *Consider a two-tier network consisting of the central macrocell B_0 and a single femtocell BS B_1. The matrix $\mathbf{\Gamma G}$ is given as*

$$\mathbf{\Gamma G} = \begin{pmatrix}0 & \Gamma_c G_{01}\\ \Gamma_f G_{10} & 0\end{pmatrix}. \tag{4.14}$$

Setting $\mathbf{F} = 0, \mathbf{q}_c = G_{01}, \mathbf{q}_f = G_{10}$ in (4.8), one obtains

$$\rho(\mathbf{\Gamma G}) = \sqrt{\Gamma_c G_{01}\Gamma_f G_{10}} \Rightarrow (\Gamma_c, \Gamma_f) \in \left\{(x, y) \in \mathbb{R}_+^2 : xy < \frac{1}{G_{01}G_{10}}\right\}. \tag{4.15}$$

Intuitively, the product of the per-tier SINR targets is limited by the inverse product of the cross-tier gains between the cellular user to the femtocell AP and vice versa.

Remark 5. *Equation* (4.8) *generically applies in a wireless network with* $N+1$ *users for finding the best SINR target for a particular user – by appropriately adjusting the entries in* $\mathbf{q}_c$, $\mathbf{q}_f$ *and* $\mathbf{F}$ *– for a given set of* N *SINR targets. However, the subsequent analysis (Lemma 5) specializes* (4.8) *to a two-tier cellular system and works only when the cellular user is isolated.*

With Γ_c obtained from (4.8) and SINR targets $\mathbf{\Gamma}^* = [\Gamma_c, \Gamma_1, \Gamma_2, \ldots, \Gamma_N]^T$, a centralized power allocation is given as

$$\mathbf{p}^* = (\mathbf{I} - \mathbf{\Gamma}^*\mathbf{G})^{-1}\boldsymbol{\eta}^*, \text{ where } \boldsymbol{\eta}^* \triangleq \text{diag}\left(\frac{\sigma^2}{g_{1,1}}, \frac{\sigma^2}{g_{2,2}}, \ldots, \frac{\sigma^2}{g_{N+1,N+1}}\right)\mathbf{\Gamma}^*. \tag{4.16}$$

Next, assume that the N femtocells $B_1 \ldots B_N$ choose a *common* SINR target $\Gamma_i = \Gamma_f (i \geq 1)$. Although the assumption of a common SINR target at all femtocells seems rather restrictive at first glance, it provides intuition on near-far effects in a two-tier network which will be discussed in the next section. The following corollary derives the Pareto contours between the best SINR targets for macrocell and femtocell users respectively.

Corollary 3. Assume a common positive target femtocell SINR target $\Gamma_f < 1/\rho(\mathbf{F})$, and a target spectral radius $\rho(\mathbf{\Gamma G}) = \kappa$, where $\Gamma_f \rho(\mathbf{F}) < \kappa < 1$. The Pareto contours maintaining a spectral radius of κ are given as

$$\left\{(\Gamma_c, \Gamma_f) : 0 \leq \Gamma_f < \frac{1}{\rho(\mathbf{F})}, \Gamma_c = \frac{\kappa^2}{\Gamma_f \mathbf{q}_c^T[\mathbf{I} - (\Gamma_f/\kappa)\mathbf{F}]^{-1}\mathbf{q}_f}\right\}. \tag{4.17}$$

Remark 6 (**Pareto optimality**)**.** *Given a target spectral radius* κ*, the* $(\Gamma_c, \mathbf{\Gamma}_f)$ *tuples derived in* (4.8) *(and hence* (4.17)*) are Pareto optimal. From Property* **??***, a "better pair"* $\mathbf{\Gamma}'_f \geq \mathbf{\Gamma}_f$ *(component-wise) and* $\Gamma'_c > \Gamma_c$ *cannot be obtained without* $\rho(\mathbf{\Gamma G})$ *exceeding* κ*.*

Lemma 5. With a set of feasible femtocell SINRs thresholds $\Gamma_i (i \geq 1)$ and $\rho(\mathbf{\Gamma}_f \mathbf{F}) < 1$, a necessary condition for any cellular SINR target Γ_c to be feasible is given as

$$\Gamma_c \leq \frac{1}{\mathbf{q}_c^T \mathbf{\Gamma}_f \mathbf{q}_f}. \tag{4.18}$$

Consequently, assuming a common positive SINR target $\Gamma_f < 1/\rho(\mathbf{F})$ at femtocells ($1/\rho(\mathbf{F})$ being the max-min target), any feasible SINR pair (Γ_c, Γ_f) satisfies the following inequality

$$\Gamma_c \Gamma_f < \frac{1}{\mathbf{q}_c^T \mathbf{q}_f}. \tag{4.19}$$

Proof. Computing the Perron complement of $\mathbf{\Gamma}_f \mathbf{F}$ in (4.6) and applying Lemma 4:

$$\kappa = \rho(\Gamma_f \mathbf{F} + \Gamma_f \mathbf{q}_f \Gamma_c \mathbf{q}_c^T / \kappa) \overset{(b)}{\geq} \rho(\Gamma_f \mathbf{q}_f \Gamma_c \mathbf{q}_c^T / \kappa) \tag{4.20}$$

where step (b) in (4.20) follows by applying [73, Corollary 8.1.19]. Upper bounding κ^2 by unity and applying $\rho(\mathbf{q}_f \mathbf{q}_c^T) = \mathbf{q}_c^T \mathbf{q}_f$ to (4.20) yields (4.18). Alternatively, one can expand $\mathbf{I} - (\Gamma_f/\kappa)\mathbf{F}$ and replace $\mathbf{q}_c^T [\mathbf{I} - (\Gamma_f/\kappa)\mathbf{F}]^{-1} \mathbf{q}_f$ by the lower bound $\mathbf{q}_c^T \mathbf{q}_f$. □

Intuitively, (4.19) restates that $1/\mathbf{q}_c^T \mathbf{q}_f$ is an upper bound on the product of the per-tier SINRs, achieved when $\mathbf{F} = \mathbf{0}$ in (4.8), i.e. the interference between neighboring femtocells is vanishingly small. Ignoring $\mathbf{F}$ is justifiable because 1. the propagation between femtocells suffers at least a double wall partition losses (from inside a femtocell to outdoor and from outdoor onto the neighboring femtocell), and 2. there is only one partition loss term while considering the propagation loss between a cellular user to femtocells.

Thus, a simple relationship between the highest per-tier SINRs is expressed as:

For small $\mathbf{F}$*, the sum of the per-tier decibel SINRs equals a channel dependant constant* $L_{dB} = -10 \log_{10}(\mathbf{q}_c^T \mathbf{q}_f)$. We denote this constant $L = \frac{1}{\mathbf{q}_c^T \mathbf{q}_f}$ as the *Link*

Budget. Choosing a cellular SINR target of x dB necessitates any feasible femtocell SINR target to be no more than $L_{\text{dB}} - x$ dB. To keep L large, it is desirable that the normalized interference powers are decorrelated (or $\mathbf{q}_c$ and $\mathbf{q}_f$ do not peak simultaneously). In a certain sense, the link budget provides an "efficiency index" of closed access femtocell operation, since open (or public) femtocell access potentially allows users to minimize their interference by handoffs.

Example 7 (N **Femtocells**)**.** *Assume a path loss based model wherein the channel gains $g_{i,j} = D_{i,j}^{-\alpha}$ ($D_{i,j}$ represents the distance between user j to BS B_i. The term α is the path loss exponent (assumed equal indoors and outdoors for convenience). Femtocell user i is located at distances R_f from its AP B_i and D_f from B_0. The cellular user is located at distances D from its macrocell BS B_0 and D_c from each femtocell AP (See Fig. 4.2 for $N = 2$ femtocells).*

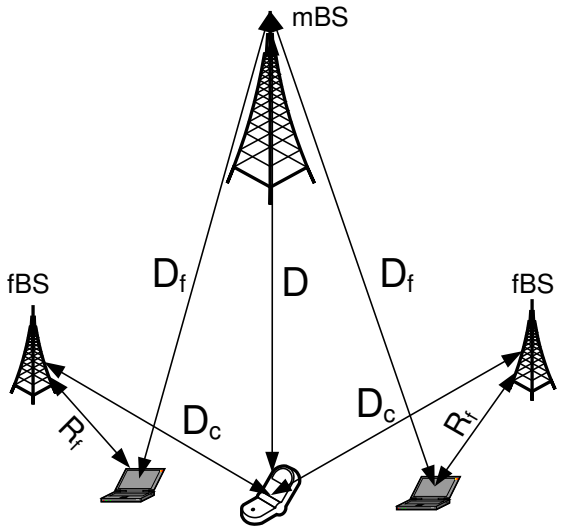

Figure 4.2: Simple example with $N = 2$ femtocells for determining how link budgets vary with the normalized interference distance $D_f D_c / R_f D$.

In this setup, $\mathbf{q}_c^T = [\left(\frac{D_f}{D}\right)^{-\alpha}, \left(\frac{D_f}{D}\right)^{-\alpha}, \ldots, \left(\frac{D_f}{D}\right)^{-\alpha}]$. *The vector* $\mathbf{q}_f = [\left(\frac{D_c}{R_f}\right)^{-\alpha}, \left(\frac{D_c}{R_f}\right)^{-\alpha}, \ldots$

The decibel link budget L_{dB} varies with α as a straight line and given as

$$L \triangleq \frac{1}{\mathbf{q}_c^T \mathbf{q}_F} = \frac{1}{N}\left(\frac{D_f D_c}{DR_f}\right)^{\alpha} \Rightarrow L_{dB} = \underbrace{-10\log_{10} N}_{intercept} + \underbrace{10\log_{10}\left(\frac{D_f D_c}{DR_f}\right)}_{slope}\alpha. \tag{4.21}$$

Define $Q \triangleq \frac{D_f D_c}{DR_f}$ as the interference distance product normalized by the signaling distance product. *Then, L_{dB} monotonically increases with α whenever the slope $Q_{dB} > 0$ and decreases otherwise. Consequently, the condition $Q \gtrless 1$ determines the sensitivity of link budgets to the path-loss exponent.*

4.3.1 Design Interpretations

This subsection studies how the per-tier SINRs and link budgets vary with user and femtocell locations in practical path loss scenarios. Assume that the cellular user 0 is located at a distance $D_{0,0} = D$ from the macrocell B_0. At a distance D_f from B_0 (see Fig. 4.3), N surrounding cochannel femtocells $\{B_i\}, i = 1 \cdots N$ are arranged in a square grid – e.g. residential neighborhood – of area $D^2_{\text{grid}} = 0.25$ sq. km. with $\sqrt{N}$ femtocells per dimension. Each femtocell has a radio range equaling R_f meters. Let $D_{i,j}$ denote the distance between transmitting mobile j and BS B_i.

For simplicity, neither Rayleigh fading nor lognormal shadowing are modeled. Assuming a reference distance $D_{\text{ref}} = 1$ meter [56] for all users, the channel gains $g_{i,j}$ are represented using the simplified path loss model in the IMT-2000 specification [1], given as

$$g_{i,j} = \begin{cases} K_c \min\left(D^{-\alpha_c}, 1\right) & i = j = 0, \\ K_{fi} R_f^{-\beta} & i = j > 1, \\ K_{fo}\phi \min\left(D_{0,j}^{-\alpha_{fo}}, 1\right) & i = 0, j > 0, \\ K_c \phi \min\left(D_{i,j}^{-\alpha_c}, 1\right) & i > 0, j = 0, \\ K_{fo}\phi^2 \min\left(D_{i,j}^{-\alpha_{fo}}, 1\right) & i \neq j, i, j > 0 \end{cases} \tag{4.22}$$

In (4.22), $\alpha_c, \beta, \alpha_{fo}$ respectively denote the cellular, indoor and indoor to outdoor femtocell path loss exponents. Defining $f_{c,\text{MHz}}$ as the carrier frequency in MHz,

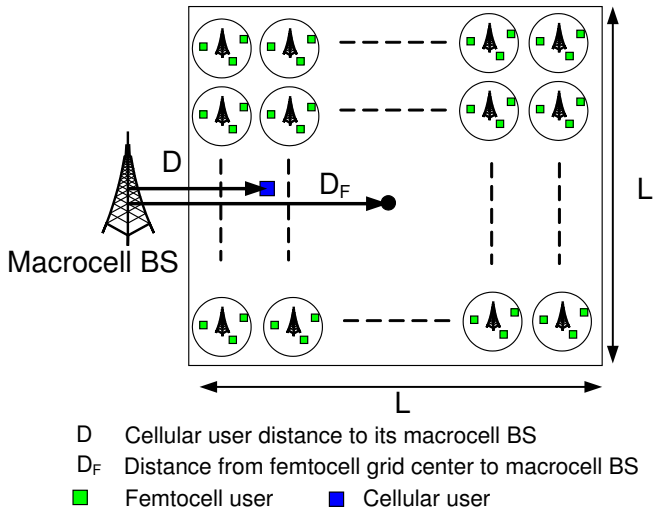

Figure 4.3: Single transmitting cellular user coexisting with an underlaid grid of cochannel femtocells.

$K_{c,\text{dB}} = 30\log_{10}(f_{c,\text{Mhz}}) - 71$ dB equals the fixed decibel propagation loss during cellular transmissions to B_0. The term K_{fi} is the fixed loss between femtocell user i to their BS B_i. Finally, K_{fo} denotes the fixed loss between femtocell user i to a different BS B_j, and assumed equal to K_c. The term W explicitly models partition loss during indoor-to-outdoor propagation (see numerical values for all system parameters in Table 4.2).

AS 4. *Assume equal outdoor path loss exponents from a cellular user and a femtocell user to the macrocell B_0. That is, $\alpha_c = \alpha_{fo} = \alpha$.*

Following AS4, substituting (4.22) in (4.19) and assuming that users are at least 1 meter away from BSs (or $D_{i,j}^{-\alpha} < 1 \forall i, j$), the link budget L is given as

$$L = \frac{K_{fi} R_f^{-\beta}}{W^2 K_{fo}} D^{-\alpha} \left(\sum_{i=1}^{N} D_{0,i}^{-\alpha} D_{i,0}^{-\alpha} \right)^{-1}. \tag{4.23}$$

We first plot the SINR contours in Fig. 4.4 for different normalized D and D_f values. The target spectral radius $\kappa = \rho(\mathbf{\Gamma G})$ in (4.8) equals $\max\{1 - 10^{-4}, \rho(\mathbf{F}) +$

$(1 - 10^{-4})(1 - \rho(\mathbf{F}))\}$ (ensuring that $\rho(\mathbf{\Gamma}_f\mathbf{F}) < \rho(\mathbf{\Gamma G}) < 1$). For comparison, the upper bound in (4.19) was also plotted. Three different positions – normalized w.r.t the cellular radius – of the user and the grid are considered namely a) $D = D_F = 0.1$, b) $D = 0.1$ and $D_F = 0.5$ and c) $D = D_F = 0.9$. In case (a), note that the macrocell BS is located in the *interior* of the femtocell grid.

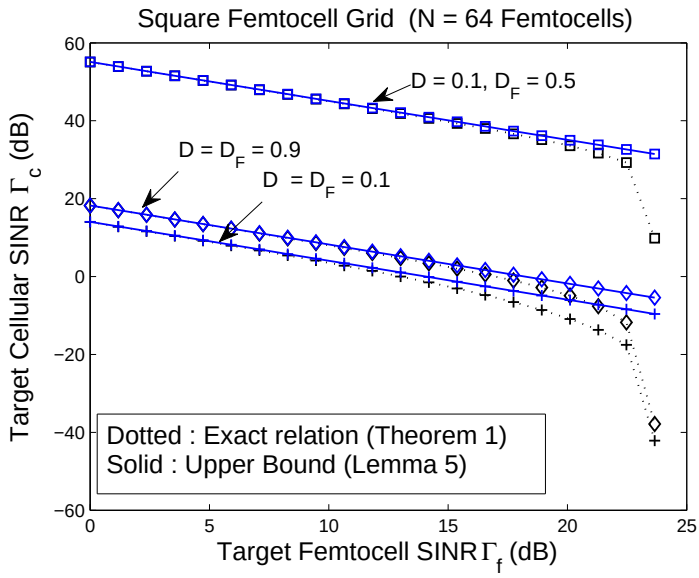

Figure 4.4: Per-Tier SINR contours for different cellular user and femtocell locations

We observe that employing (4.19) is a good approximation for the exact result given in (4.17). The highest per-tier SINRs occurs in configuration (b) suggesting a low level of normalized interference ($\mathbf{q}_c$ and $\mathbf{q}_f$). Interestingly, when both users and hotspots are close to the macrocell BS [configuration (a)], the per-tier SINRs are *worse* compared to the cell-edge configuration (c). This counterintuitive result suggests that unlike a conventional cellular system where the regular placement of BSs causes the worst-case SINRs typically at cell-edge, the *asymmetric locations of interfering transmissions in a two-tier network potentially diminishes link budgets in the cell-interior as well.* The reason is because power control "warfare" due to cross-tier interference from femtocells near the macrocell BS necessitates both tiers to lower

their SINR targets.

Assume that user 0 is located at the center of the femtocell grid ($D = D_f$ in Fig. 4.3). The following lemma provides a necessary condition under which the link budget increases with α.

Proposition 1. Under assumption 4 and assuming fixed locations of all users w.r.t their BSs, the link budget monotonically increases with α whenever

$$\frac{\sum_{i=1}^{N}(D_{0,i}D_{i,0})^{-\alpha}\ln(D_{0,i}D_{i,0})}{\sum_{i=1}^{N}(D_{0,i}D_{i,0})^{-\alpha}} > \ln(D). \tag{4.24}$$

Proof. Taking the first derivative of the link budget in (4.23) with respect to α yields (4.24). □

Fig. 4.5(a) plots the Link Budget in (4.23) for $\alpha = 3.5, 4$ and $N = 4, 16, 64$ femtocells with the cellular user colocated at the grid center ($D = D_F$). The link budgets with $\alpha = 4$ are higher relative to those obtained when $\alpha = 3.5$ indicating link budgets tend to increase with higher path loss exponents in practical scenarios. Fig. 4.5(b) plots the cumulative distribution function (CDF) of L_{dB} considering randomly distributed femtocells inside a circular region of radius $D_{\text{grid}}/\sqrt{\pi}$ and center at distance D_f from B_0. With $N = 64$ femtocells, both the regular and random configurations in Figs. 4.5(a)-4.5(b) show diminishing L in the cell-interior suggesting significant levels of cross-tier interference.

The above results motivate adapting femtocell SINRs with the following objectives namely 1. to maximize their own SINRs, and 2. limit their cross-tier interference.

4.4 Utility-Based Distributed SINR Adaptation

Due to the absence of coordination between tiers, implementing centralized power control $\mathbf{p}^* = (\mathbf{I} - \mathbf{\Gamma}^*\mathbf{G})^{-1}\boldsymbol{\eta}^*$ will likely be prohibitively difficult. In this section,

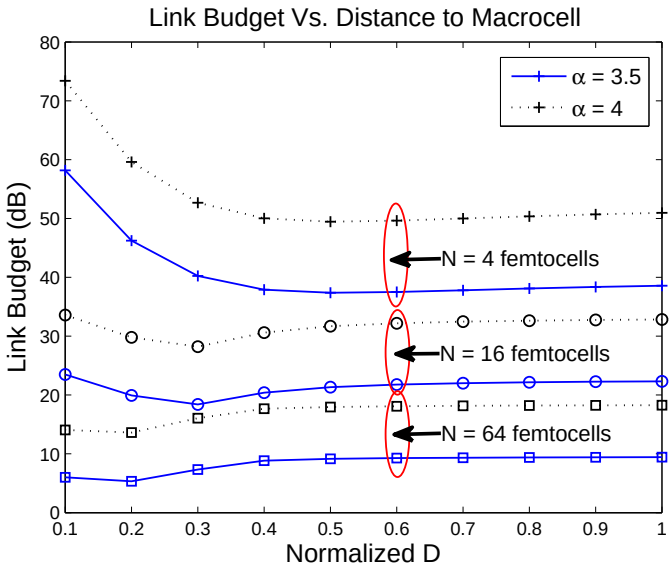

(a) Link budget with a square femtocell grid configuration

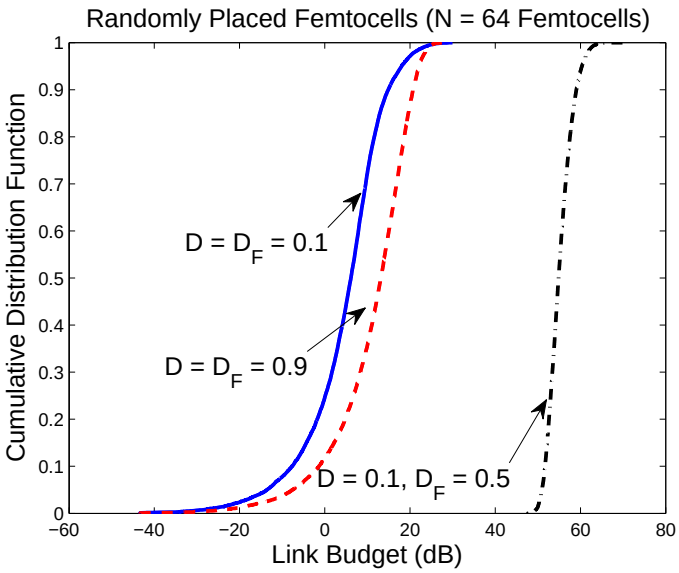

(b) Cumulative distribution function of the decibel link budget $10\log_{10}(1/\mathbf{q}_c^T\mathbf{q}_f)$ with randomly located femtocells centered about D_f

Figure 4.5: Decibel link budget $10\log_{10}(1/\mathbf{q}_c^T\mathbf{q}_f)$ considering a square femtocell grid and randomly placed femtocells

we present a utility-based SINR adaptation scheme. Using microeconomic concepts, we shall assume that cellular and femtocell users participate in a $N+1$ player non-cooperative power control game $G = [\mathcal{N}, \{P_i\}, \{U_i(.)\}]$. Here $\mathcal{N} = \{0, 1, \ldots N\}$ refers to the player index set and P_i is the strategy set describing the domain of transmission powers for user i. User i maximizes its individual utility U_i (or payoff) in a distributed fashion. Consequently, their actions – selecting their transmission power – are the best response to the actions of other participants. For notational convenience, define $[x]^+ \triangleq \max\{x, 0\}$. Given user i, designate $\mathbf{p}_{-i}$ as the vector of transmit powers of all users other than i and define $I_i(\mathbf{p}_{-i}) \triangleq \sum_{j \neq i} p_j g_{i,j} + \sigma^2$ as the interference power experienced at B_i.

Formally, for all users $0 \leq i \leq N$, this power control game is expressed as

$$\max_{0 \leq p_i \leq p_{\max}} U_i(p_i, \gamma_i | \mathbf{p}_{-i}) \text{ for each user in } \mathcal{N}. \tag{4.25}$$

We are interested in computing the equilibrium point (a vector of $N+1$ transmit powers) wherein each user in $\mathcal{N}$ individually maximizes its utility in (4.25), *given* the transmit powers of other users. Such an equilibrium operating point(s) in optimization problem (4.32) is denoted as the *Nash equilibrium* [112]. Denote $\mathbf{p}^* = (p_0^*, p_1^*, \ldots, p_N^*)$ as the transmission powers of all users under the Nash equilibrium. At the Nash equilibrium, no user can unilaterally improve its individual utility. Mathematically,

$$U_i(p_i^*, \gamma_i^* | \mathbf{p}_{-i}^*) \geq U_i(p_i, \gamma_i^* | \mathbf{p}_{-i}^*) \quad \forall p_i \neq p_i^*, p_i \in P_i, \ \forall i \in \mathcal{N}. \tag{4.26}$$

We shall make the following assumptions for the rest of the work.

AS 5. *All mobiles have a maximum transmission power constraint p_{max}, consequently the strategy set for user i is given as $P_i = [0, p_{max}]$.*

AS 6. *Assume a* closed-loop feedback power control*, i.e BS B_i periodically provides status feedback to user $i \in \mathcal{N}$ if its current SINR $\gamma_i = p_i g_{ii} / I_i(\mathbf{p}_{-i})$ is above/below its minimum SINR target Γ_i.*

4.4.1 Cellular Utility Function

Given a current cellular SINR γ_0 and a minimum SINR target $\Gamma_0 > 0$ at B_0, we model the cellular user 0's objective as

$$\max_{0 \leq p_0 \leq p_{\max}} U_0(p_0, \gamma_0 | \mathbf{p}_{-0}) = -(\gamma_0 - \Gamma_0)^2. \tag{4.27}$$

The intuition behind the strictly concave utility in (4.27) is that user 0 desires to achieve its minimum SINR target Γ_0 – assuming feasibility – while expending no more than the minimum required transmission power below $p_{\max}$. Alternatively, given a cellular SINR $\gamma_0 > \Gamma_0$ for a given interference $I_0(\mathbf{p}_{-0})$ at B_0, user 0 could improve its utility by decreasing p_0 until $\gamma_0 = \Gamma_0$.

4.4.2 Femtocell Utility Function

Given interfering powers $\mathbf{p}_{-i}$ and current SINR γ_i, user i in femtocell B_i obtains an individual utility $U_i(p_i, \gamma_i | \mathbf{p}_{-i})$. Having installed the femtocell AP B_i in their self-interest, user i seeks to maximize its individual SINR while meeting its minimum SINR requirement. At the same time, transmitting with too much power will create unacceptable cross-tier interference at the primary infrastructure B_0. Consequently, it is natural to discourage femtocells from creating large cross-tier interference. We therefore model the utility function for femtocell user i as consisting of two parts.

$$U_i(p_i, \gamma_i | \mathbf{p}_{-i}) = R(\gamma_i, \Gamma_i) + b_i \frac{C(p_i, \mathbf{p}_{-i})}{I_i(\mathbf{p}_{-i})}. \tag{4.28}$$

Reward function. The *reward function* $R(\gamma_i, \Gamma_i)$ denotes the payoff to user i as a function of its individual SINR γ_i and minimum SINR target $\Gamma_i \leq \frac{p_{\max} g_{i,i}}{\sigma^2}$.

Penalty function. The *penalty function* $b_i \frac{C(p_i, \mathbf{p}_{-i})}{I_i(\mathbf{p}_{-i})}$ is related to the interference experienced at the macrocell BS B_0. The penalty C reduces the net utility obtained by i for creating cross-tier interference at B_0 by virtue of transmitting at power p_i. Here b_i is a constant which reflects the relative importance of the penalty

w.r.t the reward of user i. Scaling the penalty by $I_i(\mathbf{p}_{-i})$ ensures that femtocells experiencing higher interference are penalized less.

Using the framework of [81], we make the following assumptions for femtocell user $i \in \mathcal{N} \setminus \{0\}$.

AS 7. *For the ith user, given fixed p_i, its utility $U_i(p_i, \gamma_i|\mathbf{p}_{-i})$ is a* monotonically increasing concave upward *function of its SINR γ_i.*

AS 8. *For the ith user, given fixed γ_i, the utility $U_i(p_i, \gamma_i|\mathbf{p}_{-i})$ is a* monotonically decreasing concave downward *function of its transmit power p_i.*

Assumption 7 models declining satisfaction (marginal utility) obtained by user i, once its current SINR γ_i exceeds Γ_i. Assumption 8 models increased penalty incurred by user i for causing more interference. Under assumptions 7 and 8:

$$\frac{\partial U_i}{\partial \gamma_i} > 0 \Rightarrow \frac{\mathrm{d}R}{\mathrm{d}\gamma_i} > 0 \qquad \frac{\partial U_i}{\partial p_i} < 0 \Rightarrow \frac{\mathrm{d}C}{\mathrm{d}p_i} < 0 \tag{4.29}$$

$$\frac{\partial^2 U_i}{\partial \gamma_i^2} < 0 \Rightarrow \frac{\mathrm{d}^2 R}{\mathrm{d}\gamma_i^2} < 0 \qquad \frac{\partial^2 U_i}{\partial p_i^2} < 0 \Rightarrow \frac{\mathrm{d}^2 C}{\mathrm{d}p_i^2} \leq 0 \tag{4.30}$$

Taking the second-order total derivative of U_i w.r.t p_i and applying (4.30),

$$\frac{\mathrm{d}^2 U_i}{\mathrm{d}p_i^2} = \frac{\mathrm{d}^2 R(\gamma_i, \Gamma_i)}{\mathrm{d}\gamma_i^2} \left(\frac{g_{ii}}{I_i(\mathbf{p}_{-i})} \right)^2 + \frac{b_i}{I_i(\mathbf{p}_{-i})} \frac{\mathrm{d}^2 C(p_i, \mathbf{p}_{-i})}{\mathrm{d}p_i^2} < 0 \tag{4.31}$$

This suggests that given interferer powers $\mathbf{p}_{-i}$, the femtocell utility function U_i at B_i is *strictly concave* with respect to the user i's transmission power p_i.

Assume that each femtocell individually maximizes its utility $U(p_i, \gamma_i|\mathbf{p}_{-i})$ as a best response to the cellular user and neighboring femtocell users' transmit powers $\mathbf{p}_{-i}$. The problem statement is given as

$$\max_{0 \leq p_i \leq p_{\max}} U_i(p_i, \gamma_i|\mathbf{p}_{-i}) = \max_{0 \leq p_i \leq p_{\max}} \left[R(\gamma_i, \Gamma_i) + b_i \frac{C(p_i, \mathbf{p}_{-i})}{I_i(\mathbf{p}_{-i})} \right]. \tag{4.32}$$

4.4.3 Existence of Nash Equilibrium

Observe that for all $i \in \mathcal{N}$, U_i is continuous in $\mathbf{p}$ and U_i is strictly concave w.r.t p_i from (4.31) over a convex, compact set $[0, p_{\max}]$. We now employ the following theorem from Glicksberg [55], Rosen [120] and Debreu [38]:

Theorem 8. A Nash equilibrium exists in game $G = [\mathcal{N}, \{P_i\}, \{U_i(.)\}]$ if, for all $i = 0, 1, \ldots, N$,

1. P_i is a nonempty, convex and compact subset of some Euclidean space $\mathbb{R}^{N+1}$.

2. $U_i(\mathbf{p})$ is continuous in $\mathbf{p}$ and quasi-concave in p_i.

Following Theorem 8, the optimization problems in (4.27) and (4.32) have a Nash Equilibrium. The following theorem derives the SINR equilibria at each femtocell.

Theorem 9. *The SINR Nash equilibrium at femtocell BS $B_i, i \in \mathcal{N} \setminus 0$ equals $\gamma_i^* = p_i^* g_{i,i}/I_i(\mathbf{p}_{-i}^*)$, where p_i^* is given as*

$$p_i^* = \min\left\{\left[\frac{I_i(\mathbf{p}_{-i}^*)}{g_{i,i}} f_i^{-1}\left(-\frac{b_i}{g_{i,i}}\frac{\mathrm{d}C}{\mathrm{d}p_i}\right)\right]^+, p_{max}\right\} \text{ and } f_i(x) \triangleq \left[\frac{\mathrm{d}R(\gamma_i, \Gamma_i)}{\mathrm{d}\gamma_i}\right]_{\gamma_i = x}. \tag{4.33}$$

Proof. See Appendix B.1. □

4.4.3.1 Femtocell Utility Selection

Assume the $R(\gamma_i, \Gamma_i)$ and $C(p_i, \mathbf{p}_{-i})$ in (4.28) as shown below.

$$R(\gamma_i, \Gamma_i) = 1 - e^{-a_i(\gamma_i - \Gamma_i)}, \gamma_i \geq 0,\ C(p_i, \mathbf{p}_{-i}) = -p_i g_{0,i}. \tag{4.34}$$

The exponential reward intuitively models femtocell users' desire for higher SINRs relative to their minimum SINR target. The linear cost $C(p_i, \mathbf{p}_{-i}) = -p_i g_{0i}$ discourages femtocell user i from decreasing the cellular SINR by transmitting at high power.

Assuming $a_i, b_i \neq 0$, it can be verified that the above choice of $R(\gamma_i, \Gamma_i)$ and $C(p_i, \mathbf{p}_{-i})$ satisfies the conditions outlined in (4.29) and (4.30).

$$\frac{\mathrm{d}R}{\mathrm{d}\gamma_i} = a_i e^{-a_i(\gamma_i - \Gamma_i)} > 0 \qquad \frac{b_i}{I_i(\mathbf{p}_{-i})}\frac{\mathrm{d}C}{\mathrm{d}p_i} = -\frac{b_i g_{0,i}}{I_i(\mathbf{p}_{-i})} < 0 \tag{4.35}$$

$$\frac{\mathrm{d}^2R}{\mathrm{d}\gamma_i^2} = -a_i^2 e^{-a_i(\gamma_i - \Gamma_i)} < 0 \qquad \frac{b_i}{I_i(\mathbf{p}_{-i})}\frac{\mathrm{d}^2C}{\mathrm{d}p_i^2} = 0 \tag{4.36}$$

Lemma 6. *With the utility-based cellular SINR adaptation [resp. femtocell SINR adaptation] in* (4.27) *[resp.* (4.32) *with reward-cost functions in* (4.34)*], the unique SINR equilibria at BS $B_i, i \in \mathcal{N}$ are given as $\gamma_i^* = \frac{p_i^* g_{ii}}{I_i(\mathbf{p}_{-i})}$ where p_i^* is given as*

$$\textit{Femtocell User}: p_i^* = \min\left\{\frac{I_i(\mathbf{p}_{-i}^*)}{g_{i,i}}\left[\Gamma_i + \frac{1}{a_i}\ln\left(\frac{a_i g_{i,i}}{b_i g_{0,i}}\right)\right]^+, p_{max}\right\}. \tag{4.37}$$

$$\textit{Cellular User}: p_0^* = \min\left\{\frac{I_0(\mathbf{p}_{-0}^*)}{g_{0,0}}\Gamma_0, p_{max}\right\}. \tag{4.38}$$

Proof. See Appendix B.2. □

In a practical tiered cellular deployment, (B.5) can be implemented in a distributed fashion since each femtocell user i only needs to know its own target SINR Γ_i and its channel gain to B_0 and B_i given as g_{0i} and g_{ii} respectively. Estimating $g_{0,i}$ at femtocell B_i may require site specific knowledge [32]. Possibly, femtocells would infer their locations using indoor GPS, or even estimate the path losses from the macrocell downlink signal in a TDD system (assuming reciprocity).

Remark 7. *Given equal minimum SINR targets at all femtocells and assuming identical coefficients in the utility functions ($a_i = a, b_i = b\ \forall i \in \mathcal{N} \setminus \{0\}$), femtocell users with higher $g_{i,i}/g_{0,i}$ (or a higher received signal strength relative to cross-tier macrocell interference) obtain a higher relative improvement in their SINR equilibria.*

The choice of the coefficients a_i and b_i entails careful consideration of the trade-offs between the femtocell users' desire to maximize their own data rates and

the relative importance of satisfying the cellular users' QoS requirement. The Nash equilibrium defined in (B.3) has the following properties.

1. For large a_i ($a_i \to \infty$), the equilibria $\gamma_i^* \to \Gamma_i$. This corresponds to hotspot users with *little inclination* to exceed their minimum rate requirement (e.g. voice users). In such a case, (B.5) is equivalent to the Foschini-Miljanic (FM) algorithm $p_i^{(k+1)} = \min\left\{p_i^{(k)} \frac{\Gamma_i}{\gamma_i^{(k)}}, p_{\max}\right\}$ [46, 59].

2. If a_i is chosen such that $a_i g_{i,i} < b_i g_{0,i}$, the hotspot users' SINR equilibria are lesser than their minimum target Γ_i, because they pay a greater penalty for causing cross-tier macrocell interference.

3. Choosing $a_i < 1$ and $\frac{a_i}{b_i} \gg 1$ increases the importance provided to the reward function relative to the cost function at each femtocell. Indeed, taking the derivative of $\frac{1}{a_i} \ln\left(\frac{a_i g_{i,i}}{b_i g_{0,i}}\right)$ w.r.t a_i yields

$$\frac{\mathrm{d}}{\mathrm{d}a_i}\left[\frac{1}{a_i}\ln\left(\frac{a_i g_{i,i}}{b_i g_{0,i}}\right)\right] = \frac{1}{a_i^2}\left(1 - \ln\left(\frac{a_i g_{i,i}}{b_i g_{0,i}}\right)\right) > 0 \ \forall \frac{a_i g_{i,i}}{b_i g_{0,i}} < e = 2.71828\ldots \tag{4.39}$$

   Therefore, the highest gains over the minimum SINR target Γ_i are obtained when $a_i g_{i,i} = e b_i g_{0,i}$. Such a choice is not necessarily preferable since the potentially large cross-tier interference from femtocells may result in $\gamma_0^* < \Gamma_0$.

4.4.4 Reducing Femtocell SINR Targets : Cellular Link Quality Protection

Whenever the cellular SINR target Γ_0 is infeasible, user 0 transmits with maximum power according to (B.6). Assume, after the Mth iterate (assuming large M), user 0's SINR $\gamma_0^{(M)} < (1-\epsilon)\Gamma_0$ where ϵ is a pre-specified SINR tolerance for the cellular user.

$$(1-\epsilon)\Gamma_0 > \gamma_0^{(M)} = \frac{p_{\max} g_{0,0}}{\sum_{i=1}^{N} p_i^{(M)} g_{0,i} + \sigma^2}. \tag{4.40}$$

For guaranteeing that user 0 achieves its SINR target within its tolerance, that is $\gamma_0^{(M)} \geq (1-\epsilon)\Gamma_0$, we propose that a femtocell subset $\Pi \subseteq \{B_1, B_2, \ldots, B_N\}$ reduce their SINR equilibria in (B.3) by a factor $t > 1$. A centralized selection of t ensures

$$(1-\epsilon)\Gamma_0 \leq \frac{p_{\max} g_{0,0}}{\frac{1}{t} \sum\limits_{i:B_i \in \Pi} p_i^{(M)} g_{0,i} + \sum\limits_{j:B_j \in \Pi^C} p_j^{(M)} g_{0,j} + \sigma^2} \tag{4.41}$$

where Π^C denotes the set complement of Π. Combining (4.40) & (4.41), a sufficient condition to obtain $\gamma_0 \geq \Gamma_0$ at B_0 is that there exists $t > 1$ and $\Pi \subseteq \{B_1, B_2, \ldots, B_N\}$ such that

$$\left(1 - \frac{1}{t}\right) \sum_{i:B_i \in \Pi} p_i^{(M)} g_{0,i} \geq p_{\max} g_{0,0} \left(\frac{1}{\gamma_0^{(M)}} - \frac{1}{(1-\epsilon)\Gamma_0} \right). \tag{4.42}$$

In (4.42), whenever $\Pi_1 \subseteq \Pi_2 \subseteq \{B_1, \ldots B_N\}$, then $t_{\Pi_1} \geq t_{\Pi_2}$. That is, choosing an expanding set of femtocell BSs to reduce their SINR targets requires a monotonically decreasing SINR reduction factor for each femtocell. Further, if reducing SINR targets inside a femtocell set Π_1 does not achieve Γ_0 at B_0, then a bigger femtocell set $\Pi_2 \supset \Pi_1$ should be chosen. Centralized selection of t and Π may be practically hard especially in two-tier networks employing OFDMA because the macrocell BS may need to communicate the t's and Π sets for each frequency sub band. A simpler strategy is to distributively adapt the femtocell SINR targets based on periodic feedback from the macrocell BS.

AS 9. *Following every Mth update in* (B.5)*, an SINR status feedback occurs from B_0 to B_i's whether $\gamma_0^{(M)} < (1-\epsilon)\Gamma_0$.*

Given M iterative updates, define the set $\Pi_{(M)}$ [resp. its complement $\Pi^c_{(M)}$] as the *dominant [resp. non-dominant] interferer* set, consisting of femtocells whose interference at B_0 individually exceeds [resp. below] a threshold $y > 0$. Mathematically, $\Pi_{(M)}(y) \triangleq \{B_i : p_i^{(M)} g_{0,i} > y\}$. Whenever femtocell user i determines that $B_i \in \Pi(y)$, it scales down its SINR target γ_i^* in (B.3) by $t > 1$. Denoting the set

cardinality by $|X|$, the above selection chooses the $|\Pi(y)|$ strongest femtocell interferers for reducing their transmit powers. Periodically decreasing y by a factor δy after every M iterations increases $|\Pi(y)|$. Specifically, for all $j \geq i$, choosing $y_{Mj} \leq y_{Mi}$ ensures that $\Pi_{Mj} \supseteq \Pi_{Mi}$. Given a tolerance ϵ, the SINR reduction procedure is repeated after every M updates until the cellular user's SINR is greater than $(1-\epsilon)\Gamma_0$. See Algorithm 1 for the pseudocode. Table 4.1 shows the algorithm performance in a practical scenario of a macrocell overlaid with 16 femtocells.

Algorithm 1 Maintain Cellular Link Quality at Macrocell BS B_0

repeat
  Initialize $k \leftarrow 1, \mathbf{p} \leftarrow \mathbf{p}_{\max}$ {Initialize iteration count and TX powers.}
  while $k \leq$ `MAXITER` **do**
    Cellular user 0 adapts transmission power according to $p_0^{(k+1)} = \min\left\{\frac{\Gamma_0}{\gamma_0^{(k)}} p_0^{(k)}, p_{\max}\right\}$
    For all $i = 1, 2, \ldots, N$, femtocell user i adapts transmit power according to $p_i^{(k+1)} = \min\left\{\frac{p_i^{(k)}}{\gamma_i^{(k)}}\gamma_i^*, p_{\max}\right\}$ where $\gamma_i^* \triangleq \left[\Gamma_i + \frac{1}{a_i}\ln\left(\frac{a_i g_{i,i}}{b_i g_{0,i}}\right)\right]^+$
    $k \Leftarrow k+1$
  end while
  Macrocell B_0 broadcasts status indicator `flag` $= \mathbf{1}[\gamma_0^* \geq (1-\epsilon)\Gamma_0]$ to all femtocells where $\epsilon \in [0,1]$ is a pre-specified tolerance.
  if `flag` $== 0$ **then**
    $\{g_{0,i}$ is channel gain from B_i to $B_0\}$
    Form status indicator at femtocell B_i: $\texttt{flag}_i = \mathbf{1}(p_i^* g_{0,i} > y)$, where $y > 0$
    if $\texttt{flag}_i == 1$ **then**
      {Reduce reduce γ_i^* since femtocell user i causes excessive cross-tier Interference.}
      SINR Target Update: $\gamma_{i,\text{dB}}^* \Leftarrow \gamma_{i,\text{dB}}^* - t_{\text{dB}}$, where $t > 1$
    end if
    $y \Leftarrow y/\delta y$ {Induce more femtocell users to lower SINR Target.}
  end if{Check if cellular user 0's SINR is within $(1-\epsilon)\Gamma_0$}
until `flag` $== 1$

Provided the SINR at B_0 equals $(1-\epsilon)\Gamma_0$, the *mean femtocell dB SINR* $\langle\gamma_{dB}^*\rangle$, the *average percentage of degraded femtocells* $\langle N\rangle$ and the *average percentage dB SINR*

Table 4.1: Example: Link quality protection for a cellular user (row 2) with $N = 16$ femtocells

User i	$\mathbf{D}_{0,i}/\mathbf{R}$	**dB Target** $\mathbf{\Gamma}$	$\mathbf{\Gamma}^*_M$ (dB)	$\mathbf{\Gamma}^*_{19M}$ (dB)	$\mathbf{p}^*_{19M}$ (dBm)
0	0.1000	**21.0034**	7.8979	**20.1932**	30.0000
1	0.2915	**25.3945**	25.5374	**23.9538**	0.4138
2	0.1716	**27.8943**	27.9605	**21.6260**	3.1487
3	0.1716	**22.6351**	22.8535	**18.1027**	−0.2808
4	0.2915	**27.1217**	27.2182	**24.8428**	1.4084
5	0.2506	14.0872	15.6355	14.8437	−3.6491
6	0.0850	**14.4560**	15.3847	**5.8830**	1.3216
7	0.0850	**28.3470**	28.3891	**15.7201**	11.1628
8	0.2506	**25.7148**	25.8408	**21.8818**	3.5317
9	0.3100	**17.9488**	18.7032	**17.9114**	−0.5868
10	0.2014	**8.4026**	12.3111	**7.5602**	3.0034
11	0.2014	**28.3375**	28.4014	**19.6914**	15.1274
12	0.3100	12.3944	14.6515	14.6515	−3.5588
13	0.4301	8.6965	13.1272	13.1272	−10.4070
14	0.3598	**19.4412**	20.0152	**19.2234**	0.7828
15	0.3598	**20.3513**	20.8225	**20.0306**	1.7930
16	0.4301	26.7008	26.8211	26.8211	3.4629

User 0 designates cellular user. Users 1 through 16 represent femtocell users.
Bold faced entries designate users unable to meet their SINR target.
Initial spectral radius $\rho(\mathbf{\Gamma G}) = 4.4391$
Final spectral radius $\rho(\mathbf{\Gamma}^*_{19M}\mathbf{G}) = 0.9999$ (M=1000 iterations/update)

degradation $\langle\Delta(\gamma^*)\rangle$ at femtocells (assuming zero SINR degradation at femtocells with $\gamma_i^* \geq \Gamma_i$) are given as

$$\begin{aligned}
\langle\gamma_{\text{dB}}^*\rangle &= \frac{1}{N}\sum_{i=1}^{N} 10\log_{10}\gamma_i^* \\
\langle|\Pi|\rangle &= \frac{1}{N}\left|\{B_i \in \Pi : \gamma_i^{(M)} < \Gamma_i\}\right| \\
\langle\Delta(\gamma^*)\rangle &= \left[\frac{1}{N}\sum_{B_i\in\Pi:\gamma_i^{(M)}<\Gamma_i} \frac{10\log_{10}\Gamma_i - 10\log_{10}\gamma_i^{(M)}}{10\log_{10}\Gamma_i}\right].
\end{aligned} \tag{4.43}$$

4.5 Numerical Results

In this section, we present numerical results based on two experiments with the system parameters in Table 4.2 and the setup in Section 4.3.1.

Table 4.2: System Parameters

Variable	**Parameter**	**Sim. Value**
R_c	Macrocell Radius	1000 m
R_f	Femtocell Radius	30 m
D_{grid}	Grid size	500 m
f	Carrier Frequency f_{Mhz}	2000 MHz
$p_{\max}$	Max. Transmission Power per Mobile	1 Watt
$\Gamma_{c,\min}, \Gamma_{c,\max}$	Max. and Min. Cellular SINR target	$3, 10$ dB
$\Gamma_{f,\min}, \Gamma_{f,\max}$	Max. and Min. Femtocell SINR target	$5, 25$ dB
K_{fi}	Indoor Loss	37 dB
W	Partition Loss	$5, 10$ dB
α, β	Outdoor and Indoor path loss exponents	$4, 3$
t_{dB}	Femtocell SINR target reduction	0.8 dB
δy	Interference threshold reduction	3 dB

The AWGN power σ^2 in (4.1) was determined assuming a cell-edge user obtains a cellular SNR equaling 20 dB at B_0 employing maximum transmission power. Results are reported for 5000 different SINR trials in each experiment. The minimum femtocell SINR targets were randomly selected (uniform distribution) in the

interval $[\Gamma_{f,\min}, \Gamma_{f,\max}]$ dB. In any given trial, if the generated set of minimum SINR targets $\mathbf{\Gamma}_f$ resulted in $\rho(\mathbf{\Gamma}_f\mathbf{F}) > 1$ in (4.6), then our experiments scaled $\mathbf{\Gamma}_f$ by a factor $\rho(\mathbf{\Gamma}_f\mathbf{F})(1 + 10^{-3})$ for ensuring feasible femtocell SINR targets.

The first experiment obtains the improvements in femtocell SINRs relative to their minimum SINR targets with our proposed SINR adaptation. A cell-edge location of the cellular user ($D = 0.9$) and the femtocell grid ($D_F = 0.9$) is considered. To maximize the chance of obtaining a feasible set of $(N + 1)$ SINRs, the cellular SINR target Γ_0 is equal to either its minimum target $\Gamma_{c,\min} = 3$ dB, or scaling its highest obtainable target in (4.8) by $\Delta_{c,\text{dB}} = 5$ dB (which ever is larger) and given as

$$\Gamma_0 = \max\left\{\Gamma_{c,\min}, \frac{1}{\Delta_c}\frac{\kappa^2}{\mathbf{q}_c^T[\mathbf{I} - (\mathbf{\Gamma}_f/\kappa)\mathbf{F}]^{-1}\mathbf{\Gamma}_f\mathbf{q}_f}\right\}. \tag{4.44}$$

Assuming $a_i = a$ and $b_i = b$ $\forall i \geq 1$ in (B.3), Fig. 4.6 plots the mean decibel femtocell SINRs ($D = D_f = 0.9$) in (4.43) for different a and b values. Selecting $a < 1$ models femtocell users seeking a greater SINR reward relative to their minimum SINR target. With $a = 0.1, b = 1$ and $N = 64$ femtocells, there is a nearly 30 % improvement in mean femtocell SINRs relative to their average minimum SINR target. With a higher interference penalty at femtocells ($b = 1$), our utility adaptation yields a nearly 2 dB improvement in mean femtocell SINRs above their mean SINR target. When $a >> 1$, femtocell users have little inclination to exceed their minimum SINR targets. In fact, with $N \geq 64$ femtocells, the mean equilibrium femtocell SINRs are *below the mean SINR target* because femtocell users turn down their transmit powers to improve the cellular link quality.

The second experiment considers randomly selected decibel cellular SINR targets chosen uniformly in the interval $[\Gamma_{c,\min}, \Gamma_{c,\max}]$ dB. All femtocells selected identical coefficients $a_i = b_i = 1$ in in (B.3). Femtocells scaled down their SINR targets in (B.5) until the cellular user 0 approached within 95% of its minimum SINR target.

Fig. 4.7 shows the average femtocell decibel SINRs $\langle\gamma^*_{\text{dB}}\rangle$ using the distributed power control in (B.5)-(B.6) and cellular link quality protection. The black dotted

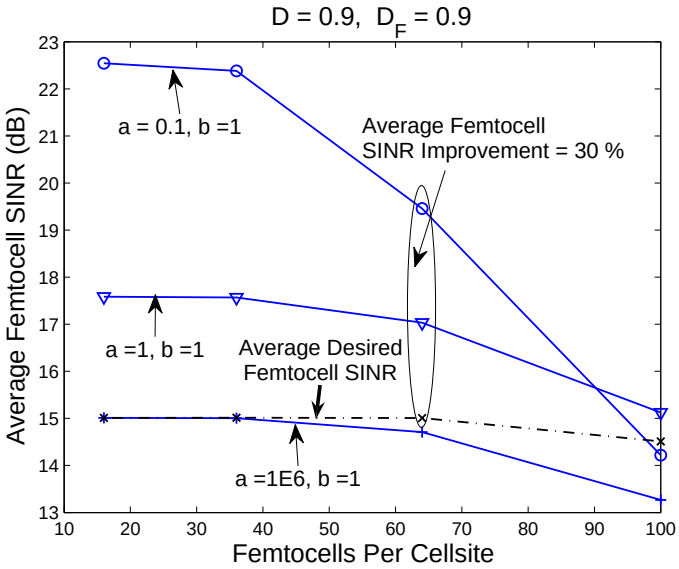

Figure 4.6: Mean femtocell SINR targets (grid center at cell-edge) for different reward and cost coefficients.

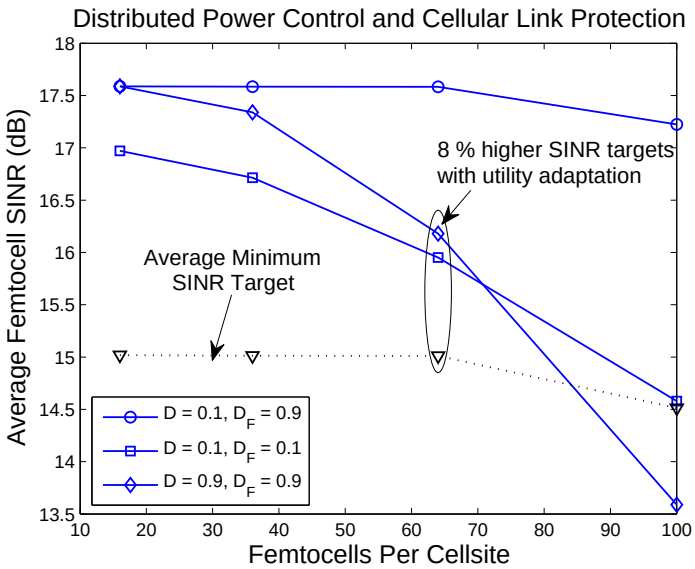

Figure 4.7: Mean femtocell SINR targets with distributed power control and cellular link quality protection.

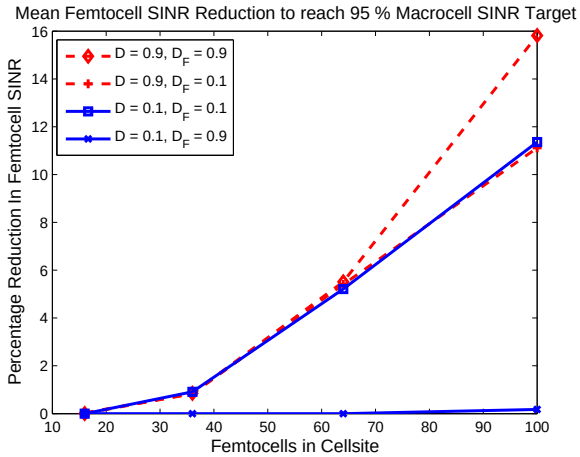

(a) Mean Percentage SINR Reduction at Femtocells

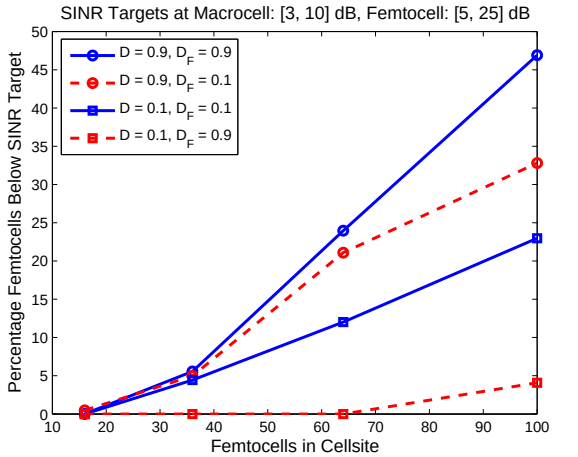

(b) Average percentage of femtocells below their SINR target

Figure 4.8: Femtocell SINR reduction when cellular SINR target is uniformly distributed in $[3, 10]$ dB, and initial femtocell SINR targets are uniformly distributed in $[5, 25]$ dB

lines plot the average minimum decibel femtocell SINR target given as $10\log_{10}(\sqrt{\Gamma_{f,\min}\Gamma_{f,\max}})$. With $N = 64$ femtocells, a nearly 8% SINR improvement is obtained with a cell-edge location of the cellular user and femtocell APs.

Figs. 4.8(a)-4.8(b) plot the mean percentage reduction in femtocell SINRs $\langle\Delta(\gamma^*)\rangle$ and the mean percentage of "degraded" femtocells $\langle|\Pi|\rangle$ in (4.43). With $N = 100$ femtocells and a cell-edge location ($D = 0.9, D_F = 0.9$), although Fig. 4.8(b) shows that nearly 45% of femtocells operate below their minimum SINR target, the worst-case femtocell SINR reduction at femtocells is only 16% [Fig. 4.8(a)]. In all other cases, the mean percentage SINR reduction is less than 6%. This shows that our cellular link quality protection algorithm guarantees reliable cellular coverage without significantly affecting femtocell SINR targets.

4.6 Conclusion

Cellular operators will obtain better spectral usage and reduced costs by deploying macrocell and femtocell users in a shared region of spectrum. Our work has addressed three related questions. The first is that of determining the radio link quality for a cellular user, given a set of N transmitting femtocells with different SINR targets. The takeaway is that achieving higher SINR targets in one tier fundamentally constricts the highest SINRs obtainable in the other tier. The reason is because of near-far effects caused by the asymmetric positions of interfering users w.r.t nearby BSs. The second and third questions seek to determine femtocell data rates when home users perform utility-based SINR adaptation; providing link quality protection to an active cellular user may necessitate femtocells to deliberately lower their SINR targets. We provide a link quality protection algorithm for progressively reducing the SINR targets at strong femtocell interferers when a cellular user is unable to meet its SINR target. Simulation results confirm the efficacy of the proposed algorithm and its minimal impact (worst case femtocell SINR reduction of only 16%) on femtocell SINRs. Being distributed, the power control algorithm ensures minimal network

overhead in a practical two-tier deployment.

The next chapter extends the analytical framework in Chapters 3-4 to account for multi-antenna transmission at either tier. Specifically, we determine how exploiting the additional spatial degrees of freedom provided using multi-antenna transmission improves coverage and alleviates the near-far effect in a two-tier cellular network.

Chapter 5

Coverage in Multi-Antenna Two-Tier Networks

5.1 Introduction

In two-tier networks with universal frequency reuse, the near-far effect from cross-tier interference creates dead spots where reliable coverage cannot be guaranteed to users in either tier. Employing multiple antenna transmission at the macrocell and femtocells provides independent and spatially distinct copies of the transmitted signal, thereby providing increased spatial reuse and increased robustness against near-far effects at the user terminal. This chapter considers how multi-antenna transmission influences the coverage and spatial reuse in a two-tier network with universal frequency reuse. Two transmission strategies namely single user (SU) multiple antenna transmission and multiple user (MU) multiple antenna transmission schemes are considered. We derive per-tier coverage zones wherein cross-tier interference bottlenecks cellular and hotspot coverage. A decentralized carrier-sensing approach is presented for regulating hotspot transmit powers based on their location.

5.2 Background on Multi-Antenna Transmission

Using multiple antennas (MIMO) at the transmitter and receiver exploits the rich spatial diversity offered by the wireless channel to obtain robustness and increased wireless capacity. MIMO enables simultaneous transmission of multiple data streams – spatial multiplexing (SM) – providing a linear increase in capacity with the number of antennas [47, 137]. Alternatively, MIMO can improve robustness by exploiting transmit or receive diversity, with or without channel state information at

the transmitter (CSIT) [6, 111, 115]. In point-to-point MIMO, practical adaptation schemes have been proposed for alternating between SM and diversity based on, but not restricted to, the current channel condition (see [24, 70, 71] and the references therein) and the spatial selectivity of the wireless channel [43, 44].

In point-to-point MIMO with full channel state information (CSI) – both the transmitter and receiver have full channel knowledge – the channel capacity scales as $\min(M, N)$ [137], where M is the number of transmit antennas and N is the number of receive antennas. Rather surprisingly, at high Signal-to-Noise Ratio (SNR), an identical scaling occurs with CSI at the receiver only. Since this scaling behavior occurs even for small M, N – as long as the channel can be estimated accurately at the receiver– MIMO has found widespread appeal in 4G wireless standards such as 3GPP's LTE and WiMAX (IEEE 802.16e).

In point-to-multipoint systems (broadcast channel), the multiplexing gain – defined as the quantity $\lim_{P\to\infty} \frac{C_{\text{sum}}}{\log_2 P}$ – characterizes the scaling behavior of the sum capacity C_{sum} at high SNR. Given M transmit antennas at the BS, N receive antennas and n users and assuming CSIT, prior works have shown that a multiplexing gain of $\min(M, \max(N, n))$ can be provided [69, 82]. Assuming $N < M$, the high SNR capacity can therefore scale linearly with the number of transmit antennas at the BS, if the number of users is made larger than M (as is typically the case).

The sum capacity of the MIMO broadcast channel is achieved using a Dirty-Paper Coding (DPC) transmission strategy [145]. Although optimal, DPC transmission requires high complexity and therefore hard to implement in practical wireless systems employing MIMO. This has motivated the use of linear MIMO transmit/receive processing techniques [83, 116] – such as zero-forcing (ZF), Minimum Mean Squared Error (MMSE) precoding – that incur low complexity while asymptotically providing the same multiplexing gain as DPC transmission.

Considering the effects of a imperfect channel information at the BS, works by [83, 164] show that even with just one base-station (no out of cell interference),

multi-user MIMO using linear ZF precoding lose their spatial multiplexing gain with a fixed number of feedback bits and/or feedback delay. With multiple base-stations, the limited number of antennas at the user terminal causes the performance of either SM or multi-user transmission schemes to deteriorate in the presence of other cell interference (OCI) [11, 23]. This degradation is due to the increased dimensionality of the received signal, which necessitates providing robustness against OCI with the available degrees of freedom [11].

Addressing OCI in multicellular systems through base-station cooperation has been the subject of intense research. Coordinated BS processing schemes using block-diagonalization (BD) techniques have been proposed in [34, 45, 88, 133, 162]. By jointly designing a linear preprocessing filter among cooperating BSs, BD transmission provides an interference-free channel to each individual user. The drawback is that BD transmission requires complete channel information at each BS regarding the channel gains between all other BSs and their respective users. To circumvent this, research in network-MIMO [19, 163] propose clustered BS cooperation, which only require local channel knowledge within each group of cooperating BSs. In spite of BS clustering, the complexity of such schemes is still daunting because of the network overhead for exchanging channel information between BSs.

In a tiered cellular network with universal frequency reuse, because of the potential proximity of femtocells to a cellular user, cross-tier femtocell interference is likely to be more severe in comparison to OCI in conventional cellular systems. Due to reasons of scalability and limited availability of backhaul bandwidth, there will be little or zero coordination between the macrocell and femtocell BSs. Consequently, centralized BS cooperation – consequently employing DPC, block diagonalization and other sophisticated transmission schemes – will likely be difficult, if not impossible to implement in a two-tier network. Considering multi-antenna transmission at either tier, this work instead proposes a decentralized carrier-sensing approach to regulate femtocell transmit powers and minimize hotspot interference at cellular users.

5.3 Problem Definition

The motivation behind this work is to understand how the available degrees of freedom from multiple antenna transmission influences coverage and spatial reuse in a two-tier network with universal frequency reuse [31]. We consider both single-user (SU) multiple antenna (SU) transmission and multiuser (MU) multiple antenna transmission employed by the macrocell base-station (BS) and femtocell APs. Array gain resulting from SU transmission (Fig. 5.1) provides robustness against cross-tier interference. Multiuser transmission, on the other hand, increases the number of simultaneous transmissions (Fig. 5.2) at the expense of reduced signal strength per user terminal.

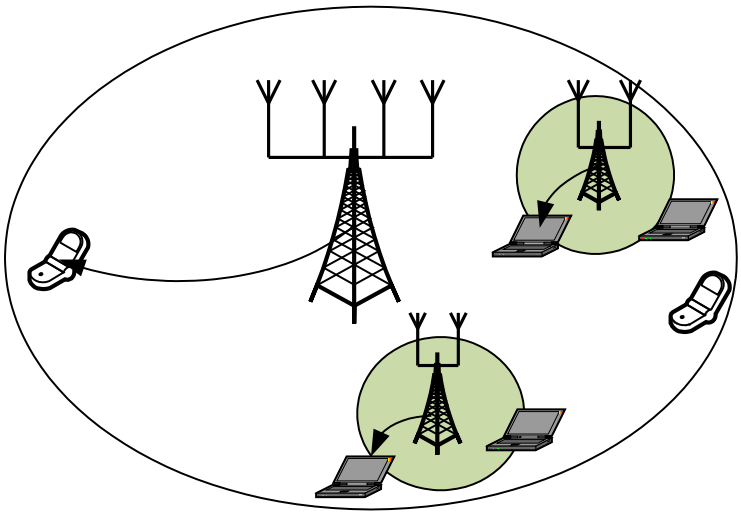

Figure 5.1: Single user multiple antenna transmission

Given a multiple antenna transmission strategy (SU or MU), let λ_f denote the maximum density (in femtocells per square meter) of simultaneously transmitting femtocells – denoted as the *maximum femtocell contention density* – that guarantees a certain minimum per-tier QoS requirement. Given a certain minimum per-tier target SIR equaling Γ, the QoS requirement stipulates that the instantaneous SIR at

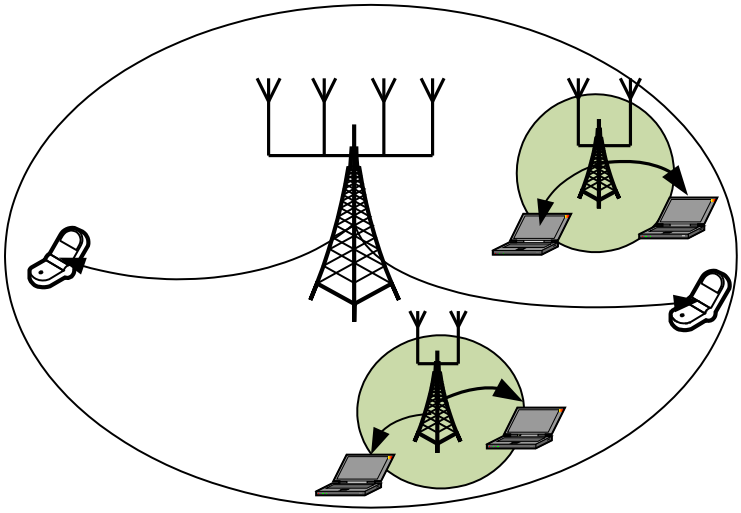

Figure 5.2: Multi-user multiple antenna transmission

each user should exceed Γ with a probability of at least $1 - \epsilon$, where ϵ is a design parameter. Since the signal power for a cellular user decays as $D^{-\alpha_c}$ (D being the distance from the macrocell BS and α_c is the outdoor path loss exponent), satisfying its QoS requirement requires λ_f to be a monotonically decreasing function of D. Conversely, satisfying the QoS requirement for a femtocell user at D necessitates λ_f to be monotonically decreasing as $D \to 0$.

This work characterizes near-far effects by defining two quantities of interest namely the *No-Coverage Femtocell Radius* and the *Cellular Coverage Radius*. The no-coverage femtocell radius D_f determines the minimum SIR feasible femtocell distance (Fig. 5.3) from the macrocell. Any femtocell user within $D < D_f$ meters from the macrocell experiences an outage probability greater than ϵ due to excessive cellular interference. This suggests that any user at $D < D_f$ should communicate with the macrocell because of its potentially higher cellular SIR. The cellular coverage radius D_c denotes the maximum SIR feasible distance (Fig. 5.4) from the macrocell BS up to which a cellular user can satisfy its outage probability constraint in the presence

of hotspot interference. Since there is no coordination between tiers for managing interference, providing greater spatial reuse using femtocells trades off the coverage radiuses and vice-versa. Because the cellular network serves as the primary network to mobile outdoor users, it is desirable to maximize D_c in the presence of hotspot interference.

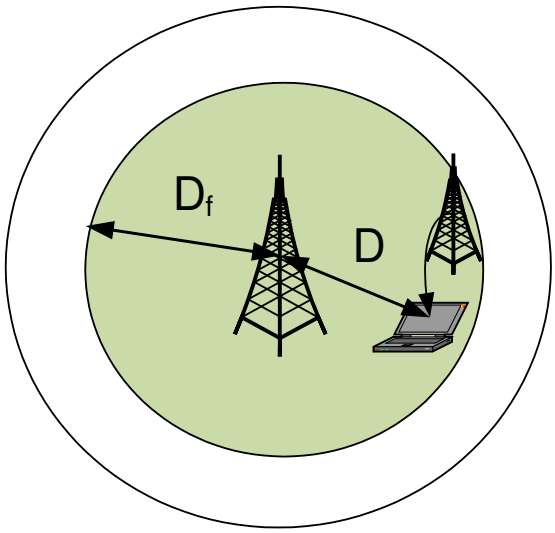

Figure 5.3: No-coverage femtocell radius D_f

Assuming that each tier employs either transmit beamforming (BF) [for SU transmission] or zero-forcing precoding [for MU transmission] with transmission powers P_c and P_f in each resource (eg. frequency sub-band), this work poses the following questions:

- What is the maximum femtocell contention density λ_f as a function of the location D with respect to (w.r.t) the macrocell, the ratio P_c/P_f, the transmission strategy (SU vs. MU transmission), the number of transmit antennas per macrocell and femtocell AP, the target per-tier SIR Γ, the maximum outage probability ϵ and the path loss exponents?

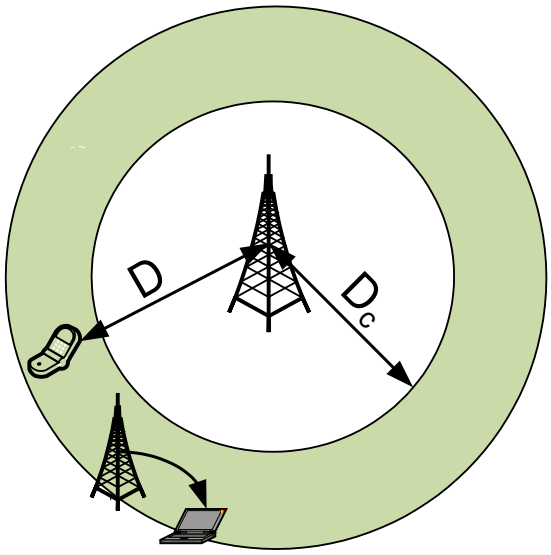

Figure 5.4: Cellular coverage radius D_c.

- Given an average of N_f transmitting femtocells per cell-site, how much cellular coverage can the macrocell provide to its users?
- How does the no-coverage femtocell radius vary with SU and MU femtocell transmission strategies?
- How should femtocells adapt their transmission power as a function of their location w.r.t the macrocell for ensuring that nearby cellular users satisfy their QoS requirements?

5.3.1 Related Works

The subject of this work is related to Huang *et al.* [75] which derives per-tier transmission capacities with spectrum underlay and spectrum overlay. In contrast to their work which assumes relay-assisted cell-edge users, our work proposes to improve coverage by regulating femtocell transmit powers. Hunter *et al.* [76] have derived transmission capacities in an *ad hoc* network with spatial diversity. Our work, in

contrast, derives the coverage loss from cross-tier interference in a cellular-underlaid *ad hoc* network with multi-antenna BSs. To the best of our knowledge, there is little related work addressing diversity performance in tiered networks (e.g [90] which proposes tilted antenna arrays to reduce cross-tier interference).

To overcome the near-far problem in femtocell networks, prior works have proposed hybrid femtocell frequency assignments [62], adjusting the maximum transmit power of femtocell users [86] and adaptive femtocell access [33]. Related works on cognitive radios (CR) include (but not restricted to) 1) analyzing sensing-throughput tradeoffs [104] for computing optimal sensing time by CR users and 2) limit transmit powers of CR users [53, 66, 74, 119]. The differentiating aspect of our work is a decentralized femtocell transmit power selection scheme which ensures a per-tier outage probability below a desired threshold.

5.3.2 Contributions

Given T_c antennas at the macrocell and T_f antennas at each femtocell, per-tier transmission powers equaling P_c at the macrocell and P_f at each femtocell, and path loss exponents given as α_c (from outdoor cellular transmission) and α_{fo} (from femtocell transmission to outdoor users and neighboring femtocells) respectively, our work provides the following contributions.

Coverage. We derive coverage zones wherein cross-tier interference prevents users in each tier from satisfying their QoS requirements. Single user macrocell transmission is shown to increase the cellular coverage radius by a factor T_c^{2/α_c} relative to MU transmission. Single-user femtocell transmission is shown to decrease the no-coverage femtocell radius D_f by a factor of $(T_f/\epsilon^{1-1/T_f})^{1/\alpha_c}$ relative to MU femtocell transmission. This suggests that the array gain provided by SU transmission results in superior coverage in either tier. Moreover, a femtocell located just a few meters outside the no-coverage zone can tolerate interference from greater than 100 hotspots

per cellsite. This suggests that femtocell performance is regulated by cellular interference and hotspot interference is negligible in comparison.

Hotspot Contention Density. We derive the maximum femtocell contention density $\lambda_f^*(D)$ at distance D from the macrocell BS. Two distinct operating regimes are shown namely a 1. Cellular-limited regime, wherein femtocell users are primarily affected by cellular interference and 2. Hotspot-limited regime wherein both cellular and hotspot users are affected by hotspot interference. Regime 1 determines the coverage provided to femtocell users, while Regime 2 determines $\lambda_f^*(D)$ and the cellular coverage radius. In Regime 2, SU macrocell transmission is shown to increase $\lambda_f^*(D)$ by a factor of $\mathbf{\Gamma}(1-2/\alpha_{fo})T_c^{4/\alpha_{fo}}$ (where $\mathbf{\Gamma}(z) \triangleq \int_0^\infty t^{z-1}e^{-t}\,\mathrm{d}t\ \forall \mathrm{Re}(t) > 0$ is the Gamma function) relative to MU transmission. Femtocells maximize their area spectral efficiency by choosing their transmission strategy depending on α_{fo}, with SU transmission being desirable with considerable hotspot interference ($\alpha_{fo} < 4$). This suggests that per-tier SU transmission is preferable from a spatial reuse perspective.

Power control. We propose a carrier-sensing approach in which a femtocell chooses its transmission power P_f in order to minimize hotspot interference and to ensure uniform cellular coverage. We derive lower and upper bounds for P_f depending on the femtocell location, the number of macrocell and femtocell antennas and the path loss exponents. We demonstrate that our strategy enables uniform cellular coverage with up to 60 femtocells per cell site (with typical cellular parameters).

5.4 System Model

Assume a central macrocell B_0 using T_c antennas to service a geographical region $\mathcal{C}$, assumed as a circular disc with radius R_c and area $|\mathcal{C}| = \pi R_c^2$. Each femtocell is equipped with T_f antennas. Femtocell users are located on the circumference of a disc of radius R_f centered at their femtocell AP. Both cellular users and femtocell users are assumed to be equipped with single-antenna receivers. In a given time/frequency

slot, each macrocell [resp. femtocell] employs its T_c [resp. T_f] antennas for serving $1 \leq U_c \leq T_c$ cellular [resp. $1 \leq U_f \leq T_f$ indoor] users. Although user selection has a potentially beneficial impact, it is not considered in this work for analytical tractability.

This work employs a stochastic geometry framework for modeling the random spatial distribution of the underlying femtocells. The randomly located femtocells are assumed to be distributed according to a Spatial Poisson Point Process (SPPP) Π_f (see [65, 91] for background, prior works include [14, 26, 48, 160]). Provided Π_f is a homogeneous SPPP (or the intensity λ_f in femtocells per square meter stays constant over $\mathcal{C}$), the average number of actively transmitting femtocells is readily obtained as $N_f = \lambda_f |\mathcal{C}|$ femtocells per cellsite. Because of near-far effects inherent to a two-tier network, the maximum hotspot intensity varies with the location D in the cell-site.

5.4.1 Terrestrial Path Loss Model

The signal decay encountered using terrestrial propagation to users in either tier is represented using a distance based path loss model. Temporal amplitude variations of the complex vector downlink channel are modeled as frequency-flat Rayleigh fading–e.g. each frequency sub-band in frequency division multiple access (FDMA) transmission–with individual complex entries distributed as $\mathcal{CN}(0, 1)$. For analytical simplicity, this work does not consider random lognormal shadow fading. Instead, we shall assume a fixed partition loss, based on Qualcomm's home BS propagation model [2], which accounts for wall losses encountered during outdoor-to-indoor and indoor-to-indoor propagation. Shown below, we use the IMT-2000 channel model [1, Page 26] for modeling indoor (derived from the COST231 indoor model [1, Page 44]) and outdoor path losses.

Macrocell to Cellular Users. The decibel path loss between B_0 and cellular user 0 is modeled as $\mathrm{PL}_{c,\mathrm{dB}} = A_{c,\mathrm{dB}} + 10\alpha_c \log_{10} D$ where α_c is the outdoor path loss exponent, $A_{c,\mathrm{dB}} = 30 \log_{10} f_c - 71$ represents the fixed decibel loss during outdoor

propagation, f_c is the carrier frequency in MHz and D is the distance between B_0 and its user.[1]

Macrocell to Femtocell Users. We model each femtocell as a point object, hence all indoor users served by a given femtocell experience identical path loss from cellular interference. This decibel path loss is given as $\mathrm{PL}_{f,c,\mathrm{dB}} = A_{f,c,\mathrm{dB}} + 10\alpha_c \log_{10}(D)$ where $A_{f,c,\mathrm{dB}} = 30\log_{10} f_c - 71 + W_{\mathrm{dB}}$ designates the fixed decibel path loss, D is the distance between B_0 and the femtocell and W_{dB} equals the decibel wall partition loss during outdoor-to-indoor wireless propagation.

Femtocell to Subscribed Home Users. The decibel path loss between a femtocell to its licensed, subscribed indoor users is modeled as $\mathrm{PL}_{fi,\mathrm{dB}} = A_{fi,\mathrm{dB}} + 10\alpha_{fi} \log_{10}(R_f)$ where $A_{fi,\mathrm{dB}} = 37$ dB models the fixed propagation loss in decibels between the femtocell to its desired user, α_{fi} represents the indoor path loss exponent. For analytical simplicity and modeling the worst-case scenario, we assume that indoor users are located on the edge of their respective femtocells.

Femtocell to Outdoor Cellular Users. Given a transmitting femtocell, any cellular user located at distance D will experience cross-tier interference with decibel path loss modeled as $\mathrm{PL}_{c,f\mathrm{dB}} = A_{c,f,\mathrm{dB}} + 10\alpha_{fo} \log_{10}(D)$. Here, the fixed decibel path loss is designated by $A_{c,f,\mathrm{dB}} = P_{\mathrm{dB}} + 37$, while α_{fo} denotes the path loss exponent during indoor-to-outdoor wireless propagation.

Femtocell to Neighboring Femtocells. The decibel path loss of the hotspot interference caused by a transmitting femtocell at another femtocell is given as $\mathrm{PL}_{f,f\mathrm{dB}} = A_{f,f,\mathrm{dB}} + 10\alpha_{fo} \log_{10}(D)$ where $A_{f,f,\mathrm{dB}} = 2W_{\mathrm{dB}} + 37$ denotes the fixed decibel path loss (the factor of 2 models the double wall partition loss during indoor to indoor propagation) and D is the distance between the two femtocells.

[1]Strictly speaking, the IMT-2000 pedestrian test model adopts a fixed path loss exponent $\alpha_c = 4$ (with path loss $\mathrm{PL}_{\mathrm{dB}} = 30\log_{10} f_c + 40\log_{10}(D) - 71$). To keep the analysis general, this work parameterizes the outdoor path loss exponent.

5.5 Per-Tier Signal-to-Interference Ratios

Assume that the macrocell B_0 serves $1 \leq U_c \leq T_c$ users. Define $\mathbf{h}_j \in \mathbb{C}^{T_c \times 1}$ as the channel from B_0 to cellular user $j \in \{0, 1, \ldots, U_c - 1\}$ with its entries distributed as $h_{k,j} \sim \mathcal{CN}(0, 1)$. The direction of each vector channel is represented as $\tilde{\mathbf{h}}_j \triangleq \frac{\mathbf{h}_j}{||\mathbf{h}_j||}$. Designate $\tilde{\mathbf{H}} = [\tilde{\mathbf{h}}_0,\ \tilde{\mathbf{h}}_1,\ \ldots,\ \tilde{\mathbf{h}}_{U_c-1}]^\dagger \in \mathbb{C}^{U_c \times T_c}$ as the concatenated matrix of channel directions, where the symbol † denotes conjugate transpose.

AS 10. *Perfect channel state information (CSI) is assumed at the central macrocell [resp. femtocells] regarding the channels to their own users.*

Although we acknowledge that imperfect channel estimation plays a potentially significant role, we defer its analysis for subsequent research and instead employ AS10 for analytical tractability.

AS 11. *For analytical tractability, cochannel Interference from neighboring cellular transmissions is ignored.*

This work assumes linear zero-forcing (ZF) precoding transmission because it has low complexity, yet achieves the same multiplexing gain as higher complexity schemes such as dirty-paper coding [83]. With ZF precoding transmission, macrocell BS B_0 chooses its precoding matrix $\mathbf{V} \in \mathbb{C}^{T_c \times U_c} = [\mathbf{v}_i]_{1 \leq i \leq U_c}$ as the normalized columns of the pseudoinverse $\tilde{\mathbf{H}}^\dagger(\tilde{\mathbf{H}}\tilde{\mathbf{H}}^\dagger)^{-1} \in \mathbb{C}^{T_c \times U_c}$. Similarly, each femtocell $F_j \in \Pi_F$ serves $1 \leq U_f \leq T_f$ users with the channel directions between F_j to its individual users represented as $\tilde{\mathbf{G}}_j^\dagger = [\tilde{\mathbf{g}_{0,j}},\ \tilde{\mathbf{g}_{1,j}},\ \ldots\ \tilde{\mathbf{g}}_{U_f-1,j}]$ and the entries of $\tilde{\mathbf{g}}_{k,j}$ distributed as $\mathcal{CN}(0, 1)$. With ZF precoding, the columns of the precoding matrix $\mathbf{W}_j = [\mathbf{w}_{j,i}]_{1 \leq i \leq U_f} \in \mathbb{C}^{T_f \times U_f}$ equal the normalized columns of $\tilde{\mathbf{G}_j}^\dagger(\tilde{\mathbf{G}_j}\tilde{\mathbf{G}_j}^\dagger)^{-1} \in \mathbb{C}^{T_f \times U_f}$.

5.5.1 SIR Analysis at a Femtocell User

Consider a reference femtocell F_0 at distance D from the macrocell B_0. During a given signaling interval, the received signal at user 0 at distance R_f w.r.t F_0 is given

as

$$y_0 = \underbrace{\sqrt{A_{fi}} R_f^{-\frac{\alpha_{fi}}{2}} \mathbf{g}_0^\dagger \mathbf{W}_0 \mathbf{r}_0}_{\text{Desired Signal}} + \sqrt{A_{f,f}} \underbrace{\sum_{F_j \in \Pi_f \setminus F_0} |X_{0,j}|^{-\frac{\alpha_{fo}}{2}} \mathbf{g}_{0,j}^\dagger \mathbf{W}_j \mathbf{r}_j}_{\text{Intra-tier Interference}}$$
$$+ \underbrace{\sqrt{A_{f,c}} D^{-\frac{\alpha_c}{2}} \mathbf{f}_0^\dagger \mathbf{V} \mathbf{s}}_{\text{Cross-tier Interference}} + \mathbf{n}$$

where the vectors $\mathbf{s} \in \mathbb{C}^{U_c \times 1}$ and $\mathbf{r}_j \in \mathbb{C}^{U_f \times 1}$ designate the transmit data symbols for users in B_0 and F_j, which satisfy $\mathbb{E}[|\mathbf{s}||^2] \leq P_c$ and $\mathbb{E}[||\mathbf{r}_j||^2] \leq P_f$ respectively (assuming equal power allocation) and $\mathbf{n}$ represents background noise. The term $\mathbf{f}_0 \in \mathbb{C}^{T_c \times 1}$ [resp. $\mathbf{g}_{0,j}$] designates the downlink vector channel from B_0 [resp. interfering femtocell F_j] to user 0. Neglecting receiver noise for analytical simplicity, the received SIR for user 0 is given as

$$\mathrm{SIR}_f(F_0, D) = \frac{\frac{P_f}{U_f} A_{fi} R_f^{-\alpha_{fi}} |\mathbf{g}_0^\dagger \mathbf{w}_{0,0}|^2}{\frac{P_c}{U_c} A_{f,c} D^{-\alpha_c} ||\mathbf{f}_0^\dagger \mathbf{V}||^2 + \frac{P_f}{U_f} A_{f,f} \sum_{F_j \in \Pi_f \setminus F_0} ||\mathbf{g}_{0,j}^\dagger \mathbf{W}_j||^2 |X_{0,j}|^{-\alpha_{fo}}}. \quad (5.1)$$

For successfully decoding the message intended for user 0, $\mathrm{SIR}_f(F_0, D)$ should be greater than equal to the minimum SIR target Γ. For clarity of exposition, we define

$$\mathcal{P}_f = \frac{P_c}{P_f} \frac{A_{f,c}}{A_{f,f}} D^{-\alpha_c}, \ \mathcal{Q}_f = \frac{A_{f,f}}{A_{fi}} R_f^{\alpha_{fi}} U_f. \quad (5.2)$$

User 0 can successfully decode its signal provided $\mathrm{SIR}_f(F_0, D)$ is at least equal to its minimum SIR target Γ. Combining (5.1) and (5.2), the probability of successful reception is given as

$$\mathbb{P}[\mathrm{SIR}_f(F_0, D) \geq \Gamma] =$$
$$\mathbb{P}\left[|\mathbf{g}_0^\dagger \mathbf{w}_{0,0}|^2 \geq \Gamma \mathcal{Q}_f \left(\frac{\mathcal{P}_f}{U_c} ||\mathbf{f}_0^\dagger \mathbf{V}||^2 + \frac{1}{U_f} \sum_{j \in \Pi_F} ||\mathbf{g}_{0,j}^\dagger \mathbf{W}_j||^2 |X_{0,j}|^{-\alpha_{fo}} \right) \right]. \quad (5.3)$$

$$\text{Let } \kappa = \frac{\mathcal{P}_f \mathcal{Q}_f \Gamma}{U_c} = \Gamma \frac{P_c/U_c}{P_f/U_f} \frac{A_{f,c}}{A_{fi}} \frac{D^{-\alpha_c}}{R_f^{-\alpha_{fi}}}. \quad (5.4)$$

Note that $\kappa \geq 0$ and the expression $\frac{\kappa}{\kappa+1} \in [0, 1)$ characterizes the relative strength of cellular interference. As κ increases (or $\frac{\kappa}{\kappa+1} \to 1$), user 0 experiences progressively poor coverage due higher cellular interference. Conversely, as $\kappa \to 0$, $\mathrm{SIR}_f(F_0, D)$ is limited by interference from neighboring femtocells.

Definition 6. *Given a Beta distributed random variable $X \sim Beta(a, b)$ with two positive shape parameters a and b, denote its cumulative distribution function (cdf) $F_X(x) \triangleq \mathbb{P}[X \leq x]$ – namely the regularized incomplete beta function – as $\mathcal{I}_x(a, b)$.*

Definition 7. *Given a Beta distributed random variable $X \sim Beta(a, b)$ with cdf $F_X(x) = \mathcal{I}_x(a, b)$, denote its inverse cdf $x \triangleq \mathcal{I}^{-1}(y; a, b)$ as that value of x for which $\mathcal{I}_x(a, b) = y$. Because of the underlying monotonicity of a cdf, $\mathcal{I}^{-1}(y; a, b)$ is well-defined.*

For satisfying the femtocell QoS requirement, $\mathbb{P}[\mathrm{SIR}_f(F_0, D) \geq \Gamma] \geq 1 - \epsilon$ in equation (5.3). The following theorem gives the *no-coverage femtocell radius* D_f as a function of ϵ, Γ, T_f, U_f and U_c.

Theorem 10. *Any femtocell F_0 within $D < D_f$ meters of the macrocell B_0 cannot satisfy its QoS requirement $\mathbb{P}[SIR_f(F_0, D) \leq \Gamma] \leq \epsilon$, where D_f is given as*

$$D_f = \left[\frac{K}{\Gamma}\frac{P_f/U_f}{P_c/U_c}\left(\frac{\mathcal{I}^{-1}(\epsilon; T_f - U_f + 1, U_c)}{1 - \mathcal{I}^{-1}(\epsilon; T_f - U_f + 1, U_c)}\right)\right]^{-1/\alpha_c} \tag{5.5}$$

where $K = \frac{A_{fi}}{A_{f,c}} R_f^{-\alpha_{fi}}$.

Proof. Refer to Appendix C.1. □

Proposition 2. *The inverse function $\mathcal{I}^{-1}(x; a, b)$ is monotonically increasing with a and monotonically decreasing with b for any $a, b \geq 0$.*

Proof. Refer to Appendix C.2 □

Remark 8. *With SU femtocell transmission ($U_f = 1$), the no-coverage radius $D_{f,SU}$ is strictly smaller than the no-coverage radius $D_{f,MU}$ with MU transmission ($1 < U_f \leq T_f$). This follows by applying Proposition 2 to* (5.5) *in Theorem 10.*

Corollary 4. *With K as defined in Theorem 10 and $U_c = 1$, the reduction in the no-coverage radius using a SU transmission strategy at femtocells relative to MU transmission to $U_f = T_f$ users [resp. single antenna transmission] is given as*

$$\frac{D_{f,SU}}{D_{f,MU}} = \left[\left(\frac{1-\epsilon^{1/T_f}}{\epsilon^{1/T_f}}\right)\frac{\epsilon}{1-\epsilon}\frac{1}{T_f}\right]^{1/\alpha_c} \approx \left[\frac{\epsilon^{1-1/T_f}}{T_f}\right]^{1/\alpha_c}$$
$$\frac{D_{f,SU}}{D_{f,1\ Antenna}} = \left[\left(\frac{1-\epsilon^{1/T_f}}{\epsilon^{1/T_f}}\right)\frac{\epsilon}{1-\epsilon}\right]^{1/\alpha_c} \approx \epsilon^{\frac{1}{\alpha_c}\left(1-1/T_f\right)}.$$

Proof. Refer to Appendix C.3. □

Remark 9. *For fixed T_f, U_f and U_c, the no-coverage femtocell radius D_f in* (5.5) *scales with the ratio of the per-tier transmission powers P_f/P_c as $(P_f/P_c)^{-1/\alpha_c}$. Decreasing D_f by a factor of k requires each femtocell to increase their transmit power by $10\alpha_c \log_{10} k$ decibels. This suggests that the graph of D_f versus P_f/P_c (see Fig. 5.5) is a straight line on a log-log scale with slope $-1/\alpha_c$.*

Any femtocell located at a distance $D > D_f$ w.r.t the macrocell can tolerate interference from both the cellular transmissions as well as neighboring hotspot transmissions. Next, we derive the maximum obtainable spatial reuse from multiple antenna femtocells when they share spectrum with cellular transmissions. Mathematically, the *maximum femtocell contention density* satisfying (5.3) is expressed as

$$\lambda_f^*(D) = \arg\max \lambda_f, \text{ subject to } \mathbb{P}(\mathrm{SIR}_f(F_0, D) \geq \Gamma) \geq 1-\epsilon. \tag{5.6}$$

The following theorem derives $\lambda_f^*(D)$.

Theorem 11. *In a two-tier network, the maximum femtocell contention density $\lambda_f^*(D)$ at distance D from the macrocell B_0, which satisfies* (5.6) *(in the small-ϵ regime) is given as*

$$\lambda_f^*(D) = \frac{1}{\mathcal{C}_f(\mathcal{Q}_f\Gamma)^{\delta_f}}\left[\frac{\epsilon - \mathcal{I}_{\frac{\kappa}{\kappa+1}}(T_f - U_f + 1, U_c)}{\frac{1}{\mathcal{K}_f} - \mathcal{I}_{\frac{\kappa}{\kappa+1}}(T_f - U_f + 1, U_c)}\right] \tag{5.7}$$

where $\delta_f = 2/\alpha_{fo}$, $\mathcal{Q}_f$ is given by (5.2)*, κ is given by* (5.4)*, and*

$$\mathcal{C}_f = \pi\delta_f U_f^{-\delta_f}\sum_{k=0}^{U_f-1}\binom{U_f}{k}B(k+\delta_f, U_f - k - \delta_f) \tag{5.8}$$

$$\mathcal{K}_f = \left[1 + \frac{1}{(1+\kappa)^{U_c}}\sum_{j=0}^{T_f-U_f-1}\left(\frac{\kappa}{\kappa+1}\right)^j\binom{U_c+j-1}{j}\sum_{l=1}^{T_f-U_f-j}\frac{1}{l!}\prod_{m=0}^{(l-1)}(m-\delta_f)\right]^{-1} \tag{5.9}$$

where $B(a,b) = \frac{\mathbf{\Gamma}(a)\mathbf{\Gamma}(b)}{\mathbf{\Gamma}(a+b)}$ denotes the Beta function and $\mathcal{K}_f = 1$ whenever $U_f = T_f$.

Proof. Refer to Appendix C.4 □

Theorem 11 provides the maximum femtocell contention density at D considering both cross-tier cellular and hotspot interference from neighboring femtocells. Alternatively, given an average of λ_f transmitting femtocells per square meter, (5.7) can be inverted (numerically) to obtain the minimum D which guarantees that (5.6) is feasible. Theorem 11 provides two fundamental operational regimes depending on the hotspot location relative to the macrocell.

Cellular-limited regime. A necessary condition for a positive femtocell contention density at distance D is $\mathcal{I}_{\frac{\kappa}{\kappa+1}}(T_f - U_f + 1, U_c) < \epsilon$, or $\kappa(D)$ in (5.4) is upper bounded as

$$\kappa \leq \frac{\mathcal{I}^{-1}(\epsilon, T_f - U_f + 1, U_c)}{1 - \mathcal{I}^{-1}(\epsilon, T_f - U_f + 1, U_c)}.$$

From Theorem 10, violating this condition implies that the hotspot cannot guarantee reliable coverage because of cross-tier interference.

Hotspot-limited regime. As $\kappa \to 0$ or $D^{-\alpha_c} \to 0$, the SIR at any femtocell located at D is primarily influenced by hotspot interference. Consequently, $\lambda_f^*(D)$ in (5.7) approaches the limit $\breve{\lambda}_f$ given as

$$\breve{\lambda}_f = \lim_{\kappa \to 0} \lambda_f^*(D) = \frac{\epsilon\, \breve{\mathcal{K}}_f}{\mathcal{C}_f (\mathcal{Q}_f \Gamma)^{\delta_f}}$$
$$, \text{ where } \breve{\mathcal{K}}_f = \lim_{\kappa \to 0} \mathcal{K}_f = \left[1 + \sum_{l=1}^{T_f - U_f} \frac{1}{l!} \prod_{m=0}^{l-1} (m - \delta_f) \right]^{-1}. \tag{5.10}$$

The limit $\breve{\mathcal{K}}_f$ determines the maximum contention density in the special case of an *ad hoc* network–no cellular interference–of homogeneously distributed transmitters equipped with multiple antennas [76]. Their work shows that $\breve{\mathcal{K}}_f$ and $\mathcal{C}_f$ scales with T_f and U_f as

$$\breve{\mathcal{K}}_f \sim \Theta[(T_f - U_f + 1)^{\delta_f}],\ \mathcal{C}_f \mathcal{Q}_f^{\delta_f} \sim \Theta(U_f^{\delta_f}). \tag{5.11}$$

Further, $\forall \kappa \geq 0, \mathcal{K}_f \leq \breve{\mathcal{K}}_f$ and $\breve{\mathcal{K}}_f$ is bounded as $(T_f - U_f + 1)^{\delta_f} \leq \breve{\mathcal{K}}_f \leq \breve{\mathcal{K}}_{f,\max} = \mathbf{\Gamma}(1 - \delta_f)(T_f - U_f + 1)^{\delta_f}$ [76]. We shall now consider two cases in the hotspot-limited regime ($D^{-\alpha_c} \to 0$). First, with multiuser transmission to $U_f = T_f$ femtocell users and using (5.11), the femtocell area spectral efficiency (in b/s/Hz/m^2) which is given as $(1 - \epsilon) U_f \breve{\lambda}_f \log_2(1 + \Gamma)$ scales according to $\Theta(T_f^{1-\delta_f})$. With SU transmission, the ASE scales as $\Theta(T_f^{\delta_f})$. This suggests that in path loss regimes with $\alpha_{fo} < 4$, higher spatial reuse is obtainable (order-wise) provided femtocells employ their antennas to transmit to just one user. In contrast, MU femtocell transmission provides higher network-wide spatial reuse (orderwise) only when hotspot interference is significantly diminished ($\alpha_{fo} > 4$).

5.5.2 SIR Analysis at a Cellular User

We now consider a reference cellular user 0 at distance D from their macrocell B_0. During a given signaling interval, the received signal at user 0 is then given as

$$y_0 = \sqrt{A_c} D^{-\frac{\alpha_c}{2}} \mathbf{h}_0^\dagger \mathbf{V}\mathbf{s} + \sqrt{A_{c,f}} \sum_{F_j \in \Pi_f} \mathbf{e}_j^\dagger \mathbf{W}_j \mathbf{r}_j |X_j|^{-\frac{\alpha_{fo}}{2}} \tag{5.12}$$

where $\mathbf{s} \in \mathbb{C}^{U_c \times 1}, \mathbb{E}[||\mathbf{s}||^2] \leq P_c$ and $\mathbf{r}_j \in \mathbf{C}^{U_f \times 1}, \mathbb{E}[||\mathbf{r}_j||^2] \leq P_f$ represent the transmit data symbols for users in each tier. Further, $|X_j|$ and $\mathbf{e}_j \in \mathbb{C}^{T_c \times 1}$ respectively denote the distance and the downlink vector channel from the interfering femtocell F_j to user 0. The received SIR for user 0 is given as

$$\mathrm{SIR}_c(B_0, D) = \frac{\frac{P_c}{U_c} A_c D^{-\alpha_c} ||\mathbf{h}_0||^2}{\frac{P_f}{U_f} A_{c,f} \sum_{F_j \in \Pi_f} ||\mathbf{e}_j^\dagger \mathbf{W}_j||^2 |X_j|^{-\alpha_{fo}}}. \tag{5.13}$$

For successfully decoding user 0's signal, $\mathrm{SIR}(0, D)$ should be greater than equal to the minimum SIR target Γ. Define $\mathcal{Q}_c = U_c \frac{P_f}{P_c} \frac{A_{c,f}}{A_c} D^{\alpha_c}$. Then, the probability of successful reception at 0 is given as

$$\mathbb{P}[\mathrm{SIR}_c(0, D) \geq \Gamma] = \mathbb{P}\left[\frac{|\mathbf{h}_0^\dagger \mathbf{v}_0|^2}{\frac{1}{U_f} \sum_{F_j \in \Pi_f} ||\mathbf{e}_j^\dagger \mathbf{W}_j||^2 |X_j|^{-\alpha_{fo}}} \geq \mathcal{Q}_c \Gamma\right]. \tag{5.14}$$

Both the desired channel powers denoted as $|\mathbf{h}_0^\dagger \mathbf{v}_0|^2$ and the interfering marks [91] given by $||\mathbf{e}_j^\dagger \mathbf{W}_j||^2$ follow a chi-squared distribution with $2(T_c - U_c + 1)$ and $2U_f$ degrees of freedom respectively. Using [76], the maximum femtocell contention density $\lambda_f(D)$ for which (5.14) satisfies the maximum outage probability constraint $\mathbb{P}(\mathrm{SIR}(0, D) \geq \Gamma) \geq 1 - \epsilon$ of a cellular user is given as

$$\lambda_f^*(D) = \frac{\epsilon \mathcal{K}_c}{\mathcal{C}_f (\mathcal{Q}_c \Gamma)^{\delta_f}}, \text{ where } \mathcal{K}_c = \left[1 + \sum_{j=1}^{T_c - U_c} \frac{1}{j!} \prod_{k=0}^{j-1} (k - \delta_f)\right]^{-1} \tag{5.15}$$

where $\delta_f = 2/\alpha_{fo}$ as before and $\mathcal{C}_f$ is given by (5.8). From [76], $\mathcal{K}_c$ is bounded as

$$(T_c - U_c + 1)^{\delta_f} \leq \mathcal{K}_c \leq \mathbf{\Gamma}(1 - \delta_f)\ (T_c - U_c + 1)^{\delta_f} \tag{5.16}$$

where the upper bound is a good approximation for $\mathcal{K}_c$; for example, with $T_c = 4$, $U_c = 1$ and $\alpha_{fo} = 3.8$, the term K_c equals 3.47 while the upper bound equals 3.87.

Remark 10. *Since* (5.15) *varies as* $\mathcal{K}_c/U_c^{\delta_f}$*, approximating* $\mathcal{K}_c$ *by the upper bound in* (5.16) *shows that the maximum contention density for single user beamforming given as* $\lambda^*_{f,SU}(D)$ *is proportional to* $\mathbf{\Gamma}(1-\delta_f)T_c^{\delta_f}$*. With* $1 < U_c < T_c$ *transmitted users, the maximum femtocell contention density denoted as* $\lambda^*_{f,MU}(D)$ *is proportional to* $\mathbf{\Gamma}(1-\delta_f)(T_c - U_c + 1)^{\delta_f}/U_c^{\delta_f}$*. Therefore, SU transmission increases the maximum hotspot density by a factor of* $[T_cU_c/(T_c - U_c + 1)]^{\delta_f}$*. With* $U_c = T_c$ *users (implying* $\mathcal{K}_c = 1$*), one obtains* $\lambda^*_{f,MU}(D)$ *to be proportional to* $T_c^{-\delta_f}$*, so that* $\lambda^*_{f,SU}(D)/\lambda^*_{f,MU}(D)$ *equals* $\mathbf{\Gamma}(1-\delta_f)T_c^{2\delta_f}$*.*

Given an average of λ_f femtocells per sq. meter, inverting (5.15) yields the maximum distance up to which the cellular outage probability lies below ϵ. This cellular coverage radius D_c is given as

$$D_c = \left(\frac{1}{\Gamma U_c}\frac{A_c}{A_{c,f}}\frac{P_c}{P_f}\right)^{1/\alpha_c}\left(\frac{\epsilon\mathcal{K}_c}{\lambda_f\mathcal{C}_f}\right)^{\frac{1}{\delta_f\alpha_c}}. \tag{5.17}$$

Remark 11. *Since* D_c *varies as* $(P_c/P_f)^{1/\alpha_c}$*, increasing the cellular coverage radius by a factor of* k *necessitates increasing* P_c *by* $10\alpha_c\log_{10}k$ *decibels relative to* P_f*.*

Remark 12. *In* (5.17)*,* D_c *is proportional to* $(\frac{\mathcal{K}_c^{1/\delta_f}}{U_c})^{\frac{1}{\alpha_c}}$*. With SU transmission [resp. MU transmission to* $U_c = T_c$ *users] at the macrocell and applying* (5.16)*, the cellular coverage distance* D_c *scales with* T_c *as* $D_{c,SU} \sim \Theta(T_c^{1/\alpha_c})$*,* $D_{c,MU} \sim \Theta(T_c^{-1/\alpha_c})$*. This suggests that SU macrocell transmission provides coverage improvement by a factor of* T_c^{2/α_c} *(order-wise) relative to MU transmission.*

5.5.3 Design Interpretations

In this section, we provide design interpretations of the preceding results derived in Sections 5.5.1 and 5.5.2 in realistic path loss scenarios. We shall use the system parameters given in Table 5.1 and the path loss model described in Section 5.4.1.

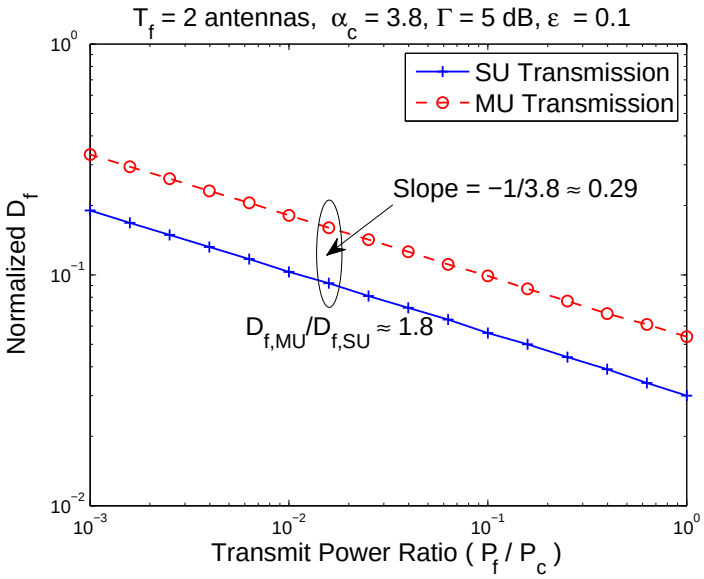

Figure 5.5: No-coverage femtocell radius for different values of $\frac{P_f}{P_c}$.

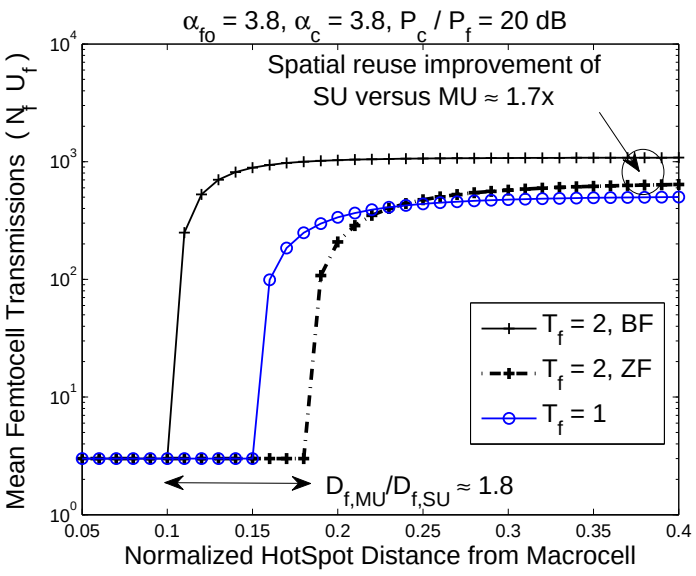

Figure 5.6: Maximum number of simultaneous femtocell transmissions $N_f U_f$ computed with SU and MU precoding at each femtocell.

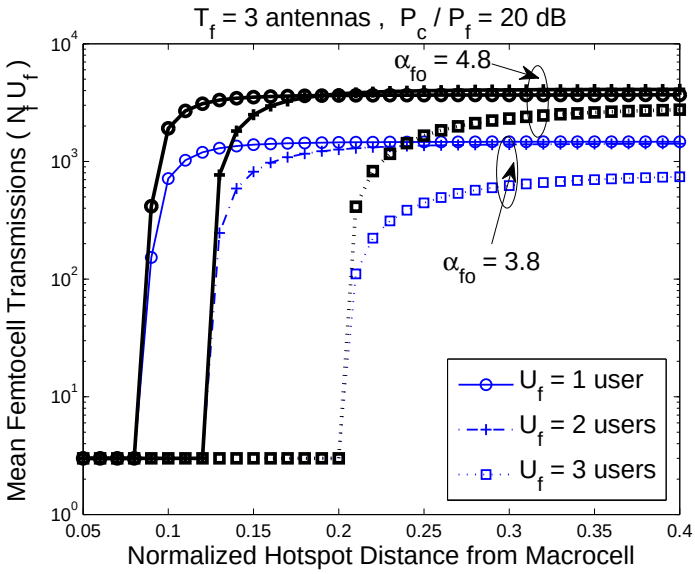

Figure 5.7: Maximum number of simultaneous femtocell transmissions $N_f U_f$ for different values of α_{fo}.

Figure 5.5 plots the normalized no-coverage femtocell radius D_f versus P_f/P_c on a log-log scale. Figs. 5.6-5.7 plot the maximum number of simultaneous femtocell transmissions given as $N_f(D)U_f$ where $N_f(D) = \pi R_c^2 \lambda_f^*(D)$, considering SU and MU femtocell transmissions and different values of α_{fo}. Shown below are the three key observations.

Coverage improvement. In the cellular-limited regime with $T_f = 2$ antennas, Fig. 5.6 shows that SU transmission obtains a nearly 1.5x reduction in the no-coverage femtocell radius D_f w.r.t single antenna transmission. Next, both Figs. 5.5-5.6 show that SU transmission reduces D_f by a factor of nearly 1.8x relative to MU transmission. Both these observations agree with the predicted improvements in Corollary 4. This indicates that SU transmission significantly improves hotspot coverage.

Dominance of cellular interference. In Figs. 5.6-5.7, N_f increases from zero (at the no-coverage femtocell radius) to greater than 100 femtocells per cell-site

within a few meters outside the no-coverage radius. This step-like transition from the cellular-limited to the hot-spot limited regime suggests that cross-tier cellular interference is the capacity-limiting factor even in densely populated femtocell networks and interference between femtocells is negligible because of the proximity of home users to their APs and double wall partition losses.

Spatial Reuse. In the hotspot-limited regime with $\alpha_{fo} = 3.8$, SU transmission consistently outperforms MU transmission. For example, with $T_f = 2$ antennas, there is a nearly 1.7x spatial reuse gain ($N_f U_f = 1080$ with SU transmission versus $N_f U_f = 640$ with MU transmission). Only when hotspot interference is *significantly diminished* – Fig. 5.7 with $T_f = 3$ antennas and $\alpha_{fo} = 4.8$ – MU transmission to $U_f = 2$ hotspot users provides a marginally higher spatial reuse relative to SU transmission. The conclusion is that achieving the multiplexing benefits of MU transmission requires relative isolation (or large α_{fo}) between actively transmitting femtocell APs.

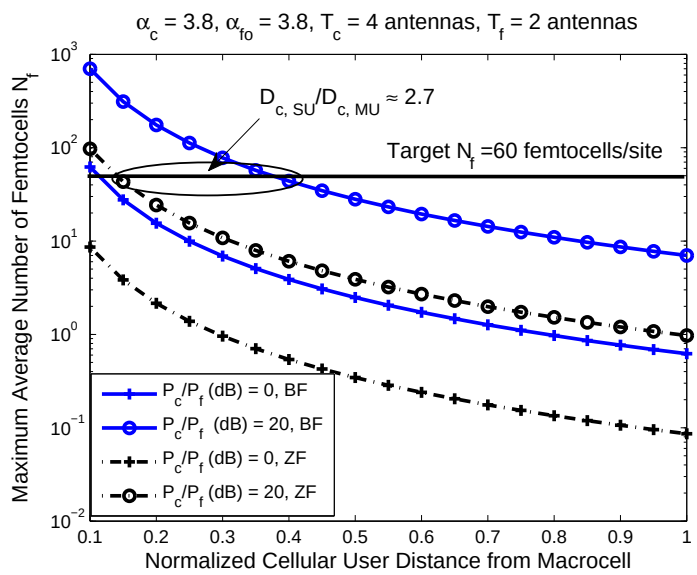

Figure 5.8: Maximum number of simultaneous femtocell transmissions given a maximum outage probability constraint ϵ per cellular user.

Fig. 5.8 plots the maximum number of transmitting femtocells $N_f = \pi R_c^2 \, \lambda_f^*(D)$ as a function of the cellular user distance D. With $(P_c/P_f)_{\text{dB}} = 20$ and a desired $N_f = 60$ femtocells/cellsite, SU macrocell transmission provides a normalized cellular coverage radius $D_c \approx 0.35$. In contrast, the coverage provided by MU transmission is only $D_c \approx 0.13$, resulting in a coverage loss of 2.7x relative to SU transmission (Remark 12 gives an order-wise loss of $\Theta(T_c^{\delta_f}) = 2.07$). With SU transmission and $(P_c/P_f)_{\text{dB}} = 0$, a cellular user at $D = 0.1$ can tolerate interference from nearly $N_f = 62$ femtocells/cellsite. In contrast, with MU transmission, N_f reduces to nearly 8 femtocells/cellsite. The observed improvement in the maximum femtocell contention density (equaling 7.75x) is well approximated by the predicted improvement $(\mathbf{\Gamma}(1-\delta_f)T_c^{2\delta_f} = 8.04\text{x})$ in Remark 10.

The preceding observations reveal 1. since MU performance is significantly limited by residual hotspot interference, the macrocell should maximize cellular coverage by transmitting to just a single cellular user and 2. that femtocells should adapt their transmit powers depending on their location in order to ensure reliable cellular coverage.

5.6 Interference Management using Carrier-Sensing at Femtocells

To motivate carrier-sensing at femtocells, Fig. 5.6 shows that even with $(P_c/P_f)_{\text{dB}} = 20$, a femtocell at normalized distance $D = 0.4$ can tolerate hotspot interference from greater than 1000 neighboring femtocells. This suggests that in dense femtocell deployments (eg. 60 femtocells in a radius of $R_c = 1$ km), $(P_c/P_f)_{\text{dB}}$ can be increased to minimize hotspot interference without violating the QoS requirement at femtocells. This section presents a carrier-sensing interference management strategy for choosing the femtocell transmission power provided there is a cellular user in its vicinity.

AS 12. *Each cellular user periodically transmits over a set of uplink pilot slots (time or frequency resource) with power $P_{UT,pilot}$ for communicating their channel information to the macrocell.*

AS 13. *Each femtocell is capable of inferring its distance from its closest macrocell.*

During carrier-sensing, each femtocell performs energy detection while monitoring uplink pilot cellular transmissions. In the absence of a cellular user, the femtocell maintains a constant transmit power P_f. When the detected energy of a cellular user exceeds a threshold, the femtocell chooses its P_f based on its location D within the underlying macrocell.

5.6.1 Minimum Required Sensing Range and Per-Tier Transmit Power Ratio Bounds

We shall first derive the minimum required sensing distance D_{sense} such that any transmitting femtocell located within $R < D_{\text{sense}}$ meters of the cellular user violates its maximum outage probability requirement. Define the notation $\mathcal{B}(D_{\text{sense}})$ to denote a circular region of radius D_{sense} containing $|\mathcal{B}(D_{\text{sense}})|$ femtocells. Given an intensity of λ_f femtocells per square meter and assuming the cellular user 0 is located at normalized distance D w.r.t the macrocell, its outage probability is lower bounded as

$$\begin{aligned}\mathbb{P}[\text{SIR}_c(B_0, D) \leq \Gamma] &\overset{(a)}{\geq} \mathbb{P}[\text{SIR}_c(B_0, D) \leq \Gamma, |\mathcal{B}(D_{\text{sense}})| > 0] \\ &\overset{(b)}{=} \mathbb{P}\left[\text{SIR}_c(B_0, D) \leq \Gamma \middle| |\mathcal{B}(D_{\text{sense}})| > 0\right] \cdot (1 - e^{-\lambda_f \pi D_{\text{sense}}^2}) \\ &\overset{(c)}{>} \mathbb{P}\left[\text{SIR}_c(B_0, D) \leq \Gamma \middle| |\mathcal{B}(D_{\text{sense}})| = 1, R = D_{\text{sense}}\right] \cdot (1 - e^{-\lambda_f \pi D_{\text{sense}}^2})\end{aligned} \tag{5.18}$$

where step (a) in (5.18) is a lower bound as it ignores the event of zero hotspots occurring within $\mathcal{B}(D_{\text{sense}})$. Step (b) rewrites (a) in terms of the conditional probability. Finally, step (c) is a lower bound because it considers the event that $|\mathcal{B}(D_{\text{sense}})| = 1$ and the hotspot is located exactly at $R = D_{\text{sense}}$ meters (thereby experiencing the

highest path loss). A necessary condition for ensuring $\mathbb{P}[\mathrm{SIR}_c(B_0, D) \leq \Gamma] \leq \epsilon$ is that the right hand side in step(c) in (5.18) consisting of the product of two probabilities should be less than ϵ. The first term represents the outage probability from interfering hotspots due to the time-varying channel powers and the second term represents the probability that $\mathcal{B}(D_{\text{sense}})$ is non-empty.

Assuming large λ_f (or $1 - e^{-\lambda_f \pi D_{\text{sense}}^2} \to 1$), a reasonable choice for selecting D_{sense} is to set the conditional outage probability , given exactly one interfering femtocell AP F_0 at distance D_{sense} from the cellular user, to equal ϵ. Evaluating this probability,

$$\begin{aligned}
\mathbb{P}\left[\mathrm{SIR}_c(B_0, D) \leq \Gamma \middle| |\mathcal{B}(D_{\text{sense}})| = 1, R = D_{\text{sense}}\right] &= \mathbb{P}\left[\frac{\frac{P_c}{U_c} A_c D^{-\alpha_c} |\mathbf{h}_0^\dagger \mathbf{v}_0|^2}{\frac{P_f}{U_f} A_{c,f} ||\mathbf{e}_0^\dagger \mathbf{W}_0||^2 D_{\text{sense}}^{-\alpha_{fo}}} \leq \Gamma\right] \\
&= \mathbb{P}\left[\frac{|\mathbf{h}_0^\dagger \mathbf{v}_0|^2}{||\mathbf{e}_0^\dagger \mathbf{W}_0||^2} \leq \frac{\Gamma \mathcal{Q}_c D_{\text{sense}}^{-\alpha_{fo}}}{U_f}\right] \\
&\overset{(a)}{=} \mathbb{P}\left[Z \leq \theta \frac{U_f}{T_c - U_c + 1}\right] \\
&\overset{(b)}{=} \mathcal{I}_{\frac{\theta}{\theta+1}}(T_c - U_c + 1, U_f) \qquad (5.19)
\end{aligned}$$

where $\mathcal{Q}_c = U_c \frac{P_f}{P_c} \frac{A_{c,f}}{A_c} D^{\alpha_c}$ as before, while $|\mathbf{h}_0^\dagger \mathbf{v}_0|^2 \sim \chi^2_{2(T_c - U_c + 1)}$ and $||\mathbf{e}_0^\dagger \mathbf{W}_0||^2 \sim \chi^2_{2U_f}$ denote the chi-squared distributed desired and interfering channel powers, as given earlier in (5.14). Step (a) in (5.19) follows by defining $\theta \triangleq \mathcal{Q}_c \Gamma D_{\text{sense}}^{-\alpha_{fo}} / U_f$ and defining the normalized ratio $Z = \frac{|\mathbf{h}_0^\dagger \mathbf{v}_0|^2 / (T_c - U_c + 1)}{||\mathbf{e}_0^\dagger \mathbf{W}_0||^2 / U_f}$ which is F-distributed [5]. Step (b) follows by substituting the cdf of the F-distributed r.v Z. The minimum required sensing radius at D is consequently given as

$$D_{\text{sense}} \geq \left[\left(\frac{\mathcal{Q}_c \Gamma}{U_f}\right)\left(\frac{1 - \mathcal{I}^{-1}(\epsilon; T_c - U_c + 1, U_f)}{\mathcal{I}^{-1}(\epsilon; T_c - U_c + 1, U_f)}\right)\right]^{1/\alpha_{fo}}. \qquad (5.20)$$

Using the numerical values in Table 5.1, Fig. 5.9 plots D_{sense} for different values of the path loss exponents α_c and α_{fo} as well as different cellular user locations

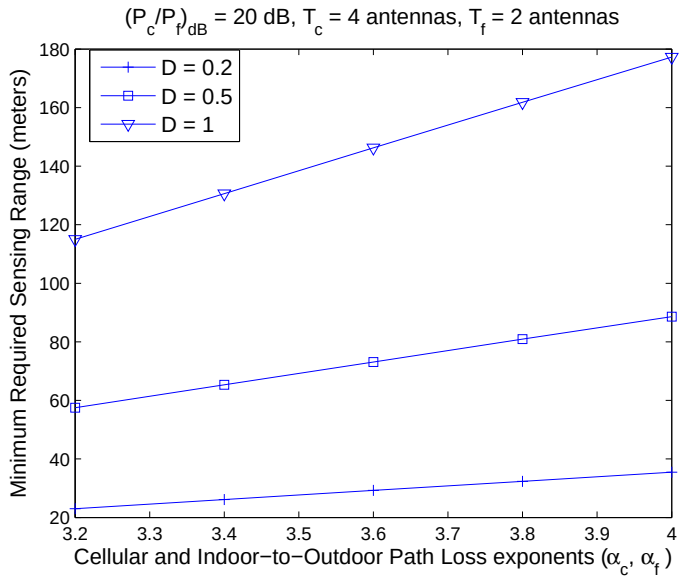

Figure 5.9: Required sensing range (in meters) per femtocell (assuming SU transmission in each tier) as a function of the path loss exponents α_c, α_f and the normalized distance D of the cellular user.

D. Assuming SU transmission in both tiers, $(P_c/P_f)_{\text{dB}} = 20$ dB and $\alpha_c = \alpha_{fo} = 3.8$, a minimum sensing range $D_{\text{sense}} \approx 160$ meters is required at the cell-edge ($D = R_c$).

Next, the following lemma derives bounds on P_c/P_f that satisfy the per-tier outage probability requirements at distance D from the macrocell.

Lemma 7. Given a mean intensity of λ_f femtocells per square meter and minimum per-tier SIR target Γ, satisfying the per-tier outage probability requirement at distance D from the macrocell necessitates (P_c/P_f) to be bounded as $(P_c/P_f)_{\text{lb}}[D] \leq P_c/P_f \leq (P_c/P_f)_{\text{ub}}[D]$, which are given as

$$\left(\frac{P_c}{P_f}\right)_{\text{lb}}[D] = \Gamma\left(\frac{A_{c,f}}{A_c}\right)\left(\frac{U_c}{D^{-\alpha_c}}\right)\left(\frac{\mathcal{C}_f\lambda_f}{\epsilon\mathcal{K}_c}\right)^{1/\delta_f} \tag{5.21}$$

$$\left(\frac{P_c}{P_f}\right)_{\text{ub}}[D] = \left(\frac{1}{\Gamma}\right)\left(\frac{A_{fi}}{A_{f,c}}\right)\left(\frac{U_c R_f^{-\alpha_{fi}}}{U_f D^{-\alpha_c}}\right)\frac{\mathcal{I}^{-1}(\tilde{\epsilon}; T_f - U_f + 1, U_c)}{1 - \mathcal{I}^{-1}(\tilde{\epsilon}; T_f - U_f + 1, U_c)} \tag{5.22}$$

where $\delta_f = 2/\alpha_{fo}$ as before, $\mathcal{K}_c$ is given by (5.15), $\mathcal{Q}_f$ is given by (5.2), $\mathcal{C}_f$ is given by (5.8) and

$$\tilde{\epsilon} = \frac{\epsilon - \lambda_f \mathcal{C}_f (\mathcal{Q}_f \Gamma_f)^{\delta_f} / \breve{\mathcal{K}}_{f,\max}}{1 - \lambda_f \mathcal{C}_f (\mathcal{Q}_f \Gamma_f)^{\delta_f}} \text{ and } \breve{\mathcal{K}}_{f,\max} = (T_f - U_f + 1)^{\delta_f} \mathbf{\Gamma}(1 - \delta_f). \tag{5.23}$$

Proof. A lower limit on P_c/P_f is obtained by computing the minimum P_c required to satisfy the outage probability requirement for a cellular user at distance D. Combining (5.15) and (5.16) yields $(P_c/P_f)_{\text{lb}}$ in (5.21). Conversely, given a cellular transmit power P_c, an upper limit for P_c/P_f is obtained by computing the minimum required P_f for satisfying $\mathbb{P}[\text{SIR}(F_0, D) \leq \Gamma] \leq \epsilon$. Substituting the upper bound for $\mathcal{K}_f$ and inverting (5.7) to compute $(P_c/P_f)_{\text{ub}}$ yields (5.22). □

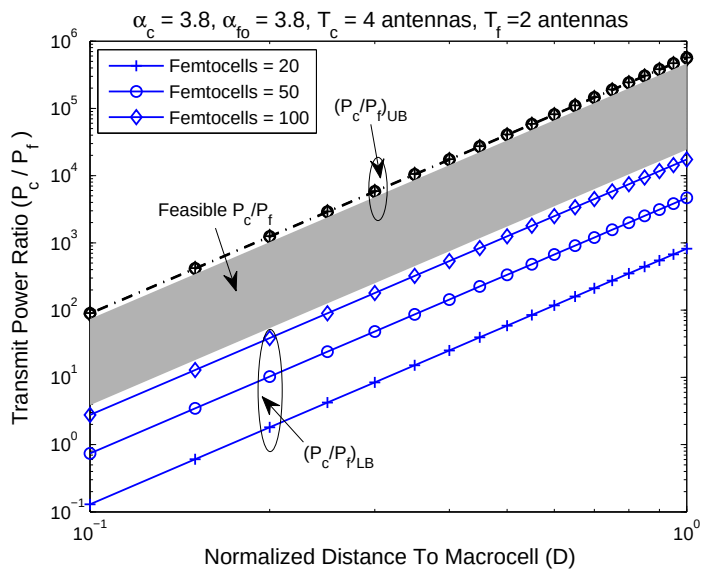

Figure 5.10: Lower and upper bounds on P_c/P_f with SU transmission as a function of the distance D. Shaded region shows feasible P_c/P_f's at location D, which satisfies the per-tier outage probability requirement for different average numbers of femtocells per cell-site.

The lower bound $(P_c/P_f)_{\text{lb}}[D]$ in (5.21) considers D as the distance of a cellular user from their macrocell. Conversely, $(P_c/P_f)_{\text{ub}}[D]$ considers D as the distance of

the reference femtocell from the macrocell. Inspecting (5.21) and (5.22) reveals that the difference between the decibel upper and lower bounds is constant for all D.

Fig. 5.10 plots $(P_c/P_f)_{\text{lb}}$ and $(P_c/P_f)_{\text{ub}}$ at different distances D from the macrocell. As an example, for a cell-edge ($D = 1$) location, the bounds on the required $(P_c/P_f)_{\text{dB}}$ are given as $40 \leq (P_c/P_f)_{\text{dB}} \leq 55$ dB.

5.6.2 Energy Detection based Carrier-Sensing of Cellular Users

Assume that each femtocell monitors a set of contiguous pilot slots (we assume time-slotted transmission in the subsequent discussion) and employs energy detection[140]. We briefly describe the sensing procedure below and refer to [39, 53, 104, 140] for further details.

Let T denote the sensing time (number of sensing time slots times the slot duration) and W designate the sensed bandwidth. Given a received signal $x(t)$ in the pilot slots and $n(t)$ being complex Gaussian noise process with power $N_0W/2$ per complex dimension, define the following hypotheses namely 1. $\mathcal{H}_0$: Absence of cellular user $[x(t) = n(t)]$ and 2. $\mathcal{H}_1$: Presence of an active cellular user $[x(t) = hs(t) + n(t)]$. The femtocell compares the energy detector output $Y = 2/N_0 \int_0^T |x(t)|^2 \, \mathrm{d}t$ against a threshold λ for inferring the presence (or absence) of a cellular user. Define m to equal the time-bandwidth product TW (assumed to be an integer). The average sensed pilot Signal-to-Noise Ratio (SNR) at the femtocell is given as

$$\begin{aligned} \overline{\gamma} &= \frac{P_{\text{UT,pilot}} D^{-\alpha_c} A_{f,c}}{N_0 W} \\ \text{where } (N_0W)_{\text{dB}} &= P_{c,\text{dB}} - A_{c,\text{dB}} - 10\alpha_c \log_{10}(R_c) - \overline{\gamma}_{\text{edge,dB}} \end{aligned} \tag{5.24}$$

where D denotes the distance of the cellular user from the femtocell. The noise power N_0W is chosen with reference to a cell-edge user obtaining an average downlink SNR $\overline{\gamma}_{\text{edge}} > \Gamma$. Assuming Selection Combining (SC) is used at the T_f available diversity branches for choosing the maximum SNR branch, the false-alarm probability P_{false}

and the detection probability $P_{\text{detect,SC}}$ are respectively given as [39, 53]

$$P_{\text{false}} = \mathbb{P}[Y > \lambda|\mathcal{H}_0] = \frac{\mathbf{\Gamma}(2m, \lambda)}{\mathbf{\Gamma}(2m)} \tag{5.25}$$

$$P_{\text{detect,SC}} = \mathbb{P}[Y > \lambda|\mathcal{H}_1] = T_f \cdot \sum_{k=0}^{T_f-1} \frac{(-1)^k}{k+1} \binom{T_f - 1}{k} P_{d,\text{Ray}} \left(\frac{\overline{\gamma}}{k+1} \right),$$

$$\text{where } P_{\text{detect,Ray}}(\overline{\gamma}) = \frac{\mathbf{\Gamma}(2m-1, \lambda)}{\mathbf{\Gamma}(2m-1)} + e^{-\frac{\lambda}{(1+m\overline{\gamma})}} \left(1 + \frac{1}{m\overline{\gamma}}\right)^{2m-1} \left[1 - \frac{\mathbf{\Gamma}(2m-1, \frac{\lambda m\overline{\gamma}}{(1+\lambda m\overline{\gamma})})}{\mathbf{\Gamma}(2m-1)}\right]. \tag{5.26}$$

where $\mathbf{\Gamma}(a, x) = \int_x^\infty t^{a-1}e^{-t}\mathrm{d}t$ is the upper incomplete gamma function. Because of the complex baseband signal model, there is a factor of 2 discrepancy in (5.25) with respect to [53].

Fig. 5.11 plots the maximum femtocell sensing range D_{sense} versus different values of the time-bandwidth product m. For example, with $P_{\text{UT,pilot}} = 20$ dBm (3 dB below the maximum UT transmit power), and target probabilities $P_{\text{detect},SC} = 0.9$ and $P_{\text{false}} = 0.1$ respectively, obtaining a sensing range of $D_{\text{sense}} = 230$ meters requires a minimum time-bandwidth product $m = 500$.

5.7 Numerical Results

This section reports the results of computer simulations using the system parameters in Table 5.1. The simulation consisted of 1000 different random drops of femtocell hotspots with 1000 trials per drop to simulate Rayleigh fading. Additive white Gaussian noise power was chosen to obtain an average cell-edge SNR of $\overline{\gamma}_{\text{edge, dB}} = 12$ dB. Single-user transmission is assumed in either tier considering its superior coverage and spatial reuse performance. With an average of $N_f = 60$ femtocells per cell-site, we evaluate whether the 10 percentile outage capacity ($\epsilon = 0.1$) satisfies the minimum required per-tier spectral efficiency $\log_2(1 + \Gamma)$ b/s/Hz (or nearly 2.06 b/s/Hz for $\Gamma_{\text{dB}} = 5$).

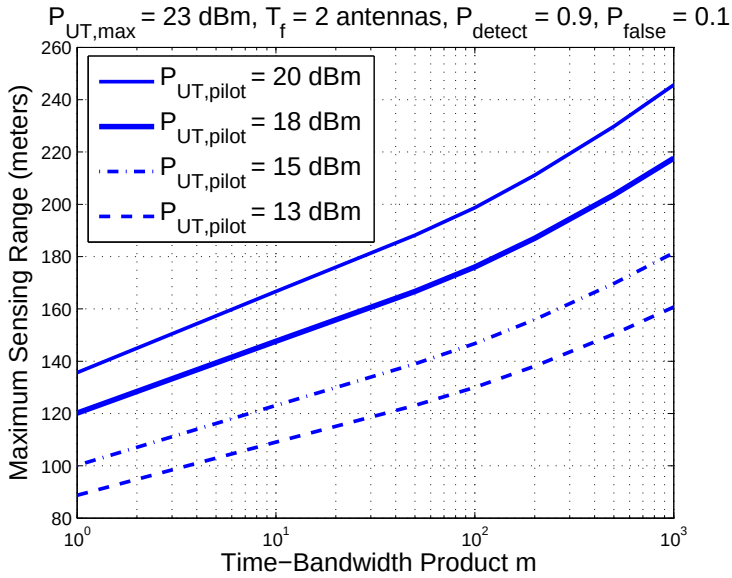

Figure 5.11: Maximum sensing range (in meters) at each femtocell as a function of the sensing time-bandwidth product and uplink pilot transmission powers.

Table 5.1: System Parameters

Variable	**Parameter**	**Sim. Value**
Γ	Minimum per-tier SIR Target for successful reception	5 dB
$\overline{\gamma}_{\text{edge,dB}}$	Average SNR of cell-edge user	12 dB
ϵ	Maximum tolerable per-tier outage probability	10%
R_c	Macrocell Radius	1000 m
R_f	Femtocell Radius	30 m
T_c	Transmit Antennas at macrocell	4 antennas
T_f	Transmit Antennas at femtocell	2 antennas
P_c	Maximum Transmit Power at macrocell	43 dBm
P_f	Maximum Transmit Power at femtocell	23 dBm
P_{UT}	Maximum Transmit Power at User Terminal	23 dBm
W_{dB}	Indoor to Outdoor Wall Partition Loss	5 dB
f_c	Carrier Frequency	2000 MHz
α_c	Outdoor path loss exponent	3.8
α_{fo}	Indoor to Outdoor path loss exponent	3.8
α_{fi}	Indoor path loss exponent	3

During carrier-sensing, each femtocell can detect active cellular users within a sensing radius equaling 230 meters (determined using computer simulations), which exceeds the minimum required sensing range of $D_{\text{sense}} = 160$ meters. We consider both a fixed P_c/P_f (without carrier-sensing or power control at femtocells) and a location based selection of P_c/P_f (wherein femocells adjust their P_f upon sensing a cellular user). Under ambient conditions (no detected cellular user), a fixed $(P_c/P_f)_{\text{dB}} = 20$ dB is chosen. Upon sensing a cellular user, a femtocell chooses its P_f such that $(P_c/P_f)[D, \text{dB}] = 0.7(P_c/P_f)_{\text{ub}}[D, \text{dB}] + 0.3(P_c/P_f)_{\text{lb}}[D, \text{dB}]$, which are given in (5.21)-(5.22). Two scenarios are considered namely

Reference Cellular User. A cellular user is placed at normalized distances ($D = 0.8$ and $D = 1.0$) w.r.t the macrocell. The cdfs of the achievable cellular data rates have been reported.

Reference Hotspot. A reference hotspot is placed at normalized distances ($D = 0.11, 0.4, 0.6, 0.8$ and 0.9 respectively from the macrocell. A reference cellular user is co-linearly placed at a distance $D_{\text{sense}}/2$ w.r.t the hotspot. The conditional cdfs of the hotspot data rates (assuming idealized sensing) have been reported.

Fig. 5.12 shows the cdfs of the obtained cellular data rates for $N_f = 60$ femtocells/cell-site. Without carrier-sensing, the 10 percentile outage capacities are below 0.5 b/s/Hz. By employing carrier-sensing, the 10 percentile outage capacities (corresponding to $\epsilon = 0.1$) equal 3.21 b/s/Hz and 2.22 b/s/Hz for cellular user locations of $D = 0.8$ and $D = 1.0$ respectively. Thus, our scheme ensures uniform cell-edge coverage with large numbers of femtocells.

Fig. 5.13 shows the cdfs of the obtained hotspot data rates with carrier-sensing and transmit power control at hotspots. The 10 percentile hotspot outage capacities are respectively equal to $2.15, 3.63, 3.56, 3.32$ and 3.22 b/s/Hz for the different hotspot locations given above which exceeds the minimum desired target spectral efficiencies. The lowest outage capacity is obtained when the femtocell is located close to the

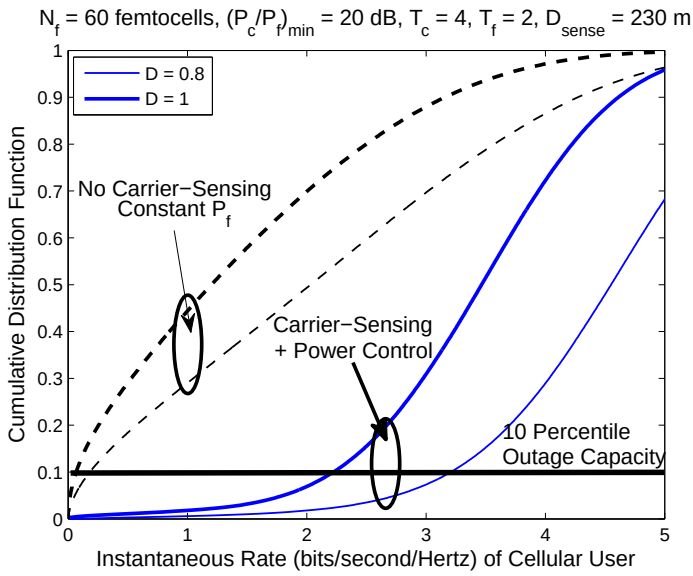

Figure 5.12: Cumulative distribution function of the cellular data rate (in b/s/Hz) with SU transmission in each tier.

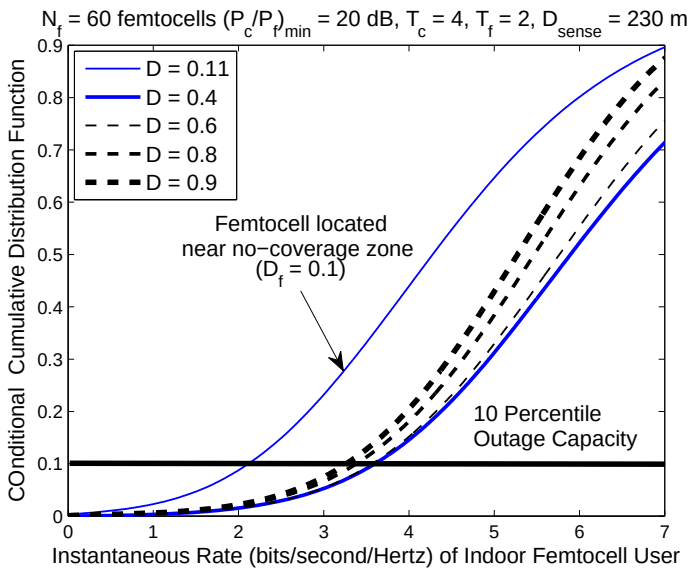

Figure 5.13: Conditional cumulative distribution function of the femtocell data rate (in b/s/Hz) (assuming a carrier-sensed cellular user at distance $D_{\text{sense}}/2$). Single-user transmission is employed in each tier.

no-coverage zone ($D = 0.11$). In the hotspot-limited regime, because of the location-based power control, the outage capacities monotonically decrease with increasing hotspot distance to the macrocell.

5.8 Conclusions

In two-tier cellular systems with universal frequency reuse, cross-tier interference will likely be the main obstacle preventing uniform coverage. This work has derived analytical expressions for the coverage zones in such a tiered architecture with spatial diversity considering the number of antennas, the maximum tolerable outage probability accounting for path-loss and Rayleigh fading. Single-user transmission in either tier is analytically shown to provide significantly superior coverage and spatial reuse while performance of multiple-user transmission suffers from residual cross-tier interference. For providing uniform cellular coverage, we have proposed a location-assisted power control scheme for regulating femtocell transmit powers. This scheme is fully decentralized and provides uniform cellular and hotspot coverage on the cell-edge, as opposed to randomized hotspot transmissions without carrier-sensing. These results motivate deploying closed-access tiered cellular architectures while requiring minimal network overhead.

Chapter 6

Spectrum Allocation in Two-Tier Networks

6.1 Introduction

In Chapters 3 through 5, interference avoidance schemes and power control techniques have been presented for mitigating cross-tier interference in a two-tier network. Alternatively, cross-tier interference is completely eliminated by placing cellular users and femtocell users in orthogonal frequency resources. In two-tier networks with frequency division based systems such as Orthogonal Frequency Division Multiple Access (OFDMA), it is likely that partitioning bandwidth between each tier will be more viable, compared to centralized frequency assignment strategies. This chapter proposes and analyzes an optimum decentralized spectrum allocation policy for two-tier networks that employ frequency division multiple access (including OFDMA). The proposed allocation is optimal in terms of Area Spectral Efficiency (ASE), and is subjected to a sensible Quality of Service (QoS) requirement, which guarantees that both macrocell and femtocell users attain at least a prescribed data rate.

6.1.1 The Return of FDMA

Frequency division multiple access (FDMA)'s resurgence in emerging OFDMA wireless standards such as the 3rd Generation Partnership Project's Long Term Evolution (LTE), the Worldwide Interoperability for Microwave Access (WiMAX) enable the macrocell to perform flexible rate assignment [10] across frequency sub bands to users and provide interference management by fractional frequency reuse. In femtocell deployments, due to reasons of scalability, security and limited availability of

backhaul bandwidth, it is reasonable to assume the absence of coordination between femtocells and the central macrocell. Further, femtocells are placed opportunistically or randomly by end users. Therefore, conventional frequency planning strategies will be very difficult in a two-tier network.

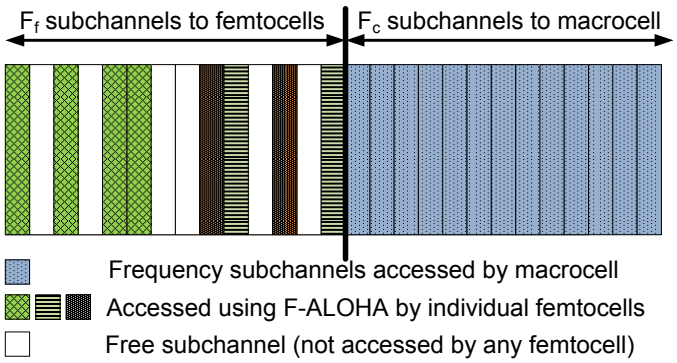

Figure 6.1: Spectrum partitioning in a two-tier network.

Assigning orthogonal spectrum resources between the central macrocell and femtocell BSs eliminates cross-tier interference. This motivates the orthogonal access spectrum allocation strategy (Fig. 6.1) proposed in this work [27]. Next, to avoid persistent collisions with neighboring femtocells in their allotted spectrum, this work proposes that each femtocell accesses a random subset of the candidate frequency subchannels, wherein each subchannel is accessed with equal probability. We term this spectrum access strategy as F-ALOHA (Frequency ALOHA)[1]. We motivate F-ALOHA for three reasons. First, F-ALOHA avoids transmission delays and increased RF sensitivity requirements for sensing frequency subchannels in the presence of channel fading[122]. Next, F-ALOHA provides randomized interference avoidance, since

[1]Slotted ALOHA, by convention, implies that the slots are in the time domain

neighboring femtocells are unlikely to consistently access identical frequency subchannels. Finally, such a transmission strategy offers a decentralized spectrum access by femtocells and low complexity.

F-ALOHA Spectrum Access: If a femtocell transmits over all its allotted subchannels, it may cause excessive interference to surrounding femtocells; conversely, accessing only a few subchannels could result in a poor spatial reuse. With F-ALOHA, there should be an optimal fraction of spectrum access for each femtocell in order to maximize the spatial reuse of spectrum, or in effect the net number of simultaneous transmissions per unit area [13, 143]. The spatial reuse is readily expressible using the *Area Spectral Efficiency* (ASE) in b/s/Hz/m^2 [7], which is defined as the network-wide spatially averaged throughput per frequency subchannel divided by the product of the subchannel bandwidth and the area over which the transmissions take place. Based on the stated reasons, we assume (1) downlink transmissions from the macrocell and femtocells are frequency orthogonal and (2) femtocells transmit using F-ALOHA, and pose the following questions:

- What is the expected subchannel throughput inside the macrocell [resp. femtocell], as a function of interference from neighboring macrocells [resp. femtocells], and terrestrial propagation parameters such as path loss exponent and lognormal shadowing?
- Given the expected subchannel throughput, the average number of femtocells per cell-site and the number of users associated with each BS, how should the bandwidth be partitioned between tiers in order to satisfy a Quality of Service (QoS) requirement in each tier?
- With this spectrum allocation strategy, how much improvement in network-wide ASE does opportunistic channel aware macrocell scheduling offer relative to channel blind scheduling?

6.1.2 Related Work

The problem considered in this work is related to Yeung and Nanda [156], who propose frequency partitioning in a microcell/macrocell system based on mobile speeds and the loading of users in each cell. Their frequency partitioning is derived based on choosing handoff velocity thresholds and maximizing the overall system capacity, subject to per-tier blocking probability constraints that ignore co-channel interference. Similar dynamic channel allocation schemes have been proposed in [102] and [50]. In Ahn *et al.* [4], an algorithmic approach is presented for macrocell-microcell deployment depending on spatio-temporal traffic loads, but relies on event-driven simulations. In contrast, our work analytically determines the spectrum allocation, which maximizes the network-wide area spectral efficiency considering interference from neighboring BSs, path losses and prevailing channel conditions.

Transmission capacities in a two-tier network have been derived in [75] for both spectrum sharing and spectrum partitioning approaches. In decentralized networks, Jindal *et al.* [84] have derived the optimal number of frequency subchannels F for a frequency-hopped ad hoc network assuming a fixed data rate requirement per transmitter-receiver pair and a target outage probability. Our work, in contrast, assumes a fixed F (as is the case with Orthogonal FDMA), allowing for multiple subchannels to be accessed by each BS, with variable rate transmission per accessed subchannel. In a hybrid network composed of ad-hoc nodes and BS infrastructure nodes, Zemlianov and de Veciana [161] and Liu *et al.* [106] have derived asymptotic scaling laws relating to the per user throughput as the number of infrastructure nodes increase. In addition to the hierarchical nature of our model, the main difference is that this work assumes single-hop communication. In wireless local area networks, Bahl *et al.* [16] have proposed variable center frequencies and variable channel widths for improving the spectrum utilization and fairness for heavily loaded access points (APs). Finally, game-theoretic approaches have been investigated for both non-cooperative [42, 60] and cooperative [136] spectrum sharing in decentralized

networks.

6.1.3 Contributions

The three contributions of this work are as follows.

Expected per-tier throughput. The expected per-tier throughput is derived for the macrocell and femtocell users accounting for interference from neighboring cells. The maximum ASE of the femtocell network is shown to be unchanged with addition of hotspots beyond a threshold. At low femtocell densities, the highest femtocell ASEs are attained when each femtocell accesses the entire available spectrum. In higher densities, femtocells should use a decreasing fraction of the spectrum; e.g. with an average of 100 femtocells in each cell site, each femtocell should access 30% of the available spectrum.

Spectrum allocation with Quality of Service (QoS). The proposed spectrum allocation maximizes the spatial reuse in a two-tier network, subject to a network-wide QoS requirement, which guarantees a minimum expected throughput per-user. Differing QoS constraints produce markedly different spectrum allocations due to the competing spatial coverage scales in each tier. Notably, a QoS requiring equal per-user throughputs in each tier means assigning greater than 90% of spectrum to the macrocell. Conversely, an even division of spectrum occurs when the QoS constraints favor femtocells to provide significantly higher data rates.

Scheduling and Spectrum Requirements. Channel aware macrocell scheduling gains permeate to femtocells, resulting in a significant spectrum reduction with the proposed allocation. With an average of 50 femtocells/cell site and target per-tier data rates of 0.1 Mbps/macrocell user and 10 Mbps/hotspot user, a channel aware macrocell scheduler provides nearly 50% reduction in necessary spectrum compared to a channel blind scheduler. As number of hotspot users increases, the spectrum requirements in a two-tier network show two extremes. One is a low interference sce-

nario where addition of femtocell hotspots provides increased spatial reuse, ensuring that the necessary spectrum is unchanged up to 110 femtocells/cell site. In a high interference scenario however, the ensuing co-channel interference may necessitate a linear increase in required spectrum with hotspot density.

6.2 System Model

The setup consists of a hexagonal region $\mathcal{H}$ of radius R_c with a central macrocell BS C providing coverage area $|\mathcal{H}| = \frac{3\sqrt{3}}{2}R_c^2$, which is surrounded by two rings of interfering macrocells. The macrocell is overlaid with femtocell hotspots of radius R_f, which are randomly distributed on $\mathbb{R}^2$ according to a homogeneous SPPP Ω_f with intensity λ_f [91]. The mean number of femtocells per cell site is readily obtained as $N_f = \lambda_f|\mathcal{H}|$. Cellular users are assumed to be uniformly distributed inside each cell site. Femtocells are assumed to provide "closed access" to licensed indoor users who fall within the radio range R_f of their respective home BSs. Let $U = U_c + N_f U_f$ denote the average number of users in each cell site. These U users are distributed into U_c uniformly distributed tier 1 mobile outdoor users and U_f users per femtocell.

6.2.1 Per-Tier Spectrum Access

The available spectrum comprises F frequency subchannels each with bandwidth W Hz. We wish to determine the optimal partitioning (F_c, F_f), where F_c subchannels are available for macrocell transmissions and $F_f = F - F_c$ subchannels are available for femtocell transmissions. Denote $\rho = F_c/F$ as the *fraction of spectrum* assigned to the macrocell BS with the following key assumptions:

AS 14. *Each femtocell schedules its users in a Channel Blind Round Robin (RR) fashion. The macrocell schedules its users according to either a RR or a Channel Aware Proportional Fair (PF) scheduler.*

AS 15. *The fraction ρ is a positive real number in $[0, 1]$. For simplicity, the paper does*

not quantize ρ for having an integer number of frequency subchannels. Consequently, $F_c = [\rho F]$ and $F_f = F - F_c$, where we use $[x]$ to denote the integer part of a number x.

Assumption 1 makes it clear that the long term expected throughput per indoor user equals $1/U_f$th of the average femtocell throughput. The long term expected macrocell throughput is assumed to be equally divided among the U_c outdoor users with RR and PF scheduling at the macrocell. With a PF scheduler, this assumption is reasonable considering mobility, which ensures that all users receive an identical average Signal-to-Interference Ratio (SIR) over the long term.

If each femtocell accesses exactly k frequency subchannels among their allotted F_f subchannels, the net portion of accessed spectrum per femtocell equals $\rho_f(1-\rho)$ where $\rho_f \triangleq k/F_f$. Provided femtocells choose their frequency subchannels independently and with equal probability, F-ALOHA "thins" the mean number of interfering femtocells in each frequency subchannel by their subchannel access probability. The probability p of a femtocell choosing a given frequency subchannel for transmission is given as

$$p = \frac{\binom{F_f}{k} - \binom{F_f-1}{k}}{\binom{F_f}{k}} = \frac{k}{F_f} = \rho_f. \tag{6.1}$$

Consequently, the set of interfering femtocells per frequency subchannel is a *Marked SPPP* [91] Λ_f with intensity $\lambda_f \rho_f = \lambda_f k/F_f$. When $\rho_f = 1$, all femtocells in Ω_f access the entire spectrum but mutually interfere in all subchannels. For $\rho_f \ll 1$, femtocells transmit in a small region of spectrum and avoid causing mutual interference. This strategy provides a higher spectral efficiency over each frequency subchannel, but incurs reduced spectrum utilization because femtocells do not transmit over the entire available spectrum.

6.2.2 Channel Model and Variable Rate Transmission

The downlink channel between each BS and its users is composed of a fixed distance dependent path loss, a slowly varying component modeled by lognormal shadowing and Rayleigh fast fading with unit average power. For simplicity, thermal noise is neglected at the receiver.

AS 16. *Each user is assumed to track their SIR in each subchannel and feedback the instantaneous rate to their BS with zero delay. Further, the channel can support the requested rate as determined by the scheduled user with probability 1.*

Although imperfect feedback and/or channel estimation has a potentially big impact on system capacity, this work does not account for these effects for sake of analytical tractability.

AS 17. *BSs assign equal transmission powers to all subchannels.*

Each BS assigns rate adaptively based on the received SIR per user. Let G denote the Shannon Gap with variable rate M-QAM transmission [56]. Assume an instantaneous transmission rate of b_i bps/Hz if the instantaneous SIR lies in $[\Gamma_i, \Gamma_{i+1}), 1 \leq i \leq L$. Using adaptive modulation with L discrete rates, the instantaneous rate Wb in a W Hz wide subchannel is given as

$$b = b_i, \text{when SIR} \in [\Gamma_i, \Gamma_{i+1}), 1 \leq i \leq L. \tag{6.2}$$

$$b_i = \log_2 \left(1 + \frac{\Gamma_i}{G}\right) \text{bps/Hz}. \tag{6.3}$$

Assuming identical statistics over all frequency subchannels, the long term expected throughput (in b/s/Hz) per macrocell/femtocell in each subchannel is given as

$$S = \sum_{l=1}^{L-1} l \cdot \Pr[\Gamma_l \leq \text{SIR} < \Gamma_{l+1}] + L \cdot \Pr[\text{SIR} \geq \Gamma_L]. \tag{6.4}$$

The expected throughput provided by each macrocell [resp. femtocell] is obtained multiplying the expected throughput in (6.4) by their respective spectrum allocation ρ [resp. $\rho_f(1-\rho)$].

6.3 Spectrum Allocation and Per-Tier Expected Throughputs

Let spectrum WF be allocated such that the macrocell BS transmits over a portion ρ, while femtocell BSs transmit over the remaining $1-\rho$ fraction of the spectrum. Let $S_c(\rho, U_c)$ be the long term throughput (in b/s/Hz) in each subchannel provided by the macrocell[2]. Obtaining S_c requires calculating the average rate per subchannel in (6.4) after spatially averaging the SIR over all locations, and accounting for the interference from two rings of transmitting macrocells.

Let each femtocell access a portion ρ_f of its allotted spectrum using F-ALOHA, servicing its users in a RR schedule. Define $S_f(\rho_f\lambda_f)$ as the expected femtocell throughput in each frequency subchannel, which is determined by the intensity $\rho_f\lambda_f$ of the marked SPPP Λ_f. With universal frequency reuse across all macrocells, the area spectral efficiency (ASE) provided by each tier is given as

$$\text{ASE}_c = \frac{S_c(\rho, U_c)}{|\mathcal{H}|},\ \text{ASE}_f = \frac{N_f\rho_f S_f(\rho_f\lambda_f)}{|\mathcal{H}|}. \tag{6.5}$$

The factor $N_f\rho_f$ represents the mean number of transmitting femtocells in each subchannel in the set Λ_f. With bandwidth W, the per-tier throughputs (in b/s) per subchannel can be calculated by multiplying the ASEs in (6.5) by $W|\mathcal{H}|$. The network-wide ASE is given as

$$\text{ASE} = \rho\text{ASE}_c + (1-\rho)\text{ASE}_f = \frac{1}{|\mathcal{H}|}[\rho S_c(\rho, U_c) + (1-\rho)N_f\rho_f S_f(\rho_f\lambda_f)]. \tag{6.6}$$

The expected network throughput (in b/s) over the WF wide spectrum is obtained by multiplying (6.6) by $WF|\mathcal{H}|$. Before determining the spectrum allocation, we first stipulate a QoS requirement η, which ensures that users in either tier are guaranteed a minimum expected throughput. By implication, η also regulates the maximum amount of spectrum that any tier can receive.

[2]The use of U_c and ρ within parenthesis is to account for a macrocell scheduler which can provide diversity gains by scheduling users according to their channel variations[141]

Definition 8. *The QoS parameter* $0 < \eta \leq 0.5$ *guarantees that the expected throughput per user in one tier is* at least $\eta/(1-\eta)$ *w.r.t the other tier.*

Choosing different η enables assigning different priorities (QoS) to one tier relative to the other. For example, setting $\eta = 0.5$ ensures that users in both tiers obtain identical expected rates. Decreasing η favors assigning greater spectrum to the tier providing a higher expected throughput per active user.

Given a total available spectrum of 1 Hz, the problem is to determine the optimal spectrum allocation ρ over all possible spectrum partitioning strategies $\omega \in [0,1]$ between the macrocell and femtocells. The proposed spectrum allocation maximizes the network-wide ASE with a QoS constraint η on the minimum expected per-tier throughput/user, as shown below.

$$\rho = \frac{1}{|\mathcal{H}|} \arg\max_{0 \leq \omega \leq 1} \omega S_c(\omega, U_c) + (1-\omega) N_f \rho_f S_f(\rho_f \lambda_f) \tag{6.7}$$

$$\text{subject to } \min\{S_{c,u}(\omega), S_{f,u}(\omega)\} \geq \eta(S_{c,u}(\omega) + S_{f,u}(\omega)) \tag{6.8}$$

$$\text{where } S_{c,u}(\omega) \triangleq \frac{\omega S_c(\omega, U_c)}{U_c} \text{ and } S_{f,u}(\omega) \triangleq \frac{(1-\omega)\rho_f S_f(\rho_f \lambda_f)}{U_f}$$

Here $S_{c,u}(\omega)$ and $S_{f,u}(\omega)$ are the long term expected throughputs for a macrocell and femtocell user respectively. Whenever the average subchannel throughput $S_c(\omega, U_c)$ is independent of the spectrum ω assigned to the macrocell, the objective function in (6.7) is an affine function w.r.t ω. The following proposition derives the optimizing ρ considering that the maximum is attained at the extremal points of the constraint set:

Proposition 3. *If the expected macrocell throughput per subchannel is independent of the total spectrum allocated to the macrocell* ω*, i.e.* $S_c(\omega, U_c) = S_c(U_c)\ \forall \omega \in [0,1]$*, the optimizing* ρ *in* (6.7) *satisfies the QoS constraint with equality, belonging to a set with two candidate spectrum allocation assignments given as*

$$\rho^* \in \{x, 1-x\}, x \triangleq \left[1 + \frac{1-\eta}{\eta} \frac{S_c(U_c)}{U_c} \frac{U_f}{\rho_f S_f(\rho_f \lambda_f)}\right]^{-1}. \tag{6.9}$$

Proof. Since $S_c(\omega, U_c) = S_c(U_c)\ \forall \omega \in [0,1]$, the optimization problem in (6.7) is to determine the optimal ρ which maximizes a convex combination of S_c and $N_f \rho_f S_f(\rho_f \lambda_f)$ with a linear constraint (6.8). Consequently, the argument maximizer is located at the extremal points of the constraint set (6.8). Solving for the ρ which satisfies (6.8) with equality yields (6.9). □

Remark 13. *Without a QoS requirement (allowing $\eta \to 0$), the objective function in* (6.7) *is a convex combination of the macrocell and femtocell throughputs which is maximized at the extreme points $\rho \in \{0, 1\}$. Such a partitioning is clearly unfair since it results in a greedy allocation of the entire spectrum to one tier.*

For a generic macrocell scheduler–when Proposition 3 may be inapplicable–(6.7) is a one dimensional optimization problem that can be solved efficiently for a given η using a numerical search.

6.3.1 Macrocell Throughput: RR Scheduling

Assuming that the central macrocell BS C_0 in the hexagonal region $\mathcal{H}$ is placed at the origin, the normalized positions of the interfering BSs $C_k \in \mathcal{B}, k = 1 \ldots 18$ are represented in polar form $\mathbf{b_k}, k \in \mathcal{B}$ using MATLAB notation as

$$\mathbf{b_k}/R_c \in \left\{\sqrt{3}e^{i(\pi/6+[0:5]\pi/3)}\right\} \bigcup \left\{3e^{i([0:5]\pi/3)}\right\} \bigcup \left\{2\sqrt{3}e^{i(\pi/6+[0:5]\pi/3)}\right\}. \tag{6.10}$$

Let $|h_0|^2$ denote exponentially distributed channel power (with unit mean) between the central macrocell BS C_0 and its scheduled user 0. Denoting the Euclidean norm by $||\cdot||$, the expression for the received SIR for macrocell user 0 at position $\mathbf{r}$ is given as

$$\mathrm{SIR}_c(\mathbf{r}) = \frac{\Theta_0}{\Psi_I(\mathbf{r})}|h_0|^2\,||\mathbf{r}/R_c||^{-\alpha_c} \text{ where } \Psi_I(\mathbf{r}) = \sum_{k\in\mathcal{B}} \left|\left|\frac{\mathbf{r}-\mathbf{b}_k}{R_c}\right|\right|^{-\alpha_c} |h_{0k}|^2\Theta_{0k}. \tag{6.11}$$

Here R_c is the cell radius, α_c represents the outdoor path loss exponent and $|h_{0k}|^2 \sim \exp(1)$ is the exponentially distributed channel power between interfering BS C_k and

the user of interest. The random variable Θ_0 [resp. Θ_{0k}] is the lognormal shadowing between the central BS [resp. interfering BSs] and the desired user, which are distributed as $\mathrm{LN}(\zeta\mu_{c,\mathrm{dB}}, \zeta^2\sigma^2_{c,\mathrm{dB}})$, where $\zeta = 0.1\ln 10$ is a scaling constant. For analytical tractability in the reminder of the paper, our paper makes the following assumption regarding the distribution of a composite lognormal-exponential random variable (r.v).

AS 18. *The distribution of a composite lognormal-exponential r.v $\Theta_k|h_{0k}|^2$ is modeled as a lognormal distribution using Turkmani's approximation [138] given as*

$$f_{\Psi_i}(x) = \frac{1}{x\sigma_i\sqrt{2\pi}} \exp\left[\frac{-(\ln x - \mu_i)^2}{2\sigma_i^2}\right] \tag{6.12}$$

$$\mu_i = \zeta(\mu_{c,dB} - 2.5), \sigma_i = \zeta\sqrt{\sigma^2_{c,dB} + 5.57^2}. \tag{6.13}$$

AS 19. *For a fixed $\mathbf{r}$, using the moment generating function based technique described in Mehta* et al.*[108], the sum of $|\mathcal{B}|$ independent, but not identically distributed lognormal r.v's in the expression $\Psi_I(\mathbf{r}) = \sum_{k\in\mathcal{B}}(||\mathbf{r} - \mathbf{b_k}||/R_c)^{-\alpha_c}\Psi_k$ is approximated by a single lognormal r.v with parameters $\mathbf{LN}(\mu_I(\mathbf{r}), \sigma_I^2(\mathbf{r}))$.*

Using Assumptions 18-19 and (6.11), $\mathrm{SIR}_c(\mathbf{r})$ is distributed according to a lognormal r.v $\mathrm{LN}(\mu_C(\mathbf{r}), \sigma_C^2(\mathbf{r})$ where $\mu_C(\mathbf{r}) = \mu_S(\mathbf{r}) - \mu_I(\mathbf{r})$ and $\sigma_C(\mathbf{r}) = \sqrt{\sigma_S^2(\mathbf{r}) + \sigma_I^2(\mathbf{r})}$. Then, the distribution of the SIR for a cellular user at position $\mathbf{r}$ w.r.t the macrocell is given as

$$\Pr\left[\mathrm{SIR}_c(\mathbf{r}) \le \Gamma|\mathbf{r}\right] = 1 - \mathrm{Q}\left[\frac{\ln\left(\Gamma\,||\mathbf{r}/R_c||^{\alpha_c}\right) - \mu_C}{\sigma_C}\right]. \tag{6.14}$$

where $\mathrm{Q}(x) \triangleq \frac{1}{\sqrt{2\pi}}\int_x^\infty e^{-t^2/2}\mathrm{d}t$ is the complementary cumulative distribution function (CCDF) of a standard normal. Defining $a(\mathbf{r}) \triangleq \frac{\ln\Gamma - \mu_C(\mathbf{r})}{\sigma_C(\mathbf{r})}$ and $b \triangleq \frac{\alpha_c}{\sigma_C(\mathbf{r})}$, (6.14) simplifies to

$$\Pr\left[\mathrm{SIR}_c(\mathbf{r}) \le \Gamma|\mathbf{r}\right] = 1 - \mathrm{Q}[a(\mathbf{r}) + b(\mathbf{r})\ln||\mathbf{r}/R_c||]. \tag{6.15}$$

Averaging (6.15) over a hexagonal cell region is difficult. Alternatively, the spatially averaged cumulative distribution function (CDF) of SIR_c can be obtained approximately by considering an circular region of radius $\sqrt{|\mathcal{H}|/\pi}$, which results in the same area as the cell site $\mathcal{H}$. To calculate the spatial throughput inside this circular region, the paper divides the region into M non-overlapping annuli. For tractability, a simplifying assumption is that all users inside an annulus experience identical shadowing statistics (i.e. identical $\mu_C(\mathbf{r})$ and $\sigma_C(\mathbf{r})$). Denoting the distance of the user from C_0 by $||\mathbf{r}|| = R$, the following lemma derives the expected spatial throughput by averaging $\mathrm{SIR}_c(R)$ inside a *circular annulus* with inner radius R_1 and outer radius R_2.

Lemma 8. *The spatially averaged SIR distribution inside a circular annulus with inner radius R_1 and outer radius R_2 is given as*

$$\mathbb{E}_R[\Pr(\mathrm{SIR}_c \leq \Gamma | R_1 \leq R \leq R_2)] = 1 - \frac{1}{(R_2^2 - R_1^2)}[R_2^2 C(a_2, b) - R_1^2 C(a_1, b)] \quad (6.16)$$

$$\textit{where } C(a,b) \triangleq \mathrm{Q}(a) + \exp\left(\frac{2-2ab}{b^2}\right)\mathrm{Q}\left(\frac{2-ab}{b}\right) \quad (6.17)$$

$$a \triangleq \frac{\ln\Gamma - \mu_C(R_2)}{\sigma_C(R_2)}, b \triangleq \frac{\alpha_c}{\sigma_C(R_2)} \quad (6.18)$$

$$a_2 = a + b\ln(R_2/R_c), a_1 = a + b\ln(R_1/R_c). \quad (6.19)$$

Proof. See Appendix D.1. □

Lemma 8 provides a simple method for estimating the cell-averaged macrocell throughput per subchannel. The probability that a user lies in an annulus with inner radius R_{m-1} and outer radius R_m ($1 \leq m \leq M$ with $R_0 = 0$) equals $\frac{\pi(R_m^2 - R_{m-1}^2)}{|\mathcal{H}|}$. We make use of assumptions 18 through 19 for computing the shadowing parameters σ_C and μ_C at discrete locations $R_m, 1 \leq m \leq M$ where $R_M = \sqrt{\frac{|\mathcal{H}|}{\pi}}$. The spatially

averaged SIR distribution for a macrocell user is therefore approximated as follows

$$\Pr(\mathrm{SIR}_c \leq \Gamma) = \mathbb{E}_R[\Pr(\mathrm{SIR}_c(R) \leq \Gamma)] \tag{6.20}$$

$$\approx \sum_{m=1}^{M} \mathbb{E}_R[\Pr(\mathrm{SIR}_c \leq \Gamma | R_{m-1} \leq R \leq R_m)] \cdot \frac{\pi(R_m^2 - R_{m-1}^2)}{|\mathcal{H}|} \tag{6.21}$$

$$= 1 - \frac{\pi R_1^2}{|\mathcal{H}|} C\left(a_1 + b_1 \ln \frac{R_1}{R_c}, b_1\right)$$
$$- \sum_{m=2}^{M} \frac{\pi}{|\mathcal{H}|}\left[R_m^2 C\left(a_m + b_m \ln \frac{R_m}{R_c}, b_m\right) - R_{m-1}^2 C\left(a_m + b_m \ln \frac{R_{m-1}}{R_c}, b_{m+1}\right)\right] \tag{6.22}$$

where $a_m \triangleq \dfrac{\ln \Gamma - \mu_C(R_m)}{\sigma_C(R_m)}$ and $b_m \triangleq \alpha_c/\sigma_C(R_m)$

where (6.21) approximates (6.20) by spatially averaging SIR_c over M different annulus. Equation (6.22) is obtained by substituting (6.16) inside the conditional expectation in (6.21) and the corresponding probability that the user lies in annulus $m, 1 \leq m \leq M$. Combining equations (6.4) and (6.20), the average macrocell throughput S_c in a given subchannel is given as

$$S_c = \sum_{l=1}^{L-1} l \cdot \mathbb{E}_R[\Pr(\Gamma_l \leq \mathrm{SIR}_c(R) < \Gamma_{l+1})] + L \cdot \mathbb{E}_R[\Pr(\mathrm{SIR}_c(R) \geq \Gamma_L)]$$
$$= \sum_{l=1}^{L-1} l \cdot (\mathbb{E}_R[\Pr(\mathrm{SIR}_c(R) \leq \Gamma_{l+1})] - \mathbb{E}_R[\Pr(\mathrm{SIR}_c(R) < \Gamma_l)])$$
$$+ L \cdot \mathbb{E}_R[\Pr(\mathrm{SIR}_c(R) > \Gamma_L)]. \tag{6.23}$$

Figure 6.2 plots S_c (in b/s/Hz) with RR scheduling as a function of the outdoor path loss exponent α_c for the system parameters in Table 6.1. The close agreement between theory and numerical simulations indicates that the theoretically obtained SIR distribution is an accurate approximation for practical throughput in a macrocellular environment.

6.3.2 Macrocell Throughput: PF Scheduling

In contrast to a RR scheduler, a PF scheduler enables macrocell users to compete for resources based on their requested rates normalized by their average throughput thus far. Consequently, the macrocell selects the user with the highest rate relative to their average rate. During the transmission interval n in subchannel m, denote $R_k[m,n]$ as the requested rate for user $k, 1 \leq k \leq U_c$, located at position $\mathbf{r}_k$ w.r.t the central macrocell C. Let $\bar{R}_k[n]$ be the windowed mean throughput obtained by user k over the F_c frequency subchannels allocated for macrocell transmission. The PF scheduler selects the user $\tilde{k}$ whose current supportable rate is highest relative to their mean rate. The scheduling policy per subchannel m with equal per-subchannel transmission powers (Assumption 17) is described as

$$\tilde{k}(m,n) = \arg\max_{1 \leq k \leq U_c} \frac{R_k[m,n]}{\bar{R}_k[n]}. \tag{6.24}$$

Note that mobile user k calculates $R_k[m,n]$ using (6.2) and (6.11) respectively. The windowed throughput per user prior to transmission interval $(n+1)$ is updated according to the rule,

$$\bar{R}_k[n+1] = (1 - \frac{1}{N})\bar{R}_k[n] + \frac{1}{N}\sum_{m=1}^{F_c} R_k[m,n]\mathbf{1}[k = \tilde{k}(m,n)], 1 \leq k \leq U_c \tag{6.25}$$

where $\mathbf{1}[\cdot]$ is the indicator function determining whether user k is scheduled during transmission interval n in frequency link or not. The window size N is a parameter that is selected considering the delay tolerance for each user. Choosing a smaller N enables a given user to be scheduled more often, whereas choosing larger N relaxes the fairness constraint and allows the scheduler to wait longer before scheduling a user. By the strong law of large numbers, the average throughput per frequency subchannel for a given set of user positions is obtained from the sample average over a long duration and expressed as

$$\mathbb{E}[\bar{R}(F_c, U_c)|\mathbf{r}_1, \cdots \mathbf{r}_{U_c}] = \lim_{n \to \infty} \frac{1}{n}\sum_{j=1}^{n}\sum_{m=1}^{F_c} \frac{R_{\tilde{k}}[m,j]}{F_c}, \tilde{k} \in \{1, 2 \cdots U_c\} \tag{6.26}$$

where the expectation on the left hand side is over the joint pdf of all channel gains between users and their serving and interfering BSs. The spatial averaged subchannel macrocell throughput is obtained by averaging (6.26) w.r.t the joint pdf $f_{\mathbf{R}_1,\cdots\mathbf{R}_{U_c}}(\cdot)$ and given as

$$T_c(\rho, U_c) = \mathbb{E}_{\mathbf{R}_1,\cdots\mathbf{R}_{U_c}}[\mathbb{E}[\bar{R}(F_c, U_c)|\mathbf{R}_1 = \mathbf{r}_1, \cdots \mathbf{R}_{U_c} = \mathbf{r}_{U_c}]]. \tag{6.27}$$

Using (6.27) to compute $T_c(\rho, U_c)$ is analytically intractable. this work resorts to numerical simulation to empirically estimate $S_c(\rho, U_c)$, which is used to derive the bandwidth partitioning. In the simulation, the number of subchannels is set as $F_c = 1$ with a link bandwidth $W = 15$ KHz and a PF window parameter $N = 500$ OFDM symbols. Each mobile is moving at $v = 13.34$ m/s (30 mph) and the per-link throughput (6.26) is averaged over 500 drops, with 8000 trials/drop for modeling time-varying Rayleigh fading. The Rayleigh fading is held fixed over a duration $S_c = 0.4/f_d$ where $f_d = \frac{vf_c}{3*10^8}$ is the doppler frequency at a carrier frequency $f_c = 2$ GHz. Fig. 6.3 compares the performance of PF (numerically evaluated) versus RR scheduling for different U_c. Exploiting channel variations through proportional fairness *roughly doubles* the expected subchannel throughput.

6.3.3 Femtocell Throughput

Using F-ALOHA, the interfering femtocells with respect to a (typical) reference femtocell F_0 form a marked SPPP $\Lambda_f \subseteq \Phi_f$ with intensity $\rho_f \lambda_f$. In a given frequency subchannel, the cochannel interference $I_{f,f}$ experienced by an indoor user served by F_0 is given as

$$I_{f,f} = \sum_{k \in \Lambda_f} A_f \Theta_{0k} |h_{0k}|^2 |x_{0k}|^{-\alpha_f} \tag{6.28}$$

where $\Theta_{0k} \sim \mathrm{LN}(\zeta\mu_{fo,\mathrm{dB}}, \zeta^2\sigma^2_{fo,\mathrm{dB}})$ represents the lognormal shadowing, and $|h_{0k}|^2$ is the exponentially distributed channel power between interfering femtocell F_k and user 0. Denoting the exponentially distributed channel power between F_0 and user 0

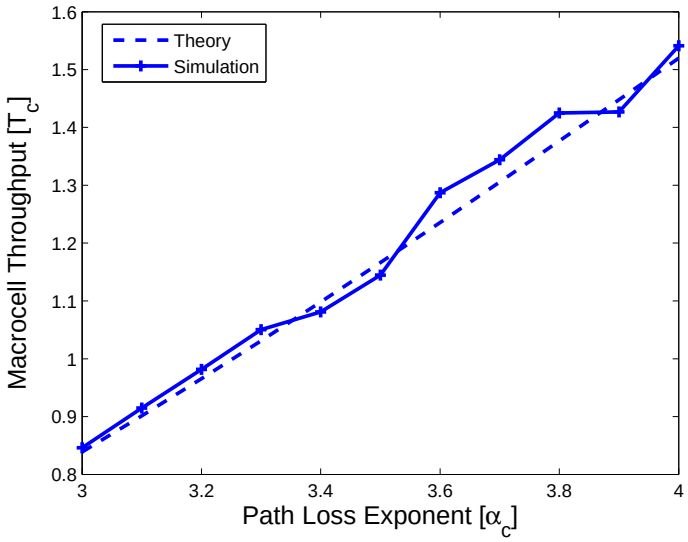

Figure 6.2: S_c (in bps/Hz) versus outdoor path loss exponent α_c.

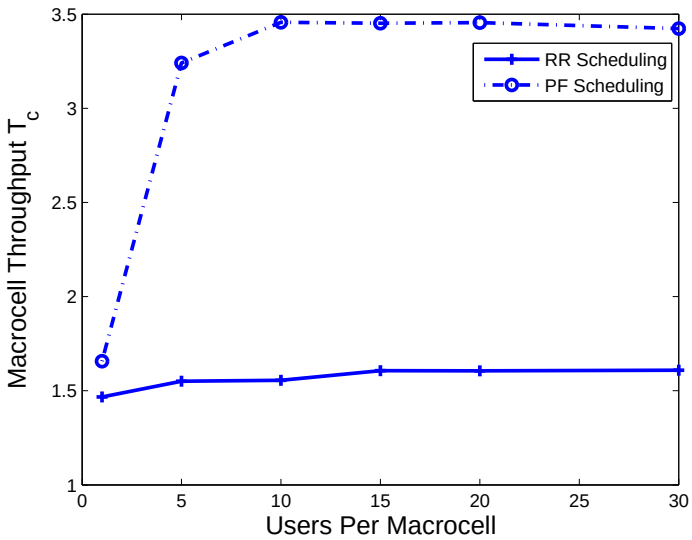

Figure 6.3: S_c (in bps/Hz) with RR and PF Scheduling, $\alpha_c = 4$.

as $|h_0|^2$ and assuming that user 0 is located at distance R_f w.r.t F_0, the received SIR is given as

$$\mathrm{SIR}_f = \frac{B_f \Theta_0 |h_0|^2 |R_f|^{-\beta_f}}{\sum\limits_{k \in \Lambda_f} A_f \Theta_{0k} |h_{0k}|^2 |x_{0k}|^{-\alpha_f}}. \tag{6.29}$$

Here, $|x_{0k}|$ are the distances of the interfering femtocells F_k w.r.t user 0, while $\Theta_0 \sim \mathrm{LN}(\zeta \mu_{fi,\mathrm{dB}}, \zeta^2 \sigma^2_{fi,\mathrm{dB}})$ designates the indoor lognormal shadowing experienced by user 0. The terms α_f [resp. β_f] represent the path loss exponents resulting from interfering transmissions [resp. in-home transmissions] to user 0. A simple model is used to distinguish between the fixed losses arising from in-home and interfering transmissions: specifically, home users are insulated against interfering femtocell transmissions through double partition losses arising from external wall partitions [2]. Consequently, A_f and B_f (in dB) are related as $A_{f,\mathrm{dB}} = B_{f,\mathrm{dB}} + 2P_{f,\mathrm{dB}}$ where $P_f = \sqrt{\frac{A_f}{B_f}}$ is the wall partition loss.

Using Assumption 18, $\Theta_0 |h_0|^2$ is well approximated as a lognormal r.v $\Psi_0 \sim \mathrm{LN}(\mu_S, \sigma_S^2)$. Similarly, the channel powers $\Theta_{0k}|h_{0k}|^2 \forall k$ are approximated as identical and independently distributed r.v's $\Psi_I \sim \mathrm{LN}(\mu_I, \sigma_I^2)$. Equation (6.29) then simplifies to

$$\mathrm{SIR}_f = \frac{\Psi_0 |R_f|^{-\beta_f}}{\sum\limits_{k \in \Lambda_f} P_f^2 \Psi_{0k} |x_k|^{-\alpha_f}}. \tag{6.30}$$

The closed form distribution of interference from neighboring femtocells $I_{f,f}$ is known only for $\alpha_f = 4$[107]. However, tight lower bounds on $\Pr(I_{f,f} > y)$ are obtained by only considering femtocells whose interference *individually* exceeds y. The following lemma, derived in Weber *et al.* [143] provides an asymptotically tight lower bound on the tail distribution of $I_{f,f}$.

Lemma 9. *[143, Theorem 3] With randomized transmissions and lacking power control, the lower bound on distribution of $I_{f,f}$ is given as*

$$\Pr(I_{f,f} > y) \geq 1 - \exp\left[-\pi \lambda_f \rho_f \mathbb{E}[\Psi_I^{\delta_f}] P_f^{2\delta_f} y^{-\delta_f}\right] \tag{6.31}$$

where $\delta_f \triangleq \frac{2}{\alpha_f}$. *When* $\alpha_f = 4$, $I_{f,f}$ *is distributed Ch5:AS:*

$$\Pr(I_{f,f} > y) = 1 - \operatorname{erfc}\left(\frac{\pi^{3/2}\lambda_f \rho_f P_f \mathbb{E}[\Psi^{1/2}]}{2\sqrt{y}}\right). \tag{6.32}$$

Lemma 9 provides the relationship between the density $\lambda_f \rho_f$ of interfering femtocells in Λ_f and the distribution of the CCI at a femtocell. For fixed y, as $\rho_f \to 0$, the tail probability $\Pr(I_{f,f} > y) \to 0$ in (6.31) indicating that selecting fewer subchannels using F-ALOHA transmission provides greater resilience against persistent collisions from nearby femtocells. The femtocell SIR distribution in (6.29) is given as

$$\Pr\left(\mathrm{SIR}_f \leq \Gamma\right) = \Pr\left(\frac{\Psi_0 |R_f|^{-\beta_f}}{\sum\limits_{k \in \Lambda_f} P_f^2 \Psi_{0k} |x_k|^{-\alpha_f}} \leq \Gamma\right) \tag{6.33}$$

$$= \mathbb{E}_{\Psi_0}\left[\Pr\left(\sum_{k \in \Lambda_f} P_f^2 \Psi_{0k} |x_k|^{-\alpha_f} \geq \frac{\psi_0 |R_f|^{-\beta_f}}{\Gamma} \Big| \Psi_0 = \psi_0\right)\right] \tag{6.34}$$

$$\geq 1 - \mathbb{E}_{\Psi_0}\left\{\exp\left[-\pi \lambda_f \rho_f \mathbb{E}[\Psi_I^{\delta_f}]\left(\frac{P_f^2 \Gamma}{\Psi_0 |R_f|^{-\beta_f}}\right)^{\delta_f}\right]\right\} \tag{6.35}$$

$$= 1 - \mathbb{E}_{\Psi_0}[\exp\left(-\rho_f \kappa_f \Gamma^{\delta_f} \Psi_0^{-\delta_f}\right)] \tag{6.36}$$

where, $\kappa_f \triangleq \pi \lambda_f \mathbb{E}[\Psi_I^{\delta_f}](P_f^2 |R_f|^{\beta_f})^{\delta_f}$

where (6.34) and (6.35) follow by conditioning on Ψ_0, assuming independence of Ψ_0 and Ψ_{0k} $\forall k \in \Lambda_f$, and applying (6.31). Although it is not possible to obtain a closed form expression for the expectation in (6.36), the distribution of SIR_f can be calculated numerically. The mean subchannel throughput S_f is calculated by combining (6.4) and (6.36):

$$S_f(\rho_f \lambda_f) = \sum_{l=1}^{L-1} l \cdot \Pr(\Gamma_l \leq \mathrm{SIR}_f < \Gamma_{l+1}) + L \cdot \Pr(\mathrm{SIR}_f \geq \Gamma_L) \tag{6.37}$$

$$\approx \sum_{l=1}^{L-1} l \cdot \mathbb{E}_{\Psi_0}[\exp\left(-\rho_f \kappa_f \Gamma_{l+1}^{\delta_f} \Psi_0^{-\delta_f}\right) - \exp\left(-\rho_f \kappa_f \Gamma_l^{\delta_f} \Psi_0^{-\delta_f}\right)]$$

$$+ L \cdot \mathbb{E}_{\Psi_0}[\exp\left(-\rho_f \kappa_f \Gamma_L^{\delta_f} \Psi_0^{-\delta_f}\right)]. \tag{6.38}$$

The approximation in (6.37) is because the right-hand side in (6.36) is a lower bound on $\Pr(\mathrm{SIR}_f \leq \Gamma)$. Figure 6.4 plots the femtocell throughput $(1-\rho)\rho_f S_f$ (in b/s/Hz) assuming the entire bandwidth is allocated to femtocells ($\rho = 0$). Black dash-dotted curves show results of numerical simulations. Two cases are considered namely (1) high attenuation (marked "HA" with $\alpha_f = 4, P_{f,dB} = 10$) and (2) low attenuation (marked "LA" with $\alpha_f = 3.5, P_{f,dB} = 2$) from neighboring femtocells. Setting $\rho_f = 1$ and assuming $N_f = 50$ femtocells/cell site, the femtocell throughput falls from approximately 4.5 b/s/Hz in a HA environment to nearly 0.5 b/s/Hz in LA scenario, indicating the sensitivity of femtocell throughput to propagation from nearby femtocells.

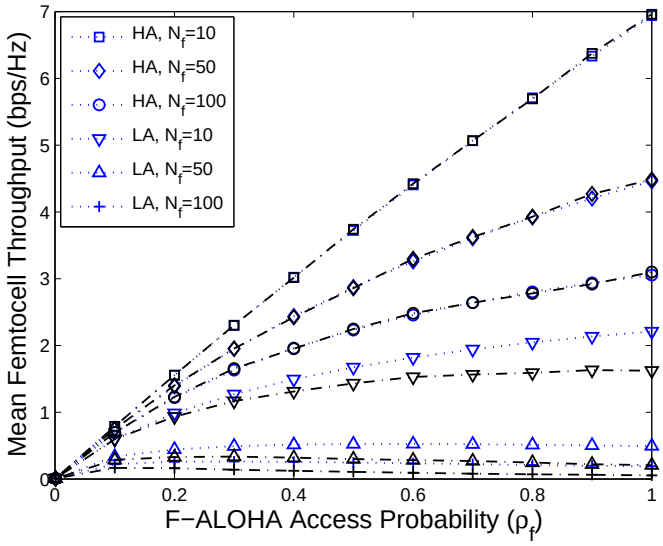

Figure 6.4: Theoretical and empirical throughput per femtocell $\rho_f S_f$ (b/s/Hz).

To calculate the optimum ρ_f, we determine the optimal fraction of subchannels accessed by each femtocell for maximizing spatial reuse, given as the solution to the following optimization problem

$$\rho_f^* = \lambda_f \arg\max_{0<\theta\leq 1} \theta S_f(\theta\lambda_f), \;\; \mathrm{ASE}_f^* = \rho_f^* \lambda_f S_f(\rho_f^* \lambda_f). \tag{6.39}$$

To justify (6.39), observe that there are an average of $|\mathcal{H}|\rho_f\lambda_f$ transmitting femtocells per subchannel. With F-ALOHA access of $0 < \theta \leq 1$, each femtocell obtains an average subchannel throughput of $S_f(\theta)$, resulting in ASE_f equaling $\lambda_f\theta \cdot S_f(\theta\lambda_f)$. Alternatively, given any allocation ρ, (6.39) computes the F-ALOHA spectrum access ρ_f which maximizes the mean *overall* throughput $(1-\rho)\rho_f S_f(\rho_f\lambda_f)$ per femtocell.

Remark 14 (**Boundedness of the ASE**). *The ASE in* (6.39) *depends only on the effective intensity $\lambda_f\rho_f^*$ of interfering femtocells per subchannel. With increasing λ_f, provided $\rho_f^* < 1$, then the intensity of Λ_f given as $\lambda_f\rho_f^*$ remains constant, implying that the optimal ρ_f decreases inversely as λ_f. Consequently, if $\rho_f < 1$ for a given λ_f, the maximum ASE per subchannel is fixed. This also means that with increasing λ_f, the network-wide femtocell throughput equaling $|\mathcal{H}|WF \cdot (1-\rho)\text{ASE}_f^*$ grows linearly with $(1-\rho)$.*

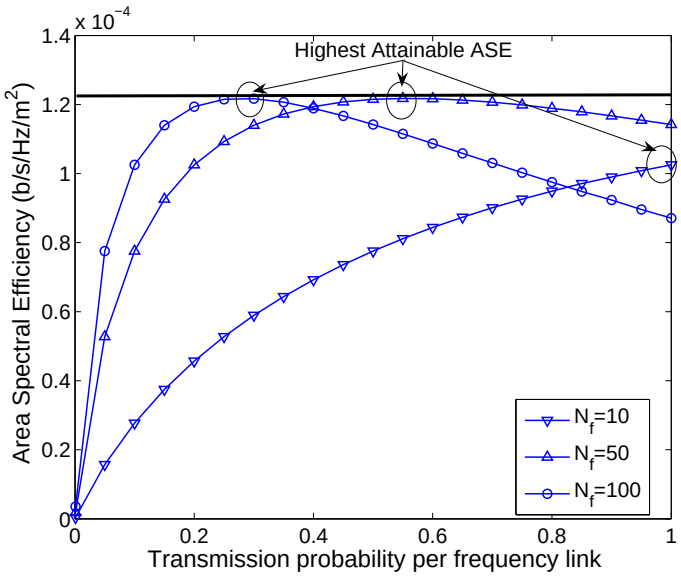

Figure 6.5: Femtocell ASE Vs F-ALOHA access probability.

Fig. 6.5 plots (6.39) for different N_f with $\alpha_f = 3.5$ and $P_{f,dB} = 2$. In all cases, the highest ASE is fixed at nearly 0.000121 b/s/Hz/m^2 validating Remark

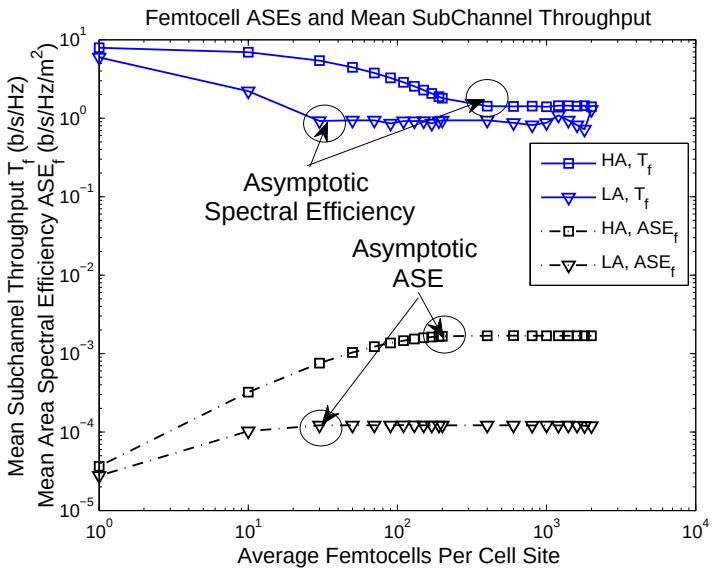

Figure 6.6: Femtocell ASEs and subchannel throughputs.

14. With a low femtocell density ($N_f = 10$ femtocells/cellsite), the best strategy is for each femtocell to access its entire allocated spectrum. In a dense network ($N_f = 100$ femtocells/cellsite), the ASE is maximized when each femtocell accesses approximately 30% of the available spectrum. Further, in (6.39), as long as $\rho_f^* = 1$, each femtocell accesses the entire available spectrum $(1-\rho)$, consequently S_f *decreases* with addition of femtocells. Whenever $\rho_f^* < 1$, $S_f = \text{ASE}_f/(\lambda_f \rho_f^*)$ remains constant with increasing λ_f (Fig. 6.6). As $\lambda_f \to \infty$, since $\rho \in (0, 1)$, the mean throughput per femtocell approaches zero, as the following limit shows:

$$\lim_{\lambda_f \to \infty} S_f(1-\rho)\rho_f \leq \lim_{\lambda_f \to \infty} S_f.\rho_f = 0 \tag{6.40}$$

One may explore the dependence of the mean overall femtocell throughput $S_f \rho_f (1-\rho)$ on the spectrum allocation ρ and F-ALOHA access ρ_f. Equivalently: *With increasing femtocell density λ_f, can increasing allocated spectrum $(1-\rho)$ to femtocells counterbalance decreasing F-ALOHA access ρ_f to result in a higher mean femtocell throughput?*

This question is answered by the following condition: Given an allocation ρ_l

at femtocell density λ_f, let $T_{f,l}$ and $\rho_{f,l}$ be the mean subchannel throughput and the optimal F-ALOHA access respectively. On increasing λ_f by $\delta\lambda_f$ with allocation ρ_h, let the corresponding quantities equal $T_{f,h}$ and $\rho_{f,h}$. The femtocell network is defined as *fully-utilized [resp. sub-utilized]* if a marginal increment in the femtocell density *reduces [resp. improves]* the mean throughput per femtocell given as

$$\begin{aligned} (1-\rho_l)\rho_{f,l}T_{f,l} &\gtreqless (1-\rho_h)\rho_{f,h}T_{f,h} \\ \iff (1-\rho_l)\frac{\mathrm{ASE}_{f,l}}{\lambda_f} &\gtreqless (1-\rho_h)\frac{\mathrm{ASE}_{f,h}}{\lambda_f+\delta\lambda_f} \\ \iff \frac{1-\rho_h}{1-\rho_l} &\lesseqgtr \frac{\mathrm{ASE}_{f,l}}{\mathrm{ASE}_{f,h}}\cdot\frac{\lambda_f+\delta\lambda_f}{\lambda_f} = \frac{T_{f,l}}{T_{f,h}}\frac{\rho_{f,l}}{\rho_{f,h}}. \end{aligned} \tag{6.41}$$

Equation (6.41) reflects the competing effects of increasing allocation $(1-\rho)$ and decreasing F-ALOHA access ρ_f (or increasing λ_f) in determining the net femtocell throughput.

6.4 Numerical Results

Results are presented in Figs. 6.7 through 6.10 with the system parameters in Table 6.1. The number of users in each tier is controlled by varying N_f. To model the different data-rates demanded by femtocell users relative to cellular users, QoS values of $\eta = 0.5$ (equal per-user throughputs in each tier) and $\eta = 0.01$ (favoring 100x higher throughput per femtocell user relative to a cellular user) are considered. Two propagation scenarios are presented namely 1) High Attenuation (HA) of neighboring femtocell transmissions with parameters $\alpha_f = 4$ and $P_{f,dB} = 10$ and 2) a Low Attenuation (LA) scenario by setting $\alpha_f = 3.5$ and $P_{f,dB} = 2$.

Fig. 6.7 shows the allocation using (6.9) with RR scheduling per-tier. With equal average per-user throughputs ($\eta = 0.5$), nearly 90% of the overall bandwidth is assigned to the macrocell. The central macrocell serves a higher number of users, who experience relatively poor reception over a bigger area. Equalizing per-user throughputs consequently requires assigning almost the entire spectrum to the macrocell. As

Table 6.1: System Parameters

Symbol	Description	Value
R_c, R_f	Macrocell, Femtocell Radius	288 m, 40 m
U	Total users per cell site	300
U_f	Users per femtocell	2
$P_{f,\text{dB}}$	Wall partition loss	2 dB, 10 dB
G, L	Shannon Gap, Modulation Levels	3 dB, 8
α_c	Path loss exponent (Cellular)	4
α_f	Path loss exponent (Femtocell to Femtocell)	$3.5, 4$
β_f	Path loss exponent (Inside Home Femtocell)	3
$\sigma_{c,\text{dB}}, \sigma_{fi,\text{dB}}, \sigma_{fo,\text{dB}}$	Lognormal Shadow Parameters	8 dB, 4 dB, 12 dB

η decreases, femtocells require more spectrum for providing greater indoor capacity; eg. in a LA scenario with $\eta = 0.01$ and $N_f = 50$ femtocells/cell site, nearly 70% of spectrum is allocated to femtocells.

Fig. 6.8 plots the ASEs of the two-tier network using (6.6). In a LA scenario with $\eta = 0.01$, the high degree of co-channel interference results in the ASE maximized with fewer than $N_f = 50$ femtocells. Following Remark 14, this indicates that adding more femtocells does not provide additional spatial reuse. In all other cases, the ASEs monotonically increase with N_f indicating increasing spatial reuse with addition of femtocells. To show benefits of opportunistic scheduling, a PF scheduler provides nearly 2.3x [resp. 1.35x] ASE gains relative to a RR scheduler in a HA scenario with QoS parameter $\eta = 0.5$ [resp. $\eta = 0.01$] and $N_f = 110$ femtocells/cell site.

Fig. 6.9 plots the expected throughput per femtocell $(1-\rho)\rho_f S_f$ as a function of N_f and η. For $\eta = 0.5$, the throughputs monotonically increase with N_f indicating that increasing spectrum allocation $(1-\rho)$ counteracts the effects of decreasing $\rho_f S_f$; in effect, the femtocell network is sub-utilized. With $\eta = 0.01$ in a LA environment however, the femtocell throughputs decrease with increasing N_f, indicating that the femtocell network is fully-utilized.

Fig. 6.10 plots the minimum required spectrum WF, satisfying a target av-

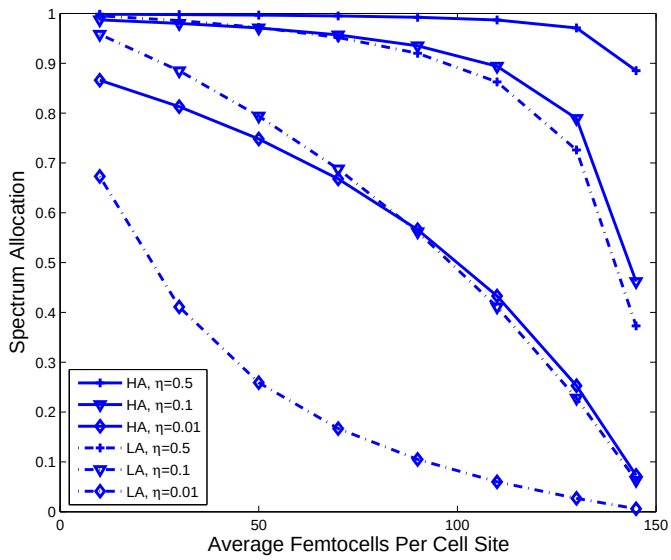

Figure 6.7: Optimal spectrum allocation ρ for varying QoS parameter η.

erage data rate of $D_c = 0.1$ Mbps for each macrocell user. For each femtocell, we consider QoS parameter values $\eta = 0.5$ and $\eta = 0.01$ corresponding to target average data rates $D_f = D_c(1-\eta)/\eta$ equaling 0.1 and 10 Mbps per hotspot user. Since Proposition 3 ensures that the QoS constraint in (6.7) is binding, the required spectrum WF is given Ch5:AS:

$$WF = \frac{U_c}{\rho S_c} D_c = \frac{U_f}{(1-\rho)\rho_f S_f} D_f. \tag{6.42}$$

Two key observations are: First, a macrocell with a channel aware PF scheduling obtains significant spectrum savings to guarantee D_f and D_c; eg. with $\eta = 0.01$ and $N_f = 50$ femtocells/cell site in a HA scenario, the spectrum reduction is nearly 40% (10 MHz) relative to RR scheduling. Next, with $\eta = 0.01$ and a LA scenario, adding femtocells requires a linear increase in spectrum WF indicating the femtocell network is fully-utilized in (6.41). Conversely, in a HA scenario, the femtocell network is sub-utilized in (6.41), hence adding femtocells increases the mean throughput per femtocell.

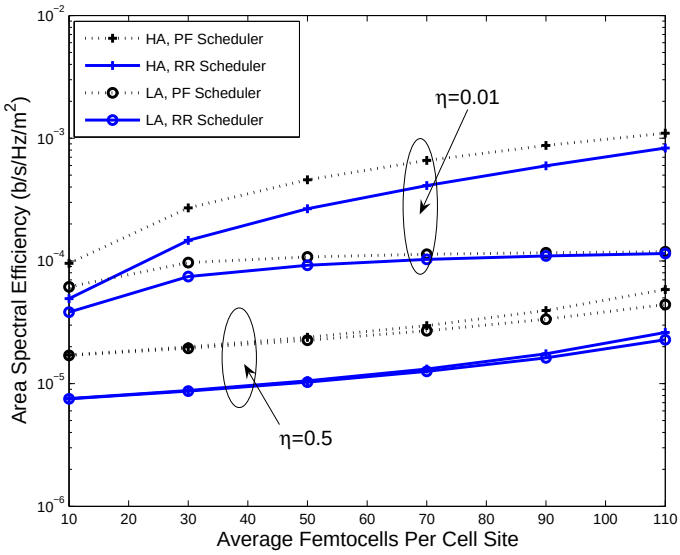

Figure 6.8: Area Spectral Efficiencies in a two-tier network for varying QoS parameter η.

6.5 Conclusions

This work has proposed a decentralized spectrum allocation strategy as an alternative to centralized/coordinated frequency assignment in a two-tier network. The proposed allocation depends on the per-tier throughputs, the loading of users in each tier and the QoS requirements, accounting for co-channel interference and path losses. With a randomized spectrum access strategy, femtocells should access a decreasing fraction of their allocated spectrum with increasing femtocell density, in order to maximize spatial reuse. Spatial reuse benefits derived from channel aware macrocell scheduling result in nearly 50% spectrum reduction for meeting target per-tier data rates. In a low interference scenario where addition of hotspots provides increased spatial reuse, the spectrum requirement is unchanged up to 110 femtocells/cell site. On the other hand, the limited spatial reuse in high interference scenarios necessitates increasing spectrum with addition of femtocells. These insights provide guidelines on

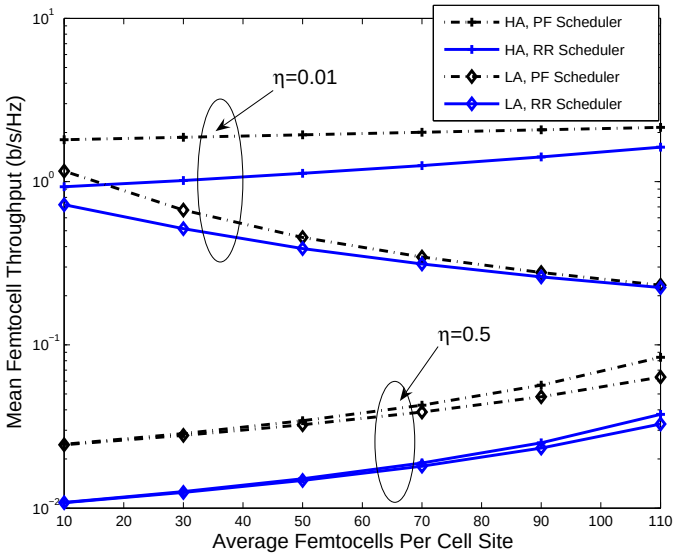

Figure 6.9: Average network-wide throughput $\rho_f S_f(1-\rho)$ (in b/s/Hz) provided by femtocells in their allocated spectrum $(1-\rho)$.

performance of decentralized spectrum allocation in the two-tier networks.

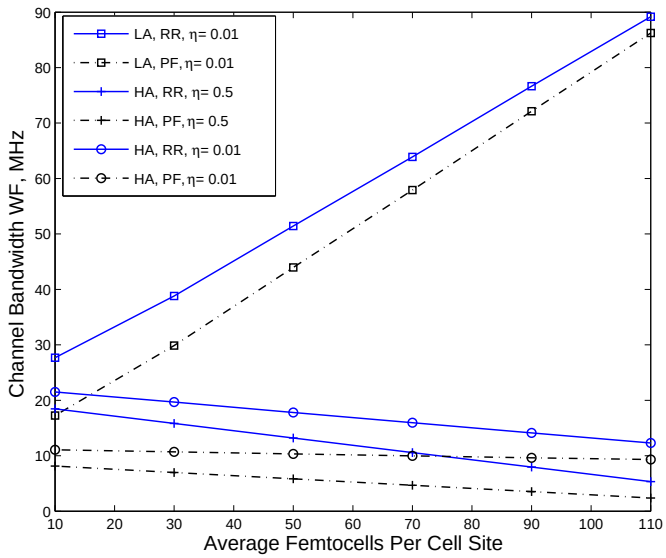

Figure 6.10: Required spectrum WF meeting a target average data rate of $D_c = 0.1$ Mbps for each macrocell user, given Round-Robin and Proportional-Fair scheduling at the macrocell.

Chapter 7

Conclusions and Future Work

7.1 Conclusions

The conventional paradigm of expanding cellular system capacity was by installing ever increasing numbers of macrocell BS towers (in addition to improved modulation and coding techniques). The key problem with adding more macrocell (or microcell) BSs was a) substantial resource and capital investments for the cellular operator, and b) these deployments do not scale well with the ever increasing demand for data rates for reasons of economy and scarce availability of spectrum.

In contrast, supplementary hotspot infrastructure in the form of femtocells, distributed antennas and relays ameliorate wireless capacity by exploiting the relative proximity of users to their AP (thereby reducing the average transmit-receive communication distance), resulting in a greater number of cochannel transmissions per square meter. Because these technologies potentially require less capital and scale with the number of users, cellular operators can recoup their initial investments within a relatively shorter duration and offer better service, while consuming less bandwidth.

This dissertation has addressed the key technical challenges confronting tiered cellular wireless systems when cellular and hotspot users either share radio spectrum or operate over orthogonal spectrum. Our main thesis is that tiered networks with universal frequency reuse will be significantly encumbered by significant levels of cross-tier interference, which results from the significant disparity in communication distances over the cellular and hotspot networks. Specifically, there is a fundamental

tradeoff between providing reliable cellular coverage and providing reliable hotspot operation. Addressing this problem is challenged due to the absence of coordination between the macrocell and femtocell BS transmissions due to reasons of scalability, security and limited backhaul capacity. The net consequence is that accommodating greater numbers of hotspots (or providing higher hotspot data rates) reduces the number of cellular users that can reliably operate in the same spectrum. Without interference management, adding femtocells will likely be self-defeating, because of the potentially likely disruption in reliable outdoor coverage at the primary cellular infrastructure.

The focus of this work has been to address decentralized radio interference management in femtocell-aided cellular architectures, encompassing a variety of physical layer technologies, through a combination of interference avoidance, power control and spectrum allocation techniques for alleviating cross-tier interference and improving system capacity. With interference avoidance, cellular and hotspot users attempt to avoid causing mutual collisions (through time-hopping and antenna sectorization). Interference mitigation is achieved by forcing femtocells to choose their target data rates (and hence their transmit powers) for minimizing cross-tier interference inflicted on cellular users. This thesis has developed power control schemes which require femtocells to adjust their target data rates either upon sensing the presence of an active cellular user within its radio range, or upon receiving a broadcast from the macrocell BS. The efficacy of these power control schemes has been demonstrated in typical cellular path loss scenarios even when large number of femtocells are deployed. Finally, the spectrum allocation scheme suggested in this thesis maximizes spatial reuse in two-tier networks employing FDMA, while guaranteeing a minimum desirable Quality-of-Service to users in either tier.

7.2 Future Work

Adaptive Access. Open-access (or public access) femtocell operation will enable cellular users experiencing poor macrocell coverage to undergo handoff to a nearby femtocell, thereby reducing radio interference at both the macrocell and femtocell BSs. It is reasonable to assume that a practical system would assign weighted priorities to serviced users with the paying home consumers receiving higher priority. Closed-access operation, on the other hand, provides privileged access to the home user which is desirable when backhaul capacity is limited. Because the femtocells transport their traffic over the internet backhaul, the available excess backhaul capacity will most likely influence whether a femtocell should serve an unlicensed user without deteriorating the Quality-of-Service provided to the tariff paying home consumer.

An open research problem is to analyze which mode of operation (open-access or closed-access) is preferable either from the perspective of the paying home consumer (as an instance, which operation yields a higher average throughput), or from the perspective of the entire network (a centralized entity could maximize the network-wide spatial reuse by determining two classes of hotspots: one would provide open access, and the other set would operate with closed access). The implication is that femtocells would adaptively configure their access mode depending on their location, the prevailing levels of co-channel interference, the channel conditions between users to their BSs, the number of already serviced users in each femtocell and their prevailing target data-rates.

Coverage and Handoffs. In open-access operation, the network overhead arising from handoffs from the cellular BS to a femtocell hotspot will seriously challenge practical deployments of large numbers of femtocells. One method of minimizing frequent handoff events is that femtocells dynamically adapt their coverage radius – also called "cell breathing" [95] – depending on their channel conditions, and the

number of users served by each femtocell. Femtocell handoff procedures should carefully choose the femtocell pilot signal strengths in order to load balance users across tiers [37, 156]. The problem of determining the "optimal" femtocell coverage radius as a function of the available excess backhaul bandwidth, the time-varying channel strength and cellular user mobility (governing dwell times) is an open avenue for further research.

Appendices

Appendix A

Appendix to Chapter 3

A.1 Lemma 1

With TH-CDMA transmission over N_{hop} slots and antenna sectoring with N_{sec} directed BS antennas in each tier, the interfering field at a given antenna sector can be mapped to the SPPPs Φ_c and Φ_f on $\mathbb{R}^2$ with intensities $\eta_c = \lambda_c/(N_{hop}N_{sec})$ and $\eta_f = \lambda_f(1 - e^{-U_f})/(N_{hop}N_{sec})$ respectively.

Proof. Consider the Poisson field of interferers as seen at any antenna sector (either macrocell or femtocell BS) with antenna alignment angle θ. Assuming a perfect antenna radiation pattern, the interfering Poisson field forms heterogeneous SPPPs $\hat{\Omega}_c$ and $\hat{\Omega}_f$ with intensities respectively given as

$$\begin{aligned}\hat{\lambda}_c(r,\phi) &= \frac{\lambda_c}{N_{\text{hop}}} \cdot \mathbf{1}\left(\phi \in \left[\theta, \theta + \frac{2\pi}{N_{\text{sec}}}\right]\right) \\ \hat{\lambda}_f(r,\phi) &= \frac{\lambda_f}{N_{\text{hop}}}(1 - e^{-U_f}) \cdot \mathbf{1}\left(\phi \in \left[\theta, \theta + \frac{2\pi}{N_{\text{sec}}}\right]\right)\end{aligned} \tag{A.1}$$

where the indicator $\mathbf{1}(\cdot)$ is defined as $\mathbf{1}(x \in \mathcal{X}) \triangleq 1$ if $x \in \mathcal{X}$ and zero otherwise. Equation (A.1) is justified for the following reasons namely,

Hopping slot selection: The set of cellular users and femtocell BSs transmitting over any hopping slot is obtained by independent Bernoulli thinning of the individual SPPPs Ω_c and Ω_f by the probability of choosing that hopping slot namely $1/N_{\text{hop}}$.

Active femtocell selection: The factor $(1 - e^{-U_f})$ arises because the set of femtocells with *at least one actively transmitting user* is obtained using independent

Bernoulli thinning of Ω_f [91]. Observe that a femtocell with $U \geq 1$ actively transmitting users satisfies $\mathbb{E}[U] = \frac{U_f}{1-e^{-U_f}}$.

The event consisting of marking femtocells by the probability that they contain at least one actively transmitting user and the event of marking femtocells by the probability of choosing a common hopping slot are independent; this implies that the resulting SPPP $\hat{\Omega}_f$ has intensity $\frac{\lambda_f}{N_{\text{hop}}}(1-e^{-U_f})$. Finally, using the Mapping theorem [91, Section 2.3] for Poisson processes, one can map the heterogeneous SPPPs $\hat{\Omega}_c$ and $\hat{\Omega}_f$ over one antenna sector to homogeneous SPPPs Φ_c and Φ_f over $\mathbb{R}^2$ with intensities $\eta_c = \frac{\lambda_c}{N_{\text{hop}}N_{\text{sec}}}$ and $\eta_f = \frac{\lambda_f}{N_{\text{hop}}N_{\text{sec}}}(1-e^{-U_f})$ respectively. □

A.2 Theorem 1

With a path loss exponent $\alpha = 4$, the interference terms $I_{c,f}$ and $I_{f,f}$ are identically distributed as a Poisson shot-noise process $Y = \sum_{i\in\Phi_f} Q_f \Psi_i |X_i|^{-\alpha}$ with identical and independently distributed marks Ψ_i and probability density function (pdf) and cumulative distribution function (cdf) given as

$$f_Y(y) = \sqrt{\frac{\kappa_f}{\pi}} y^{-3/2} e^{-\kappa_f/y}, F_Y(y) = \text{erfc}\left(\sqrt{\frac{\kappa_f}{y}}\right) \tag{A.2}$$

where $\kappa_f \triangleq \eta_f^2 \pi^3 Q_f (\mathbb{E}[\Psi^{1/2}])^2/4$.

Proof. From (3.2), $I_{c,f}$ (and $I_{f,f}$) are distributed as a Poisson SNP $\hat{Y} = \sum_{i\in\hat{\Omega}_f} Q_f \Psi_i |X_i|^{-\alpha}$ over an antenna sector of width $2\pi/N_{\text{sec}}$. The statistics of $\hat{Y}$ can be obtained using the following two steps.

1. Invoke Lemma 1 for mapping $\hat{\Omega}_f$ to a homogeneous SPPP Φ_f on $\mathbb{R}^2$. This implies that $\hat{Y}$ is distributed identically as $Y = \sum_{i\in\Phi_f} Q_f \Psi_i |X_i|^{-\alpha}$.

2. Map the planar SPPP defining Φ_f with intensity η_f to a one-dimensional SPPP with intensity $\pi\eta_f$ using Proposition 1, Theorem 2 in [78]. For doing so, rewrite Y as, $Y = \sum_{i\in\Phi_f} Q_f \Psi_i (|X_i|^2)^{-\alpha/2}$ which represents a SPPP on the line with Poisson arrival times $|X_i|^2$ and intensity $\pi\eta_f = \frac{\pi\lambda_f}{N_{\text{hop}}\cdot N_{\text{sec}}}(1-e^{-U_f})$.

Consequently, Y is identically distributed as a one-dimensional SPPP with intensity $\pi\eta_f$, which represents a Lévy-stable distribution with a stability exponent $\delta = 2/\alpha$ [124]. When $\alpha = 4$ (or stability exponent $\delta = 0.5$), the cumulative distribution function in (3.5) is obtained from Equation (30) in [107]. □

A.3 Theorem 2

With Poisson in-cell macrocell interference $I_{c,in}$, Gaussian out-of-cell interference $I_{c,out}$ and Lévy-stable femtocell interference $I_{c,f}$ given by (3.5)*, the outage probability at the macrocell BS antenna sector is given as*

$$\epsilon \geq \mathbb{P}^c_{out} = 1 - \frac{1}{1 - e^{-\eta_c|\mathcal{H}|}} \sum_{m=1}^{\lfloor \rho_c/P^c_r \rfloor} \frac{e^{-\eta_c|\mathcal{H}|}(\eta_c|\mathcal{H}|)^m}{m!} G_c(\tilde{\rho}_c) \tag{A.3}$$

where $\eta_c = \frac{\lambda_c}{N_{hop}N_{sec}}, \rho_c = \frac{P^c_r G}{\Gamma N_{hop}}, \tilde{\rho}_c = \rho_c - (m-1)P^c_r$ *and* $G_c(t) \triangleq \int_0^t f_{I_{c,out}}(t - y)F_{I_{c,f}}(y)\ dy$.

Proof. At the macrocell BS, the interference terms denoted by $I_{c,in}, I_{c,out}$ and $I_{c,f}$ are mutually independent random variables. The macrocell outage probability $\mathbb{P}^c_{\text{out}}$ defined in (3.3) can be computed by the probability of the complementary event, corresponding to the probability that the cumulative interference does not exceed the SIR threshold $\rho_c = GP^c_r/(\Gamma N_{\text{hop}})$. The cdf of $(I_{c,in} + I_{c,out} + I_{c,f})$ can be computed using a three-fold convolution. Observe that the event that the intra-tier macrocell interference from $(k-1)$ in-cell tier 1 interferers $I_{c,in}$ equals $(k-1)P^c_r$, given at least one active tier 1 user (user of interest), is equivalent to the event that Φ_c has exactly k elements within $\mathcal{H}$. The probability of this event is given as,

$$\mathbb{P}\left[I_{c,in} = (k-1)\cdot P^c_r \middle| k \geq 1\right] = \mathbb{P}\left[|\Phi_c| = k \middle| |\Phi_c| \geq 1\right] = \frac{1}{1 - e^{-\eta_c|\mathcal{H}|}} \frac{e^{-\eta_c|\mathcal{H}|}(\eta_c|\mathcal{H}|)^k}{k!}. \tag{A.4}$$

The total interference caused by the $(k-1)$ interfering macrocell users equals $(k-1)\cdot P^c_r$. Outage does not occur if the residual interference $I_{c,out} + I_{c,f}$ is less than

$\rho_c - (k-1)P_r^c$. Using Theorem 1 and independence of $I_{c,out}$ and $I_{c,f}$, the result follows. $\square$

A.4 Theorem 3

At any femtocell antenna sector located at distance $0 < R_0 \leq R_c$ from the macrocell BS along the hexagonal axis:

1. *The complementary cumulative distribution function (ccdf) of the cross-tier interference $I_{f,c}$ at a femtocell antenna sector is lower bounded as $\bar{F}_{I_{f,c}}(y) \geq 1 - F^{lb}_{I_{f,c}}(y)$, where*

$$F^{lb}_{I_{f,c}}(y) = \exp\left\{-\frac{\lambda_c}{N_{hop}} \iint\limits_{\mathcal{H}_{sec}} S(r,\phi;y) r\, dr\, d\phi\right\}, S(r,\phi;y) \triangleq \bar{F}_\Psi\left[\frac{yr}{P_r^c(|re^{\mathbf{i}\phi} + R_0|)^\alpha}\right]. \tag{A.5}$$

Here $\bar{F}_\Psi$ is the ccdf of $\Psi : 10\log_{10}\Psi \sim \mathcal{N}(0, 2\sigma^2_{dB})$, $\mathbf{i} \triangleq \sqrt{-1}$, θ is the femtocell BS antenna alignment angle and $\mathcal{H}_{sec} \subseteq \mathcal{H}$ denotes the region inside the reference macrocell enclosed between $\theta \leq \phi \leq \theta + 2\pi/N_{sec}$.

2. *For a corner femtocell $R_0 = R_c$ with an omnidirectional femtocell antenna $N_{sec} = 1$, the ccdf of $I_{f,c}$ is lower bounded as $\bar{F}_{I_{f,c}}(y) \geq 1 - F^{lb}_{I_{f,c}}(y)$, where*

$$F^{lb}_{I_{f,c}}(y) = \exp\left\{-3\frac{\lambda_c}{N_{hop}} \iint\limits_{\mathcal{H}} S(r,\phi;y) r\, dr\, d\phi\right\}. \tag{A.6}$$

Proof. The interference experienced at a femtocell BS antenna sector $\theta \leq \phi \leq \theta + 2\pi/N_{\text{sec}}$ is lower bounded by the cellular interference arising within $\mathcal{H}_{sec}$. If the femtocell BS is located at distance R_0 from the reference macrocell, then any macrocell user located at polar coordinates (r_i, ϕ_i) w.r.t the femtocell BS causes an interference equaling $P_r^c \Psi_i(|R_0 + re^{\mathbf{i}\phi}|/r)^\alpha$ at the femtocell BS. Corresponding to the heterogeneous SPPP Π_c (see Def. 3), outage events at the femtocell BS arising from

cellular interference $I_{f,c}$ can be categorized into two types: In the first type, outage events arise due to interference caused by a single user in Π_c. The second class of outage events occur due to the macrocell interferers whose *cumulative* interference causes outage [144]. This class precludes all interferers falling in the first category. Mathematically, for an outage threshold y at the femtocell BS, split Π_c into two disjoint heterogeneous Poisson SPPPs $\Pi_c = \Pi_{c,y} \cup \Pi_{c,y}^C$ corresponding to the set of *dominant* and *non-dominant* cellular interferers:

$$\Pi_{c,y} \triangleq \{(r_i, \phi_i) \in \Pi_c : P_r^c \Psi_i (|r_i e^{\mathbf{i}\phi_i} + R_0|/r_i)^\alpha \geq y\}, \Pi_{c,y}^C = \Pi_c \setminus \Pi_{c,y}. \tag{A.7}$$

At any point $(r, \phi) \in \mathcal{H}$, the intensity of $\Pi_{c,y}$ denoted by $\lambda_{c,y}(r, \phi)$ is given as,

$$\lambda_{c,y}(r, \phi) = \frac{\lambda_c}{N_{\text{hop}}} \bar{F}_\Psi \left[\frac{y r^\alpha}{P_r^c |r e^{\mathbf{i}\phi} + R_0|^\alpha} \right] \cdot \mathbf{1} \left(\phi \in \left[\theta, \theta + \frac{2\pi}{N_{\text{sec}}} \right] \right). \tag{A.8}$$

In the event of $\Pi_{c,y}$ being non empty, the femtocell BS experiences outage, arising from the interference caused by a user in $\Pi_{c,y}$. Therefore, $\mathbb{P}_{\text{out}}^f$ is lower bounded by the probability that $\Pi_{c,y}$ has at least one element. Equation (A.5) results from the Poisson void probability of the complementary event $\mathbb{P}[|\Pi_{c,y}| = 0]$ [91]. This completes the proof for the first assertion.

To prove (3.8), recognize that a corner femtocell with an omnidirectional BS antenna encounters cellular interference from the three surrounding cellsites. The dominant macrocell interferer set $\Pi_{c,y}$ can be expressed as $\Pi_{c,y} = \bigcup_{i=1}^3 \Pi_{c,y}^i$, where $\Pi_{c,y}^i$ denotes the dominant macrocell interferer set in neighboring cellsite i. The heterogeneous SPPPs $\Pi_{c,y}^i$ are non-intersecting with an intensity expressed by (A.8). The ccdf of $I_{f,c}$ is then lower bounded by the probability of $\Pi_{c,y}$ being non empty, which can be deduced from the event that $\Pi_{c,y}^i, i \in \{1, 2, 3\}$ are empty.

$$F_{I_{f,c}}^{lb}(y) = \prod_{i=1}^{3} \mathbb{P}(|\Pi_{c,y}^i| = 0) = \exp\left\{ -3 \frac{\lambda_c}{N_{\text{hop}}} \iint_{\mathcal{H}} S(r, \phi; y) r \, \mathrm{d}r \mathrm{d}\phi \right\}. \tag{A.9}$$

To complete the proof, use pairwise independence of the events that $\Pi_{c,y}^i$ and $\Pi_{c,y}^j$ are empty and $S(r, \phi; y)$ in (A.5) to show that $\bar{F}_{I_{f,c}}(\cdot)$ is lower bounded as $\bar{F}_{I_{f,c}}(y) \geq 1 - F_{I_{f,c}}^{lb}(y)$ in (A.9). $\square$

A.5 Theorem 4

For small λ_c, the femtocell outage probability $\mathbb{P}^f_{out}$ is lower bounded as

$$\epsilon \geq \mathbb{P}^{f,lb}_{out} \approx 1 - \frac{e^{-U_{f,sec}}}{1-e^{-U_{f,sec}}} \sum_{m=1}^{\lfloor \rho_f/P^f_r \rfloor} \frac{U^m_{f,sec}}{m!} \cdot G_f(\tilde{\rho}_f) \tag{A.10}$$

where $U_{f,sec} \triangleq \frac{U_f}{N_{sec}}, \rho_f \triangleq \frac{GP^f_r}{N_{hop}\cdot\Gamma}$, $\tilde{\rho}_f = \rho_f - (m-1)\cdot P^f_r$ *and* $G_f(t) \triangleq F_{I_{f,f}}(t) + \int_0^t f_{I_{f,f}}(t-y)\ln\left(F^{lb}_{I_{f,c}}(y)\right)\, dy$.

Proof. The number of femtocell users within a femtocell BS antenna sector is Poisson distributed with mean U_f/N_{sec}. The overall interference is composed of three terms namely $I_{f,in}, I_{f,f}$ and $I_{f,c}$ which are mutually independent. Given m actively transmitting femtocell users including the user of interest, the interference from users within the femtocell equals $I_{f,in} = (m-1)P^f_r$. The threshold for $I_{f,f} + I_{f,c}$ to cause outage therefore equals $\tilde{\rho}_f = \rho_f - (m-1)P^f_r, \rho_f \triangleq GP^f_r/(\Gamma N_{\text{hop}})$ using (3.3). A lower bound on $\mathbb{P}^f_{\text{out}}$ is obtained as,

$$\begin{aligned} 1 - \mathbb{P}^{f,lb}_{out} &= \frac{e^{-U_{f,\text{sec}}}}{1-e^{-U_{f,\text{sec}}}} \sum_{m=1}^{\lfloor \rho_f/P^f_r \rfloor} \frac{U^m_{f,\text{sec}}}{m!} \cdot F_{I^{lb}_{f,c}+I_{f,f}}(\tilde{\rho}_f) \\ &\overset{(a)}{=} \frac{e^{-U_{f,\text{sec}}}}{1-e^{-U_{f,\text{sec}}}} \sum_{m=1}^{\lfloor \rho_f/P^f_r \rfloor} \frac{U^m_{f,\text{sec}}}{m!} \cdot [F^{lb}_{I_{f,c}} * f_{I_{f,f}}](\tilde{\rho}_f) \\ &\overset{(b)}{\approx} \frac{e^{-U_{f,\text{sec}}}}{1-e^{-U_{f,\text{sec}}}} \sum_{m=1}^{\lfloor \rho_f/P^f_r \rfloor} \frac{U^m_{f,\text{sec}}}{m!} \cdot [(1+\ln(F^{lb}_{I_{f,c}})) * f_{I_{f,f}}](\tilde{\rho}_f). \end{aligned} \tag{A.11}$$

Equation (A.11) uses the lower bound on macrocell interference $I^{lb}_{f,c}$ arising from the set of dominant macrocell interferers (A.7). Step (a) uses pairwise independence of $I_{f,f}$ and $I_{f,c}$ for performing a convolution of the respective probabilities. Finally, Step (b) follows from a first-order Taylor series approximation of $F^{lb}_{I_{f,c}}$ in (A.5) using $e^x \approx (1+x)$ for small λ_c in the low outage regime. □

A.6 Lemma 2

With a femtocell exclusion region of radius $R_{f,exc}$ around the reference macrocell BS, the ccdf of cross-tier femtocell interference $I_{c,f}$ is lower bounded as

$$\bar{F}_{I_{c,f}}(y) \geq 1 - e^{-\pi\eta_f H(y)} \tag{A.12}$$

where $H(y)$ is defined as,

$$\begin{aligned} H(y) &\triangleq \left(\frac{Q_f}{y}\right)^{\delta} (\mathbb{E}[\Psi^{\delta}] - F_{\Psi}(u)\mathbb{E}[\Psi^{\delta}|\Psi \leq u]) - (R_{f,exc})^2 \bar{F}_{\Psi}(u) \\ \Psi &= \sum_{i=1}^{U} \Psi_i, \text{ where } 10\log_{10}\Psi_i \sim \mathcal{N}(0, 2\sigma_{dB}^2) \\ \delta &= 2/\alpha, u = \frac{yR_{f,exc}^{2/\delta}}{Q_f}, U \sim X|X \geq 1, X \sim \text{Poisson}(U_f). \end{aligned} \tag{A.13}$$

Proof. Outside the femtocell exclusion region $\mathcal{R}_f^{exc} \subset \mathcal{H}$, corresponding to an outage threshold y, the SPPP Φ_f (see Def.2) of intensity $\eta_f = \frac{\lambda_f}{N_{\text{hop}}N_{\text{sec}}}(1 - e^{-U_f})$ can be split into the dominant and non-dominant interfering femtocells denoted by $(\Phi_{f,y}, \Phi_{f,y}^C)$ respectively. The heterogeneous SPPP $\Phi_{f,y} = \{(r_i, \phi_i) \in \Phi_f : Q_f\Psi_i r_i^{-\alpha} \geq y\}$ consists of actively transmitting femtocells over $\mathbb{R}^2$ which are capable of individually causing outage at a macrocell BS. At any (r, ϕ) w.r.t macrocell BS, the intensity of $\phi_{f,y}$ equals $\eta_f \cdot \bar{F}_{\Psi}(yr^{\alpha}/Q_f)$. The ccdf of the femtocell interference $I_{f,c}$ is lower bounded by the probability that $\Phi_{f,y}$ is non-empty. For if $\Phi_{f,y}$ contains at least one element, then the macrocell BS antenna sector is in outage (by construction of $\Phi_{f,y}$). The lower bound

$\bar{F}^{lb}_{I_{c,f}}(y)$ is then given as

$$1 - \bar{F}^{lb}_{I_{c,f}}(y) = \exp\left\{-2\pi\eta_f \int\limits_{R_{f,\text{exc}}}^{\infty} \bar{F}_\Psi\left(\frac{yr^\alpha}{Q_f}\right) r \ \mathrm{d}r\right\} \tag{A.14}$$

$$\overset{(a)}{=} \exp\left\{-\pi\eta_f Q_f^\delta y^{-\delta} \int\limits_{u}^{\infty} \bar{F}_\Psi(t) \ \mathrm{d}(t^\delta)\right\}$$

$$\overset{(b)}{=} \exp\left\{-\pi\eta_f Q_f^\delta y^{-\delta} \left[\int\limits_{u}^{\infty} t^\delta f_\Psi(t) \ \mathrm{d}t - \bar{F}_\Psi(u)(R_{f,\text{exc}})^2\right]\right\}.$$

Step (a) follows by substituting $t = yr^\alpha/Q_f$ and $\delta = 2/\alpha$ in (A.14), while Step (b) is obtained using integration by parts and setting $u = (\frac{y}{Q_f})(R_{f,\text{exc}})^{2/\delta}$. Using $\int_u^\infty t^\delta f_\Psi(t) \ \mathrm{d}t = \mathbb{E}[\Psi^\delta] - F_\Psi(u)\mathbb{E}[\Psi^\delta|\Psi \leq u]$ in Step (b) completes the proof. □

A.7 Lemma 3

With a tier selection policy in which any user within a radius R_f of a femtocell undergoes handoff to the femtocell BS, the intensity of tier 1 users within $\mathcal{H}$ after handoff is given as $\lambda_c^{TS}(r) = \lambda_c e^{-\lambda_f \pi {R_f}^2}$ whenever $r > R_{f,exc}$, where $R_{f,exc}$ is the femtocell exclusion radius.

Proof. In the region $0 \leq r \leq R_{f,\text{exc}}$ around the reference macrocell, actively transmitting femtocells are absent, so that there are no femtocells for handoff to occur for any user in Ω_c. Consequently, the intensity of the tier 1 cellular users in $0 < r < R_{f,\text{exc}}$ equals λ_c. For $r > R_{f,\text{exc}}$, the intensity of the cellular users is found by computing the probability that any point in Ω_c (prior tier selection) does not fall within R_f meters of a femtocell BS. This is equivalent to computing the void probability of Ω_f within a circle of radius R_f of every point in Ω_c, which equals $e^{-\lambda_f \pi R_f^2}$.

This proof assumes an independent Bernoulli thinning of each point in Ω_c by the probability that a tier 1 user falls with R_f of a femtocell. Strictly speaking,

this statement is not correct: Given two closely spaced tier 1 users in Ω_c, the event that the first user undergoes femtocell handoff is correlated with a nearby user in Ω_c undergoing handoff with the same femtocell. However, we justify that this assumption is reasonable while considering the small size of each femtocell. Then, the intensity of tier 1 users following the femtocell handoff is obtained by independent Bernoulli thinning [91] of Ω_c by the void probability $e^{-\lambda_f \pi R_f^2}$, which completes the proof. $\square$

Appendix B

Appendix to Chapter 4

B.1 Theorem 9

The SINR Nash equilibrium at femtocell BS $B_i, i \in \mathcal{N}\backslash 0$ equals $\gamma_i^* = p_i^* g_{i,i}/I_i(\mathbf{p}_{-i}^*)$, where p_i^* is given as

$$p_i^* = \min\left\{\left[\frac{I_i(\mathbf{p}_{-i}^*)}{g_{i,i}} f_i^{-1}\left(-\frac{b_i}{g_{i,i}}\frac{\mathrm{d}C}{\mathrm{d}p_i}\right)\right]^+, p_{max}\right\} \text{ and } f_i(x) \triangleq \left[\frac{\mathrm{d}R(\gamma_i,\Gamma_i)}{\mathrm{d}\gamma_i}\right]_{\gamma_i=x}. \quad \text{(B.1)}$$

Proof. Since femtocell user i individually optimizes its utility as a best response to other users, we first fix interfering powers $\mathbf{p}_{-i}$. Because $U_i(p_i, \gamma_i|\mathbf{p}_{-i})$ is a strictly concave function of p_i, its partial derivative $U_i'(p_i, \gamma_i|\mathbf{p}_{-i})$ – assuming differentiability – monotonically decreases with increasing p_i. A necessary condition for the existence of local optima is that the derivative of U_i in the interval $[0, p_{max}]$ equals zero. Therefore, if there is no local optima in the interval $[0, p_{\max}]$, the user i chooses its equilibrium transmit power p_i^* depending on the sign of the derivative $U_i'(p_i, \gamma_i)$ – transmit at full power (if $U_i'(p_i, \gamma_i) > 0$ in $[0, p_{\max}]$) or zero power otherwise.

On the contrary, $\forall i \in \mathcal{N}, i \geq 1$, if the Nash equilibrium p_i^* is a local optima in $[0, p_{\max}]$,

$$\left[\frac{\mathrm{d}U_i(p_i,\gamma_i|\mathbf{p}_{-i})}{\mathrm{d}p_i}\right]_{p_i=p_i^*} = 0 \Rightarrow \left[\frac{\mathrm{d}R(\gamma_i,\Gamma_i)}{\mathrm{d}\gamma_i}\frac{g_{i,i}}{I_i(\mathbf{p}_{-i})} + \frac{b_i}{I_i(\mathbf{p}_{-i})}\frac{\mathrm{d}C}{\mathrm{d}p_i}\right]_{p_i=p_i^*} = 0. \quad \text{(B.2)}$$

Since $I_i(\mathbf{p}_{-i}) \geq \sigma^2 > 0$, one may cancel $I_i(\mathbf{p}_{-i})$ on both sides of (B.2). The first- and second-order conditions (4.29)-(4.30) ensure that $\mathrm{d}R(\gamma_i, \Gamma_i)/\mathrm{d}\gamma_i$ [resp. $-\mathrm{d}C/\mathrm{d}p_i$] are

monotone decreasing [resp. monotone non-decreasing] in p_i. The solution to (B.2) corresponds to the intersection of a monotone decreasing function $g_{i,i}\mathrm{d}R(\gamma_i, \Gamma_i)/\mathrm{d}\gamma_i$ and a monotone increasing function $-b_i\mathrm{d}C/\mathrm{d}p_i$ w.r.t the transmitter power p_i. This intersection is therefore unique [81, Section 3] and corresponds to the Nash equilibrium at $p_i = p_i^*$. Using the notation $f_i(x) \triangleq \left[\frac{\mathrm{d}R(\gamma_i,\Gamma_i)}{\mathrm{d}\gamma_i}\right]$ evaluated at $\gamma_i = x$ yields (B.1). This completes the proof. □

B.2 Lemma 6

With the utility-based cellular SINR adaptation [resp. femtocell SINR adaptation] in (4.27) *[resp.* (4.32) *with reward-cost functions in* (4.34)*], the unique SINR equilibria at BS* $B_i, i \in \mathcal{N}$ *are given as* $\gamma_i^* = \frac{p_i^* g_{ii}}{I_i(\mathbf{p}_{-i})}$ *where* p_i^* *is given as*

$$\textit{Femtocell User}: p_i^* = \min\left\{\frac{I_i(\mathbf{p}_{-i}^*)}{g_{i,i}}\left[\Gamma_i + \frac{1}{a_i}\ln\left(\frac{a_i g_{i,i}}{b_i g_{0,i}}\right)\right]^+, p_{max}\right\}. \tag{B.3}$$

$$\textit{Cellular User}: p_0^* = \min\left\{\frac{I_0(\mathbf{p}_{-0}^*)}{g_{0,0}}\Gamma_0, p_{max}\right\}. \tag{B.4}$$

Proof. The cellular user's utility function $U_0(p_0, \gamma_0|\mathbf{p}_{-0})$ is strictly concave w.r.t p_0 given $\mathbf{p}_{-0}$. Consequently, the argument maximizer in (4.27) occurs either in the interior at $p_0^* = \Gamma_0\frac{I_0(\mathbf{p}_{-0})}{g_{00}}$ or at the boundary point $p = p_{\max}$ if $U_0'(p_0, \gamma_0|\mathbf{p}_{-0}) = 2(\Gamma_0 - p_0\frac{g_{00}}{I_0(\mathbf{p}_{-0}^*)}) > 0$ in $[0, p_{\max}]$. At femtocell AP B_i, the equilibrium SINR in Equation (B.3) follows immediately by applying (B.1) in Theorem 9 to the utility functions given in (4.34).

To show uniqueness of the Nash equilibria, we rewrite Equations (B.3)-(B.4) as an iterative power control update $\mathbf{p}^{(k+1)} = \mathbf{f}(\mathbf{p}^{(k)})$ – wherein the component $f_i(p_i)$

represents the power update for user i – with individual power updates given as

$$\text{Femtocell User}: p_i^{(k+1)} = \min\left\{\frac{p_i^{(k)}}{\gamma_i^{(k)}}\left[\Gamma_i + \frac{1}{a_i}\ln\left(\frac{a_i g_{i,i}}{b_i g_{0,i}}\right)\right]^+, p_{\max}\right\}. \tag{B.5}$$

$$\text{Cellular User}: p_0^{(k+1)} = \min\left\{\frac{p_0^{(k)}}{\gamma_i^{(k)}}\Gamma_0, p_{\max}\right\}. \tag{B.6}$$

Yates [154] has shown that, provided a power control iteration of the form $\mathbf{p}^{(k+1)} = \mathbf{f}(\mathbf{p}^{(k)})$ has a fixed point and whenever $\mathbf{f}(\mathbf{p})$ satisfies the following properties namely a) positivity $f(\mathbf{p}) > 0$, b) monotonicity $\mathbf{p}_1 > \mathbf{p}_2 \Rightarrow \mathbf{f}(\mathbf{p}_1) > \mathbf{f}(\mathbf{p}_2)$ and c) scalability $\alpha\mathbf{f}(\mathbf{p}) > \mathbf{f}(\alpha\mathbf{p})\ \forall\alpha > 1$, then the power control iteration converges to the fixed point, which is unique. In such a case, $\mathbf{f}$ is called a *standard interference function*. Since the RHSs in (B.5)-(B.6) form a standard interference function, its fixed point (or the Nash equilibrium given by (B.3)-(B.4)) is *unique* and the iterates are guaranteed to converge to the equilibrium transmit powers. This completes the proof. □

Appendix C

Appendix to Chapter 5

C.1 Theorem 10

Any femtocell F_0 within $D < D_f$ meters of the macrocell B_0 cannot satisfy its QoS requirement $\mathbb{P}[SIR_f(F_0, D) \leq \Gamma] \leq \epsilon$, where D_f is given as

$$D_f = \left[\frac{K}{\Gamma}\frac{P_f/U_f}{P_c/U_c}\left(\frac{\mathcal{I}^{-1}(\epsilon; T_f - U_f + 1, U_c)}{1 - \mathcal{I}^{-1}(\epsilon; T_f - U_f + 1, U_c)}\right)\right]^{-1/\alpha_c} \tag{C.1}$$

where $K = \frac{A_{fi}}{A_{f,c}} R_f^{-\alpha_{fi}}$ and $x \triangleq \mathcal{I}^{-1}(\epsilon; a, b)$ denotes the value of x for which the cumulative distribution function (cdf) of a Beta-distributed random variable X with parameters a and b [namely the regularized incomplete Beta function $\mathcal{I}_x(a, b) = \mathbb{P}(X \leq x)$] equals ϵ.

Proof. The probability of successful reception in (5.3) can be upper bounded as

$$\mathbb{P}[\mathrm{SIR}_f(F_0, D) \geq \Gamma] \leq \mathbb{P}\left[|\mathbf{g}_0^\dagger \mathbf{w}_{0,0}|^2 \geq \Gamma \mathcal{Q}_f \left(\frac{\mathcal{P}_f}{U_c}||\mathbf{f}_0^\dagger \mathbf{V}||^2\right)\right]. \tag{C.2}$$

The term $|\mathbf{g}_0^\dagger \mathbf{w}_{0,0}|^2$ is distributed as a chi-squared random variable (r.v) X with $2(T_f - U_f + 1)$ degrees of freedom [103, 148] denoted as $\chi^2_{2(T_f - U_f + 1)}$. To prove this claim, whenever $U_f = 1$ (beamforming to a single user), $\mathbf{w}_{0,0} = \frac{\mathbf{g}_0}{||\mathbf{g}_0||}$, therefore, $|\mathbf{g}_0^\dagger \mathbf{w}_{0,0}|^2$ is distributed as $\chi^2_{2T_f}$. When $1 < U_f \leq T_f$, $|\mathbf{g}_0^\dagger \mathbf{w}_{0,0}|^2 = |\frac{\mathbf{g}_0^\dagger}{||\mathbf{g}_0||}\mathbf{w}_{0,0}|^2 \cdot ||\mathbf{g}_0||^2$ which equals the product of two independent r.v's which are distributed as Beta$(T_f - U_f + 1, U_f - 1)$ (see [49, Theorem 1.1] for proof) and $\chi^2_{2T_f}$ respectively. Proposition 4 shows that $|\mathbf{g}_0^\dagger \mathbf{w}_{0,0}|^2$ is distributed as a $\chi^2_{2(T_f - U_f + 1)}$ r.v. The probability density function of $|\mathbf{g}_0^\dagger \mathbf{w}_{0,0}|^2$ is given as $f_{|\mathbf{g}_0^\dagger \mathbf{w}_{0,0}|^2}(x) = x^{T_f - U_f} e^{-x}/\Gamma(T_f - U_f + 1)$ $\forall x \geq 0$ where $\Gamma(k) = (k-1)!$ for any positive integer k.

Similarly, the r.v $||\mathbf{f}_0^\dagger \mathbf{V}||^2 = \sum_{k=0}^{U_c-1} |\mathbf{f}_0^\dagger \mathbf{v}_k|^2$ is the sum of U_c r.v's, wherein each term $|\mathbf{f}_0^\dagger \mathbf{v}_k|^2$ equals the squared modulus of a linear combination of T_c complex normal r.v's, which is exponentially distributed. Consequently, $||\mathbf{h}_{0,c}^\dagger \mathbf{V}||^2$ is distributed as a $\chi^2_{2U_c}$ r.v.

Define $Z = \frac{|\mathbf{g}_0^\dagger \mathbf{w}_{0,0}|^2}{||\mathbf{f}_0^\dagger \mathbf{V}||^2}$. Then Z is the ratio of two independent χ^2 r.v's with $2(T_f - U_f + 1)$ and $2U_c$ degrees of freedom respectively. Therefore, Z follows a canonical F_c-distribution[5] and $\frac{Z\ U_c}{(T_f - U_f + 1)}$ is an F-distributed r.v with parameters $2(T_f - U_f + 1)$ and $2U_c$ respectively. Substituting κ in (5.4) and taking the complement of (C.2), one obtains

$$\begin{aligned}
\mathbb{P}[\mathrm{SIR}_f(F_0, D) \leq \Gamma] &\geq \mathbb{P}[Z \leq \kappa] \\
&= \mathbb{P}\left[\frac{Z\ U_c}{T_f - U_f + 1} \leq \kappa \frac{U_c}{T_f - U_f + 1}\right] \\
&= \mathcal{I}_{\frac{\kappa}{\kappa+1}}(T_f - U_f + 1, U_c). \qquad \text{(C.3)}
\end{aligned}$$

A necessary condition for meeting the QoS requirement ϵ for indoor users served by F_0 is given as

$$\mathcal{I}_{\frac{\kappa}{\kappa+1}}(T_f - U_f + 1, U_c) \leq \epsilon \Rightarrow \kappa^* = \frac{\mathcal{I}^{-1}(\epsilon; T_f - U_f + 1, U_c)}{1 - \mathcal{I}^{-1}(\epsilon; T_f - U_f + 1, U_c)}. \qquad \text{(C.4)}$$

Substituting the definition of κ in (5.4), one obtains D_f. This completes the proof. □

C.2 Proposition 2

The inverse function $\mathcal{I}^{-1}(x; a, b)$ is monotonically increasing with a and monotonically decreasing with b for any $a, b \geq 0$.

Proof. We use the following two expansions [61, Page 29] for $\mathcal{I}_x(a, b)$.

$$\mathcal{I}_x(a, b) \overset{(a)}{=} 1 - \sum_{i=1}^{a} \frac{\Gamma(b+i-1)}{\Gamma(b)\Gamma(i)} x^{i-1}(1-x)^b \overset{(b)}{=} \sum_{i=1}^{b} \frac{\Gamma(a+i-1)}{\Gamma(a)\Gamma(i)} x^a (1-x)^{i-1}. \qquad \text{(C.5)}$$

where the Gamma function $\mathbf{\Gamma}(k) = (k-1)!$ for any positive integer k. Relation (a) shows that $\mathcal{I}_x(a,b)$ monotonically decreases with a. The equivalent Relation (b) shows that $\mathcal{I}_x(a,b)$ is monotone increasing w.r.t b. Consequently, the inverse function $\mathcal{I}^{-1}(x;a,b)$ monotonically increases with a and monotonically decreases with b. $\square$

C.3 Corollary 4

With K as defined in Theorem 10 and $U_c = 1$, the reduction in the no-coverage radius using a SU transmission strategy at femtocells relative to MU transmission to $U_f = T_f$ users [resp. single antenna transmission] is given as

$$\frac{D_{f,\mathrm{SU}}}{D_{f,\mathrm{MU}}} = \left[\left(\frac{1-\epsilon^{1/T_f}}{\epsilon^{1/T_f}}\right)\frac{\epsilon}{1-\epsilon}\frac{1}{T_f}\right]^{1/\alpha_c} \approx \left[\frac{\epsilon^{1-1/T_f}}{T_f}\right]^{1/\alpha_c}.$$

$$\frac{D_{f,\mathrm{SU}}}{D_{f,1\text{ Antenna}}} = \left[\left(\frac{1-\epsilon^{1/T_f}}{\epsilon^{1/T_f}}\right)\frac{\epsilon}{1-\epsilon}\right]^{1/\alpha_c} \approx \epsilon^{\frac{1}{\alpha_c}\left(1-1/T_f\right)}.$$

Proof. With SU femtocell transmission [resp. MU transmission to $U_f = T_f$ users] and $U_c = 1$ user, the incomplete beta function $\mathcal{I}_{\frac{\kappa}{\kappa+1}}(T_f - U_f + 1, U_c)$ simplifies as

$$\mathcal{I}_{\frac{\kappa_1}{\kappa_1+1}}(T_f,1) = \left(\frac{\kappa_1}{\kappa_1+1}\right)^{T_f},\ \mathcal{I}_{\frac{\kappa_2}{\kappa_2+1}}(1,1) = \left(\frac{\kappa_2}{\kappa_2+1}\right) \tag{C.6}$$

where $\kappa_1 = \frac{1}{K}\frac{P_c}{P_f}D_{f,\mathrm{SU}}^{-\alpha_c}$ and $\kappa_2 = \frac{1}{K}\frac{P_c}{P_f/T_f}D_{f,\mathrm{MU}}^{-\alpha_c}$ respectively. Therefore, the no-coverage distances in (5.5) are respectively given as

$$D_{f,\mathrm{SU}} = \left[\frac{K}{\Gamma}\frac{P_f}{P_c}\left(\frac{\epsilon^{1/T_f}}{1-\epsilon^{1/T_f}}\right)\right]^{-1/\alpha_c},\ D_{f,\mathrm{MU}} = \left[\frac{K}{\Gamma}\frac{P_f/T_f}{P_c}\left(\frac{\epsilon}{1-\epsilon}\right)\right]^{-1/\alpha_c}. \tag{C.7}$$

Assuming small ϵ, SU femtocell transmission consequently reduces D_f by a factor of approximately $(\frac{T_f}{\epsilon^{1-1/T_f}})^{1/\alpha_c}$ relative to MU transmission. A similar argument shows that SU transmission reduces D_f by a factor of approximately $\epsilon^{-\frac{1}{\alpha_c}\left(1-1/T_f\right)}$ relative to single antenna transmission. $\square$

C.4 Theorem 11

In a two-tier network, the maximum femtocell contention density $\lambda_f^*(D)$ at distance D from the macrocell B_0, which satisfies (5.6) *(in the small-ϵ regime) is given as*

$$\lambda_f^*(D) = \frac{1}{\mathcal{C}_f(\mathcal{Q}_f\Gamma)^{\delta_f}}\left[\frac{\epsilon - \mathcal{I}_{\frac{\kappa}{\kappa+1}}(T_f - U_f + 1, U_c)}{\frac{1}{\mathcal{K}_f} - \mathcal{I}_{\frac{\kappa}{\kappa+1}}(T_f - U_f + 1, U_c)}\right] \tag{C.8}$$

where $\delta_f = 2/\alpha_{fo}$, $\mathcal{Q}_f$ is given by (5.2)*, κ is given by* (5.4)*, and*

$$\mathcal{C}_f = \pi\delta_f U_f^{-\delta_f}\sum_{k=0}^{U_f-1}\binom{U_f}{k}B(k+\delta_f, U_f - k - \delta_f) \tag{C.9}$$

$$\mathcal{K}_f = \left[1 + \frac{1}{(1+\kappa)^{U_c}}\sum_{j=0}^{T_f-U_f-1}\left(\frac{\kappa}{\kappa+1}\right)^j\binom{U_c+j-1}{j}\sum_{l=1}^{T_f-U_f-j}\frac{1}{l!}\prod_{m=0}^{(l-1)}(m-\delta_f)\right]^{-1} \tag{C.10}$$

where $B(a,b) = \frac{\Gamma(a)\Gamma(b)}{\Gamma(a+b)}$ denotes the Beta function and $\mathcal{K}_f = 1$ whenever $U_f = T_f$.

Proof. Using (5.3), the probability of successful reception $\mathbb{P}[\mathrm{SIR}_f(F_0, D) \geq \Gamma]$ is given as

$$\mathbb{P}[|\mathbf{g}_0^\dagger \mathbf{w}_{0,0}|^2 \geq \Gamma\mathcal{Q}_f(I_{f,c} + I_{f,f})]$$
$$\text{where, } I_{f,c} = \frac{\mathcal{P}_f}{U_c}||\mathbf{f}_0^\dagger\mathbf{V}||^2,\ I_{f,f} = 1/U_f\sum_{F_j\in\Pi_f\setminus F_0}||\mathbf{g}_{0,j}^\dagger\mathbf{W}_j||^2|X_{0,j}|^{-\alpha_{fo}}. \tag{C.11}$$

The interference from neighboring femtocells $I_{f,f}$ is a Poisson Shot-noise Process([107, 132]) with independent and identically distributed marks[91]. The distributions of the signal powers and marks of the interferers are chi-squared with degrees of freedom given as $|\mathbf{g}_0^\dagger\mathbf{w}_{0,0}|^2 \sim \chi^2_{2(T_f-U_f+1)}$, $||\mathbf{f}_0^\dagger\mathbf{V}||^2 \sim \chi^2_{2U_c}$ and $||\mathbf{g}_{0,j}^\dagger\mathbf{W}_j||^2 \sim \chi^2_{2U_f}$ respectively. Consequently,

$$\mathbb{P}[\mathrm{SIR}_f(F_0, D) \geq \Gamma] \overset{(a)}{=} \int_0^\infty\sum_{k=0}^{T_f-U_f}\frac{(s\mathcal{Q}_f\Gamma)^k}{k!}e^{-s\mathcal{Q}_f\Gamma}\mathrm{d}\mathbb{P}(I_{f,c} + I_{f,f} \leq s) \tag{C.12}$$

$$\overset{(b)}{=} \sum_{k=0}^{T_f-U_f}\frac{(-\mathcal{Q}_f\Gamma)^k}{k!}\frac{\mathrm{d}^k}{\mathrm{d}\theta^k}\mathcal{L}_{I_{f,c}}(\theta)\mathcal{L}_{I_{f,f}}(\theta)\Big|_{\theta=\mathcal{Q}_f\Gamma} \tag{C.13}$$

where step (a) follows by conditioning on $I_{f,c}+I_{f,f}$ and computing the complementary cumulative distribution (ccdf) of $||\mathbf{g}_0||^2$. For deriving step (b), with $k = 0$, the integral in (a) corresponds to the Laplace Transform (LT) of the r.v $I_{f,f} + I_{f,c}$ given as $\mathbb{E}[e^{-(I_{f,c}+I_{f,f})\theta}]$ evaluated at $\theta = \mathcal{Q}_f\Gamma$ (originally derived in [13]). Next, since $I_{f,c}$ and $I_{f,f}$ are independent r.v's, the LT of their sum decouples as the product of their LTs $\mathbb{E}[e^{-I_{f,c}\theta}]\mathbb{E}[e^{-I_{f,f}\theta}]$. Finally, for any $k > 0$, we have the identity $\mathcal{L}[t^k f(t)] = (-1)^k F^{(k)}(s)$, where $F^k(s)$ represents the kth derivative of $F(s)$ (this technique is borrowed from [76]).

The LTs of $I_{f,c}$ and $I_{f,f}$ may be written as

$$\mathcal{L}_{I_{f,c}}(\theta) = \mathbb{E}[e^{-\theta I_{f,c}}] = \frac{1}{(1+\mathcal{P}_f\theta/U_c)^{U_c}} \tag{C.14}$$

$$\begin{aligned}\mathcal{L}_{I_{f,f}}(\theta) = \mathbb{E}[e^{-\theta I_{f,f}}] &\overset{(a)}{=} \exp\left\{-\lambda_f \int_{\mathbb{R}^2} 1 - \mathbb{E}_S[e^{-\theta\frac{S}{U_f}|x|^{-\alpha_{fo}}}]\,\mathrm{d}x\right\}, \text{where } S \sim \chi^2_{2U_f} \\ &\overset{(b)}{=} \exp\left\{-\pi\lambda_f\delta_f\left(\frac{\theta}{U_f}\right)^{\delta_f}\sum_{k=0}^{U_f-1}\binom{U_f}{k}B(k+\delta_f, U_f-k-\delta_f)\right\} \\ &\overset{(c)}{=} \exp(-\lambda_f\mathcal{C}_f\theta^{\delta_f})\end{aligned} \tag{C.15}$$

where (C.14) follows from the LT of a chi-squared r.v with $2U_c$ degrees of freedom. In (C.15), step (a) represents the LT of a Poisson Shot-Noise process with independent and identically distributed marks S_j–equaling $||\mathbf{g}^\dagger_{0,j}\mathbf{W}_j||^2$ in our case. Steps (b) and (c) follow from [76]. Substituting (C.14) and (C.15) in (C.13) leads to the following requirement for the success probability

$$\sum_{k=0}^{T_f-U_f}\frac{(-\mathcal{Q}_f\Gamma)^k}{k!}\frac{\mathrm{d}^k}{\mathrm{d}\theta^k}\frac{e^{-\lambda_f\mathcal{C}_f\theta^{\delta_f}}}{(1+\frac{\mathcal{P}_f\theta}{U_c})^{U_c}} \geq 1-\epsilon, \text{where } \theta = \mathcal{Q}_f\Gamma. \tag{C.16}$$

Using the Leibniz rule, the kth derivative of $\mathcal{L}_{I_{f,c}}(\theta)\mathcal{L}_{I_{f,f}}(\theta)$ is given as

$$\frac{\mathrm{d}^k}{\mathrm{d}\theta^k}\frac{e^{-\lambda_f\mathcal{C}_f\theta^{\delta_f}}}{(1+\frac{\mathcal{P}_f\theta}{U_c})^{U_c}} = \sum_{j=0}^{k}\binom{k}{j}\frac{\mathrm{d}^j}{\mathrm{d}\theta^j}\left(1+\frac{\mathcal{P}_f\theta}{U_c}\right)^{-U_c}\frac{\mathrm{d}^{(k-j)}}{\mathrm{d}\theta^{(k-j)}}e^{-\lambda_f\mathcal{C}_f\theta^{\delta_f}}. \tag{C.17}$$

where $\binom{a}{b}$ is the coefficient of x^b in the expansion of $(1+x)^a$. Considering the low outage regime, we shall evaluate the kth derivative of $\mathcal{L}_{I_{f,f}}(\theta)$ using a first-order Taylor series approximation around $\lambda_f \mathcal{C}_f \theta^{\delta_f} = 0$. Then, for all $k \geq 1$, the kth derivatives of $\mathcal{L}_{I_{f,c}}(\theta)$ and $\mathcal{L}_{I_{f,f}}(\theta)$ are individually given as

$$\frac{\mathrm{d}^k}{\mathrm{d}\theta^k}\left(1+\frac{\mathcal{P}_f\theta}{U_c}\right)^{-U_c} = \frac{\left[\prod_{j=0}^{k-1}(U_c+j)\right]\left(\frac{-\mathcal{P}_f}{U_c}\right)^k}{(1+\frac{\mathcal{P}_f\theta}{U_c})^{k+U_c}}. \tag{C.18}$$

$$\frac{\mathrm{d}^k}{\mathrm{d}\theta^k}e^{-\lambda_f\mathcal{C}_f\theta^{\delta_f}} = -\left[\lambda_f\mathcal{C}_f\prod_{m=0}^{k-1}(\delta_f-m)\theta^{\delta_f-k}\right]e^{-\lambda_f\mathcal{C}_f\theta^{\delta_f}} + \Theta(\lambda_f^2\mathcal{C}_f^2\theta^{2\delta_f}). \tag{C.19}$$

Combining (C.16) with (C.18) and (C.19) and substituting $\theta = \mathcal{Q}_f\Gamma$ leads to

$$\begin{aligned}
&\frac{e^{-\lambda_f\mathcal{C}_f(\mathcal{Q}_f\Gamma)^{\delta_f}}}{(1+\frac{\mathcal{P}_f\mathcal{Q}_f\Gamma}{U_c})^{U_c}}\Bigg\{\sum_{k=0}^{(T_f-U_f)}\frac{(\frac{\mathcal{P}_f\mathcal{Q}_f\Gamma}{U_c})^k}{k!\left(1+\frac{\mathcal{P}_f\mathcal{Q}_f\Gamma}{U_c}\right)^k}\prod_{m=0}^{(k-1)}(U_c+m)\\
-\;&\lambda_f\mathcal{C}_f(\mathcal{Q}_f\Gamma)^{\delta_f}\sum_{k=1}^{(T_f-U_f)}\frac{(-1)^k}{k!}\sum_{j=1}^{k}\binom{k}{j}\left[\frac{\frac{-\mathcal{P}_f\mathcal{Q}_f\Gamma}{U_c}}{1+\frac{\mathcal{P}_f\mathcal{Q}_f\Gamma}{U_c}}\right]^{k-j}\prod_{n=0}^{(k-j-1)}(U_c+n)\prod_{m=0}^{j-1}(\delta_f-m)\Bigg\}\\
+\;&\Theta(\lambda_f^2\mathcal{C}_f^2(\mathcal{Q}_f\Gamma)^{2\delta_f}) \geq 1-\epsilon.
\end{aligned}$$

Next, substituting $\kappa = \mathcal{P}_f\mathcal{Q}_f\Gamma/U_c$ from (5.4) and performing a first-order Taylor series expansion of $e^{-\lambda_f\mathcal{C}_f(\mathcal{Q}_f\Gamma)^{\delta_f}} = 1-\lambda_f C_f(\mathcal{Q}_f\Gamma)^{\delta_f} + \Theta(\lambda_f^2\mathcal{C}_f^2(\mathcal{Q}_f\Gamma)^{2\delta_f})$, the above expression simplifies as

$$\begin{aligned}
&\frac{1-\lambda_f\mathcal{C}_f(\mathcal{Q}_f\Gamma)^{\delta_f}}{(1+\kappa)^{U_c}}\Bigg\{\sum_{k=0}^{T_f-U_f}\frac{1}{k!}\left(\frac{\kappa}{\kappa+1}\right)^k\prod_{m=0}^{k-1}(U_c+m)\\
-\;&\lambda_f\mathcal{C}_f(\mathcal{Q}_f\Gamma)^{\delta_f}\sum_{k=1}^{T_f-U_f}\frac{1}{k!}\sum_{j=1}^{k}\binom{k}{j}\left[\frac{\kappa}{\kappa+1}\right]^{k-j}\prod_{n=0}^{(k-j-1)}(U_c+n)\prod_{m=0}^{j-1}(m-\delta_f)\Bigg\}\\
+\;&\Theta(\lambda_f^2\mathcal{C}_f^2(\mathcal{Q}_f\Gamma)^{2\delta_f}) \geq 1-\epsilon.
\end{aligned} \tag{C.20}$$

Note that $\prod_{m=0}^{k-1}(U_c+m)/k! = \binom{U_c+k-1}{k}$. Using Proposition 5 in Appendix C.6, we have the identity

$$\sum_{k=0}^{(T_f-U_f)}\left(\frac{\kappa}{\kappa+1}\right)^k\binom{U_c+k-1}{k} = (1+\kappa)^{U_c}[1-\mathcal{I}_{\frac{\kappa}{\kappa+1}}(T_f-U_f+1;U_c)]. \tag{C.21}$$

With straightforward algebraic manipulation, it is easily shown that

$$\sum_{k=1}^{(T_f-U_f)} \frac{1}{k!} \sum_{j=1}^{k} \binom{k}{j} \left[\frac{\kappa}{\kappa+1}\right]^{k-j} \prod_{n=0}^{k-j-1} (U_c+n) \prod_{m=0}^{j-1} (m-\delta_f)$$
$$= \sum_{j=0}^{T_f-U_f-1} \left(\frac{\kappa}{\kappa+1}\right)^{j} \binom{U_c+j-1}{j} \sum_{l=1}^{T_f-U_f-j} \frac{1}{l!} \prod_{m=0}^{(l-1)} (m-\delta_f). \tag{C.22}$$

Using (C.22), we now define $\mathcal{K}_f$ in (5.9), where $\mathcal{K}_f = 1$ whenever $U_f = T_f$ (since (C.16) does not contain derivative terms). By substituting (C.21) and $\mathcal{K}_f$ in (C.20) and discarding (for small λ_f) the $\Theta(\lambda_f^2 \mathcal{C}_f^2 (\mathcal{Q}_f \Gamma)^{2\delta_f})$ terms (which are $\mathrm{o}(\lambda_f \mathcal{C}_f (\mathcal{Q}_f \Gamma)^{\delta_f})$), the upper bound on λ_f is given as

$$\lambda_f \leq \frac{1}{\mathcal{C}_f (\mathcal{Q}_f \Gamma)^{\delta_f}} \frac{\epsilon - \mathcal{I}_{\frac{\kappa}{\kappa+1}}(T_f - U_f + 1, U_c)}{\frac{1}{\mathcal{K}_f} - \mathcal{I}_{\frac{\kappa}{\kappa+1}}(T_f - U_f + 1, U_c)}. \tag{C.23}$$

Since the *maximum contention density* λ_f^* maximizes the number of simultaneous femtocell transmissions, λ_f^* satisfies (C.23) with equality. This completes the proof. □

C.5 Distribution of the product of independent Beta distributed and Gamma distributed random variates

Proposition 4. *Let $X \sim Beta(a, b)$ be a Beta distributed random variable (r.v) with shape parameters $a > 0$ and $b > 0$ respectively. Let $Y \sim Gamma(a + b, 1)$ be an independent Gamma r.v with shape parameter $a + b$. Then the product XY is gamma distributed with shape parameter a, that is $XY \sim Gamma(a, 1)$.*

Proof. Since Y is Gamma distributed with shape parameter $a + b$, its moment generating function (MGF) is given as

$$\mathbb{E}[e^{tY}] = (1-t)^{-(a+b)} = (1-t)^{-a} \cdot (1-t)^{-b}$$
$$\Rightarrow Y \stackrel{d}{=} Y_1 + Y_2, Y_1 \sim \mathrm{Gamma}(a, 1), Y_2 \sim \mathrm{Gamma}(b, 1) \text{ and } Y_1 \perp Y_2 \tag{C.24}$$

where $\stackrel{d}{=}$ denotes equality in distribution and $\perp$ denotes independence of r.v's. That is, Y is equal in distribution to the sum of two independent Gamma r.v's with shape parameters a and b respectively (since the MGF of the sum of two independent r.v's equals the product of their respective MGF's).

Next, the ratio $\frac{Y_1}{Y_1+Y_2}$ is Beta distributed with shape parameters a and b respectively, that is,

$$\frac{Y_1}{Y_1+Y_2} \sim \text{Beta}(a,b) \Rightarrow \frac{Y_1}{Y} \sim \text{Beta}(a,b) \Rightarrow XY \stackrel{d}{=} Y_1 \sim \text{Gamma}(a,1).$$

In other words, the product XY is equal in distribution to a Gamma distributed random variable with shape parameter a. This completes the proof. □

C.6 A new expression for the regularized incomplete Beta function

Proposition 5. For any $x \geq 0$, and non-negative integers n, m and r where $n \geq r$,

$$\sum_{k=0}^{n-r} \left(\frac{x}{x+1}\right)^k \binom{m+k-1}{k} = (1+x)^m \, \mathcal{I}_{\frac{1}{x+1}}(m, n-r+1). \tag{C.25}$$

Proof. Multiplying the left hand side of (C.25) by $(1+x)^{n-r}$,

$$\sum_{k=0}^{n-r} x^k (1+x)^{n-r-k} \binom{m+k-1}{k} = \sum_{k=0}^{n-r} \sum_{l=0}^{n-r-k} \binom{n-r-k}{l} \binom{m+k-1}{k} x^{k+l}. \tag{C.26}$$

The coefficient of x^q, where $0 \leq q \leq n-r$, is given as $\sum_{j=0}^{q} \binom{n-r-j}{q-j}\binom{m+j-1}{j} = \binom{n-r+m}{q}$ (using the combinatorial identity [58, Page 22, (3.2)]). Consequently, we have

$$\sum_{k=0}^{n-r} x^k (1+x)^{n-r-k} \binom{m+k-1}{k} = \sum_{k=0}^{n-r} \binom{n-r+m}{k} x^k. \tag{C.27}$$

Next, by definition of the incomplete Beta function,

$$
\begin{aligned}
(1+x)^m \mathcal{I}_{\frac{1}{x+1}}(m, n-r+1) &\overset{(a)}{=} \sum_{j=m}^{n-r+m} \binom{n-r+m}{j} \frac{x^{n-r+m-j}}{(1+x)^{n-r}} \\
&\overset{(b)}{=} \sum_{k=0}^{n-r} \binom{n-r+m}{k} \frac{x^k}{(1+x)^{n-r}} \qquad \text{(C.28)}
\end{aligned}
$$

where step (a) follows by definition, while step (b) follows by replacing the index j in step (a) by $k = n - r + m - j$. Combining (C.27) and (C.28) gives the desired result. $\square$

Appendix D

Appendix to Chapter 6

D.1 Lemma 8

The spatially averaged SIR distribution inside a circular annulus with inner radius R_1 and outer radius R_2 is given as

$$\mathbb{E}_R[\Pr(\mathrm{SIR}_c \leq \Gamma | R_1 \leq R \leq R_2)] = 1 - \frac{1}{(R_2^2 - R_1^2)}[R_2^2 C(a_2, b) - R_1^2 C(a_1, b)] \quad \text{(D.1)}$$

$$\text{where } C(a,b) \triangleq \mathrm{Q}(a) + \exp\left(\frac{2-2ab}{b^2}\right)\mathrm{Q}\left(\frac{2-ab}{b}\right) \quad \text{(D.2)}$$

$$a \triangleq \frac{\ln\Gamma - \mu_C(R_2)}{\sigma_C(R_2)}, b \triangleq \frac{\alpha_c}{\sigma_C(R_2)} \quad \text{(D.3)}$$

$$a_2 = a + b\ln(R_2/R_c), a_1 = a + b\ln(R_1/R_c), \quad \text{(D.4)}$$

Proof. Inside a circular annulus of small width, one can assume that a user experiences identical shadowing statistics from interfering BSs. For convenience, the parameters a and b are chosen when the user is at the outer edge ($R = R_2$) of the annulus, as shown in equation (6.18). Given $R_1 \leq R \leq R_2$ with the pdf function $f_R(r|R_1 \leq R \leq R_2) = \frac{2r}{R_2^2 - R_1^2}$, the spatially averaged outage probability is obtained as

$$\begin{aligned}
\mathbb{E}_R[\Pr(\mathrm{SIR}_c \leq \Gamma | R_1 \leq R \leq R_2)] &= 1 - \mathbb{E}_R[\mathrm{Q}(a + b\ln R/R_c) \mid R_1 \leq R \leq R_2] \\
&= 1 - \frac{2}{R_2^2 - R_1^2}\int_{R_1}^{R_2} \mathrm{Q}[a + b\ln r/R_c] r \, \mathrm{d}r \quad \text{(D.5)} \\
&= 1 - \frac{1}{R_2^2 - R_1^2}\left\{R_2^2 \int_0^{R_2} \frac{2}{R_2^2}\mathrm{Q}[a_2 + b\ln r/R_2] r \, \mathrm{d}r \right. \\
&\left. - R_1^2 \int_0^{R_1} \frac{2}{R_1^2}\mathrm{Q}[a_1 + b\ln r/R_1] r \, \mathrm{d}r \right\} \quad \text{(D.6)}
\end{aligned}$$

where (D.6) is obtained by substituting $a_2 \triangleq a + b \ln R_2/R_c$ and $a_1 \triangleq a + b \ln R_1/R_c$ in (D.5). Combining the definitions in (6.17) and (6.19) with the identity [56, Pg. 55]:

$$C(a, b) = \frac{2}{R^2} \int_0^R \mathrm{Q}(a + b \ln r/R) r \ \mathrm{d}r \tag{D.7}$$

and plugging into (D.6), the result follows. □

Bibliography

[1] Guidelines for evaluation of radio transmission technologies for IMT-2000. *ITU Recommendation M.1225*, 1997.

[2] HNB and HNB-macro propagation models. In *3rd Generation Partnership Project, Tech. Rep. R4-071617*, October 2007.

[3] J.M. Aein. Power balancing in systems employing frequency reuse. *COMSAT tech. rev.*, 3(2), 1973.

[4] Byungchan Ahn, Hyunsoo Yoon, and Jung Wan Cho. A design of macro-micro CDMA cellular overlays in the existing big urban areas. *IEEE Journal on Selected Areas in Comm.*, 19(10):2094–2104, October 2001.

[5] Y. Akyildiz and B. D. Rao. Statistical performance analysis of optimum combining with co-channel interferers and flat rayleigh fading. In *Proc., IEEE Global Telecomm. Conference*, volume 6, pages 3663–3667, San Antonio, TX, USA, 2001.

[6] S. M. Alamouti. A simple transmit diversity technique for wireless communications. *IEEE Journal on Selected Areas in Comm.*, 16(8):1451–1458, October 1998.

[7] M. S. Alouini and A. J. Goldsmith. Area spectral efficiency of cellular mobile radio systems. *IEEE Transactions on Veh. Tech.*, 48(4):1047–1066, July 1999.

[8] T. Alpcan, T. Basar, R. Srikant, and E. Altman. CDMA uplink power control as a noncooperative game. In *Proceedings of the IEEE Conference on Decision and Control*, volume 1, pages 197–202, Orlando, FL, USA, 2001.

[9] E. Altman, T. Boulogne, R. El-Azouzi, T. Jiminez, and L. Wynter. A survey of network games in telecommunications. *Computers and Operations Research*, pages 286–311, February 2006.

[10] J. G. Andrews, A. Ghosh, and R. Muhamed. *Fundamentals of WiMAX*. Prentice-Hall, 2007.

[11] J.G. Andrews, W. Choi, and R.W. Heath, Jr. Overcoming interference in spatial multiplexing MIMO cellular networks. *IEEE Wireless Comm. Magazine*, 14(6):95–104, December 2007.

[12] D. Avidor, S. Mukherjee, J. Ling, and C. Papadias. On some properties of the proportional fair scheduling policy. In *Proc., IEEE International Symposium on Personal, Indoor and Mobile Radio Communications*, volume 2, pages 853–858, September 2004.

[13] F. Baccelli, B. Blaszczyszyn, and P. Muhlethaler. An ALOHA protocol for multihop mobile wireless networks. *IEEE Transactions on Info. Theory*, 52(2):421–436, February 2006.

[14] F. Baccelli, B. Blaszczyszyn, and F. Tournois. Spatial averages of coverage characteristics in large CDMA networks. *Wireless Networks*, 8(6):569–586, November 2002.

[15] F. Baccelli, M. Klein, M. Lebourges, and S. Zuyev. Stochastic geometry and architecture of communication networks. *J. Telecommunication Systems*, 7:209–227, 1997.

[16] Paramvir Bahl, Ranveer Chandra, Thomas Moscibroda, Yunnan Wu, and Yuan Yuan. Load aware channel-width assignments in wireless LANs. *Microsoft Research Tech. Report MSR-TR-2007-79*, July 2007.

[17] N. Bambos, S. C. Chen, and G. J. Pottie. Channel access algorithms with active link protection for wireless communication networks with power control. *IEEE/ACM Transactions on Networking*, 8(5):583–597, October 2000.

[18] I. Bazar, Y. Onozato, and Z. Jie. Effects of cell distance on capacity of two-tier cellular networks. In *Proc., IEEE International Conference on Universal Personal Communications*, volume 1, pages 537–541, Florence, Italy, October 1998.

[19] F. Boccardi and H. Huang. Limited downlink network coordination in cellular networks. In *Proc., IEEE International Symposium on Personal, Indoor and Mobile Radio Communications*, pages 1–5, September 2007.

[20] H. Boche and S. Stanczak. Strict convexity of the feasible log-SIR region. *IEEE Trans. on Comm.*, 56(9):1511–1518, September 2008.

[21] J. Castaneda-Camacho and D. Lara-Rodriguez. Performance of a new micro-cell/macrocell cellular architecture with CDMA access. In *Proc., IEEE Veh. Tech. Conference*, volume 1, pages 483–486, Tokyo, Japan, 2000.

[22] D. Catrein, L. A. Imhof, and R. Mathar. Power control, capacity, and duality of uplink and downlink in cellular CDMA systems. *IEEE Trans. on Comm.*, 52(10):1777–1785, October 2004.

[23] S. Catreux, P. F. Driessen, and L. J. Greenstein. Attainable throughput of an interference-limited multiple-input multiple-output (MIMO) cellular system. *IEEE Trans. on Comm.*, 49(8):1307–1311, August 2001.

[24] S. Catreux, V. Erceg, D. Gesbert, and R.W. Heath, Jr. Adaptive modulation and MIMO coding for broadband wireless data networks. *IEEE Comm. Magazine*, 40(6):108–115, June 2002.

[25] D. Cavalcanti, D. Agrawal, C. Cordeiro, B. Xie, and A. Kumar. Issues in Integrating Cellular Networks, WLANs, and MANETs: a Futuristic Heterogeneous Wireless Network. *IEEE Wireless Comm. Magazine*, pages 30–41, June 2005.

[26] Chun Chung Chan and S.V. Hanly. Calculating the outage probability in a CDMA network with Spatial Poisson traffic. *IEEE Transactions on Veh. Tech.*, 50(1):183–204, January 2001.

[27] V. Chandrasekhar and J. G. Andrews. Spectrum allocation in two-tier femtocell networks. *To Appear, IEEE Trans. on Comm.*, 2009.

[28] V. Chandrasekhar and J. G. Andrews. Uplink capacity and interference avoidance in two-tier femtocell networks. *To appear, IEEE Trans. on Wireless Comm.*, 2009.

[29] V. Chandrasekhar, J. G. Andrews, and A. Gatherer. Femtocell networks: a survey. *IEEE Comm. Magazine*, 46(9):59–67, September 2008.

[30] V. Chandrasekhar, J. G. Andrews, T. Muharemovic, Z. Shen, and A. Gatherer. Power control in two-tier femtocell networks. *Submitted, IEEE Trans. on Wireless Comm.*, 2008.

[31] V. Chandrasekhar, M. Kountouris, and J. G. Andrews. Coverage in multi-antenna two-tier networks. *Submitted, IEEE Trans. on Wireless Comm.*, 2009.

[32] J. K. Chen, T. S. Rappaport, and G. de Veciana. Site specific knowledge for improving frequency allocations in wireless LAN and cellular networks. In *Proc., IEEE Veh. Tech. Conference*, pages 1431–1435, September/October 2007.

[33] D. Choi, P. Monajemi, Shinjae Kang, and J. Villasenor. Dealing with loud neighbors: The benefits and tradeoffs of adaptive femtocell access. In *Proc., IEEE Global Telecomm. Conference*, pages 1–5, November/December 2008.

[34] Lai-U Choi and R. D. Murch. A transmit preprocessing technique for multiuser MIMO systems using a decomposition approach. *IEEE Transactions on Wireless Comm.*, 3(1):20–24, January 2004.

[35] Wan Choi and J. G. Andrews. Downlink performance and capacity of distributed antenna systems in a multicell environment. *IEEE Transactions on Wireless Comm.*, 6(1):69–73, January 2007.

[36] H. Claussen, L. T. W. Ho, and L. G. Samuel. Financial analysis of a picocellular home network deployment. In *Proc., IEEE International Conference on Communications*, pages 5604–5609, June 2007.

[37] H. Claussen, L. T. W. Ho, and L. G. Samuel. Self-optimization of coverage for femtocell deployments. *Proc., IEEE Wireless Telecomm. Symposium*, pages 278–285, April 2008.

[38] G. Debreu. A social equilibrium existence theorem. *Proceedings of the National Academy of Sciences*, 38:886–893, 1952.

[39] F. F. Digham, M. S. Alouini, and M. K. Simon. On the energy detection of unknown signals over fading channels. In *Proc., IEEE International Conference on Communications*, volume 5, pages 3575–3579, May 2003.

[40] A. Doufexi, E. Tameh, A. Nix, S. Armour, and A. Molina. Hotspot wireless LANs to enhance the performance of 3G and beyond cellular networks. *IEEE Communications Magazine*, 41(7):58–65, July 2003.

[41] T. ElBatt and A. Ephremides. Joint scheduling and power control for wireless ad hoc networks. *IEEE Transactions on Wireless Comm.*, 3(1):74–85, January 2004.

[42] R. Etkin, A. Parekh, and D. Tse. Spectrum sharing for unlicensed bands. *IEEE Journal on Selected Areas in Comm.*, 25(3):517–528, April 2007.

[43] A. Forenza, M. Airy, M. Kountouris, R.W. Heath, Jr., and S. Shakkottai. Performance of the MIMO downlink channel with multi-mode adaptation and scheduling. *Proc. 6th IEEE Workshop on Signal Proc. Advances in Wireless Commun. (SPAWC)*, pages 695–699, June 2005.

[44] A. Forenza, M. R. McKay, A. Pandharipande, R.W. Heath, Jr., and I. B. Collings. Adaptive MIMO transmission for exploiting the capacity of spatially correlated channels. *IEEE Transactions on Veh. Tech.*, 56(2):619–630, March 2007.

[45] G. J. Foschini, H. Huang, K. Karakayali, R. A. Valenzuela, and S. Venkatesan. The value of coherent base station cooperation. In *Proc., Conference on Information Sciences and Systems*, June 2005.

[46] G. J. Foschini and Z. Miljanic. A simple distributed autonomous power control algorithm and its convergence. *IEEE Transactions on Veh. Tech.*, 42(4):641–646, November 1993.

[47] G.J. Foschini and M.J. Gans. On limits of wireless communications in a fading environment when using multiple antennas. *WL. Pers. Commun.*, 6(3):311–335, March 1998.

[48] S. G. Foss and S. A. Zuyev. On a Voronoi aggregative process related to a bivariate Poisson process. *Advances in Applied Probability*, 28(4):965–981, December 1996.

[49] P. Frankl and H. Maehara. Some geometric applications of the beta distribution. *Annals of the Institute of Statistical Mathematics*, 42(3):463–474, September 1990.

[50] H. Furukawa and Y. Akaiwa. A microcell overlaid with umbrella cell system. In *Proc., IEEE Veh. Tech. Conference*, pages 1455–1459, Stockholm, Sweden, June 1994.

[51] A. Ganz, C. M. Krishna, D. Tang, and Z. J. Haas. On optimal design of multitier wireless cellular systems. *IEEE Communications Magazine*, 35(2):88–93, February 1997.

[52] J.J. Gaytan and D. Murioz-Rodriguez. Analysis of capacity gain and BER performance for CDMA systems with desensitized embedded microcells. In *Proc., IEEE International Conference on Universal Personal Communications*, volume 2, pages 887–891, Florence, Italy, October 1998.

[53] A. Ghasemi and E. Sousa. Spectrum sensing in cognitive radio networks: the cooperation-processing tradeoff. *Wirel. Commun. Mob. Comput.*, 7(9):1049–1060, 2007.

[54] A. Ghasemi and E. S. Sousa. Collaborative spectrum sensing for opportunistic access in fading environments. In *IEEE Int. Symp. on New Frontiers in Dynamic Spectrum Access Networks*, pages 131–136, November 2005.

[55] I. L. Glicksberg. A further generalization of the Kakutani fixed point theorem with application to Nash equilibrium points. *Proceedings of the American Mathematical Society*, 3(1):170–174, 1952.

[56] Andrea Goldsmith. *Wireless Communications*. Cambridge University Press, 2005.

[57] D. Goodman and N. Mandayam. Power control for wireless data. *IEEE Personal Communications Magazine*, 7(2):48–54, April 2000.

[58] H.W. Gould. *Combinatorial Identities*. MorganTown Printing and Binding Co., 1972.

[59] S. A. Grandhi and J. Zander. Constrained power control in cellular radio systems. In *Proc., IEEE Veh. Tech. Conference*, June 1994.

[60] L. Grokop and D. N. C. Tse. Spectrum sharing between wireless networks. In *Proc., IEEE INFOCOM*, pages 201–205, Phoenix, AZ,, April 2008.

[61] A. K. Gupta and S. Nadarajan. *Handbook of Beta distribution and its applications.* Marcel Dekker Inc., 2004.

[62] I. Guvenc, Moo-Ryong Jeong, F. Watanabe, and H. Inamura. A hybrid frequency assignment for femtocells and coverage area analysis for co-channel operation. *IEEE Comm. Letters*, 12(12), December 2008.

[63] M. Haddad, M. Debbah, and A. M. Hayar. Distributed power allocation for cognitive radio. In *Proc., International Symposium on Signal Processing and its Applications*, pages 1–4, February 2007.

[64] M. Haenggi. On distances in uniformly random networks. *IEEE Transactions on Info. Theory*, 51(10):3584–3586, October 2005.

[65] M. Haenggi, J. G. Andrews, F. Baccelli, O. Dousse, and M. Franceschetti. Stochastic geometry and random graphs for the analysis and design of wireless networks. *Submitted, IEEE Journal on Sel. Areas on Comm.*, 2009.

[66] K. Hamdi, Wei Zhang, and K. Ben Letaief. Power control in cognitive radio systems based on spectrum sensing side information. In *Proc., IEEE International Conference on Communications*, pages 5161–5165, June 2007.

[67] S. V. Hanly. An algorithm for combined cell-site selection and power control to maximize cellular spread spectrum capacity. *IEEE Journal on Selected Areas in Comm.*, 13(7):1332–1340, September 1995.

[68] A. Hasan and J. G. Andrews. The guard zone in wireless ad hoc networks. *IEEE Transactions on Wireless Comm.*, 6(3):897–906, March 2007.

[69] B. Hassibi and M. Sharif. Fundamental limits in MIMO broadcast channels. *IEEE Journal on Selected Areas in Comm.*, 25(7):1333–1344, September 2007.

[70] R.W. Heath, Jr. and D. J. Love. Multimode antenna selection for spatial multiplexing systems with linear receivers. *IEEE Transactions on Sig. Proc.*, 53:3042–3056, August 2005.

[71] R.W. Heath, Jr. and A. J. Paulraj. Switching between diversity and multiplexing in MIMO systems. *IEEE Trans. on Comm.*, 53(6):962–968, June 2005.

[72] L. T. W. Ho and H. Claussen. Effects of user-deployed, co-channel femtocells on the call drop probability in a residential scenario. In *Proc., IEEE International Symposium on Personal, Indoor and Mobile Radio Communications*, pages 1–5, September 2007.

[73] R.A. Horn and C.R. Johnson. *Matrix Analysis*. Cambridge University Press, 1985.

[74] N. Hoven and A. Sahai. Power scaling for cognitive radio. In *International Conf. on Wireless Networks, Communications and Mobile Computing*, volume 1, pages 250–255, June 2005.

[75] K. Huang, V. Lau, and Y. Chen. Spectrum sharing between cellular and mobile ad hoc networks: Transmission-capacity trade-off. *To appear, IEEE Journal on Sel. Areas on Comm. (Issue: Stoc. Geometry and Random Graphs for Wireless Nets.)*, 2009. [Online] Available at `http://arxiv.org/abs/0808.2181`.

[76] A. M. Hunter, J. G. Andrews, and S. Weber. Transmission capacity of ad hoc networks with spatial diversity. *IEEE Transactions on Wireless Communications*, 7:5058–5071, December 2008.

[77] Chih-Lin I, L. J. Greenstein, and R. D. Gitlin. A microcell/macrocell cellular architecture for low- andhigh-mobility wireless users. *IEEE Journal on Selected Areas in Comm.*, 11(6):885–891, August 1993.

[78] J. Ilow and D. Hatzinakos. Analytic alpha-stable noise modeling in a Poisson field of interferers or scatterers. *IEEE Transactions on Sig. Proc.*, 46(6):1601–1611, June 1998.

[79] Zhang J. and J.G. Andrews. Distributed antenna systems with randomness. *IEEE Transactions on Wireless Comm.*, 7(9):3636–3646, September 2008.

[80] M. G. Jansen and R. Prasad. Capacity, throughput, and delay analysis of a cellular DS CDMA system with imperfect power control and imperfect sectorization. *IEEE Transactions on Veh. Tech.*, 44:67–75, February 1995.

[81] H. Ji and C. Y. Huang. Non-cooperative uplink power control in cellular radio systems. *Wire. Net.*, 4(3):233–240, 1998.

[82] N. Jindal. High SNR analysis of MIMO broadcast channels. In *Proc., IEEE International Symposium on Information Theory*, pages 2310–2314, September 2005.

[83] N. Jindal. MIMO broadcast channels with finite-rate feedback. *IEEE Transactions on Info. Theory*, 52(11):5045–5060, November 2006.

[84] N. Jindal, J. G. Andrews, and S. Weber. Bandwidth partitioning in decentralized wireless networks. *IEEE Transactions on Wireless Comm.*, 7:5408–5419, December 2008.

[85] N. Jindal, S. Vishwanath, and A. Goldsmith. On the duality of gaussian multiple-access and broadcast channels. *IEEE Transactions on Info. Theory*, 50(5):768–783, May 2004.

[86] Han-Shin Jo, Jong-Gwan Yook, Cheol Mun, and June Moon. A self-organized uplink power control for cross-tier interference management in femtocell networks. In *Proc., Military Communications Conference*, pages 1–6, November 2008.

[87] D.A. Joseph, B.S. Manoj, and C. Siva Ram Murthy. The interoperability of Wi-Fi hotspots and packet cellular networks and the impact of user behaviour. In *Proc., IEEE International Symposium on Personal, Indoor and Mobile Radio Communications*, volume 1, pages 88–92, September 2004.

[88] M. K. Karakayali, G. J. Foschini, R. A. Valenzuela, and R. D. Yates. On the maximum common rate achievable in a coordinated network. In *Proc., IEEE International Conference on Communications*, volume 9, pages 4333–4338, June 2006.

[89] R. S. Karlsson. Radio resource sharing and capacity of some multiple access methods in hierarchical cell structures. In *Proc., IEEE Veh. Tech. Conference*, volume 5, pages 2825–2829, Amsterdam, September 1999.

[90] Dong Hee Kim, Dong Do Lee, Ho Joon Kim, and Keum Chan Whang. Capacity analysis of macro/microcellular CDMA with power ratio control and tilted antenna. *IEEE Transactions on Vehicular Technology*, 49(1):34–42, January 2000.

[91] J.F.C Kingman. *Poisson Processes*. Oxford University Press, 1993.

[92] S. Kishore, L. J. Greenstein, H. V. Poor, and S. C. Schwartz. Downlink user capacity in a CDMA macrocell with a hotspot microcell. In *Proc., IEEE Global Telecomm. Conference*, volume 3, pages 1573–1577, December 2003.

[93] S. Kishore, L. J. Greenstein, H. V. Poor, and S. C. Schwartz. Soft handoff and uplink capacity in a two-tier CDMA system. *IEEE Transactions on Wireless Comm.*, 4(4):1297–1301, July 2005.

[94] S. Kishore, L. J. Greenstein, H. V. Poor, and S. C. Schwartz. Uplink user capacity in a CDMA system with hotspot microcells: effects of Finite Transmit power and Dispersion. *IEEE Transactions on Wireless Comm.*, 5(2):417–426, February 2006.

[95] S. Kishore, L.J. Greenstein, H.V. Poor, and S.C. Schwartz. Uplink user capacity in a CDMA macrocell with a hotspot microcell: Exact and approximate analyses. *IEEE Transactions on Wireless Comm.*, 2(2):364–374, March 2003.

[96] S. Kishore, L.J. Greenstein, H.V. Poor, and S.C. Schwartz. Uplink user capacity in a multicell CDMA system with hotspot microcells. *IEEE Transactions on Wireless Comm.*, 5(6):1333–1342, June 2006.

[97] S. Kishore, L.J. Greenstein, S.C. Schwartz, and H.V. Poor. Uplink user capacity of a multi-cell CDMA system with hotspot microcells. In *Proc., IEEE Veh. Tech. Conference*, volume 2, pages 992–996, 2002.

[98] S. Kishore, L.J. Greenstein, S.C. Schwartz, and H.V. Poor. User capacity in a CDMA macrocell with a hotspot microcell: effects of Transmit power constraints and finite dispersion. In *Proc., IEEE Global Telecomm. Conference*, volume 3, pages 1558–1562, December 2003.

[99] T. E. Klein and Seung-Jae Han. Assignment strategies for mobile data users in hierarchical overlay networks: performance of optimal and adaptive strategies. *IEEE Journal on Selected Areas in Comm.*, 22(5):849–861, June 2004.

[100] S. Koskie and Z. Gajic. A Nash game algorithm for SIR-based power control in 3G wireless CDMA networks. *IEEE Transactions on Networking*, 13(5):1017–1026, October 2005.

[101] Z. Kostic, I. Maric, and X. Wang. Fundamentals of dynamic frequency hopping in cellular systems. *IEEE Journal on Selected Areas in Comm.*, 19(11):2254–2266, November 2001.

[102] X. Lagrange. Multitier cell design. *IEEE Comm. Magazine*, 35(8):60–64, August 1997.

[103] J. Lee and N. Jindal. High SNR analysis for MIMO broadcast channels: Dirty paper coding versus linear precoding. *IEEE Transactions on Info. Theory*, 53(12):4787–4792, December 2007.

[104] Ying-Chang Liang, Yonghong Zeng, E. C. Y. Peh, and Anh Tuan Hoang. Sensing-throughput tradeoff for cognitive radio networks. *IEEE Transactions on Wireless Comm.*, 7(4):1326–1337, April 2008.

[105] B. Lin, Pin-Han Ho, L. L. Xie, and X. Shen. Optimal relay station placement in IEEE 802.16j networks. In *Proceedings of the 2007 international conference on Wireless communications and mobile computing*, pages 25–30, 2007.

[106] B. Liu, Z. Liu, and D. Towsley. On the capacity of hybrid wireless networks. In *Proc., IEEE INFOCOM*, volume 2, pages 1543–1552, March/April 2003.

[107] S.B. Lowen and M.C. Teich. Power-law shot noise. *IEEE Transactions on Info. Theory*, 36(6):1302–1318, November 1990.

[108] N. B. Mehta, Jingxian Wu, A. F. Molisch, and Jin Zhang. Approximating a sum of random variables with a lognormal. *IEEE Transactions on Wireless Comm.*, 6(7):2690–2699, July 2007.

[109] C. Meyer. Uncoupling the Perron eigenvector problem. *Linear Algebra and its Appl.*, 114–115:69–94, March 1989.

[110] A. M. Monk and L. B. Milstein. Open-loop power control error in a land mobile satellite system. *IEEE Journal on Selected Areas in Comm.*, 13(2):205–212, February 1995.

[111] A. F. Naguib, N. Seshadri, and A. R. Calderbank. Increasing data rate over wireless channels. *IEEE Signal Processing Magazine*, 17(3):76–92, May 2000.

[112] J. F. Nash. Non-cooperative games. *Ann. Math.*, 54:289–295, 1951.

[113] D. Niyato and E. Hossain. Call admission control for QoS provisioning in 4G wireless networks: issues and approaches. *IEEE Network*, 19(5):5–11, September/October 2005.

[114] O. Oyman, J. N. Laneman, and S. Sandhu. Multihop relaying for broadband wireless mesh networks: From theory to practice. *IEEE Communications Magazine*, 45(11):116–122, November 2007.

[115] A. Paulraj, R. Nabar, and D. Gore. *Introduction to Space-Time Wireless Communications*. Cambridge, 2003.

[116] C. B. Peel, B. M. Hochwald, and A. L. Swindlehurst. A vector-perturbation technique for near-capacity multiantenna multiuser communication-part i: channel inversion and regularization. *IEEE Trans. on Comm.*, 53(1):195–202, January 2005.

[117] S. W. Peters and R.W. Heath, Jr. The future of WiMAX: Multihop relaying with IEEE 802.16j. *IEEE Communications Magazine*, 47(1):104–111, January 2009.

[118] Presentations by Airvana, ABI Research, Picochip. *2nd International Conference on Home Access Points and Femtocells*, December 2007. [Online] Available at `http://www.avrenevents.com/dallasfemto2007/`.

[119] L. Qian, X. Li, J. Attia, and Z. Gajic. Power control for cognitive radio ad hoc networks. In *IEEE Workshop on Local & Metro. Area Netwks.*, pages 7–12, June 2007.

[120] J. B. Rosen. Existence and uniqueness of equilibrium points for concave n-person games. *Econometrica*, 33(3):520–534, 1965.

[121] W. Rudin. *Principles of Mathematical Analysis.* New York: McGraw Hill, 1976.

[122] A. Sahai, N. Hoven, S. M. Mishra, and R. Tandra. Fundamental tradeoffs in robust spectrum sensing for opportunistic frequency reuse. Technical report, 2006.

[123] A. Saleh, A. Rustako, and R. Roman. Distributed antennas for indoor radio communications. *IEEE Trans. on Comm.*, 35(12):1245–1251, December 1987.

[124] G. Samorodnitsky and S. Taqqu. *Stable Non-Gaussian Random Processes.* Chapman and Hall, 1994.

[125] C. U. Saraydar, N. B. Mandayam, and D. J. Goodman. Pricing and power control in a multicell wireless data network. *IEEE Journal on Selected Areas in Comm.*, 19(10):1883–1892, October 2001.

[126] C. U. Saraydar, N. B. Mandayam, and D. J. Goodman. Efficient power control via pricing in wireless data networks. *IEEE Trans. on Comm.*, 50(2):291–303, February 2002.

[127] A. Shah and A. M. Haimovich. Performance analysis of optimum combining in wireless communications with rayleigh fading and cochannel interference. *IEEE Trans. on Comm.*, 46(4):473–479, April 1998.

[128] V. Shah, N. B. Mandayam, and D. J. Goodman. Power control for wireless data based on utility and pricing. In *Proc., IEEE International Symposium on Personal, Indoor and Mobile Radio Communications*, volume 3, pages 1427–1432, Boston, MA, USA, September 1998.

[129] J. Shapira. Microcell engineering in CDMA cellular networks. *IEEE Transactions on Vehicular Technology*, 43(4):817–825, November 1994.

[130] Z. Shen and S. Kishore. Optimal multiple access to data access points in tiered CDMA systems. In *Proc., IEEE Veh. Tech. Conference*, volume 1, pages 719–723, September 2004.

[131] M. Souryal, B. Vojcic, and R. Pickholtz. Ad hoc, multihop CDMA networks with route diversity in a rayleigh fading channel. In *Proc., Military Communications Conference*, volume 2, pages 1003–1007, 2001.

[132] E.S. Sousa and J.A. Silvester. Optimum transmission ranges in a direct-sequence spread-spectrum multihop packet radio network. *IEEE Journal on Selected Areas in Comm.*, 8(5):762–771, June 1990.

[133] Q. H. Spencer, A. L. Swindlehurst, and M. Haardt. Zero-forcing methods for downlink spatial multiplexing in multiuser MIMO channels. *IEEE Transactions on Sig. Proc.*, 52(2):461–471, February 2004.

[134] C. W. Sung. Log-convexity property of the feasible SIR region in power-controlled cellular systems. *IEEE Comm. Letters*, 6(6):248–249, June 2002.

[135] C. W. Sung and K. K. Leung. A generalized framework for distributed power control in wireless networks. *IEEE Transactions on Info. Theory*, 51(7):2625–2635, July 2005.

[136] J. E. Suris, L. A. DaSilva, Z. Han, and A. B. MacKenzie. Cooperative game theory for distributed spectrum sharing. In *Proc., IEEE International Conference on Communications*, pages 5282–5287, June 2007.

[137] E. Telatar. Capacity of multi-antenna gaussian channel. *European Trans. Telecommunications*, 10:585–595, November 1999.

[138] A. M. D. Turkmani. Probability of error for m-branch macroscopic selection diversity. In *Communications, Speech and Vision, IEE Proceedings I*, volume 139, pages 71–78, February 1992.

[139] S. Ulukus and R. D. Yates. Stochastic power control for cellular radio systems. *IEEE Trans. on Comm.*, 46(6):784–798, June 1998.

[140] H. Urkowitz. Energy detection of unknown deterministic signals. *Proceedings of the IEEE*, 55(4):523–531, April 1967.

[141] P. Viswanath, D. N. C. Tse, and R. Laroia. Opportunistic beamforming using dumb antennas. *IEEE Transactions on Info. Theory*, 48(6):1277–1294, June 2002.

[142] S.P. Weber, J.G. Andrews, and N. Jindal. Transmission capacity: Applying stochastic geometry to uncoordinated ad hoc networks. *Submitted, IEEE Journal on Selected Areas in Comm.*, August 2008.

[143] S.P. Weber, J.G Andrews, and Nihar Jindal. The effect of fading, channel inversion, and threshold scheduling on ad hoc networks. *IEEE Transactions on Info. Theory*, 53(11):4127–4149, November 2007.

[144] S.P. Weber, Xiangying Yang, J.G. Andrews, and G. de Veciana. Transmission capacity of wireless ad hoc networks with outage constraints. *IEEE Transactions on Information Theory*, 51(12):4091–4102, December 2005.

[145] H. Weingarten, Y. Steinberg, and S. Shamai. The capacity region of the Gaussian Multiple-Input Multiple-Output broadcast channel. *IEEE Transactions on Info. Theory*, 52(9):3936–3964, September 2006.

[146] White Paper by Analysys. *Picocells and Femtocells: Will indoor base-stations transform the telecoms industry?*, 2007.

[147] White Paper by Tropos Networks. *Picocell Mesh: Bringing Low-Cost Coverage, Capacity and Symmetry to Mobile WiMAX*, March 2007.

[148] J. H. Winters, J. Salz, and R. D. Gitlin. The impact of antenna diversity on the capacity of wireless communication systems. *IEEE Trans. on Comm.*, 42:1740–1751, 1994.

[149] J.-S. Wu, J.-K. Chung, and M.-T. Sze. Analysis of uplink and downlink capacities for two-tier cellular system. *IEE Proceedings- Communications*, 144(6):405–411, December 1997.

[150] Jung-Shyr Wu, Jen-Kung Chung, and Yu-Chuan Yang. Performance study for a microcell hot spot embedded in CDMA macrocell systems. *IEEE Transactions on Vehicular Technology*, 48(1):47–59, January 1999.

[151] Mingbo Xiao, N. B. Shroff, and E. K. P. Chong. Utility-based power control in cellular wireless systems. In *Proc., IEEE INFOCOM*, volume 1, pages 412–421, Anchorage, AK, USA, 2001.

[152] Kun Yang, Yumin Wu, and Hsiao-Hwa Chen. QoS-aware routing in emerging heterogeneous wireless networks. *IEEE Communications Magazine*, 45(2):74–80, February 2007.

[153] R. Yates and C. Y. Huang. Optimal uplink power control and base station assignment. In *Proc., IEEE International Conference on Universal Personal Communications*, pages 247–251, San Diego, CA, USA, September/October 1994.

[154] R. D. Yates. A framework for uplink power control in cellular radio systems. *IEEE Journal on Selected Areas in Comm.*, 13(7):1341–1347, September 1995.

[155] R. D. Yates and Ching-Yao Huang. Integrated power control and base station assignment. *IEEE Transactions on Veh. Tech.*, 44(3):638–644, August 1995.

[156] K.L. Yeung and S. Nanda. Channel management in microcell/macrocell cellular radio systems. *IEEE Transactions on Veh. Tech.*, 45(4):601–612, November 1996.

[157] Y. Yuan, P. Bahl, R. Chandra, T. Moscibroda, and Y. Wu. Allocating dynamic time-spectrum blocks in cognitive radio networks. In *MobiHoc '07: Proceedings of the 8th ACM international symposium on Mobile ad hoc networking and computing*, pages 130–139, 2007.

[158] J. Zander. Distributed cochannel interference control in cellular radio systems. *IEEE Transactions on Veh. Tech.*, 41(3):305–311, August 1992.

[159] J. Zander. Performance of optimum transmitter power control in cellular radio systems. *IEEE Transactions on Veh. Tech.*, 41(1):57–62, February 1992.

[160] A. Zemlianov and G. De Veciana. Cooperation and decision-making in a wireless multi-provider setting. In *Proc., IEEE INFOCOM*, volume 1, pages 386–397, March 2005.

[161] A. Zemlianov and Gustavo De Veciana. Capacity of ad hoc wireless networks with infrastructure support. *IEEE Journal on Selected Areas in Comm.*, 23(3):657–667, March 2005.

[162] H. Zhang and H. Dai. Cochannel interference mitigation and cooperative processing in downlink multicell multiuser networks. *EURASIP journal on Wireless Communications and Networking*, pages 222–235, 2004.

[163] J. Zhang, R. Chen, J. Andrews, A. Ghosh, and R.W. Heath, Jr. Networked MIMO with clustered linear precoding. *To Appear, IEEE Transactions on Wireless Comm.*, 2009.

[164] J. Zhang, R.W. Heath, Jr., M. Koutouris, and J. G. Andrews. Mode switching for MIMO broadcast channel based on delay and channel quantization.

To Appear, EURASIP special issue on Multiuser MIMO Transmission with Limited Feedback, Cooperation, and Coordination, 2009. [Online] Available at `http://arxiv.org/abs/0812.3120`.

Vita

Vikram Chandrasekhar was born in Chennai, India in 1979. He was a recipient of the National Talent Search scholarship awarded by the Government of India in 1994. He completed his B.Tech (honors) at Indian Institute of Technology, Kharagpur in 2000 and received his M.S. at Rice University in 2003. After his M.S., he held a staff engineer position at National Instruments for two and half years where he was a finalist for the best new employee of the year. He was an intern at Texas Instruments in the summers of 2007 and 2008, working on power control schemes in femtocell networks and maximizing sum rates in multi-cell systems. He had previously interned at Freescale Semiconductor in 2006 working on synchronization algorithms for downlink cell-search in the 3GPP's Longterm Evolution standard. His PhD dissertation focuses on fundamental limits and algorithms for microcellular and hotspot-aided broadband cellular networks. His research paper on spectrum allocation in two-tier networks was adjudged as the second best paper among 108 submissions in the student paper contest in the 2008 IEEE Asilomar conference on signals, systems and computers. His research was supported by Texas Instruments.

Permanent address: 7117 Woodhollow Dr.
Austin, Texas 78731

This dissertation was typeset with LaTeXby the author.